Calcium Signalling in *Dictyostelium discoideum*

Submitted by

Claire Yvonne Allan

B. Biol. Sc. (Hons)

A thesis submitted in total fulfilment of the requirements for the degree of

Doctor of Philosophy

School of Agriculture, Biomedicine and Environment

Department of Microbiology, Anatomy, Physiology & Pharmacology

La Trobe University

Victoria 3083

Australia

April 2022

Table of Contents

List of figures

List of tables

List of abbreviations and their symbols

ACD	Autophagic cell death
AMPK	AMP- activated protein kinase
ATP	Adenosine triphosphate
AV	Autophagic vacuole
Bp	Base pairs
$[Ca^{2+}]_{cyt}$	Cytosolic calcium concentration
CaBPs	Ca^{2+} Binding proteins
CaM	Calmodulin
cAMP	3',5' cyclic adenosine monophosphate
CAX	$Na^{+}/H^{+}/Ca^{2+}$ exchanger
cDNA	Complementary deoxyribonucleic acid
CICR	Ca^{2+} induce Ca^{2+} release
CV	Contractile vacuole
dH2O	Distilled water
DIF	Differentiation Inducing Factor
DMSO	Dimethyl sulfoxide
DNA	Deoxyribonucleic acid
EDTA	Ethylenediamine tetra-acetic acid
EE	Early endosome
ER	Endoplasmic reticulum
gDNA	Genomic DNA
GPCRs	G-protein coupled receptors
HBS	HEPES-buffered saline
h	Hour
IP_3	Inositol 1,4,5-trisphosphate
IP3Rs	Inositol-1,4,5-triphospate receptors
Kb	Kilobase
KD	Knockdown
KO	Knockout
LB	Luria broth
LE	Late endosome
LEL	Late endosome lysosome
M	Molar
MCU	Mitochondrial Ca^{2+} uniporter
mg	Milligram
min	Minute
mL	Milliliter
mM	Millimolar
mRNA	Messenger RNA
ng	Nanogram
PBS	Phosphate buffered saline
PCR	Polymerase chain reaction
PD	Parkinson's disease
PLC	Phospholipase C
PM	Plasma membrane
PMCA	Plasma membrane Ca^{2+}- ATPase
pmol	Picomoles
PC1	Polycystin-1

PC2	Polycystin-2
RNA	Ribonucleic acid
RNase	Ribonuclease
RT	Reverse transcription
RyRs	Ryanodine receptors
s	Second
SDS	Sodium dodecyl sulfate
SERCA	Sarco-endoplasmic reticulum Ca^{2+}- ATPase
SM	Standard medium
SOCE	Store-operated Ca^{2+} entry
SPCA	Secretory Pathway Ca^{2+}- ATPase
SR	Sarcoplasmic reticulum
SS	Saline solution
TBE	Tris-borate-EDTA-buffer
TMD	Transmembrane domain
TPC	Two Pore Channel
TRP	Transient Receptor Potential
TRPML	Transient Receptor Potential Mucolipin
TRPP	Transient Receptor Potential Polycystin
U	Units
v/v	Volume per volume ratio
VDCC	Voltage-dependent Ca^{2+} channels
asRNA	Antisense ribonucleic acid
bp	Base pair
ON	Overnight
qPCR	Quantitative PCR
qRT-PCR	Quantitative Reverse transcription PCR
RT-PCR	Reverse transcription PCR
VGCCs	Voltage gate calcium channels
VOCCs	Voltage operated calcium channels
w/v	Weight per volume ratio
µg	Microgram
µl	Microliter
µM	Micromolar

Abstract

Calcium is a universal regulator of cell biological functions, so is crucial to cellular life and death. Increasingly, aberrant calcium signalling and homeostasis is being linked to many diseases, and as such, pharmacological intervention targeting calcium regulatory proteins is used therapeutically as disease treatment. Therefore, understanding the molecular mechanisms behind calcium dysregulation in diseased cells will be key to development of future therapies. The use of model organisms such as *Dictyostelium discoideum* to study disease associated proteins provides valuable insights into disease molecular pathogenesis. *Dictyostelium* has been used extensively to study a number of human diseases including mitochondrial disease, neurodegenerative disease and lysosomal diseases. The organism is an established model to study cellular calcium signalling and displays a diverse set of phenotypes. *Dictyostelium* encodes a simple selection of calcium channels, pumps and binding proteins that regulate calcium homeostasis and signalling. Many of these proteins have been the subject of only a limited number of studies or are completely uncharacterized. Therefore, studying the molecular function of these proteins not only add to our understanding of how they function in *Dictyostelium*, but also allows the findings to be extrapolated to the human homologues.

In this thesis I have studied two *Dictyostelium* calcium channels, Ddpolycystin and Ddmucolipin, homologues of which are associated with the diseases Polycystic kidney disease and Mucolipidosis type IV respectively. To date little is known about the function of either protein especially in relation to chemotactic calcium signalling. I overexpressed and knocked down expression of Ddpolycystin and Ddmucolipin and measured diverse phenotypes in the unicellular and multicellular stages of the *Dictyostelium* life cycle and coupled this with assays of Ca^{2+} responses using Ca^{2+}-sensitive luminescence by recombinant aequorin coexpressed in the same transformants. I showed that Ddpolycystin contributes to chemoattractant induced cytosolic calcium responses in both vegetative (folic acid responses) and aggregation competent cells (cAMP responses). Thus, Ddpolycystin being expressed in the plasma membrane contributes to facilitating the influx of extracellular calcium during these responses. While Ddmucolipin can measurably contribute to the global calcium responses when overexpressed, its role may be more related to regulating local calcium signalling associated with processes along the

endocytic pathway because it is expressed in the membranes of endocytic compartments. This is the first direct evidence to show that Ddmucolipin contributes to these calcium signals.

I also showed that Ddpolycystin and Ddmucolipin dependent calcium signalling is involved in regulation of various cellular phenotypes. Specifically, Ddpolycystin positively regulated both axenic growth rates and growth on lawns of bacteria and also affects macropinocytosis and phagocytosis, likely due to calcium dependent pathways. Ddpolycystin dependent Ca^{2+} signaling was also involved in controlling cell type specific differentiation, spore germination and autophagic cell death. Altering Ddmucolipin expression levels caused an accumulation or more acidified vesicles stained with Lysosensor Blue in vegetative cells suggesting defects in the endocytic pathway. Accordingly, strains exhibited defects in catabolism because knocking down Ddmucolipin upregulated nutrient uptake by phagocytosis and macropinocytosis but there was no corresponding increase in growth. Defective catabolism is common to lysosomal diseased cells, and as such, Ddmucolipin mutants were in a state of partial starvation and thus formed increased numbers of aggregation centers and accordingly smaller slugs and fruiting bodies. Many of the phenotypes displayed in my Ddmucolipin strains are common to other *Dictyostelium* lysosomal diseases models. This work supports the use of *Dictyostelium* to study both Polycystic kidney disease and Mucolipidosis type IV particularly in relation to calcium regulation.

Finally, I have investigated the role of two *Dictyostelium* homologues of the P-type Ca^{2+}-ATPases (calcium pumps), in the *Dictyostelium* lifecycle and in particular chemoattractant elicited calcium responses. Until now these putative calcium pumps have been completely uncharacterized in *Dictyostelium*. Dysfunctions in the human proteins are associated with varying diseases such as mental disorders, cystic fibrosis, neurodegenerative disorders and muscular dystrophies, and the molecular mechanisms of these proteins is still being elucidated. Thus, *Dictyostelium* provides an untapped resource to aid in our understanding of Ca^{2+}-ATPases dysfunction in human disease. By knocking down expression of two Ca^{2+}-ATPases, termed PAT3 and PAT4, I showed that they display functional redundancy. When a single pump is knocked down, other pumps can be up-regulated, because the Ca^{2+} signalling system is homeostatically regulated at the

transcriptional level. Therefore, single pump knockdown strains were phenotypically the same as wildtype cells. The cytosolic calcium responses to folic acid in vegetative cells differed to the wild type only by a subtly change in kinetics of the responses, which indicated that that PAT3 and PAT4 have different responsiveness to cytosolic calcium, with PAT4 exerting a larger influence than PAT3 on the Ca^{2+} responsiveness of the response kinetics. On the other hand, in developed cells both the kinetics and mechanism of the cAMP responses were altered. This suggests that PAT3 and PAT4 contribute more to shaping cAMP cytosolic Ca^{2+} responses, than folic acid responses thus playing a more prominent role of calcium regulation during development.

Statement of Authorship

This thesis includes work by the author that has been published or accepted for publication as described in the text. Except where reference is made in the text of the thesis, this thesis contains no other material published elsewhere or extracted in whole or in part from a thesis accepted for the award of any other degree or diploma. No other person's work has been used without due acknowledgement in the main text of the thesis. This thesis has not been submitted for the award of any degree or diploma in any other tertiary institution.

Claire Yvonne Allan

Date: 13th April 2022

Acknowledgements

I would like to thank my supervisor Professor Paul Fisher for his guidance and support.

I would like to thank my lab members for their friendship, support and encouragement throughout the years.

I would like to thank my family and friends for their support especially my partner Scott Gould for his encouragement.

This work was supported by an Australian Government Research Training Program Scholarship through an Australian Postgraduate Award.

List of publications

Allan, C.Y. and Fisher P.F. (2022). The *Dictyostelium* model for Mucolipidosis Type IV. *Front. Cell Dev. Biol.* **(10)** doi: 10.3389/fcell.2022.741967

Oral Presentations

Claire Y. Allan and Paul R Fisher. (2008). Calcium Signalling in *Dictyostelium* and its implications in Polycystic Kidney Disease and Mucolipidosis Type IV. Dicty2008. Annual International *Dictyostelium* Conference 2008. Abstract 12-3 p. 49. 15th-20th September, 2009. Tsukuba-Shi, Japan.

Claire Y Allan and Paul R Fisher (2005). Chimeric receptors and calcium signaling in *Dictyostelium*. Melbourne *Dictyostelium* Conference 2005. 21st July 2005. Melbourne, Australia.

Poster Presentations

Claire Y Allan and Paul R Fisher (2011). *Dictyostelium discoideum* as a model for Mucolipidosis Type IV. Cell Signal-omics 2011. Integrated cellular pathology – systems biology of human disease under the auspices of the European Research Institute for Integrated Cellular Pathology. Session 8 Gene expression networks in health and disease Poster 1. Abstract p. 167. 26th – 28th January 2011. European Conference Centre, Luxembourg.

Claire Y Allan and Paul R Fisher (2008). Calcium signalling in *Dictyostelium*. Australian Society for Microbiology Annual Conference 2008. Abstract P04.02. 6th – 10th July, 2008. Melbourne Convention Centre, Australia.

Chapter One

The molecular basis and biological roles of calcium signalling in *Dictyostelium*

The ubiquitous cellular messenger, calcium, is unique in its ability to regulate a plethora of biological functions that are essential to cellular life and death. The following chapter discusses calcium signalling and regulation in the eukaryotic slime mold *Dictyostelium discoideum* and its biological role. The review is comprised of two main parts: Section one discusses what is known about the molecular mechanisms of calcium regulation and signalling in *D. discoideum* discussed in the context of knowledge in other eukaryotes. Section two provides a summary of what is known about the biological roles that calcium plays in the lifecycle *D. discoideum*.

1.1 The molecular basis of calcium signalling in *Dictyostelium*

1.1.1 Overview of calcium signalling in *Dictyostelium discoideum*

Calcium is a vital cellular messenger in all organisms (Berridge *et al*., 2000). The role of calcium in *Dictyostelium* is paramount to many cellular processes and is involved at all stages of the lifecycle. Various Ca^{2+} sensing effectors, such as Ca^{2+}-binding or Ca^{2+}-activated proteins, can translate signals into specific cellular physiological responses. Therefore, spatiotemporal regulation of intracellular Ca^{2+} concentrations, both cytoplasmic and within organelles, is crucial for the homeostatic maintenance of basal concentrations and facilitation of global and local Ca^{2+} signalling. Ca^{2+} signals can originate from the extracellular environment or from within intracellular Ca^{2+} stores including the endoplasmic reticulum (ER), mitochondria, contractile vacuole (CV), acidocalcisomes, Golgi apparatus and acidic vesicles of the endocytic pathway. The concentration of Ca^{2+} within these organelles can reach micromolar levels, much higher than the basal cytosolic Ca^{2+} concentration in *Dictyostelium* of approximately 70 nM (Nebl and Fisher 1997; Traynor *et al*., 2000; Wilczynska *et al*., 2005). There are many proteins that are involved in initiating, shaping, maintaining and terminating Ca^{2+} signals. These include Ca^{2+} channels that can release Ca^{2+} into the cytosol, pumps that energetically sequester Ca^{2+} ions across cellular membranes, cation exchange transporters and binding proteins that can regulate free Ca^{2+} concentrations (Clapham, 2007).

The *Dictyostelium* genome encodes a collection of Ca^{2+} transport and binding proteins involved in Ca^{2+} signalling and homeostasis some of which have been studied experimentally. The ER, a major Ca^{2+} store, contains two calcium binding proteins calnexin and calreticulin (Muller-Taubenberger *et al*., 2001) and two putative Ca^{2+}-ATPases are likely to be located in the plasma or ER membranes (Wilczynska *et al*., 2005). PAT1, a vacuolar Ca^{2+}-ATPase (Moniakis *et al*., 1995) localises to the membranes of the contractile vacuole (CV) and acidocalcisomes (Marchesini *et al*., 2002). Five ATP gated P2X Ca^{2+} channels are also functional in the CV membrane (Fountain *et al*., 2007; Ludlow *et al*., 2008). The gene *cax2* encoding a type II cation exchange Ca^{2+} antiporter (CAX) has been identified but not studied (Shigaki *et al*., 2006). A putative Ca^{2+} channel IplA (Traynor *et al*., 2000; Lusche *et al*., 2012) and a transient receptor potential (TRP) like channel

Ddpolycystin (Wilczynska *et al*., 2005; Lima *et al*., 2014; Traynor and Kay, 2017) are primarily localised in the plasma membrane. Vesicles of the endocytic pathway, particularly post lysosomes, colocalise with a TRP homologue Ddmucolipin (Lima *et al*., 2012), where the putative two pore calcium channel (DdTPC) is likely to also localise (Chang *et al*., 2020; Wilczynska *et al*., 2005). The mitochondrial uniporter (DdMCU) may facilitate mitochondrial Ca^{2+} uptake (Kovács *et al*., 2014) (Fig 1.1). In mammals the Golgi apparatus harbors various calcium pumps, channels and binding proteins (Pizzo *et al*., 2011), however in *Dictyostelium* no calcium translocating proteins have been identified at the Golgi to date.

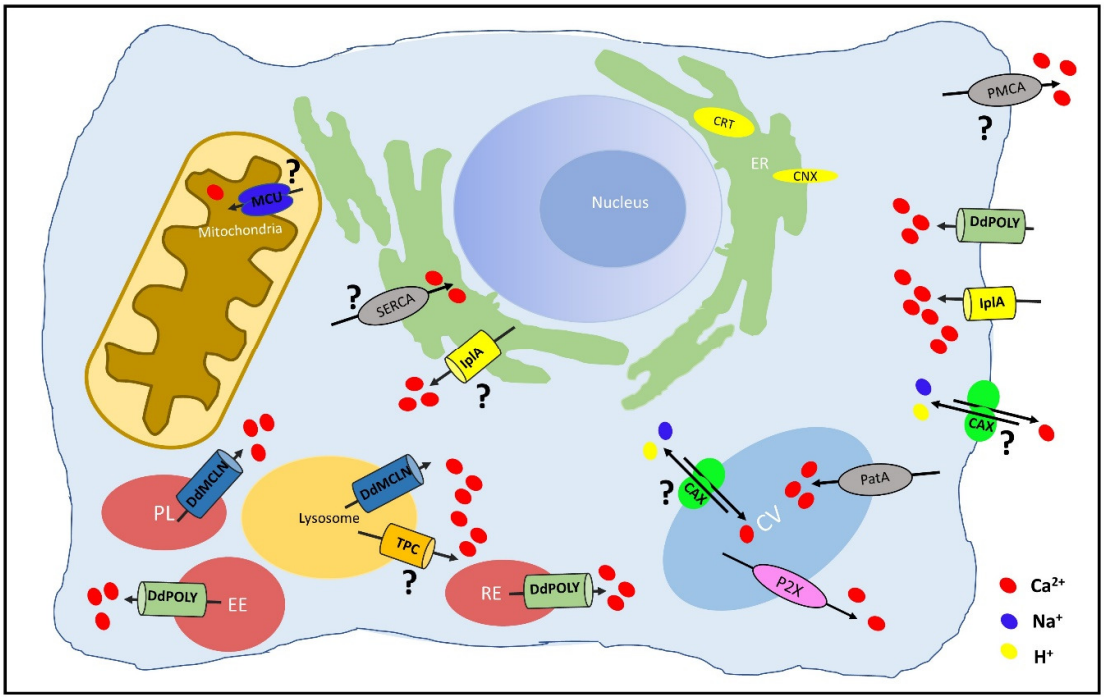

Figure 1.1 *Dictyostelium* calcium channels, pumps, exchangers and binding proteins.
The channel Ddpolycystin (DdPOLY) has been localised primarily to the PM, but was also observed in early endosomes (EE) and recycling endosomes (RE) likely as a consequence of the endocytic cycle (Lima *et al*., 2014). The DdTPC homologue has been identified but its subcellular localisation is unknown (indicated by "?"), it likely resides in the endo-lysosomal membranes as is described in other organisms (Wang *et al*., 2012). Ddmucolipin (DdMCLN) has been localised to endosomal compartments and the post lysosome (PL) (Lima *et al*., 2012). The IplA channel has been localised to the PM and in the membranes of undescribed cytoplasmic vesicles (Lusche *et al*., 2012). While IplA has not been localised to the ER (specific ER markers have not been used to determine colocalization), this subcellular location may be possible (indicated by the "?") as is described for other InsP3 receptors (Taylor *et al.,* 1999). The ER also contains the calcium binding proteins,

calnexin, a class 1 transmembrane protein, and calreticulin resides in the lumen (Muller-Taubenberger *et al*., 2001). Five P2X receptor homologues are located in the membrane of the contractile vacuole (CV) (Ludlow *et al*., 2009). The P-type-Ca^{2+}-ATPase, PAT1 also localises to the CV membrane. Two other predicted homologues of PMCA/SERCA, dictyBase accession numbers DDB_G0284605 and DDB_G0289473 are encoded in the genome, but have not been experimentally investigated (Wilczynska *et al*., 2005). One may be located in the PM and one in the ER (as indicated by the "?"). The putative $Na^+/H^+/Ca^{2+}$ exchanger (CAX) has been predicted (DDB_G0279301) (Shigaki *et al*., 2006) although not experimentally studied, may reside in the PM or CV. The *Dictyostelium* mitochondrial uniporter (MCU) localises to the inner mitochondrial membrane when expressed in HEK-293T cell lines, however it's subcellular localisation in *Dictyostelium* is unknown as indicated by "?" (Kovács-Bogdán *et al*., 2014).

1.1.2 The shape of Ca^{2+} signals: spikes, waves and oscillations

Eukaryotic Ca^{2+} signals begin by release of ions into the cytoplasm via Ca^{2+} channel activation. Free Ca^{2+} in the cytoplasm is tightly buffered so that Ca^{2+} ions can only diffuse less than 1 micrometer over a few microseconds before being translocated by pumps and exchangers, or bound by Ca^{2+} binding proteins (Clapham, 1995). As such, signals must be propagated by coordinated release from neighboring channels. Signals can exist in the form of spikes, that consist of brief bursts of Ca^{2+} release which only travel short distances to signal locally from the site of release. These spikes can also be organized into regenerative waves by further activation of surrounding Ca^{2+} channels, which increase the spatiotemporal reach of the signal and these waves can further form oscillations that act globally throughout the cell (Clapham, 2007; Parkash and Asotra, 2012; Samanta and Parekh, 2017). In this manner, functions of a single channel can have whole cell implications (Fig 1.2). Cytosolic Ca^{2+} 'buffers' such as parvalbumins, calbindin-D9k, calbindin-D28k, and calretinin, can also modulate the shape of the signal by binding free Ca^{2+}, and also contribute to signal termination (Gilabert, 2012). Termination of the signal is accomplished by sequestration of ions from the cytoplasm by Ca^{2+}-ATPases or CAX or both (Clapman, 2007). Oscillations can take several seconds to reach maximum amplitude, and termination can occur over tens of seconds (Thul *et al*., 2015). The initiation and propagation of Ca^{2+} signals are largely shaped by the type and location of the Ca^{2+} channel activated. Ca^{2+} channels belong to three main groups, as discussed in the following sections.

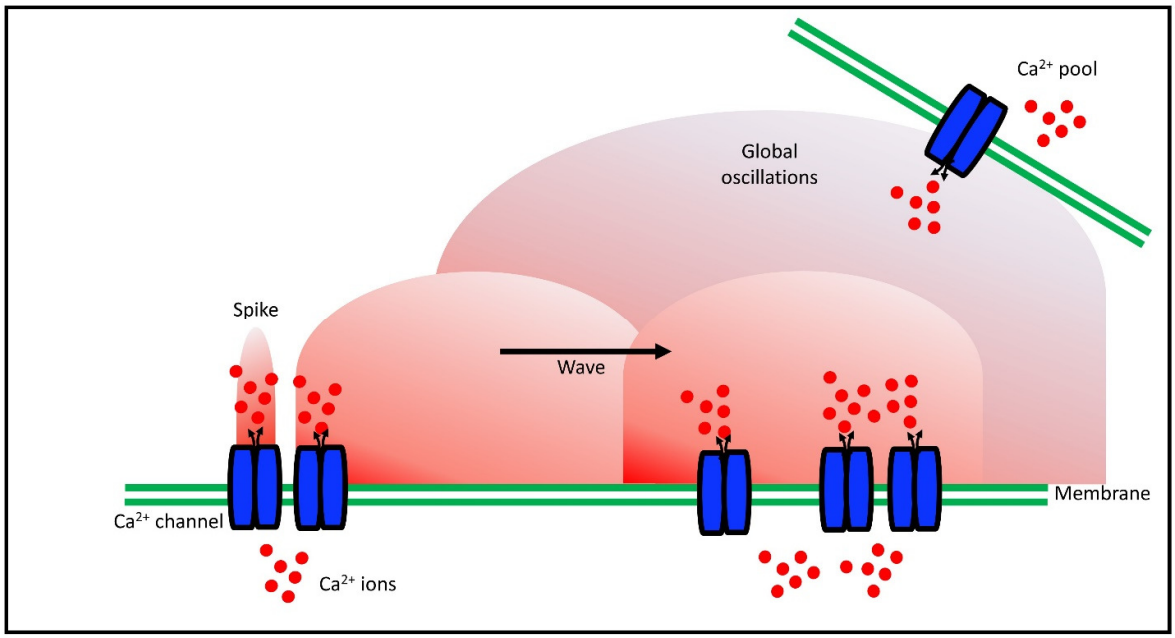

Figure 1.2 Ca^{2+} spikes, waves and oscillations.

Release of Ca^{2+} through Ca^{2+} channels can be in the form of small spikes that consist of brief bursts of Ca^{2+} that only travel short distances to signal locally from the site of release. These spikes can also be organized into regenerative waves (indicated by the small shaded domes) by further activation of surrounding Ca^{2+} channels, which increase the spatiotemporal reach of the signal. The waves can further form oscillations (indicated by the larger shaded dome) that act globally throughout the cell by activating Ca^{2+} release from Ca^{2+} pools in other areas of the cell. Adapted from Foskett *et al*. (2007).

1.1.3 The Ca^{2+} channels that shape Ca^{2+} signals

1.1.3.1 Ligand gated Ca^{2+} channels

Ligand gated ion channels open in response to interaction of a specific ligand, such as ATP, inositol 1,4,5-trisphosphate (IP_3) or a neurotransmitter, with the ligand binding domain. They can function in both the plasma membrane and membranes of intracellular organelles, to both initiate and amplify Ca^{2+} signals (Foskett *et al*., 2007). The *Dictyostelium* ATP-gated P2X and InsP3-activated IplA channels fall into this category and are discussed in sections (1.1.4.7) and (1.1.4.3).

1.1.3.2 Transient receptor potential channels

Transient receptor potential (TRP) channels comprise a large superfamily of Ca^{2+} channels that include six subfamilies: the TRP polycystin, TRP mucolipin, TRP canonical, TRP ankyrin, TRP vanilloid and TRP melastatin (Gees *et al*., 2010). TRPs are associated with sensory

physiology such as touch, temperature, pain and taste and are activated by an enormous variety of stimuli from both outside and within the cell, including phosphorylation, hyperpolarization, heat, cold, osmolarity, diacylglycerol and Ca^{2+} store depletion (Montell, 2002; Clapham, 2003). The *Dictyostelium* homologues of TRPP (Ddpolycystin), TRPML (Ddmucolipin) are discussed further in sections (1.1.4.1) and (1.1.4.2) respectively.

1.1.3.3 Voltage gated Ca^{2+} channels (VGCC)

Transmission of extracellular and intracellular stimuli into a Ca^{2+} signal cascade requires channel activation. The mechanism of channel activation depends on the type of channel. Voltage gated Ca^{2+} channels (VGCC) comprise a large family of Ca^{2+} channels in excitable cells and are activated by membrane depolarization (Miller, 1992). They are extremely fast at conducting Ca^{2+} signals with a single channel able to release ~10^6 Ca^{2+} ions per second (Clapham, 2007). No homologues of VGCCs have been described in *Dictyostelium*.

1.1.3.4 EF-hand calcium binding domains

To be regulated by calcium themselves, calcium-regulating proteins contain specific regulatory Ca^{2+} binding domains. The EF-hand Ca^{2+} binding domain is a common structural motif that allows proteins to bind and be regulated by Ca^{2+} ions. Proteins containing the motif are termed EF-hand Ca^{2+}-binding proteins. A pair of helix-loop-helix motifs bundle together to form a domain capable of binding two Ca^{2+} ions which can either activate or suppress the function of the protein (Chazin, 2011) and assist in the crucial process of converting the Ca^{2+} signal into activation of intracellular signalling pathways. EF-hand Ca^{2+}-binding proteins fall into two main groups, Ca^{2+}-sensors and Ca^{2+}-buffers. The Ca^{2+}-sensors, including calmodulin (CaM), recoverin, and many other known EF-hand proteins, function by translating a change in Ca^{2+} concentration into a variety of cellular responses. Ca^{2+}-buffers, such as parvalbumin, calbindin D9k, calbindin D28k and calretinin, modulate calcium signals by binding free Ca^{2+} ions therefore acting as Ca^{2+} buffers to restrict signals (Denessiouk *et al.*, 2014). Ca^{2+}-binding EF hands have been predicted to be present in *Dictyostelium* TPC (Section 1.1.4.6) and Ddmucolipin channels (Wilczynska *et al*., 2005).

1.1.3.5 Intracellular Ca^{2+} stores and coupling to Ca^{2+} influx

Dictyostelium's major intracellular Ca^{2+} stores are the ER (Wilczynska *et al*., 2005) and acidic Ca^{2+} stores comprising acidic vesicles, acidocalcisome and CV (Schlatterer *et al*., 2001; Marchesini *et al*., 2002). In other cell types, free Ca^{2+} concentrations within the ER have been estimated to be approximately 100-700 µM (Foskett *et al*., 2007) and around 500 µM in acidic vesicles (Christensen *et al*., 2002), so that there is a 10^3 to 10^4-fold concentration gradient between the lumen of these compartments and the cytosol, where the free [Ca^{2+}] is 70-100 nM. Intracellular Ca^{2+} stores are key to the mechanism of Ca^{2+} signal propagation. Two mechanisms for coupling between Ca^{2+} influx and release of Ca^{2+} from intracellular stores have been described in other organisms:

1) Calcium-induced calcium release (CICR) is a mechanism whereby Ca^{2+} influx over the plasma membrane activates intracellular Ca^{2+} channels in the internal stores and induces Ca^{2+} release. In this way, extracellular Ca^{2+} signals can be amplified further via intracellular Ca^{2+} release. For this mechanism to be active, the intracellular Ca^{2+} release channels must also be activated by Ca^{2+} (Bootman *et al*., 2002), thus the presence of a Ca^{2+} binding domain such as an EF-hand motif is necessary.

2) Store-operated Ca^{2+} entry (SOCE) or capacitative Ca^{2+} entry (CCE) occurs after IP_3-mediated depletion of ER Ca^{2+}, and release from other intracellular Ca^{2+} stores, which activates channels in the plasma membrane to induce Ca^{2+} influx to refill the internal stores. The channels in the plasma membrane that respond to emptying of the internal stores are called store-operated Ca^{2+} channels (SOCC) (Putney, 1986; Putney, 2009).

Evidence that CICR rather than CCE functions in *Dictyostelium* chemotactic Ca^{2+} responses has been provided (Wilczynska *et al*., 2005; Fisher and Wilczynska, 2006; Malchow *et al*., 2008). In a pharmacological study, addition of various concentrations of Ca^{2+} (0.3–3 µM Ca^{2+}) to isolated vesicle and ER fractions induced a rapid release of Ca^{2+}. The release primarily originated from the acidic vesicles because the response was reduced by 55±18% in vesicles depleted of Ca^{2+} using Concanamycin A (CMA) and by 20±11% in Ca^{2+}-depleted ER fractions (Malchow *et al*., 2008). This result also implies that both stores are capable of CICR. Genetic studies have also indicated that CICR, rather than CCE, is involved in chemotactic cytosolic Ca^{2+} transients in whole cells, discussed further in section 1.2.3 (Nebl *et al*., 2002; Wilczynska *et al*., 2005; Fisher and Wilczynska, 2006). As *Dictyostelium*

contains all the necessary elements to allow CCE to function, there remains the possibility that CCE functions during different, undescribed Ca^{2+} signalling events.

Throughout the life cycle of *Dictyostelium,* Ca^{2+} signalling is essential for proper function of many cellular processes. This review will first discuss the individual elements of the *Dictyostelium* Ca^{2+} signalling proteins and what is known about them so far. It will then go on to discuss the interconnectivity of these proteins in their various subcellular locations in controlling Ca^{2+} signalling and the cellular processes regulated by this ubiquitous second messenger.

1.1.4 The calcium translocating and binding proteins of *Dictyostelium*

1.1.4.1 The calcium channel polycystin-2

Ddpolycystin is the *Dictyostelium* homologue of mammalian polycystin-2 (PC2), a TRP type channel, homologues of which have been studied in *Caenorhabditis elegans*, *Drosophila*, mice and human models. In mammals PC2 is ubiquitously expressed (Thul *et al*., 2017) and localises to the plasma membrane (Luo *et al*., 2003; Ma *et al*., 2005), primary cilium (Nauli *et al*., 2003; Pazour *et al*., 2003) and ER (Cai *et al*., 1999; Koulen *et al*., 2002). It is responsible for Ca^{2+} entry into the cytosol, both from intracellular compartments and from the extracellular milieu, as a mediator of sensory signalling. PC2 signalling has diverse cellular roles. In mammalian cells PC2 function in the primary cilium is involved in left-right asymmetry establishment during embryonic development (Yoshiba and Hamada, 2014; Grimes *et al*., 2016). Knockout (KO) mice exhibit vascular defects, embryonic kidney cysts (Wu *et al*., 2000), defects in organ laterality (Pennekamp *et al*., 2002) and respiratory dysfunction (Sang *et al*., 2019). In *Drosophila* PC2 may function as an intracellular release channel involved in muscle contraction (Gao *et al*., 2004), and it also localises to the distal tip of sperm flagella where it is involved in fertility (Watnick *et al*., 2003; Li *et al*., 2020). In *C. elegans* the channel localises to both intracellular membranes and also sensory neuron cilia and is involved in mating behavior (Barr *et al*., 2001; O'Hagan *et al*., 2014).

PC2 is an integral membrane protein comprising 6 transmembrane domains (TMD) with cytoplasmic amino- and carboxyl-termini and pore region between TM5 and TM6 (Mochizuki *et al*., 1996). The functional channel is believed to be comprised of four PC2 units oligomerized as a tetramer (Yu *et al*., 2009). Patch clamping experiments have revealed that the channel is a non-selective cation channel with high permeability to Ca^{2+} (Hanaoka *et al*., 2000; González-Perrett *et al*., 2001), but can also conduct Na^{+} and K^{+} (Liu *et al*., 2018; Brill and Ehrlich, 2020). PC2 has an ER retention signal (Cai *et al*., 1999) and two EF-hand Ca^{2+} binding motifs in the C terminal region (Qian *et al*., 1997) which are thought to play a role in Ca^{2+}-dependent activation of the channel (Schumann *et al*., 2009; Petri *et al*., 2010; Celic *et al*., 2012; Yang *et al*., 2016). While two EF-hand Ca^{2+} binding motifs have been identified, in the human PC2 only one can functionally bind Ca^{2+}, because in the first motif there is a deletion of 4 amino acids that are required for Ca^{2+} binding (Petri *et al*., 2010). Upon binding Ca^{2+} the EF-hand of PC2 undergoes a folding transition which is sensitive to Ca^{2+} (Celic *et al*., 2008). As Ca^{2+} concentrations increase, the C-terminal cytoplasmic tail transitions from a mixture of extended oligomers to a compact dimer (Cai *et al*., 2004; Celic *et al*., 2012). In this way, the EF-hand is thought to be responsible for sensing Ca^{2+} concentrations that control the activity of the channel so that it opens and closes within the physiological range of ~100 nM to 10 µM Ca^{2+} (Kuo *et al*., 2014). Ca^{2+} concentrations regulate whether the channel is in the open configuration following a bell-shaped curve. When Ca^{2+} levels are low, the channel senses an increase in Ca^{2+} concentration which results in an increased probability that the channel will be open and as the Ca^{2+} concentration further increases, the channel open probability is subsequently reduced (Cai *et al*., 2004). Phosphorylation at Ser^{812} is also important for Ca^{2+}-stimulated activation and the open probability of the channel (Cai *et al*., 2004), while a hydrophobic residue in the distal part of the pore, L677, is thought to prevent ion permeation by forming a hydrophobic gate which mediates pore closure by forming a hydrophobic barrier (Zheng *et al*., 2018).

As well as being able to function as a cation channel alone (González-Perrett *et al*., 2001), PC2 function is also regulated by complexing with polycystin-1 (PC1), a large mechanosensitive receptor comprising 11 TMD and a large cytoplasmic C-terminal (Hughes *et al*., 1995; Oatley *et al*., 2012). PC1 and PC2 interact through coiled coil domains located at the C-terminus of both proteins (Qian *et al*., 1997) and this interaction is

important for channel localisation and function. PC1 and PC2 can also interact through their extracellular loops - the loop between TM1 and TM2 of PC2 interacts with the loop between TM6 and TM7 of PC1, and is involved in trafficking and function of the complexes (Salehi-Najafabadi *et al*., 2017). PC1 responds to fluid stress in the primary cilium by inducing Ca^{2+} influx into the cytoplasm through PC2 to control Ca^{2+}-regulated signalling processes (Hanaoka *et al*., 2000)**.** PC2 activity is also regulated by interactions with other proteins including actin bundling proteins (Cantero Mdel and Cantiello *et al*., 2015), and other intracellular Ca^{2+} channels such as the ryanodine receptor of the SR (Anyatonwu *et al*., 2007), InsP3R of the ER (Li *et al*., 2005; Sammels *et al*., 2010), and also other TRP channels (Brill and Ehrlich, 2020).

The *Dictyostelium* PC2 homologue, Ddpolycystin (dictyBase gene ID: DDB_G0272999), shares 46% protein similarity to the human homologue, is predicted to have 6 TMD, including a conserved pore region between TM5 and TM6, and a conserved C-terminal coiled-coil domain. Ddpolycystin lacks the EF-hand motif and ER retention signal seen in mammalian PC2 (Lima *et al*., 2014). Flag-tagged Ddpolycystin localized the protein primarily to the plasma membrane where it colocalised with the marker H-36, and some colocalization was observed with recycling and early endocytic compartments (Lima *et al*., 2014), however ER localisation has not been assessed. The role of Ddpolycystin in *Dictyostelium* remains ambiguous. Ddpolycystin KO strains are defective in purinergic cytosolic Ca^{2+} influx in response to ATP and ADP (Traynor and Kay, 2017) and Ca^{2+}-induced lysosomal exocytosis (Lima *et al*., 2014). These results hint at Ddpolycystin's involvement in Ca^{2+} signalling. Studies have also provided conflicting results for some phenotypes in Ddpolycystin KO cells. Lima *et al*. (2014) reported defective rheotaxis in KO cells and Waheed *et al*. (2014) reported slower axenic growth, while a recent study found no defect in either phenotype (Traynor and Kay, 2017) and Artemenko *et al*. (2016) reported no effect to responses in mechanical stimulation in Ddpolycystin null cells. Obviously further studies will need to be conducted to clarify the role of Ddpolycystin in Ca^{2+} signalling and its mode of action. Ddpolycystin might be gated by the putative PC1 homologue encoded in the *Dictyostelium* genome (dictyBase gene ID: DDB_G0289409) and could also potentially interact with IplA to contribute to Ca^{2+} signalling events analogously to the PC2 InsP3R receptor interaction reported in mammalian cells (Li *et al*., 2005; Sammels *et al*., 2010). Ddpolycystin is discussed further in chapter 3.

1.1.4.2 Transient receptor potential mucolipin 1-3 (TRPML1-3)

In *Dictyostelium,* a single homologue of the mammalian TRPML1 protein is encoded in the genome, Ddmucolipin (dictyBase gene ID DDB_G0291275) (Wilczynska *et al*., 2005). Human TRPML1 is a member of the TRP superfamily of ion channels and is one of three human TRPMLs (TRPML1-3 also called MCOLN1-3). TRPMLs are non-selective cation channels that are predicted to have six TMDs and cytosolic amino and carboxyl-terminus regions, and a pore region between TM5-TM6 (Grimm *et al*., 2007; Kim *et al*., 2010; Grimm *et al*., 2012). TRPMLs are localised to the membranes of components of the endocytic pathway, with TRPML2 and TRPML3 also localized to the plasma membrane (Kim *et al*., 2007; Dong *et al*., 2010). The cellular functions of the TRPMLs are associated with trafficking and sorting of membranes along the endocytic pathway (Cheng *et al*., 2010; Chen *et al.*, 2017; Plesch *et al*., 2018). TRPML1 is found in the late endosomal (LE) and lysosomal membranes and therefore is associated with trafficking in the late endocytic pathway including lysosome biogenesis and exocytosis (Chen *et al*., 1998). TRPML-mediated Ca^{2+} release is involved in Ca^{2+} dependent fusion/fission events of membranes along the endocytic pathway (LaPlante *et al*., 2004), the importance of Ca^{2+} for such events being well established (Luzio *et al*., 2007; Brailoiu and Brailoiu, 2016).

TRPML1 has been found to be involved in autophagy (Curcio-Morelli *et al*., 2010), lysosomal iron release (Dong *et al*., 2008), late endosome and lysosome pH regulation (Soyombo *et al*., 2006) and zinc homeostasis (Eichelsdoerfer *et al.,* 2010). Mutations in TRPML1 cause the neurodegenerative lysosomal disease Mucolipidosis Type IV (MLIV) (Sun *et al*., 2000) and the channel has also been associated with other neurodegenerative diseases including Alzheimer's, Parkinson's disease, Amyotrophic lateral sclerosis and Niemann-Pick diseases (Santoni *et al*., 2020). Mitochondrial dysfunction is associated with MLIV, and it is thought that the defective autophagy of mitochondria due to impaired lysosomal function leads to accumulation of degenerate mitochondria (Jennings *et al*., 2006).

The *Dictyostelium* mucolipin homologue, Ddmucolipin, shares homology to all three human TRPMLs. TRPMLs share conserved region of similarity between TM3 and TM6 (pos. 385–541) and protein alignments show that Ddmucolipin is 55% similar to the human protein in this region. Like its human homologues, Ddmucolipin is predicted to have six

TM domains, a large extracellular loop between TMD1 and TMD2, and a conserved pore region (pos. 498–511) (Lima *et al*., 2012). However, unlike the human proteins, Ddmucolipin contains a predicted C-terminal Ca^{2+}-binding EF-hand (pos. 614–626) (Wilczynska *et al*., 2005). Ddmucolipin has been localised to endosomal compartments rich in the endosomal marker p80, predominately to post lysosomes (Lima *et al*., 2012). In DH1-10 *Dictyostelium* cells, KO of Ddmucolipin reduces Ca^{2+} concentrations in secretory post-lysosomes, measured using dextran coupled fluorophores, and increases lysosomal exocytosis. This study also suggests that Ddmucolipin contributes to Ca^{2+} homeostasis because KO cells grew two times faster than wild type in Ca^{2+}-depleted medium. It was hypothesized that Ddmucolipin functions to channel Ca^{2+} into the lumen of the lysosomes during high local Ca^{2+} spikes helping to restrict vesicle fusion with the plasma membrane (Lima *et al*., 2012). While these results do indicate Ddmucolipin plays a role in both the endocytic cycle and Ca^{2+} signalling, more work will need to be conducted to further elucidate the cellular function of Ddmucolipin. TRPMLs are discussed in further detail in chapter 4.

1.1.4.3 Inositol 1,4,5-triphosphate receptor-like protein - IplA

The *Dictyostelium* inositol 1,4,5-triphosphate receptor like protein, IplA (dcityBase gene ID: DDB_G0292564), is a putative Ca^{2+} permeable, integral membrane channel that is a homologue of the inositol trisphosphate receptors (InsP3Rs) of higher eukaryotes (Traynor *et al*., 2000). InsP3Rs are homotetrameric Ca^{2+} channels that function in the membrane of the ER, vesicles and plasma membrane (Taylor *et al.,* 1999). InsP3R function is regulated by both Ca^{2+}, which regulates the steady state channel open probability (P_o) in a Ca^{2+} concentration dependent manner, and the second messenger InsP3, which binds at the N-terminal InsP3 binding domain to initiate Ca^{2+} flux (Foskett *et al*., 2007). Together, these two second messengers regulate Ca^{2+} homeostasis and signalling by releasing ER-stored Ca^{2+} into the cytosol. Ca^{2+} release from the ER can amplify signals from the plasma membrane through CICR signalling. Moreover, close association between the ER InsP3Rs and the plasma membrane activates SOCs and aids CCE (Putney, 1986; Putney, 1997; Lam and Galione, 2013). Importantly, the cellular and subcellular distribution of InsP3Rs also shapes the associated Ca^{2+} signals and the functional after effects of those signals, either locally or globally. For example, Ca^{2+} signalling between the ER and mitochondria is facilitated by connected microdomains called mitochondrially associated ER-membranes

(MAMs) that allow release of ER Ca^{2+} via InsP3Rs to increase the Ca^{2+} concentration at the mitochondrial membrane above cytosolic levels (Rizzuto *et al*., 1998; Marchi *et al*., 2017). As a result of this network of Ca^{2+} signals, InsP3-mediated Ca^{2+} release increases mitochondrial Ca^{2+} concentrations thus shapes mitochondrial Ca^{2+} signalling (Rizzuto *et al*., 1993; Missiroli *et al*., 2017).

The *Dictyostelium* IplA protein is predicted to be 3177 amino acids and contains a large hydrophilic N-terminal domain, multiple (6) TMDs and a small C-terminal domain. The protein shares 12% identity to the human Type 1 InsP3Rs and 14% identity to the *C. elegans* protein and retains two of 10 conserved basic amino acids for InsP3 binding in the N-terminus (Traynor *et al*., 2000). It also has a predicted calmodulin-binding helical peptide IQ motif at amino acids 148–167, consistent with regulation by Ca^{2+} (Wilczynska *et al*., 2005). IplA has been localised primarily to cytoplasmic vesicular membranes with some expression at the plasma membrane in an *IplA*$^{-}$*/IplA*$^{+}$-GFP cell line (Lusche *et al*., 2012). The protein's role at the cell surface involves extracellular Ca^{2+} binding, as *IplA*$^{-}$ cell lines bind 61-73% less $^{45}Ca^{2+}$ than control cells (Lusche *et al*., 2012), and in accordance with a role in intracellular Ca^{2+} homeostasis, *IplA*$^{-}$ mutants display lower basal intracellular Ca^{2+} concentrations than wild type cells (Schaloske *et al*., 2005). IplA function has been implicated in a number of cellular processes that are discussed in section (1.2).

1.1.4.4 Calnexin and calreticulin – Ca^{2+} binding proteins of the ER

Ca^{2+} release from the ER is modulated by the amount of free Ca^{2+} available within the lumen which is critical for the allosteric activation of the InsP3 receptor. Total luminal Ca^{2+} concentration estimated to be approximately 2 mM, and free Ca^{2+} concentration can vary dramatically from ~ 100-700 µM when full to ~ 10-50 µM after the ER channels have opened (Meldolesi and Pozzan, 1998; Yu and Hinkle, 2000; Foskett *et al*., 2007). Free Ca^{2+} is controlled by resident Ca^{2+}-binding proteins (CBPs) including BiP/Grp78 (Lièvremont *et al*., 1997), protein disulphide isomerase (Luz and Lennarz, 1996), glucose-regulated protein 94, calnexin and calreticulin (Coe and Michalak, 2009). *Dictyostelium* expresses homologues of both calnexin and calreticulin and is the only known microorganism that expresses both proteins. Ddcalnexin is encoded by *cnxA* (dictyBase accession number: DDB_G0271144) and Ddcalreticulin by *crtA* (dictyBase accession number: DDB_G0283539). While both reside in the ER, calnexin is a class 1 transmembrane protein

as it spans the membrane only once, with the N-terminus in the lumen of the ER and a cytosolic C-terminus. Calreticulin resides in the lumen of the ER and contains a C-terminal K(H)DEL signal for retention (Muller-Taubenberger *et al*., 2001). These proteins have been intensively studied in other organisms and are known for their function in protein chaperoning and folding of Asn-linked glycoproteins in the ER which are Ca^{2+} sensitive processes (Williams, 2006), however their Ca^{2+} regulatory activity is also a major function.

Calreticulin acts as a major CBP, with two Ca^{2+} binding sites, one being a high affinity (K_d =1.6 μM), low capacity site (~ 1 mol of calcium/mol of protein) in the central 134 residues, and the other in the C-terminus having high capacity (~20 mol of calcium/mol of protein) and low affinity for Ca^{2+} (K_d ~ 2 mM) (Baksh and Michalak, 1991). This enables calreticulin to bind approximately 50% of the luminal Ca^{2+} (Coe and Michalak, 2009). The C-terminal Ca^{2+} binding domain (C-domain) is highly negatively charged encompassed by residues 291-400 (Smith and Koch, 1989). It is vital for calreticulin's Ca^{2+}-binding abilities and appears not to be involved in its chaperone activity (Conte *et al*., 2007).

Calnexin not only binds Ca^{2+}, but also acts as a Ca^{2+} sensor. The C-terminal region undergoes structural changes when faced with different Ca^{2+} concentrations, which is thought to be a consequence of the distribution of charged residues along the domain. In high Ca^{2+} concentrations the C-terminus binds Ca^{2+} which brings certain acidic residues near each other and adopts a more ridged, compact structure. When Ca^{2+} concentrations drop, the C-terminal region becomes disordered. This feature seems to be important in calreticulin's function when faced with the large Ca^{2+} fluctuations of the ER (Villamil Giraldo *et al*., 2010). Evidence for calreticulin's involvement in Ca^{2+} signalling and homeostasis comes from studies in mouse embryonic fibroblasts and activated T-cells lacking calreticulin. In these cell types, the ER Ca^{2+} storage capacity and agonist-induced Ca^{2+} release are reduced (Mesaeli *et al*., 1999; Nakamura *et al*., 2001).

Calnexin is thought to have two binding sites for Ca^{2+}, one in the globular region of the luminal N-terminal, which is thought to bind a single Ca^{2+} ion (Schrag *et al*., 2001) and another potential binding site in the highly charged C-terminal cytoplasmic tail (Tjoelker *et al*., 1994). While calnexin does not have the high Ca^{2+}-binding capacity of calreticulin, it has been shown to play a role in Ca^{2+} buffering in mammalian cells (Wada *et al*., 1991)

and *Drosophila* (Rosenbaum *et al*., 2006). Aside from Ca^{2+} buffering, calnexin might help to modulate ER Ca^{2+} levels by interactions with SERCA to influence luminal Ca^{2+} uptake. Phosphorylation at the calnexin C-terminal serine residue (S562) was observed after InsP3 -induced Ca^{2+} release and this regulated calnexin's interaction with SERCA2b. In this manner, calnexin can influence cytosolic Ca^{2+} oscillations and signalling by regulating uptake into the ER (Roderick *et al*., 2000). Modulation of SERCA by calreticulin has also been observed (Camacho and Lechleiter, 1995; John *et al*., 1998; Baker *et al*., 2002), which demonstrates complexity to the fine control these proteins have over ER and cytosolic Ca^{2+}.

In *Dictyostelium*, GFP-tagged versions of Ddcalnexin and Ddcalreticulin do localise to the ER as would be predicted (Muller-Taubenberger *et al*., 2001). Evidence for the proteins functioning as ER CBPs has been demonstrated in mutants lacking either or both calnexin and calreticulin. These mutants display larger influx of Ca^{2+} into the cytosol after chemoattractant stimulation presumably due to higher intraluminal free [Ca^{2+}] resulting from the reduced Ca^{2+} buffering ability of the ER. This provides evidence for the ER's contribution to this response, and also the ability of Ddcalnexin and Ddcalreticulin to bind ER Ca^{2+} (Wilczynska *et al*., 2005; Fisher and Wilczynska, 2006). Ddcalnexin and Ddcalreticulin are also essential for nutrient uptake by phagocytosis, specifically for the formation of the phagocytic cup after particle adhesion. Whether the proteins act directly or indirectly is unclear, however the observation of close associations between the ER membrane and the forming phagocytic cup suggests that local Ca^{2+} signalling may be involved in the process (Muller-Taubenberger *et al*., 2001).

1.1.4.5 Signalling at the mitochondria: the MCU and NCLX

The mitochondria are a major Ca^{2+} signalling hub crucial for regulation of cell death pathways through activating mitochondrial permeability transition (Lemasters *et al*., 2009), bioenergetics (Glancy and Balaban, 2012; Rossi *et al*., 2019) and shaping intracellular Ca^{2+} signals (Rizzuto, 2000). The importance of these organelles in Ca^{2+} signalling was first highlighted by Rizzuto *et al*. (1992) who measured mitochondrial Ca^{2+} transients in mammalian cells which responded to agonist-stimulated changes in cytosolic Ca^{2+} concentrations. This implied a contribution of the mitochondria to cytosolic Ca^{2+} signalling events. Since then, a plethora of studies have investigated the organelle's

involvement in Ca^{2+} signalling (Santo-Domingo *et al*., 2015; Bravo-Sagua *et al*., 2017) and provided evidence for its important role in mediating Ca^{2+} crosstalk with the ER and plasma membrane in microdomains where the mitochondrial membranes are closely juxtaposed with these other membranes (Rizzuto *et al*., 2012; Carreras-Sureda *et al*., 2018). Evidence for a mitochondrial Ca^{2+} pool in *Dictyostelium* came first from Europe-Finner and Newell (1986) who observed a Ca^{2+} pool sensitive to oligomycin and dinitrophenol which are inhibitors of mitochondrial complexes and cause release of Ca^{2+} from mitochondrial stores. This mitochondrial Ca^{2+} pool was also observed in permeabilised *Dictyostelium* cells which, when pulsed with high concentrations of Ca^{2+}, took up the Ca^{2+} in a mitochondrial membrane-dependent and mitochondrial inhibitor-sensitive manner (Kovács-Bogdán *et al*., 2014). Mitochondrial Ca^{2+} signalling in *Dictyostelium* has had little attention.

Ca^{2+} levels must be maintained within both the intermembrane space and the matrix for proper biological function and to facilitate signalling. Ca^{2+} movement across the outer mitochondrial membrane (OMM) is thought to be through the voltage-dependent anion channel (VDAC). This multifunctional channel mediates the transfer of metabolites between the mitochondria and the cytosol (Shoshan-Barmatz and Ben-Hail, 2012). The open state of this channel is mitochondrial membrane potential-dependent, with the channel showing high conductance to molecules up to ~1500 Da at low potential of around −20 to +20 mV (Shoshan-Barmatz *et al*., 2010). There is some evidence, however that Ca^{2+} can transverse the OMM when VDAC is in its closed configuration (Tan and Colombini, 2007) and the exact mechanisms of Ca^{2+} flow in and out of the OMM are still not clear. The *Dictyostelium* VDAC, also known as Porin, (DDB_G0271848) has been characterized, however its Ca^{2+} channeling properties have not been assessed (Troll *et al*., 1992).

Mitochondria maintain a steep Ca^{2+} gradient across their inner mitochondrial membrane (IMM) membrane, and precisely control transport of various ions across the IMM to maintain the high membrane potential which is necessary to facilitate ATP production. Ca^{2+} movement across the IMM is controlled by the mitochondrial calcium uniporter (MCU) and $Na^{+}/Ca^{2+}/Li^{+}$ exchangers (NCLX).

1.1.4.5.1 Mitochondrial calcium uniporter (MCU)

The MCU of the IMM is a high capacity Ca^{2+} uptake transporter (Gunter and Gunter, 1994; Bernardi, 1999; De Stefani, 2011; Marchi and Pinton, 2014), which has an extremely high affinity for Ca^{2+} (dissociation constant ≤2 nM). There are an estimated 10-40 MCU per μm^2 of IMM (Kirichok *et al*., 2004). The human MCU channel (HsMCU) complexes with the essential MCU regulator (EMRE) which, as the name suggests, has been found to be essential for MCU function (Sancak *et al*., 2013) and with its regulatory proteins MICU1 and 2. The latter proteins each contain a pair of EF-hand Ca^{2+}-binding motifs (Perocchi, 2010; Mallilankaraman *et al.,* 2012; Csordás *et al*., 2013; Payne *et al*., 2017) and are able to sense cytosolic Ca^{2+} concentrations and regulate Ca^{2+} uptake when faced with both low and high cytosolic Ca^{2+} levels (Paillard *et al*., 2017; Payne *et al*., 2017). Once MCU is in the open configuration, Ca^{2+} is taken up into the mitochondria driven by the IMMs negative membrane potential. Ca^{2+} sensing by MICU1 is important to prevent uncontrolled Ca^{2+} uptake as demonstrated in MICU1 null cells which experience excessive MCU-mediated Ca^{2+} uptake (Mallilankaraman *et al.,* 2012). This is particularly important during ER Ca^{2+} release at MAMs which can quickly increase the local Ca^{2+} concentrations to ~ 10µM (Berridge *et al*., 2003).

The *Dictyostelium* DdMCU (dictyBase accession number: DDB_G0286429) has been cloned and expressed in yeast, which lack a MCU, to develop an *in vivo* reconstitution system for study. DdMCU shares close sequence and structural similarity to HsMCU, including a mitochondrial targeting sequence at the N-terminal, and two TMDs on either side of the intermembrane 'DIME motif' which is crucial for Ca^{2+} transport. Recently the crystal structure of the DdMCU n-terminal domain was determined and showed a helix-rich fold which is different from the n-terminal structure of the HsMCU which forms β-grasp-like structures. This reveals divergence of the MCU n-terminal domains (Yuan *et al*., 2020). When expressed in HEK-293T-derived cell lines in which HsMCU has been knocked out, DdMCU indeed localises to the IMM. DdMCU expression rescued Ca^{2+} uptake in these KO cells with almost identical kinetics to the HsMCU rescue. DdMCU, unlike HsMCU, is able to channel Ca^{2+} independently of EMRE, suggesting that in *Dictyostelium*, DdMCU is the single genetic element necessary for function (Kovács-Bogdán *et al*., 2014). In *Dictyostelium* cells, mitochondrial membrane potential (MMP)-dependent Ca^{2+} uptake in permeabilised cells suggests that the mitochondria possessed uniporter activity. This Ca^{2+}

uptake was sensitive to the MMP uncoupler carbonyl cyanide 3-chlorophenylhydrazone (CCCP) and uniporter inhibitors ruthenium red and Ru360 (Kovács-Bogdán *et al*., 2014). Further studies of DdMCU in *Dictyostelium* cells will reveal the protein's endogenous role in Ca^{2+} signalling.

1.1.4.5.2 $Na^+/Ca^{2+}/Li^+$ exchangers (NCLX)

Release of Ca^{2+} from the mitochondria is facilitated by Na^+ or H^+ exchangers which utilize an electrochemical gradient to extrude Ca^{2+}. H^+/Ca^{2+} exchange activity is primarily found in mitochondria of non-excitable cells, while Na^+/Ca^{2+} exchanger activity, although active in most cell types, is particularly active in excitable cells. The mitochondrial H^+/Ca^{2+} Leucine zipper-EF-hand-containing transmembrane protein1 (Letm1) has been identified, but not well studied (De Marchi *et al*., 2014; Shao *et al*., 2016). Evidence for a Na^+/ Ca^{2+} exchange mechanism was first identified in mitochondria from cardiac cells by Carafoli *et al*. (1974), however, only fairly recently the molecular identity of the exchanger was discovered to be a $Na^+/Ca^{2+}/Li^+$ exchanger (NCLX). Genetic studies implicated NCLX in mitochondrial Ca^{2+} release. Mitochondrial Na^+-dependent Ca^{2+} efflux was measured using the mitochondria-targeted Ca^{2+}-sensing protein Pericam, which is a fusion between a circular form of green fluorescent protein and CaM (Nagai *et al*., 2001). Efflux was increased in HEK-293 NCLX overexpressing cells, reduced in siRNA NCLX knockdown (KD) cells and blocked when a mutation in the catalytic site was introduced (Palty *et al*., 2010; Palty and Sekler, 2012). Since its identification, NCLX has been studied in various cell types, all supporting its role in mitochondrial Ca^{2+} release (Kim *et al.,* 2013; Parnis *et al.,* 2013; De Marchi *et al.,* 2014; Kim *et al*., 2016). An NCLX homologue has not yet been described in *Dictyostelium.*

1.1.4.6 Two pore channel (TPC)

The putative calcium channel two pore channel (DdTPC) (DDB_G0289105) is a *Dictyostelium* homologue (Wilczynska *et al*., 2005; Chang *et al*., 2020) of the mammalian TPC2, of the subfamily of the TPCs, TPC1-3. TPCs are eukaryotic iron-permeable channels structurally similar to voltage gated calcium channels and able to release Ca^{2+}, Na^+, H^+ and K^+ in response to stimuli including nicotinic acid adenine dinucleotide phosphate (NAADP), $PI(3,5)P_2$, leucine-rich repeat kinase 2 (LRRK2) and action potentials. They are inhibited

by high Mg^{2+} concentrations, Ca^{2+} and Na^{+} ion channel inhibitors, c-Jun N-terminal kinase (JNK) and p38 kinase, as well as mammalian target of rapamycin (mTOR) (Feijóo-Bandín *et al*., 2017). They are expressed in endolysosomal membranes, where they are vital for normal function including maintaining membrane potential, pH (Wang *et al*., 2012), and Ca^{2+} signalling (Brailoiu *et al*., 2009; Galione, 2015). TPC2 has also been visualised at the ER and nuclear envelope (Shuk-Kwan Lee *et al*., 2016) and TPC3 at the plasma membrane (Cang *et al*., 2014). TPCs have been implicated in an astounding array of biological functions (reviewed in Feijóo-Bandín *et al*., 2017). They are comprised of two covalently linked shaker-type homologous domains each with 6 TM domains and each containing a pore-forming loop between TM 5-6 (hence the name). TPC1 has been shown to be allosterically modulated by luminal and cytosolic Ca^{2+} at an unknown Ca^{2+} binding site (Lagostena *et al*., 2017), and Ca^{2+} release from TPCs can activate SOCE (López *et al*., 2012).

DdTPC is predicted to be located in the membranes of acidic Ca^{2+} stores, contain 12 TM domains as seen in other organisms, two EF-Ca^{2+} binding motif(s) which overlap and may be the same site (Wilczynska *et al*., 2005), also present in the *Arabidopsis* where one modulates calcium sensitivity and the other calcium gating by the channel (Schulze *et al*., 2011), but not the human channel (Lagostena *et al*., 2017). In *Dictyostelium* KO of DdTPC has shown that the protein has no involvement in mechanical stress responses (Lima *et al*., 2014), but is involved in growth, development and acidification of acidic vesicles (Chang *et al*., 2020). The role for DdTPC in calcium signalling is unclear, differentiated DdTPC null cells maintain their cAMP-mediated Ca^{2+} responses and the magnitude was comparable to that in wild type AX2 cells, however the responses are slightly delayed, suggesting a possible role for the protein in 'priming' the calcium release from the other stores. Calcium uptake into preparations of *Dictyostelium* vesicles was increased in vesicles from DdTPC KO cells compared to wild type. This suggests that DdTPC could act as a Ca^{2+} leak channel, however, KO cells had increased expression of *patA* mRNA which encodes PAT1, a Ca^{2+} ATPase responsible for refilling acidic Ca^{2+} stores, which could also explain the findings (Chang *et al*., 2020). Further work is required to understand the role of DdTPC in calcium regulation.

1.1.4.7 P2X receptors, ATP gated Ca^{2+} channels of the contractile vacuole

P2X receptors are one member of the superfamily of ligand gated ion channels. They are ATP-gated membrane channels with a unique trimeric architecture and permeability to Na^+, K^+ and Ca^{2+} (Habermacher *et al*., 2016). Channel opening occurs within milliseconds of ATP binding, which allows fast transfer of ions, but may become desensitized due to prolonged exposure to ATP, in which case ion flux is terminated before ATP dissociates from the channel and it reverts to the closed configuration (Habermacher *et al*., 2016). These receptors are found in vertebrates and lower eukaryotes and are expressed in diverse tissues and subcellular locations. In mammals, 7 members (P2X1-7) of this family have been identified and are involved in processes such as initiation of action potentials in primary nerve cells, excitatory junction potentials of smooth muscle cells, and release of pro-inflammatory cytokines from immune cells during inflammation (North, 2016).

The *Dictyostelium* genome encodes 5 putative P2X receptors, *P2xA-E* (Kreppel *et al*., 2004). The observation that extracellular ATP and ADP invokes Gβ- and *iplA*-independent, rapid and instant influx of extracellular Ca^{2+} (Ludlow *et al*., 2008) prompted investigation into the involvement of P2X receptors in this response. The *Dictyostelium* P2XA receptor (*Dd*P2XA) shares the most homology to vertebrate P2X receptors and when expressed in human embryonic kidney HEK293 cells, *Dd*P2XA indeed localises to plasma membrane. Ion currents were measured in response to 30-100uM ATP, and the channel was found to be freely permeable to Ca^{2+} ions (Fountain *et al*., 2007). However, when expressed in *Dictyostelium* AX4 cells, a GFP-tagged protein (*Dd*P2XA-GFP) actually localised to the membrane of the contractile vacuole (CV) where it plays a role in osmoregulation (Fountain *et al*., 2007). A later study found that all five *Dd*P2X receptors are intracellularly localised in the membrane of the CV, and a quintuplet KO of all five receptors in AX2 did not abolish the extracellular Ca^{2+} response to either ATP or ADP (Ludlow *et al*., 2009). These findings demonstrated a role for *Dd*P2X receptors in intracellular Ca^{2+} signalling rather than extracellular purinergic signalling. Proteinase-K digestion assays revealed the orientation of the ATP binding domain toward the lumen of the CV and N- and C- terminus in the cytoplasm (Ludlow *et al*., 2009), as was later confirmed by Sivaramakrishnan and Fountain (2013). Therefore, *Dd*P2X receptors have a role in detecting ATP signals from within the CV and modulating Ca^{2+} release from this organelle which is a major Ca^{2+} store (Sivaramakrishnan and Fountain, 2012).

Activation of *Dd*P2X receptors from within the CV lumen requires a source of ATP. HLPC analysis of vacuolar nucleotides showed only insignificant amounts of AMP and ADP, therefor luminal synthesis is not possible. Since ATP cannot passively diffuse across organellar membrane due to its strong anionic properties, the presence of an ATP transportation mechanism was investigated (Sivaramakrishnan and Fountain, 2012). Cytoplasmic levels of ATP are ~4mM, therefore isolated vacuoles were exposed to the same conditions to reveal ATP translocation across the membrane at a rate of 1.8 ± 0.4 nmol/mg/min. Addition of ATP to isolated vacuoles also initiated Ca^{2+} release which could not be mimicked by β-γ-imido-ATP, ADP, AMP or GTP. This Ca^{2+} release was reduced by 72% in *Dd*P2XA null AX4 cells and completely abolished in cells lacking all five P2X receptors, suggesting some functional redundancy amongst the *Dd*P2X receptors. The different sensitivities of the *Dd*P2XA, B and E receptors to ATP (Ludlow *et al*., 2009), suggests that expression of the various subtypes enable the CV to fine tune ATP signals and subsequently Ca^{2+} signalling (Sivaramakrishnan and Fountain, 2012).

The importance of Ca^{2+} release from the CV is still not well understood, however it is thought to play a role in osmotic regulation (Sivaramakrishnan and Fountain, 2012). The CV cycle is regulated by a family of Rab proteins that facilitate the maturation of the vacuole during hypo-osmotic shock and subsequent tethering and fusion with the plasma membrane and discharge of luminal contents (Du *et al*., 2008). *Dd*P2x4 null cells, derived from the parental strain AX4, are defective in osmoregulation and lack the regulated cell volume decrease (RVD) under hypotonic conditions (Fountain *et al*., 2007; Baines *et al*., 2013). In these strains the CV cycle was prolonged and fewer fusion events were observed (Fountain *et al*., 2007). Since Ca^{2+} is a known regulator of vesicle fusion, and CV fusion with the plasma membrane is dependent on down regulation of Rab11a in a Ca^{2+}-dependent event, Parkinson *et al*. (2014) investigated the involvement of *Dd*P2XA in the CV cycle. In wild type cells they measured an almost two-fold increase in Ca^{2+} concentrations around the CV just prior to fusion, increasing the localised Ca^{2+} concentration to 100-200nM, but this local calcium spike was absent in *Dd*P2XA (K67A/K289A) inactive mutants. This lack of Ca^{2+} release from the CV of *Dd*P2XA (K67A/K289A) deficient mutants was coupled with impaired ability of the CV to fuse with the plasma membrane.

Some confusion still pertains over the role of *Dd*P2X receptors in osmoregulation as *Dd*P2XA-E null cells and *Dd*P2XA null cells derived from the parental AX2 strain are still capable of RVD (Ludlow *et al*., 2009; Sivaramakrishnan and Fountain, 2013). While the reason for these differences in phenotypic observations between AX2- and AX4-derived strains are still unclear, they may be attributable to differences in ATP-stimulated Ca^{2+} release from CVs from AX2 and AX4 cells, as the magnitude of Ca^{2+} release from the AX2 CV is approximately 2-fold less than from AX4 vacuoles (Sivaramakrishnan and Fountain, 2013).

The connection between Ca^{2+} signalling and the CV will undoubtedly be illuminated in the future. The presence of not only *Dd*P2X Ca^{2+} channels, but also a PMCA-type Ca^{2+}-ATPase (PAT1) (Moniakis *et al*., 1999), the Ca^{2+} binding protein CaM (Zhu and Clarke, 1992) and a proton pump which creates a proton gradient to facilitate Ca^{2+}-transport (Clarke *et al*., 2002), provides strong evidence for this organelle's involvement in Ca^{2+} signalling.

1.1.4.8. Calcium Pumps and exchangers

Once Ca^{2+} has activated its downstream targets, its function has been carried out and it thus needs to be rapidly removed from the cytoplasm to restore basal levels. Maintenance of basal cytosolic Ca^{2+} levels and extrusion out of the cytosol after Ca^{2+} fluxes is regulated by cation exchangers and Ca^{2+}-ATPases.

1.1.4.8.1 Cation exchangers

Cation exchangers exchange Ca^{2+} ions for other ions such as $Na^+/H^+/K^+$ ions across cellular membranes in an electrogenic manner. The Na^+/Ca^{2+} exchanger (NCX) is the major Ca^{2+} PM efflux mechanism which has low Ca^{2+} binding affinity but high Ca^{2+} conductance. It is therefore suited to quickly clearing the cytosolic Ca^{2+} after an influx. The protein has been estimated to conduct Ca^{2+} at a maximum turnover rate of 5000 per second in cardiac cells, exchanging one Ca^{2+} for three Na^+ per turnover (Egger and Niggli, 1999). NCX isoforms function at the plasma membrane, and also intracellular membranes such as those of the nucleus and mitochondria (Brini and Carafoli, 2011). The movement of ions is entirely dependent on the electrochemical gradient and is fully reversible. These transporters contain a large cytosolic loop with two Ca^{2+} binding domains (CBD1 and CBD2) which

activate the exchanger upon Ca^{2+} binding (Hilge *et al*., 2006; reviewed in Verkhratsky *et al*., 2018). Ca^{2+}/H^{+} exchangers (CAX) function in the membranes of acidified compartments, where uptake of Ca^{2+} is driven by the steep proton gradient across the vacuolar membrane (Melchionda *et al*., 2016). In *Dictyostelium*, the putative $Na^{+}/H^{+}/Ca^{2+}$ exchanger Cax1 has been predicted (DDB_G0279301) (Shigaki *et al*., 2006) and although not experimentally studied, one might speculate that this exchanger plays a vital role in Ca^{2+} homeostasis and signalling.

1.1.4.8.2 P-type Ca^{2+} ATPases *SERCA/PMCA*

Eukaryotic Ca^{2+}-translocating ATP-ases belong to a large family of P-type cation translocases which maintain basal Ca^{2+} levels and terminate Ca^{2+} signals by excreting Ca^{2+} out of the cytosol after influx events. They are classified according to their subcellular localisation and include plasma membrane Ca^{2+} ATPases (PMCA), secretory pathway Ca^{2+} ATPases (SPCA) and those located in the ER/SR membranes, the sarco(endo)plasmic reticulum Ca^{2+} ATP-ases (SERCA) which refill internal Ca^{2+} stores. These enzymatic pumps couple the energy provided by ATP hydrolysis to power uphill transport of cations across the membrane. As opposed to the high Ca^{2+} conductance of CAX, Ca^{2+}- ATPases have a high Ca^{2+} binding affinity, but low conductance rate. This means that the proteins are particularly suited to maintaining the low basal cytosolic Ca^{2+} levels. These proteins have been extensively studied (Brini *et al*., 2012; Stammers *et al*., 2015; Brini *et al*., 2017), and will be discussed further in chapter five.

The *Dictyostelium* genome encodes three P-type Ca^{2+}-ATPases, PAT1, which localizes to the membrane of the CV (Moniakis *et al*., 1995; Moniakis *et al*., 1999) and two homologues of PMCA, dictyBase accession numbers DDB_G0284605 and DDB_G0289473 (Wilczynska *et al*., 2005). The latter two proteins both contain predicted calmodulin-binding helical peptide IQ motifs (Wilczynska *et al*., 2005). Early experiments measuring ATP-dependent Ca^{2+} release over the plasma membrane at a rate of roughly 5×10^{6} ions/cell/min, provided evidence for PMCA activity at this location (Böhme *et al*., 1987). Subsequently an ATP/Mg^{2+}-dependent, high-affinity Ca^{2+} pump at the plasma membrane was described (Milne and Coukell, 1988). The *Dictyostelium* PMCA homologues are yet to be genetically studied, however given the evidence that Ca^{2+} can be released from the ER during chemotactic Ca^{2+} responses (Wilczynska *et al*., 2005), one can assume that an active SERCA-like pump also functions at this location and is responsible for refilling the

ER Ca^{2+} store after Ca^{2+} release. The other intracellular P-type Ca^{2+}-ATPase that has been studied is PAT1 of the CV.

1.1.4.8.3 PAT1, a high affinity Ca^{2+}-ATPase in the contractile vacuole

In order to regulate Ca^{2+} concentrations within the lumen of the CV, Ca^{2+} must be sequestered back into the lumen after having been released via Ca^{2+} channels such as the P2X receptors. Due to the concentration differential across the CV membrane, Ca^{2+} ions must be actively transported across the membrane at the expense of ATP. Indeed, an ATP-dependent, high affinity Ca^{2+}- transport system associated with intracellular vesicles, was identified by Milne and Coukell (1989) who measured $^{45}Ca^{2+}$-uptake in isolated cell fractions. Similar findings were reported by Rooney and Gross (1992) who reported $^{45}Ca^{2+}$ uptake into acidosomal cell fractions. Later, Moniakis *et al*. (1995) cloned cDNAs of the gene *patA*, which encodes a P-type Ca^{2+}-ATPase, PAT1 (dictyBase ID: DDB_G0277861). PAT1 contains ~46% amino acid identity with Ca^{2+} ATPases of the plasma membrane, and consistent with its role in Ca^{2+} regulation, harbors a calmodulin-binding helical peptide IQ motif (pos. 642-661) (Wilczynska *et al*., 2005). Indirect immunofluorescence microscopy revealed that PAT1 colocalizes with CaM in the CV membrane (Moniakis *et al*. 1995, Moniakis *et al*. 1999), providing strong evidence for the protein's function as a Ca^{2+} uptake pump in the vacuolar membrane.

Extracellular Ca^{2+} concentrations affect expression of PAT1. AX2 cells were adapted to growth in medium containing 80 mM $CaCl_2$ over 3-4 weeks, and northern blot analysis revealed that *patA* transcripts were increased ~10-fold in $CaCl_2$-grown cells compared to untreated cells, and this correlated with an overexpression of PAT1 (Moniakis *et al*. 1995). Later, to determine if this up regulation was a consequence of selection for PAT1 overexpressing strains over the weeks of culturing, or if it was in fact a consequence of high extracellular $CaCl_2$, the same experiment was conducted to assess the kinetics of this response. This revealed that within 3 hours of exposure to 80 mM $CaCl_2$ *patA* mRNA transcripts increased between 10-40 fold, which correlated with the upregulation of the PAT1 protein (Moniakis *et al*. 1999). Under conditions of high $CaCl_2$ PAT1 is highly enriched at the CV membrane, and also at the plasma membrane. This hints toward a role for PAT1 in maintaining basal Ca^{2+} levels during Ca^{2+} stress. This was tested in strains expressing *patA* antisense RNA to decrease protein expression. After 4 days of growth in

medium with and without 60 mM $CaCl_2$, antisense strains grown in the presence of $CaCl_2$ had reached a density of only 20% of cultures grown without $CaCl_2$ (Moniakis *et al*. 1999). The role for PAT1 in the CV is likely to both maintain luminal Ca^{2+} concentrations and also facilitate Ca^{2+} signalling events related to CV functioning such as osmoregulation. Evidence suggests that PAT1 also helps to maintain cellular Ca^{2+} levels during Ca^{2+} stress.

1.1.4.9 Calmodulin the universal calcium binding protein and signal mediator

Ca^{2+}-binding proteins (CBP) play roles in Ca^{2+} homeostasis, and in shaping and decoding Ca^{2+} signals by controlling intracellular free Ca^{2+} concentrations (Yáñez *et al*., 2012). While CBPs encompass a wide range of heterogeneous proteins, they all share the ability to bind Ca^{2+} on specific and varied domains, some acting as Ca^{2+} stores and others as receptors. *Dictyostelium* expresses a number of CBP throughout growth and development that have been found to be important for chemotactic signalling, development and differentiation. These include α-actinin (Witke *et al*., 1993), calfumirin (Abe and Maeda, 1995), calmodulin (CaM) and CaM-related proteins (Andre *et al*., 1996).

The highly conserved Ca^{2+}-binding protein, CaM, is present in eukaryotes, including *Dictyostelium* (Bazari and Clarke, 1981; Marshak *et al*., 1984), and is involved in many cellular processes. CaM mediates Ca^{2+} signalling by sensing and binding Ca^{2+} ions and then interacting with target proteins, via their CaM binding motif, to modulate their function (O'Day, 2003). The protein is composed of two globular domains, each of which contains two EF-hand Ca^{2+} binding motifs, and both domains are separated by a flexible linker. Ca^{2+} binding causes a conformational change in the protein which changes its affinity for target proteins. There are also some targets that bind CaM in its non-Ca^{2+} bound confirmation (Apo-CaM) (Zhang *et al*., 1995; Jurado *et al*., 1999). Target proteins interact with CaM via CaM binding motifs, of which there are three classes. Class I are Ca^{2+}-dependent motifs which are basic, amphipathic α-helical domains with conserved, hydrophobic residues (pos. 1-(5)-10, 1-(8)-14 or 1–16). Class II and III are IQ motifs, and IQ-like motifs respectively (Rhoads and Friedberg, 1997; Bähler and Rhoads, 2002). Generally, Ca^{2+}-independent binding to CaM-Apo occurs via IQ and IQ-like motifs (Yap *et al*., 2000) and targets can contain both Ca^{2+}-dependent and independent motifs (Nunomura *et al*., 2000). Hundreds of CaM target proteins have been identified (reviewed Tidow and Nissen,

2013), both with and without enzymatic function. They implicate CaM in a plethora of cell physiological roles including inflammation and immune response, muscle excitation-contraction, fertilization, cell proliferation, memory, metabolism and apoptosis (Tidow and Nissen, 2013).

The *Dictyostelium* calmodulin (DdCaM) encoded by *calA* was cloned by Lui *et al*. (1992), who reported constitutive mRNA expression through growth and development suggesting that it functions at all stages of the life cycle. DdCaM is similar to vertebrate CaM, containing the four EF-hand Ca^{2+}-binding motifs and has 88.7 % AA similarity to human CaM (O'Day, 2003). DdCaM is enriched in the membrane of the CV and is also present in the cytosol (Zhu and Clarke 1992). Around 60 potential DdCaM-binding proteins have been identified, both Ca^{2+}-dependent and -independent (Catalano and O'Day, 2008). Some have been characterized, such as the Ca^{2+}-CaM-dependent protein phosphatase, calcineurin (Dammann *et al*., 1996), and the myosins which are Ca^{2+}-independent CaM binding proteins (Kollmar, 2006), however most are yet to be studied experimentally.

Given the vast number of proteins regulated by DdCaM, it is not surprising that it has been implicated in numerous cellular processes including growth and development. During development, docking of the Ca^{2+}-dependent cell-cell adhesion molecule DdCAD-1, to the CV membrane prior to being transported to the plasma membrane, is Ca^{2+}-DdCaM dependent (Sriskanthadevan *et al*., 2013). Cytokinesis is blocked in DdCaM antisense mutants (Liu *et al*., 1992), and secretion of extracellular DdCaM localised to the slime sheath has also been identified to be present throughout development, where it plays a role in cell proliferation and cAMP-mediated chemotaxis (O'Day *et al*., 2012).

DdCaM has been pharmacologically implicated in Ca^{2+} signalling and cAMP oscillatory cycles. The CaM antagonist W-7 blocked approximately 50% of active vesicular $^{45}Ca^{2+}$ uptake after cAMP-induced influx (Gröner and Malchow, 1996). W-7 also caused vesicular Ca^{2+}-leakage, thought to be a result of inhibition of V-type H^+-ATPase activity in the acidic stores, as well as enhanced light scattering and cAMP oscillation (Malchow *et al*., 2004). In contrast to W-7, treatment of cells with the CaM agonist calmidazolium, induced release of Ca^{2+} from IP_3 sensitive and acidic intracellular stores and also influx across the plasma membrane (Schlatterer and Schaloske, 1996). Calmidazolium also delayed light

scattering oscillation and cAMP relay, indicating a link between intracellular Ca^{2+} and cAMP production (Malchow *et al*., 1996). The mechanism of intracellular Ca^{2+} release by CaM inhibition is unknown, but was not a consequence of inhibition of Ca^{2+} pumping because Ca^{2+} pump inhibitors did not invoke the same change (Schlatterer and Schaloske, 1996). The difference in cellular consequences after calmidazolium and W-7 treatment are likely to be explained by the differences in the drugs themselves, particularly, solubility, target specificity and duration of effect (Malchow *et al*., 2004), however these reports do implicate DdCaM in chemotactic and Ca^{2+} signalling.

1.2 The biological roles of calcium signalling in *Dictyostelium*

1.2.1 Growth, aggregation and differentiation

The *Dictyostelium* life cycle in the soil includes a single cell vegetative stage where they consume bacteria and other microorganisms by responding chemotactically to folic acid (discussed further in section 1.2.3) and other pterins excreted by the microorganisms (Pan *et al*., 1972, Pan *et al*., 1975). Vegetative cells are dividing by mitosis and the calcium binding protein CaM is necessary for efficient cytokinesis (Liu *et al*., 1992). The involvement of calcium in the growth phase is evident as there is a correlation between the stages of the cell cycle and cellular calcium levels (Jaiswal and Nanjundiah, 2003). When nutrient sources are depleted cells initiate a developmental program where cells differentiate into multicellular slug which can disperse cells to new areas of soil. After starvation, cells develop a receptor-mediated signalling system that initiates a developmental program. As cells begin to starve they signal that they are starving to other cells by excreting conditioned medium factor (CMF), a cell density sensing factor (Gomer *et al*., 1991; Jain *et al*., 1992; Yuen *et al*., 1995; Deery *et al*., 2002). Cells also begin to periodically release cAMP which both attracts and stimulates their neighbors to do the same, thus forming a gradient in which cAMP waves are outwardly relayed through the aggregating cells (Tomchik and Devreotes, 1981). When CMF reaches a threshold, cells become chemotactically responsive to cAMP excreted by the other cells, migrating up the [cAMP] gradient to form streams which flow into an aggregation center culminating in around 10^5 cells (Cai and Devreotes, 2011). The aggregated cells then form a mound and subsequently slugs which consist of multiple cell types, prespore or prestalk, that are able to move the population as a single organism to another location in the soil. When the slug reaches an ideal location at the soils surface, the cells then differentiate into either stalk or spore cell types and continue on to form fruiting body (Kessin 2001; Willard and Devreotes, 2006).

Ca^{2+} plays a vital role during aggregation and differentiation and amoebae can be exposed to vast variations in extracellular concentrations in their soil environment. Extracellular Ca^{2+} is essential for motility and for amoebae to orient in the direction of a cAMP gradient to facilitate aggregation (Lusche *et al*., 2009). Ca^{2+} can affect the speed at which the cell

travels during aggregation, where cells that are slow have a lower intracellular Ca^{2+} content, and fast cells have a higher Ca^{2+} content. These cells also showed a different distribution of the motility-related molecules F-actin, PTEN and PI3 kinase (Goury-Sistla *et al*., 2012). The Ca^{2+}-specific indicator aequorin has been used to measured intracellular Ca^{2+} concentrations at various stages of development and showed that free $[Ca^{2+}]_{cyt}$ increases during aggregation and culmination, and increased $[Ca^{2+}]_{cyt}$ has been recorded in both the mound and slug stage (Saran *et al*., 1994a; Cubitt *et al*., 1995).

Within the slug a spatial gradient of cytoplasmic and sequestered Ca^{2+} is established, with the anterior, comprising ~ 20% of the cells in the slug, having higher Ca^{2+} levels than the posterior (Maeda and Maeda, 1973; Tirlapur *et al*., 1991; Azhar *et al*., 1994). The position of a cell within the slug determines its cell type fate, cells at the anterior are genetically defined prestalk cells and those at the posterior are prespore cells (Azhar *et al*., 1995), suggesting a link between Ca^{2+} concentrations and cell type differentiation. Differentiation can be stimulated artificially by increasing intracellular $[Ca^{2+}]$ (Tanaka *et al*., 1998). Indeed, post-aggregative cell fate is shown to be determined by the levels of intracellular Ca^{2+} such that low Ca^{2+} levels predispose cells to prespore differentiation and cells with high Ca^{2+} levels tend to become prestalk cells (Maeda and Maeda, 1973; Saran *et al*., 1994; Yumura *et al*., 1996). Stalk cell formation is favored over spore cell formation when cells are exposed to high Ca^{2+} concentrations (100-120 mM) in the medium (Maeda, 1970). Moreover, when cells are in S and early G_2 of the cell cycle, their intracellular Ca^{2+} levels are fairly high and they generally differentiate into prestalk cells, whereas lower cellar Ca^{2+} levels in mid- to late G_2 phase predispose cells to becoming prespore cells (Azhar *et al*., 2001). A study of fractions of individual cells within the slug showed that prespore cells are able to store more Ca^{2+} than prestalk cells in intracellular granulated Ca^{2+} stores. Ca^{2+} release from fractions of prestalk cells was greater than from prespore cells (Schlatterer *et al.,* 2001), this suggests that the cytoplasmic Ca^{2+} is higher in the prestalk cells because they have less buffering capacity, and that Ca^{2+} concentrations of the cells may influence cell type determination. Indeed, Ca^{2+} has been shown to be involved regulating expression of prespore and prestalk specific genes during differentiation (Pinter and Gross, 1995; Schaad *et al*., 1996; Baskar *et al*., 2000; Poloz and O'Day, 2012; Poloz and O'Day 2012a).

A number of Ca^{2+}-regulating and -regulated proteins have been demonstrated as important for development and differentiation, further implicating Ca^{2+} in these processes. A family of Ca^{2+}-upregulated genes (*cup*) have been identified that, as the name suggests, are upregulated by Ca^{2+}. These proteins are involved in aggregation since cells expressing *cup* asRNA are completely blocked in aggregation. It was suggested that these proteins may play a role in stabilizing the plasma membrane during the dramatic changes that take place during aggregation (Coukell *et al*., 2004). Similarly, overexpression of Ca^{2+}-binding protein 7 (CBP7), results in mutant strains with low cytosolic free Ca^{2+} levels that are unable to chemotax toward cAMP and are not able to aggregate. CBP7 may be involved in substrate adhesion and cell spreading needed for motility (Park *et al*., 2018). The calcium-CaM activated protein phosphatase, calcineurin, is necessary for differentiation and development. Pharmacological studies have implicated calcineurin in growth and development (Horn and Gross, 1996; Weissenmayer *et al*., 2005). Similarly, knockdown of the calcineurin regulatory subunit B by RNAi-silencing results in developmental defects and abnormal fruiting bodies (Boeckeler *et al*., 2006), as does RNAi-silencing of the catalytic subunit A (Thewes *et al*., 2014). Aggregation and development in *IplA*$^{-}$ cells also results in the formation of smaller fruiting bodies than the parent strain and is delayed by 1-2 hr. The formation of smaller fruiting bodies is due to fragmented aggregation streams that proceed to form smaller mounds (Traynor *et al*., 2000; Schaloske *et al*., 2005).

1.2.2 Autophagic cell death

Autophagy is an important process in the lifecycle of *Dictyostelium* (see Mesquita *et al*., 2017 for a recent review). During development, when cells differentiate, they become either viable spore cells, or stalk cells which undergo autophagic processes and become vacuolized cellulose-walled dead cells (Whittingham and Raper, 1960). Starvation and signalling by the polyketide differentiating inducing factor -1 (DIF-1) is necessary to induce cell death pathways (Morris *et al*., 1987; Thompson and Kay, 2000; Luciani *et al*., 2009). Regulation of autophagy by Ca^{2+} signalling in mammalian cells is well documented and has been intensively studied (Bootman *et al*., 2018), however little is known about how and if Ca^{2+} controls autophagic cell death (ACD) in *Dictyostelium*. Given that prestalk cells have increased intracellular Ca^{2+}, one might postulate a link between Ca^{2+} signalling and ACD.

Indeed, evidence that Ca^{2+} signalling is involved in ACD comes from random mutagenesis which identified IplA as necessary for DIF-induced ACD. The *IplA*$^{-}$ mutant did not vacuolize and undergo ACD in response to starvation and DIF addition, processes that are also inhibited by treatment with the Ca^{2+} chelator BAPTA, indicating that IplA and Ca^{2+} dependent processes are required for ACD. It is thought that DIF stimulates IP_3 production, which activates IplA to release Ca^{2+} into the cytosol, thereby inducing ACD possibly through calcineurin/calmodulin pathways (Lam *et al.,* 2008). DIF-1 induced phosphorylation of calcineurin might also regulate the proteins Ca^{2+}-CaM-dependent phosphatase activity (Sugden *et al*., 2015). Another study associating calcium with autophagy in *Dictyostelium* reported that after the induction of autophagy with rapamycin, intracellular Ca^{2+} increased from ~ 150 nM to ~ 700 nM over 72 hours, and this increase coincided with an increase in the autophagic marker Atg-8 (Swer *et al*., 2014). Similarly, treatment with thapsigargin, which blocks ER calcium uptake and increases cytosolic calcium, induces ACD (Luciani *et al*., 2011; Marcassa *et al*., 2017). While there is clearly a link between Ca^{2+} signalling and ACD, still little is known about these processes in *Dictyostelium*.

1.2.3 Chemotaxis

Aggregation is driven by chemotaxis, and chemotaxis is also important for amoebae to find bacterial prey during their vegetative growth phase. Chemoattractants induce changes in extracellular (Bumann *et al*., 1984) and intracellular Ca^{2+} concentrations over all stages of development (Wick *et al*., 1978; Milne and Coukell, 1991; Yumura *et al*., 1996; Malchow *et al*., 1996a; Nebl and Fisher, 1997), therefore the involvement of Ca^{2+} signalling in chemotaxis has been studied. The chemotactic signal transduction pathways and some of the molecular events that link chemotactic signals to cell physiological responses have been identified.

During chemotaxis cells perceive an external gradient of chemoattractant and instead of random extension of pseudopods during normal movement, pseudopods are extended directionally toward the source of chemoattractant (Fisher *et al*., 1989; Fisher, 1990; Soll *et al*., 2009). This directional movement is accomplished by attractant binding to cell surface receptors which induces polarization of the cell, mediated by cytoskeletal

rearrangements that cause actomyosin assembly and contraction in the rear and ruffling in a region of the plasma membrane closer to the attractant source to establish a leading edge. During polarization some signalling molecules become distributed to the posterior of the cell and others to the leading edge. Those at the leading edge promote actin polymerization and pseudopod extension toward the chemoattractant, while actomyosin filaments at the sides and posterior contract to prevent inappropriate extension (Cai and Devreotes, 2011). Concurrently, chemoattractant binding induces an influx of extracellular Ca^{2+} which has been shown to localise primarily to the rear cortex of the cell (Yumura *et al*., 1996).

1.2.3.1 The chemotactic Ca^{2+} response

During chemotaxis, attractant binding induces a rise in cytosolic Ca^{2+} concentration through influx from the extracellular medium (Wick *et al*., 1978; Milne and Coukell, 1991; Yumura *et al*., 1996; Nebl and Fisher, 1997; Traynor *et al*., 2000; Nebl *et al*., 2002), and release from intracellular stores (Wilczynska *et al*., 2005; Fisher and Wilczynska, 2006). The cell surface G-protein coupled receptors (GPCR) responsible for chemoattractant binding are a family of four cAMP binding receptors (cAR1-4) (Saxe *et al*., 1991; Hereld and Devreotes, 1992; Ginsburg *et al*., 1995), and a folic acid receptor 1, fAR1 (Pan *et al*., 2016). Signalling pathways that connect the chemoreceptors to the plasma membrane Ca^{2+} channels that facilitate Ca^{2+} influx are largely unknown. After stimulation of cells with chemoattractants, the onset of the Ca^{2+} response begins after a delay of around 8 seconds for cAMP stimulation and around 12 seconds after folic acid stimulation (Wilczynska *et al*., 2005). This delay in Ca^{2+} influx represents the time needed for the chemoreceptors to become activated, the intracellular signalling pathway to signal to plasma membrane Ca^{2+} channels, and the Ca^{2+} channels to open.

Genetic studies in mutant *Dictyostelium* cell lines have shown that Ca^{2+} influx signalled by cARs is developmentally regulated. In early starvation, signalling is dependent on the G-protein Gα2βγ, and in aggregation competent cells is independent of G-proteins (Milne and Devreotes, 1993; Milne *et al*., 1995; Nebl and Fisher, 1997; Nebl *et al*., 2002). Ca^{2+} influx by folic acid stimulation is Gα4βγ-dependent and only present in vegetative cells (Nebl *et al*., 2002). The second messenger cyclic guanosine 3,5-monophosphate (cGMP) also accumulates within cells after chemoattractant stimulation and has been linked to cAMP and folic acid stimulated Ca^{2+} influx (Menz *et al*., 1991; Flaadt *et al*., 1993;

Kuwayama and Van Haastert, 1998; Nebl *et al*., 2002). In these studies mutants of the gene *stmF,* identified by chemical mutagenesis (Ross and Newell, 1981), showed prolonged and enhanced chemoattractant induced Ca^{2+} and cGMP elevation. It was believed that *stmF* encodes a phosphodiesterase responsible for attenuation of the cGMP and thus Ca^{2+} responses. This was later proved incorrect after a null strain lacking the major cGMP-specific phosphodiesterase (*pdeD*) was analysed. In this mutant, Ca^{2+} responses in early differentiation are reduced rather than enhanced, and in later development Ca^{2+} responses are unaltered (Lusche and Malchow, 2005). Similar findings were reported in other mutants with disruptions in guanylyl cyclase and cGMP phosphodiesterase genes (Veltman *et al*., 2003). The unknown gene product of *stmF* may be involved in upstream regulation of the G-protein dependent pathway involved in regulation of both the cGMP and Ca^{2+} responses.

These cytosolic Ca^{2+} transients in response to 1 µM cAMP or folic acid have been characterized using expression of the luminescent Ca^{2+}-indicator apoaequorin. This method provides sensitive and accurate readings which can detect changes in cytosolic Ca^{2+} concentrations of as little as 2 to 3 nM, and with a temporal resolution of 20 ms (Wilczynska *et al*., 2005). The Ca^{2+} responses last ~60 seconds, during which time cytosolic $[Ca^{2+}]_{cyt}$ levels rise from basal levels of ~70 nM to ~150nM for folic acid responses and ~200 nM for cAMP responses. An example is shown in Fig. 1.3 of a Ca^{2+} response to cAMP. The responses are terminated via sequestration by Ca^{2+}-ATPases back into intracellular stores and across the plasma membrane to return cytosolic Ca^{2+} to resting levels (Nebl and Fisher, 1997; Wilczynska *et al*., 2005).

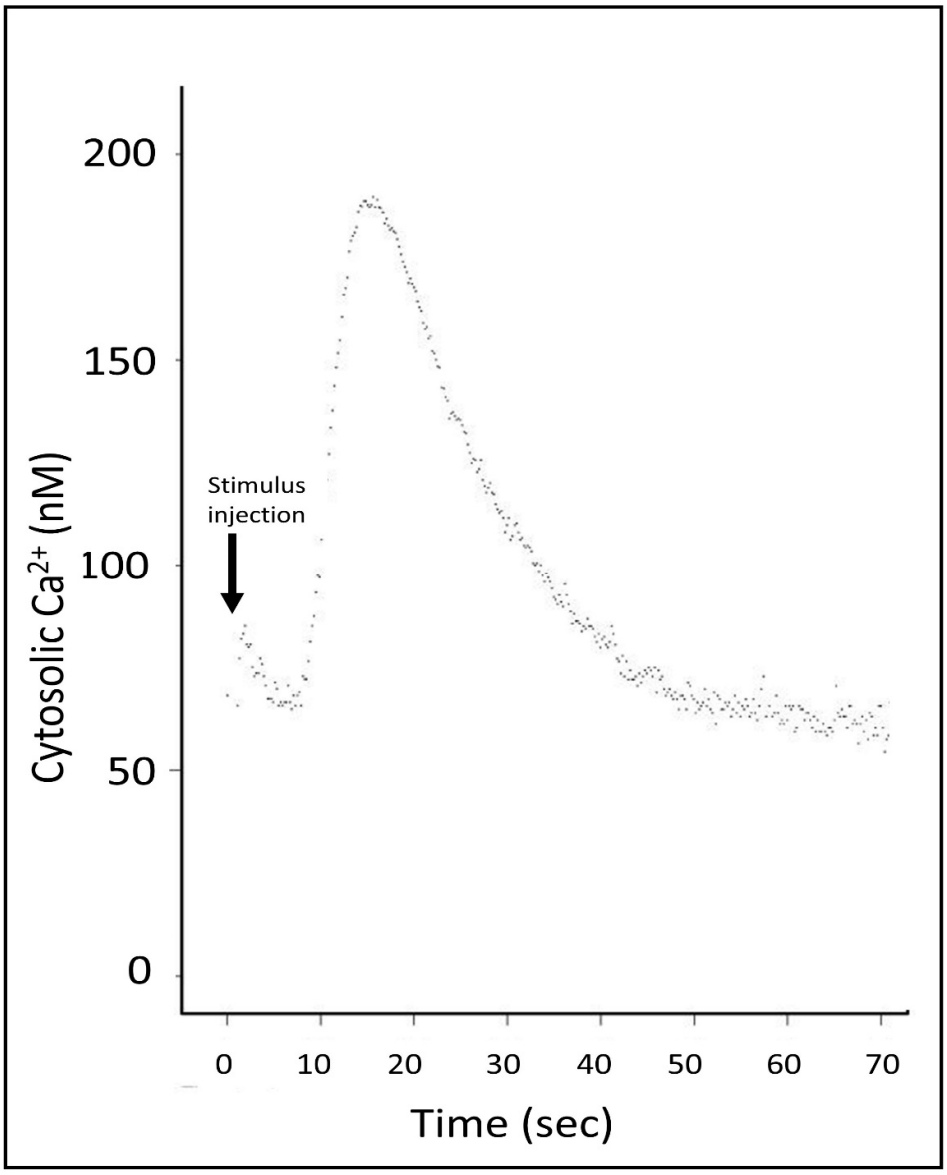

Figure 1.3 Real time recording of typical cytosolic cAMP Ca^{2+} response in *Dictyostelium.*
Basal cytosolic Ca^{2+} levels are around 70 nM. The stimulus is administered by injection into a cell suspension, after which there is a short lag time before the response begins. During the lag time the chemoreceptors to become activated, the intracellular signalling pathways activate plasma membrane Ca^{2+} channels, and the Ca^{2+} channels open. An influx of Ca^{2+} flows into the cytosol which triggers release from intracellular pools, temporally increasing the cytosolic Ca^{2+} levels. The response comes to a peak and is subsequently terminated by removal of Ca^{2+} from the cytosol through the action of pumps and binding proteins, which restores resting Ca^{2+} levels.

The source of the cytosolic Ca^{2+} influx was originally thought to be firstly an IP_3-induced release from the ER and then to be further amplified by influx over the plasma membrane in a CCE type mechanism. Several reports indicated that cAMP stimulates formation of IP_3 (Europe-Finner and Newell, 1987; Van Haastert *et al*., 1989), and that IP_3 application to permeabilised cells invoked a fast small Ca^{2+} efflux from intracellular IP_3 sensitive stores (Europe-Finner and Newell, 1986a; Flaadt *et al*., 1993). Furthermore, a pharmacological study showed that intracellular stores must be loaded with Ca^{2+} to allow cAMP-induced cytosolic Ca^{2+} influx (Schlatterer *et al*., 2004), which would suggest the Ca^{2+} release from internal stores is necessary for influx in a CCE type mechanism. This was later shown not to be the case. Mutants with no phospholipase C activity which in turn lack cAMP-mediated IP_3 increase (Drayer *et al*., 1994), display normal Ca^{2+} responses to cAMP and folic acid (Nebl *et al*., 2002). This shows that IP_3 is not necessary for the responses. Chemotactic Ca^{2+} responses have been shown to be dependent on extracellular Ca^{2+} as they are absent in Ca^{2+} free buffer (EGTA treated) (Nebl and Fisher, 1997, Traynor *et al*., 2000). Genetic studies have revealed that the ER, a Ca^{2+} storage organelle, contributes to chemotactic Ca^{2+} transients. KO mutants which lack either or both ER Ca^{2+} binding proteins, calnexin and calreticulin, have increased Ca^{2+} responses, indicating that the ER is contributing to this response (Wilczynska *et al*., 2005) but the release of Ca^{2+} from the ER is dependent on extracellular Ca^{2+} suggesting that Ca^{2+} influx causes intracellular release, such as in a CICR mode of action (Fisher and Wilczynska, 2006). Taken together this evidence, implies that CCE is not the mechanism of cytosolic Ca^{2+} influx, but rather CICR.

Another major Ca^{2+} store, known as the acidic Ca^{2+} stores, comprises the CV which is linked to mass dense acidocalcisomes, both of which possess vacuolar H^+-ATPase, and PAT1 (Marchesini *et al*., 2002). The CV appears also to be involved in the cAMP response as mutants which lack the gene for the protein *l*arge *v*olume *s*phere A (*LvsA*) display disorganized CVs which have dissociated from CaM and are severely impaired in cAMP-induced Ca^{2+} influx (Malchow *et al*., 2006). Moreover, release of Ca^{2+} from intracellular acidic stores has been suggested to be induced after cAMP stimulation by a mechanism in which activation of phospholipase A2 liberates fatty acids that induce Ca^{2+} release from acidic stores (Schaloske and Malchow, 1997; Schaloske *et al*., 1998). The Ca^{2+} channel responsible for release from the CV is unknown as recently purified vesicles lacking DdTPC

have been shown to retain arachidonic acid-induced Ca^{2+} release (Chang *et al*., 2020). Uptake by the CV of Ca^{2+} from the cytosol to help terminate the Ca^{2+} response is likely to be mediated by PAT1.

Analysis of the kinetics of both cAMP and folate responses has shown that the larger the Ca^{2+} response, the faster Ca^{2+} flows into the cytoplasm and the faster the response is terminated. This indicates that mechanisms common to cAMP and both folic acid signalling pathways control key aspects that shape the responses, such as the open and closed state of Ca^{2+} channels and activation of Ca^{2+}-ATPases. This suggests that the responses are autoregulated and that Ca^{2+} itself is responsible for Ca^{2+}-induced channel closure and activation of Ca^{2+} pumps that terminate the responses (Wilczynska *et al*., 2005). Consistent with this is the prediction that, with the exception of Ddpolycystin, all of *Dictyostelium* Ca^{2+} pumps and channels, contain Ca^{2+} regulatory domains such as the calmodulin IQ motif in the two putative DdPMCA/SERCA, PAT1 and IplA; and Ca^{2+}-binding EF hands in DdTPC and Ddmucolipin (Wilczynska *et al*., 2005). It is unknown if the DdP2X channels are also calcium regulated, however evidence suggests that huP2X receptors may contain a Ca^{2+} binding pocket and are sensitive to inhibition by high extracellular Ca^{2+} (Stojilkovic *et al*., 2014).

The Ca^{2+} channel activated by cAR1 and fAR1 that is responsible for Ca^{2+} influx across the plasma membrane has not been identified. IplA is a candidate as it has some localisation at the plasma membrane but is primarily localised to intracellular vesicles (Lusche *et al*., 2012). IplA null amoebae have been shown to lack both cAMP and folic acid Ca^{2+} responses measured by cytosolic $^{45}Ca^{2+}$ uptake (Traynor *et al*., 2000), and using a fluorescent Ca^{2+} indicator (Traynor and Kay, 2017). However, study by Schaloske *et al*. (2005) found IplA null strains retained a reduced cAMP Ca^{2+} response measured using a Ca^{2+} sensitive electrode and under lower extracellular Ca^{2+} concentrations (~1µM as opposed to 100 µM in Traynor *et al*. (2000) experiments). Different experimental conditions may account for the discrepancies, therefore, the role IplA plays in these chemotactic Ca^{2+} responses remains to be clarified. Another potential Ca^{2+} channel facilitating chemotactic Ca^{2+} uptake is Ddpolycystin. Expression of Ddpolycystin has also been observed at the plasma membrane (Lima *et al*., 2014; Traynor and Kay, 2017)

however KO cells reportedly still retain calcium responses to cAMP and folic acid (Traynor and Kay, 2017).

1.2.3.2 The role of Ca^{2+} in chemotaxis

Surprisingly, as mentioned above, Traynor *et al*. (2000) reported that chemotactic Ca^{2+} uptake by IplA null amoebae is abolished however these cells were still able to chemotax efficiently. These findings indicate that Ca^{2+} influx and signalling is not necessary for chemotaxis. However, chelation of cytosolic Ca^{2+} was shown to impair chemotaxis (Schaloske *et al*., 2005). These conflicting results may be due to differences in assays, but the question remains: why is this Ca^{2+} influx associated with chemotactic stimulation? Some evidence suggests a link between Ca^{2+} and cytoskeletal rearrangements during chemotaxis. One study reported a Ca^{2+} gradient within the cells where Ca^{2+} localises primarily to the rear cortex of freely migrating cells in the majority, but not all cells (Yumura *et al*., 1996). In the rear cortex, Ca^{2+} has been proposed to induce the localisation of myosin II which may contribute to rear retraction and prevent the pseudopod extending in the incorrect direction, thus aiding correct directional movement (Yumura and Kitanishi-Yumura, 1993; Yumura, 1996). Furthermore, many actin binding proteins are Ca^{2+} sensitive (Pikzack *et al*., 2005), as are the copines which are calcium-dependent phospholipid-binding proteins, that translocate to the plasma membrane in response to cAMP (Ilacqua *et al*., 2018), therefore Ca^{2+} can influence cytoskeleton rearrangement during chemotaxis. Extracellular Ca^{2+} has been shown to positively regulate cell uropod formation, cell velocity and increase of myosin II in the cell posterior (Lusche *et al*., 2009), similarly, chelating extracellular Ca^{2+} with EGTA impaired cell motility (Unterweger and Schlatterer, 1995; Fache *et al*., 2005), however cells were still able to orient within a chemotactic gradient (Unterweger and Schlatterer, 1995). Conversely, pseudopod extension toward chemoattractants was not inhibited in the presence of EGTA in electro-permeabilised cells, suggesting that neither intra or extracellular Ca^{2+} is required (Van Duijin and Haastert, 1992). The role of Ca^{2+} in cytoskeletal rearrangement needed for chemotaxis is still not clear and warrants further investigation.

During early differentiation, as well as acquiring receptor-mediated cAMP chemotaxis signal transduction mechanisms, cells also develop the ability to chemotax along a spatial gradient of Ca^{2+} (Scherer *et al*., 2010; Soll *et al*., 2011), and an estimated 2×10^8 high

affinity Ca^{2+} binding sites per cell has been reported (Böhme *et al*., 1987). Mutants lacking IplA (Lusche *et al.,* 2012) and two of the four myosin II heavy chain (Mhc) kinases MhckA and MhckC (Wessels *et al*., 2012) lose their ability to chemotax in a special gradient of Ca^{2+} but are normal in their chemotaxis to cAMP. IplA null cells also lost their ability to orient in the direction of the aggregation center (Lusche *et al.,* 2012). Taken together with the finding that extracellular Ca^{2+} is essential for amoebae to orient in the direction of a cAMP gradient, with the optimal concentration of 10 mM (Lusche *et al*., 2009), a hypothesis was formed that at the onset of each natural cAMP wave steep and transient Ca^{2+} gradients are formed between cells (Scherer *et al*., 2010) which could facilitate cell orientation in the direction of the aggregation center (Lusche *et al.,* 2012). IplA is a possible receptor responsible for Ca^{2+} chemotaxis, and MhckA and MhckC may somehow regulate IplA function. This provides a suggested role for the Ca^{2+} influx during cAMP chemotaxis, however is still only a hypothesis thus needs further investigation.

1.2.4 Phagocytosis and macropinocytosis

Phagocytosis and macropinocytosis are two distinct uptake methods that *Dictyostelium* amoebae use to internalize extracellular particles (phagocytosis) or fluids (macropinocytosis). In their natural soil environment, amoebae hunt and engulf microorganisms via phagocytosis (Cosson and Soldati, 2008). Laboratory cultures that can grow axenically in liquid medium have been isolated and cultured for routine use (Sussman and Sussman, 1967; Watts and Ashworth, 1970). Particles or fluids are taken up in either into a phagocytic or macropinocytic cup, in distinct processes that both involve Ca^{2+}. The Ca^{2+}-regulated actin bundling protein, fibrin, is associated with both the macrophagosome and macropinosome during formation (Pikzack *et al*., 2005). The requirement for Ca^{2+} during phagocytosis has been shown as cultures treated with the Ca^{2+} chelators EDTA or EGTA are inhibited in their uptake of fluorescently labelled yeast, and this suppression could be reversed by the addition of Ca^{2+} (Yuan *et al*., 2001). Similar results have been reported for uptake of *L. pneumophila*, where chelation of extracellular Ca^{2+} decreased phagocytosis of the bacteria, and chelation of intracellular Ca^{2+} also had a mild inhibitory effect on phagocytosis (Fajardo *et al*., 2004). Biochemical studies have shown that disrupted Ca^{2+} homeostasis due to caffeine treatment inhibited axenic growth and fluid phase pinocytosis. Caffeine induces release of Ca^{2+} from intracellular stores

which is believed to disrupt intracellular Ca^{2+} homeostasis and therefore pinocytosis. The results were mimicked by treatment with the calcium transport inhibitor La^{3+} (Gonzalez *et al*., 1990). Genetic evidence also supports a role for Ca^{2+} in phagocytosis. Mutant strains lacking both calnexin and calreticulin have low rates of phagocytosis, not due to defects in particle adhesion, but due to defective formation of the phagocytic cup and particle uptake (Muller-Taubenberger *et al*., 2001). As these mutants exhibit increased rather than reduced chemotactic Ca^{2+} responses (Wilczynska *et al*., 2005; Fisher and Wilczynska, 2006), it is unclear if the defect in phagocytosis is associated with Ca^{2+} signalling or the chaperone activities of the calnexin and calreticulin in protein folding (Muller-Taubenberger *et al*., 2001). Similarly, mutants lacking calnexin and calreticulin have low rates of *L. pneumophila* phagocytosis (Fajardo *et al*., 2004).

During the endocytic cycle, shortly after phago/pinocytisis the internalized nascent endocytic compartment (NC) progresses through the endo-lysosomal pathway which involves vesicle maturation events. The NC matures into acidified lysosome-like vesicles which then gradually mature into neutralized post-lysosomes (PL) that fuse with the plasma membrane at an exocytic patch (Jenne *et al*., 1998; Neuhaus and Soldati, 1999; Maniak, 2001; Charette and Cosson, 2008). Studies of the endolysosomal pathways of mammalian cells have shown that Ca^{2+} release from these vesicles regulates the fusion/fission of the membranes (Janice 2004, Luzio *et al*., 2007a; Patel and Cai, 2015), and also compartmental acidification (Gerasimenko *et al*.,1998). In *Dictyostelium*, given the effects of Ca^{2+} on both phagocytosis and pinocytosis, it is likely that Ca^{2+} plays a role in maturation of the endolysosomal pathway. Acidic vesicles also act as internal Ca^{2+} stores which can release and sequester Ca^{2+} to contribute to Ca^{2+} homeostasis and signalling. In mammalian cells, estimates of luminal free Ca^{2+} concentrations in lysosomes are estimated to be ~ 0.5 mM (Christensen *et al*., 2002; Luzio *et al*., 2007). In *Dictyostelium* the Ca^{2+} concentration in the PL has been estimated to be ~1-3 µM (Lima *et al*., 2012), but the concentration in the lysosome had not been measured. Studies in mammalian cells show that local Ca^{2+} bursts released from endosomal compartments can facilitate membrane fusion approximately 20-100 nm from the site of release (Neher 1998; Burgoyne and Clague, 2003). Ca^{2+} signals are then dissipated by actively transporting Ca^{2+} back to the lumen. This Ca^{2+} release and sequester is facilitated by Ca^{2+} channels, cation exchangers and pumps and is discussed further in chapter 5.

1.2.5 Mechanosensation

Mechanical forces are sensed by the cytoskeleton through plasma membrane receptors which are often linked to calcium influx (Arnadóttir and Chalfie, 2010). Numerous studies in *Dictyostelium* have investigated cellular responses to mechanical stimuli including stretch, compression, shear-flow and electrical currents and have reported that extracellular calcium is integral to stimulus response because responses are absent when extracellular calcium is depleted (Fache *et al*, 2005; Shanley *et al*., 2006; Lombardi *et al*., 2008). While there may be a role for Ddpolycystin and Ddmucolipin in mechanosensation (Lima *et al*., 2014), *Dictyostelium* also encodes a putative mechano-sensitive channel, mscS (Lombardi *et al*., 2008; Traynor and Kay, 2017), and a homologue of the Piezo mechanosensitive ion channel in the cell membrane of eukaryotes (Coste *et al*., 2010; Srivastava *et al*., 2020). *Dictyostelium* cells experience elevated $[Ca^{2+}]_{cyt}$ in response to mechanical stimuli which involves IplA dependent calcium release (Lombardi *et al*., 2008; Artemenko *et al*., 2016), and are sensitive to the calcium channel blocker gadolinium (Srivastava *et al*., 2020). The mechano-activated calcium transients are dependent on both intra- and extracellular calcium and regulate signal transduction that maintains rapid cell movement (Srivastava *et al*., 2020), directed migration and cell substrate adhesion (Zhu *et al*., 2015).

1.3 Aims of thesis

Dictyostelium exhibits diverse, readily assayed phenotypes, and is an established tractable model for molecular genetic, biochemical and cell biological and studies. The entire genome is fully sequenced, there are limited cell types compared to mammalian systems, and cells are available for study at both unicellular and multicellular life stages. This lends *Dictyostelium* to be an excellent simple model to study the function of protein targets associated with human diseases, and has already provided important insights into the molecular pathogenesis of many diseases. The human homologues of Ddpolycystin and Ddmucolipin are associated with the diseases polycystic kidney disease and mucolipidosis type IV respectively. While current published work has established *Dictyostelium* as a suitable model to study polycystin-2 and mucolipin, my phenotypic analysis will further contribute to establishing *Dictyostelium* as an important and relevant cell-based model to study the molecular mechanisms involved in the pathology of diseases. Studying PAT3 and PAT4 function in *Dictyostelium* could also help uncover the disease-relevant molecular functioning of Ca^{2+} pumps as dysregulation of these proteins is associated with a variety of neurodegenerative and mental disorders.

Calcium signalling is undoubtedly integral to both growth and development of *Dictyostelium*. The slime mould expresses a collection of calcium pumps, channels and binding proteins that are responsible for maintaining calcium homeostasis and calcium signal propagation. While many constituents of the *Dictyostelium* calcium signalling machinery have been identified, few of the proteins have been comprehensively studied. Therefore, my purpose in the work described in this thesis was to characterise four of these proteins, Ddpolycystin, Ddmucolipin and two putative Ca^{2+}-ATPases, which I have termed PAT3 and PAT4. The strategy was to create antisense inhibition and overexpression constructs for the channels, and antisense inhibition constructs for PAT3 and PAT4, and express them in the parental strain AX2. This would allow me to characterise a collection of strains in which expression of these proteins had been altered and correlate the phenotypic outcomes with an expression index for each protein (the copy numbers of the relevant constructs). To fulfil this purpose, I measured diverse phenotypes in the unicellular and multicellular stages of the *Dictyostelium* life cycle and

coupled this with assays of Ca^{2+} responses using Ca^{2+}-sensitive luminescence by recombinant aequorin coexpressed in the same transformants (Nebl and Fisher, 1997).

My first aim was to characterise the chemoattractant calcium responses to folic acid and cAMP in the knockdown and overexpression strains to determine if the channels and pumps contribute to these responses. The two calcium channels, Ddpolycystin and Ddmucolipin, are homologues of TRP Ca^{2+} channels, however their channeling activity in *Dictyostelium* is unclear. Ddpolycystin was identified by Wilczynska *et al*. (2005) and has been the subject of a small number of studies that have identified it as a plasma membrane calcium channel that is responsible for purinergic calcium responses (Lima *et al*., 2014; Traynor and Kay, 2017) but not necessary for chemotactic calcium responses to cAMP or folic acid because a knockout strain still retained these responses. However, given the overlapping and redundant functions of many calcium channels and pumps, the retention of calcium responses in the knockout does not exclude the possibility of Ddpolycystin contributing to Ca^{2+} responses to these chemoattractants. Therefore, my project aimed to determine if Ddpolycystin contributed to chemoattractant calcium signalling assayed using a different technique, the aequorin method described above.

Ddmucolipin localises to membranes of the endocytic pathway, and knockout studies have hinted at its involvement in calcium regulation (Lima *et al*., 2012), however no study has directly measured Ddmucolipin's contribution to calcium signalling. Therefore, my second aim was to determine for the first time if Ddmucolipin contributes to calcium transients in response to chemoattractants. Similarly, the putative Ca^{2+}-ATPases, PAT3 and PAT4, have not been studied experimentally, so my 3rd aim was to determine for the first time if they are involved in chemotactic calcium signalling.

My final aim was to determine how knocking down and overexpressing these proteins affects various *Dictyostelium* phenotypes. This was to be achieved by analyzing a battery of phenotypes including growth rates in liquid and on solid medium, pinocytosis, phagocytosis and multicellular morphogenesis to determine if the channels and pumps are involved. Because calcium is involved in many cellular processes, altering the cells' ability to properly handle calcium fluxes may affect these phenotypes. This is of particular importance in the case of Ddpolycystin because there have been some discrepancies in the literature in relation to some phenotypes in Ddpolycystin null cells. Growth and

rheotaxis defects have been reported in some studies, but not others. Discrepancies such as this may occur due to parental strain differences, protocol differences, or if the defects are only subtle they may not always be detected in a knockout mutant (for statistical reasons). Therefore, to try and clarify some of the discrepancies, use of the knockdown and overexpression strains, rather than knockouts, would allow me to correlate phenotypic readouts with copy number of the constructs. This approach involves larger samples of independently isolated mutant strains, offers the possibility of regression analysis of phenotype versus copy number, and the reduced likelihood of off-target unknown genetic events influencing the outcome. For these reasons, it can be more sensitive in detecting any small phenotypic abnormalities, that may not be detected in analysis of knockout strains. Similarly, a knockout approach has previously been used to analyze Ddmucolipin where the authors reported that knocking out Ddmucolipin did not cause any defects in growth rates, endocytosis rates or multicellular development. However, these phenotypes have not been assessed in strains overexpressing the channel. Therefore, I aimed in this thesis to determine if using a combined knockdown and overexpression system would unveil any phenotypic roles for Ddmucolipin that may be present.

Chapter two

Materials and methods

2.1 General Procedures

2.1.1 Sterilization

All glassware, media, tips and Eppendorf tubes were sterilized by autoclaving at 100 kPa and 120 °C for 20 min. Sterile distilled water was used as a solvent for all media and buffers unless otherwise stated.

2.1.2 Chemicals

See Appendix 1

2.1.3 Media and buffers

See Appendix 2

2.1.4 Enzymes and kits

See Appendix 3, 4 and 5 for enzymes, kits and their suppliers respectively. All protocols were followed according to the manufacturer's instructions, unless otherwise stated.

2.1.5 Nomenclature of genes used in thesis

The genes and their associated protein names, used in the study are outlined in Table 2.1.

Table 2.1 Genes cloned in this study

Gene name used in this thesis	**Protein name used in this thesis**	**dictyBase Gene ID**	**Gene product**
Ddpolycystin	**Ddpolycystin**	DDB_G0272999	polycystin-2
Ddmucolipin	**Ddmucolipin**	DDB_G0291275	mucolipin
pat3	**PAT3**	DDB_G0284605	P-type ATPase Ca^{2+}-ATPase
pat4	**PAT4**	DDB_G0289473	P-type ATPase Ca^{2+}-ATPase

2.1.6 Bacterial and *D. discoideum* strains

The bacterial and *Dictyostelium* strains used throughout the study are outlined in Tables 2.2-2.3. The plasmid constructs used to transform AX2 and create mutants are outlined in Table 2.4.

Table 2.2 Genotypes of *E. coli* strains

Strain	Genotype	Reference
DH5α	*F-endA1 hsdR17($r_k^-m_k^+$) supE44 thi-1 recA1 gyrA(Nal^r) relA1 Δ(lacZYA-argF)$_{U169}$ (m80lacZΔM15)*	Hanahan, 1983
JC11451	*F- thr-1 leuB6 proA2 his-4 thi-1 argE3 lacY1 galK2 supE44 ara-14 xyl-15 mtl-1 sbcB sup$^+$*	Kushner *et al.*, 1971
TOP10	*F-* mcr*A Δ(*mrr-hsd*RMS*-mcr*BC) Φ80*lac*ZΔM15 Δ*lac*X74* rec*A1* ara*D139 Δ(*ara leu*) 7697* gal*U* gal*K* rps*L (StrR)* end*A1* nup*G*	Invitrogen, Carlsbad, CA, USA

Key to genotype symbols:

GENOTYPE	PHENOTYPE
ara- 14	Defective in arabinose sugar utilization
argE3	Requires arginine for growth
argF	Ornithine carbamoyltransferase mutation blocks arginine utilization
endA1	Mutation suppressing endonuclease A-dependent degradation plasmid DNA
galK2	Defective in galactose sugar utilization
gal*U*	Glucose -1- phosphate uridylyltransferase mutation blocks galactose utilization
gyrA(Nal^r)	DNA gyrase mutation (nalidixic acid resistance)
his-4	Requires histidine for growth
hsd	Restriction negative and modification positive

leuB6	Requires leucine for growth
mtl-1	Defective in mannitol sugar utilization
*mcr*A	Mutation allows methylated DNA not to be recognized as a foreign DNA
nupG	Mutation for the transport of the nucleosides
ProA2	Requires proline for growth
recA	Recombination defective
relA1	Relaxed regulation of RNA synthesis
rps*L* (StrR)	Provides streptomycin resistance
sbcB	Recombination defective
supE44	Carries a tRNA suppressor gene
thi-1	Requires thiamine for growth
thr-1	Requires threonine for growth
xyl-15	Defective in xylose sugar utilization

Table 2.3 Genotypes of *Dictyostelium discoideum* strains used in this project

Strain	**Parent**	**Genotype or construct expressed**	**Reference**
AX2	NC4	*axe*A1, *axe*B1, *axe*C1	Watts and Ashworth, 1970
HPF401	AX2	Expressing pPROF120 for aequorin expression	Nebl and Fisher, 1997
HPF642 HPF831 HPF643 HPF833 HPF644 HPF835-838 HPF859	AX2	**Ddpolycystin knockdown strains.** Expressing pPROF120 for aequorin expression and pPROF646 antisense inhibiting *pkd2*	This thesis
HPF839-841 HFP651-652 HPF844-846 HPG653	AX2	**Ddpolycystin overexpression strains.** Expressing pPROF120 for aequorin expression pPROF640 for overexpression of *pkd2*	This thesis

HPF812 HPF813 HPF640 HPF815 HPF655 HPF817 HPF818	AX2	**Ddmucolipin knockdown strains.** Expressing pPROF120 for aequorin expression and pPROF650 for antisense inhibition of *mcln*	This thesis
HPF820 HPF654 HPF656 HPF823-829	AX2	**Ddmucolipin overexpression strains.** Expressing pPROF120 for aequorin expression and pPROF638 for overexpression of *mcln*	This thesis
HPF862 HPF863 HPF648-650 HPF865-871	AX2	**PAT3 knockdown strains.** Expressing pPROF120 for aequorin expression and pPROF643 for antisense inhibition of *pat3*	This thesis
HPF849-853 HPF658 HFP646 HPF856 HPF645 HPF659 HPF647	AX2	**PAT4 knockdown strains.** Expressing pPROF120 for aequorin expression and pPROF640 for antisense inhibition of *pat4*	This thesis

Key to genotype symbols:

Genotype	Phenotype
axe	AX2 able to grow on axenic medium

Table 2.4 Plasmid constructs utilized in this thesis

Construct name	**Information**	**Reference**
pA15GFP	*Dictyostelium* expression vector containing *gfp* gene and a neomycin resistance cassette	Fey *et al.*, 1995
pDNeo2	*Dictyostelium* expression vector containing Tn903 neomycin resistance cassette	Witke *et al.*, 1987
pPROF120	Plasmid used for the expression of the light sensitive photoprotein aequorin	Nebl and Fisher, 1997
pZErO-2™	Bacterial plasmid contains an expression cassette consisting of the Lac promotor/operator region and a multiple cloning site.	Invitrogen®
pPROF635	Full length *pkd2* gDNA cloned into the *Bam*HI site of pZErO-2™	This thesis
pPROF636	Full length *pkd2* gDNA subcloned from pPROF635 into the *Xho*I and *Cla*I sites of pA15GFP in replacement of GFP.	This thesis
pPROF637	Full length *mcln* gDNA cloned into the *Bam*HI site of pZErO-2™	This thesis
pPROF638	Full length *mcln* gDNA subcloned from pPROF637 into the *Xho*I and *Cla*I sites of pA15GFP in replacement of GFP.	This thesis
pPROF639	First 1397 bp of *pat4* gDNA cloned into the *Eco*RI site of pZErO-2™ Fragment size: 1382 bp	This thesis

pPROF640	First 1397 bp of *pat4* gDNA subcloned from pRPOF639 into the *Eco*RI site of pDNeo2 in the antisense orientation. Fragment size: 1382 bp	This thesis
pPROF642	First 1447 bp of *pat3* gDNA cloned into the *Bam*HI and *Kpn*I sites of pZErO-2™ in the antisense orientation. Fragment size: 1447 bp	This thesis
pPROF643	First 1447 bp of *pat3* gDNA subcloned from pRPOF642 into the *Kpn*I and *Xho*I sites of pDNeo2 in the antisense orientation. Fragment size: 1447 bp	This thesis

2.1.7 *D. discoideum* cell culture

D. discoideum cells were grown on lawns of *Enterobacter aerogenes* as a food source on SM and incubated at 21 °C for 3-4 days. Cultures were subcultured as required from a single colony. To prepare liquid cultures, 5-10 spores were inoculated into a well of a 24-well Costar plate containing 1.5 mL HL5 supplemented with geneticin (20 µg mL^{-1}), ampicillin (100 µg mL^{-1}), streptomycin (500 µg mL^{-1}) and tetracycline (100 µg mL^{-1}), and incubated at 21 °C to allow spores to germinate and form amoebae. Once confluence was reached 1 mL of culture was inoculated into 10 mL HL5 in T25 flask (Falcon) and cells were grown to the density of 1-2 x 10^6 cells mL^{-1} shaking at 150 rpm and 21 °C. Strains were subcultured once without antibiotics before use to remove possible effects on phenotypic readouts.

2.1.8 Storage of *D. discoideum* strains

D. discoideum strains were grown on lawns of *E. aerogenes* SM plates with either geneticin (20 µg mL^{-1}) for transformants or without for AX2. A mix of vegetative amoebae and

fruiting bodies from an entire plate were scraped with a sterile toothpick and resuspended in 1000 µl of *Dictyostelium* storage buffer (45 % (v/v), horse serum, 10 % (v/v) DMSO, and 45 % (v/v) sterile saline) and stored at -80 °C until required. Multiple aliquots were stored for future use.

2.1.9 Storage of bacterial strains

Bacterial strains were cultured ON in 10 mL of LB medium either without antibiotics or with appropriate selection with ampicillin (100 µg mL^{-1}) or kanamycin (25 µg mL^{-1}) to an optical density of 0.5-0.6 at 600 nm. Five mL of cells were harvested by centrifugation, 5 min at 13, 000 × *g* and the pellet resuspended in 1 mL 10 % (v/v) glycerol and stored at -80 °C until required.

2.1.10 Plasmid maps

The following provides a brief description and circular maps of plasmid backbones utilized in the production of various constructs, Figures 2.1-2.4

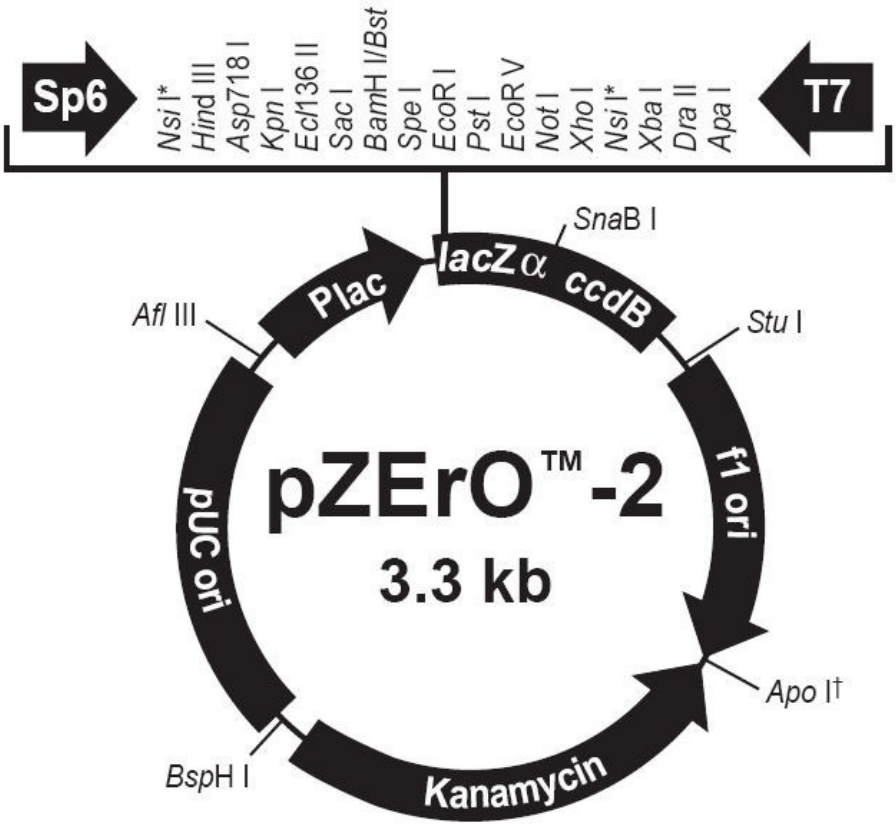

Figure 2.1 Simplified plasmid map of pZErO™-2.

The plasmid contains an expression cassette consisting of the Lac promotor/operator region and a multiple cloning site. Insertion of a gene into the multiple cloning site disrupts the expression of the lethal *ccdB* gene, allowing for selection of transformants with an insert. Selection of transformants also relies on the vegetative origin of replication, pMB1, and the kanamycin resistance gene. **Source:** Invitrogen®

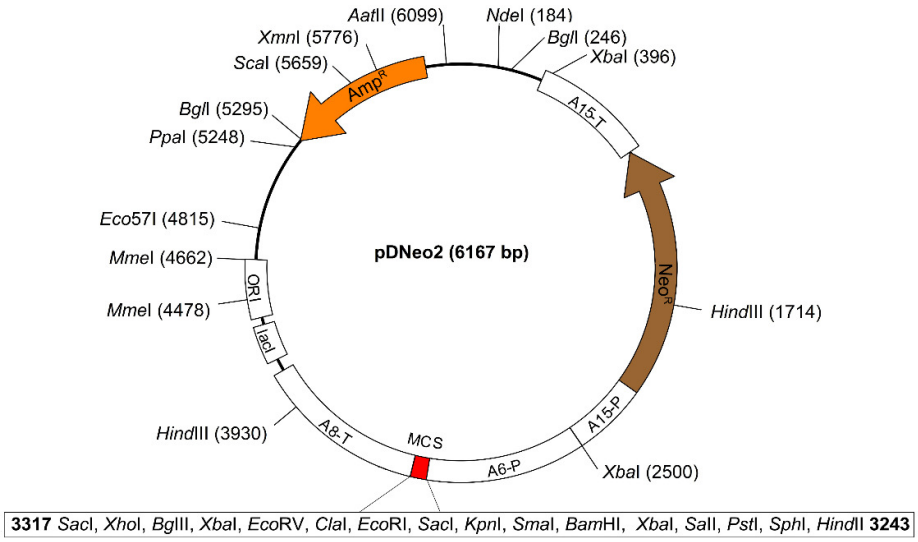

Figure 2.2 *Dictyostelium* shuttle vector pDNeo2**.** Circular map of pDNeo2 is shown.

The plasmid was used to clone antisense fragments of genes of interest. It was made by replacing the polylinker of plasmid vector pUC19 with a G418 resistance cassette and an expression cloning cassette. The G418 resistance is provided by the bacterial Tn903 neomycin resistance gene (Neo^R) under the control of the *D. discoideum* actin-15 promoter (A15-P) and terminator (A15-T). The multiple cloning site (MCS) is under the control of the *D. discoideum* actin-6 promoter (A6-P) and actin-8 gene transcription terminator (A8-T) (Witke *et al.,* 1987).

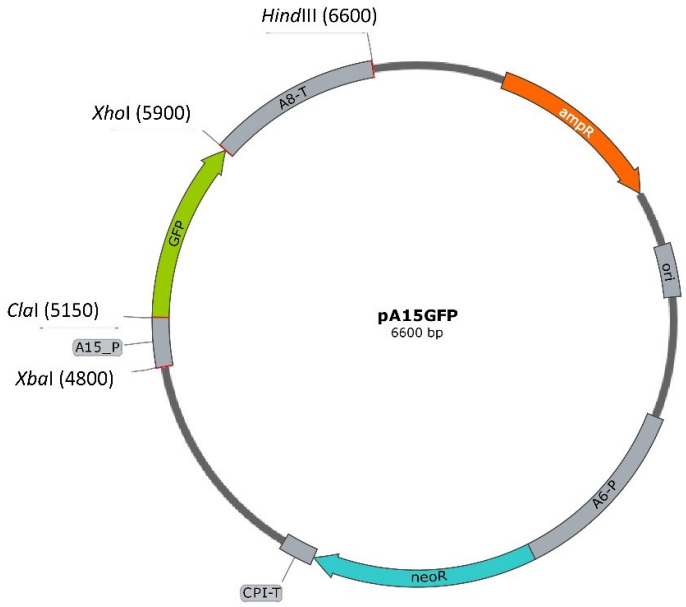

Figure 2.3 Simplified plasmid map of the *Dictyostelium* shuttle vector pA15GFP.

The plasmid was created by insertion of GFP and the actin-15 promotor (A15-P) into the pDdGal backbone. For cloning into this vector, GFP was replaced with the gene insert of interest. Expression of the bacterial neomycin resistance gene (neoR) under the control of the *Dictyostelium* actin-6 promotor (A6-P) and CPI transcription terminator (CPI-T), allows G418 resistance for selection of transformants. It also contains an ampicillin resistance (ampr) gene which confers resistance against ampicillin for bacterial selection (Fey *et al*. 1995).

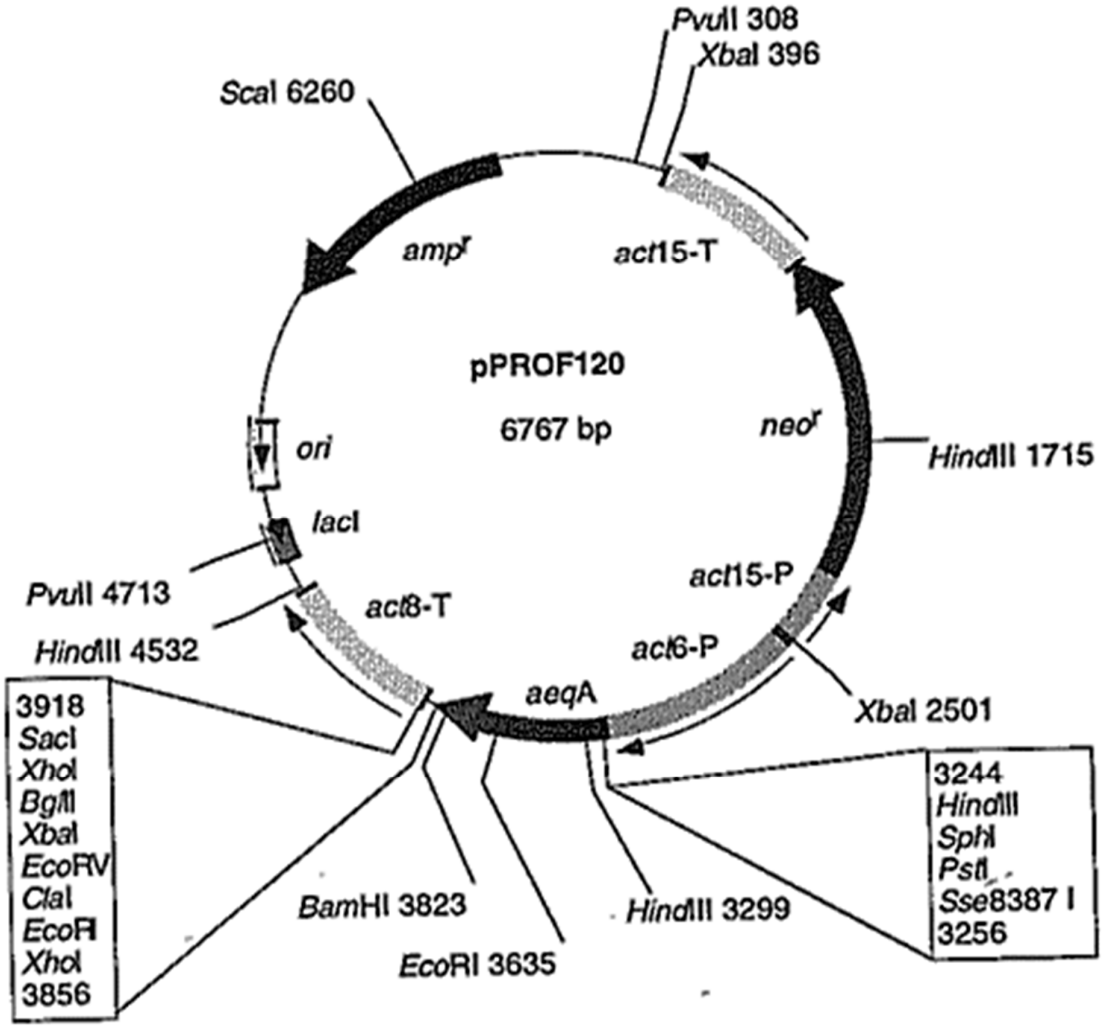

Figure 2.4 Simplified plasmid map of pPROF120.

This plasmid was used for the expression of the light sensitive photoprotein aequorin, used for *in vivo* measurements of $[Ca^{2+}]_{cyt}$. pPROF120 was created by inserting *aeqA* into the *Dictyostelium* shuttle vector pDNeo2. Regulation of apoaequorin is under the expression and termination of the *Dictyostelium* actin-6 promotor (act6-P) and actin-8 transcription terminator (act8-T) respectively. G418 resistance relies on the expression of the bacterial neomycin resistance gene (neo^r)under the control and termination of the *Dictyostelium* actin-15 promotor (act15-P) and actin-15 transcription terminator (act15-T) respectively (Nebl and Fisher 1997).

2.2 Molecular biological techniques

2.2.1 Protocol for large scale extraction of plasmid DNA

The large-scale extraction of plasmid DNA from *E. coli* was prepared using the Jetstar™ 2.0 Maxi Prep Kit 120 (Gentaur) following the supplied protocol with no deviations. A single bacterial colony was picked from an LB agar plate containing ampicillin or kanamycin and used to inoculate 125 mL of LB medium containing 100 μg mL^{-1} ampicillin or 25 μg mL^{-1} kanamycin and incubated ON at 37 °C with rapid shaking. The cultured bacteria were harvested by centrifugation in a Sorvall GSA rotor at 4, 500 × *g* for 10 min at 4 °C, and the cell pellet was resuspended in buffer containing 100 μg mL^{-1} boiled RNase A. Meanwhile the column was equilibrated with 30 mL equilibration solution. Cells were lysed for 5 min in lysis buffer before neutralisation buffer was added. Cell debris and chromosomal DNA was removed by centrifugation at 15, 000 × *g* for 20 min. The supernatant containing the plasmid DNA was then loaded into the equilibrated column where the ion exchange resin bound to the plasmid DNA. The column was then washed with 50 mL wash buffer to remove impurities, and the bound plasmid DNA eluted with elution buffer. Plasmid DNA was ethanol precipitated and pelleted by centrifugation at 15, 000 × *g* for 20 min. The pellet was dissolved in TE buffer or sterile dH_2O.

2.2.2 Small scale extraction of plasmid DNA (alkaline lysis miniprep)

The alkaline lysis method described by Birnboim and Doly (1979) was used for extraction of small amounts of plasmid DNA. This method was used to screen transformants for the desired constructs. 24 randomly selected bacterial colonies were inoculated into 3 mL LB broth supplemented with a selective antibiotic (25 μg mL^{-1} kanamycin or 100 μg mL^{-1} ampicillin) and grown ON at 37 °C shaking. A 1.5 mL aliquot of the ON culture was decanted into a sterile microcentrifuge tube and the cells pelleted by centrifugation at 2000 × *g* for 20 s in a bench top centrifuge. The supernatant was discarded, and the pellet resuspended in 100 μl of resuspension buffer (TE with 1 μg mL^{-1} RNase A). 200 μl of cell lysis buffer (0.2 M NaOH 1 % w/v SDS) was added to the suspension and mixed by inverting the tube which was then incubated on ice for 5 min. 150 μl of neutralization buffer (5 M K-acetate pH 4.8) was then added to the lysate, the sample mixed by vortexing and

incubated on ice for 5 min. Centrifugation in a bench top centrifuge at maximum speed for 5 min pelleted the cell debris and chromosomal DNA, and the supernatant was transferred to a microcentrifuge tube containing 900 µl of absolute ethanol. The microcentrifuge tube was inverted to mix the sample which was then incubated at room temperature for 5 min to precipitate DNA before pelleting by centrifugation at 14, 000 × *g* for 5 min to pellet the plasmid DNA. The pellet was then washed with 70 % ethanol dried by vacuum in a speed-vac on low temperature and resuspended in 20 µl of sterile dH_2O.

Extended procedure for JC11451 E. coli cells

The following extra steps allowed for the efficient removal of contaminating nucleases in the minipreps of JC11451 transformants under standard conditions.

After the removal of cell debris and chromosomal DNA, the supernatant was transferred to a microcentrifuge tube containing 300 µl of phenol and 300 µl of chloroform. The sample was mixed by inverting and centrifuged at maximum speed for 5 min. The upper phase was then transferred to a microcentrifuge tube containing 900 µl of absolute ethanol and 45 µl of 3 M Na-acetate to precipitate the plasmid DNA. The DNA was pelleted by centrifugation at 14, 000 × *g* for 5 min, washed with 70 % ethanol and dried in a speed-vac. The pellet was then resuspended in 20 µl of sterile dH_2O.

2.2.3 Restriction enzyme digestion of DNA

All reaction mixtures prepared for restriction endonuclease digestion contained buffers recommended for use by the suppliers. The total volume of the digestion mixtures was between 10 and 30 µl, which included 2-4 units of enzyme per µg of DNA. The reaction mixtures were incubated for 2 h at 37 °C. To terminate the reaction a one-third volume of SBE loading buffer was added or the enzyme was inactivated at 75 °C for 15 min. The DNA was then analysed by gel electrophoresis. The standard reaction mixture used for digestion of small amounts of DNA is presented in Table 2.5. For digestion of larger amounts of DNA, the amount of enzyme, and therefore buffer, was increased, and the total reaction mixture adjusted with dH_2O.

Table 2.5 Standard reaction mixture for restriction endonuclease digestion of DNA. All digestions were performed at 37 °C, with the buffer recommended by the supplier.

Component	*DNA*	*Buffer*	*H_2O*	*Restriction Enzyme*	*Total volume*
Volume (µl)	*2*	*1*	*6*	*1*	*10*

If two enzymes were used, the sample was digested separately with each enzyme and the supplier's recommended buffer for 2 h. The mixture was microdialysed (Section 2.3.4) between digestions to reduce salt concentration from the previous buffer. This method proved more efficient than use of multipurpose buffers.

2.2.4 Agarose gel electrophoresis

To perform gel electrophoresis, 1.0-1.5 % (w/v) agarose gels, depending on the size of the fragments to be separated, were prepared and placed into a Bio-Rad gel tank containing 1.5 L of 1 × TBE buffer. Electrophoresis was run for ~ 2 h at 100 V. Gene Ruler 1 kb DNA ladder (Thermo Scientific) was used as size standards, this enabled the migration of the DNA to be matched to the fragment size (50 µg loaded). To visualise DNA, ethidium bromide was added to the agarose gel to intercalate and fluoresce the DNA. The gel was placed over a transilluminator for visualization of the DNA, which was photographed with a Polaroid CU-5 camera and 655 film (Polaroid) or Bio-Rad Gel doc™ EZ imager (Bio-Rad).

.

2.2.5 Recovery of DNA fragments from agarose gel

DNA fragments were agarose gel separated and recovered using the Eppendorf Perfectprep Gel Clean-up (Progen Biosciences). The DNA fragment of interest was extracted from the gel using a sterile razor blade and placed in a 1.5 mL microcentrifuge tube, the slice was weighed, and a maximum of 400 mg was used. Three volumes of binding buffer was added and the sample was incubated at 50 °C for ~10 min until the gel had melted. A volume of isopropanol equal to the original gel slice was added and the sample mixed by inverting the tube. A spin column was placed in a 2 mL collection tube, and 800 µl of the DNA mixture added. The assembly was centrifuged at 10, 000 × g for 60 s in a microcentrifuge so the DNA could come in contact with, and bind to, the glass fibre

membrane in the spin column. The filtrate was discarded. A sample larger than 800 µl was reloaded and the DNA loaded in the column as above. The supplied wash buffer was diluted in four parts absolute ethanol, and 750 µl of this diluted wash buffer was added to the spin column. The assembly was centrifuged at 10, 000 × g for 60 s to remove salts, organics and other contaminating. The assembly was then centrifuged again to remove any residual wash buffer. The column was placed in a new collection tube and 30 µl of the supplied elution buffer pipetted onto the middle of the column. The sample was centrifuged at 10, 000 × g for 60 s and the purified DNA collected in the tube. The purified DNA was free of salts, ethidium bromide, protein, agarose and organics and ready for down-stream applications. Purified DNA thus obtained was stored at -80 °C.

2.2.6 Phenol/chloroform extraction

For recovery of DNA to be used for other applications a modified phenol extraction method from (Ausubel, 1994) was used. The DNA band of interest was extracted from the agarose gel using a sterile scalpel and placed in a 1.5 mL microcentrifuge tube. The gel slice was suspended in 500 µl of phenol, mixed by vortexing, and the sample was placed at –70 °C for 30 min. The sample was then centrifuged at 17, 000 × *g* for 10 min in a bench top microcentrifuge. The supernatant was collected and an equal volume of phenol/chloroform/iso-amyl alcohol (24:24:1 (v/v/v)) was added and mixed by inverting the tube. The sample was centrifuged at 17, 000 × *g* for 10 min and the top aqueous phase collected. Two volumes of absolute ethanol and 0.1 volume of 5 M Na acetate (pH 4.8) were added to the supernatant to precipitate the DNA. The sample was incubated at –70 °C for 30 min and then the DNA was pelleted by centrifugation at 17, 000 × *g* for 10 min. The pellet was washed with 70 % ethanol to dissolve salts and then resuspended in an appropriate amount of TE buffer. The sample was centrifuged at 17, 000 × *g* for 10 min and the top aqueous phase collected and the DNA ethanol precipitated (Section 2.2.7).

2.2.7 Ethanol precipitation

For ethanol precipitation of DNA an adapted method from Current Protocols in Molecular Biology (Ausubel, 1994) was employed. Absolute ethanol (2.5 vol) and 3 M sodium acetate (0.1 vol) was added to the DNA solution to precipitate the DNA. The sample was incubated at –70 °C for 30 min and the DNA pelleted by centrifugation at 17, 000 × *g* for 10-30 min

at 4 °C. The supernatant was discarded and to remove residual salts and organic molecules the DNA pellet washed in 70 % (v/v) ethanol. The supernatant was removed and the pellet dried in a Speed-Vac set on low heat for 5-10 min. The pellet was resuspended in an appropriate amount of dH_2O or TE buffer and incubated at room temperature for 20 min for DNA to properly dissolve. The sample was then stored at – 20 °C until required.

2.2.8 DNA sequencing

Sequencing of plasmid DNA was performed by the Australian Genome Research Facility (AGRF), Brisbane, Queensland. Purified plasmid DNA (500-800 ng) was sent with 100 pmol of forward or reverse primer separately. Sequence analyses, alignments, and database searches were conducted using web-based software through dictyBase (http://www.dictybase.org), ExPASy (http://www.expasy.org), and the Australian Genome Research Facility (http://www.agrf.org.au).

2.2.9 Genomic DNA isolation

Genomic DNA (gDNA) from *Dictyostelium* transformants was extracted using DNAzol® gDNA Isolation Reagent (Molecular Research Centre). DNAzol is a reagent designed for the isolation of gDNA from solid and liquid animal and plant samples, therefore a modified procedure to the protocol supplied was used to extract total gDNA from *Dictyostelium*. Cultures were grown to a density of ~ 2×10^6 cells mL^{-1} and 1×10^7 cells were harvested by centrifugation at 500 × *g* for 5 min. The supernatant was removed and the pellet washed in 1 mL of sterile saline. To the pellet 1 mL of DNAzol was added (1 mL per 1×10^7 cells) and the sample gently mixed by inversion to avoid shearing of the DNA. The sample was incubated at room temperature for 2 min and the homogenate sedimented at 10, 000 × g for 10 min. The supernatant was transferred to a fresh centrifuge tube and the DNA ethanol precipitated (Section 2.2.7).

2.2.10 RNA isolation

Total RNA was isolated from *Dictyostelium* strains using TRIzol reagent (Ambion, Life Technologies). Cells were grown in HL5 medium at a density of 1-2 x 10^6cells mL^{-1} and 10^7 cells were harvested by centrifugation (500 × *g* for 5 min), resuspended in 1 mL of TRIzol

reagent and incubated at room temperature for 5 min to allow complete dissociation of nucleoprotein complexes. To the sample, 0.2 mL of chloroform was added and the solution mixed by vigorous shaking for 15 s then incubated at room temperature for 2-3 min. Samples were centrifuged at 12,000 × *g* for 15 min at 4 °C and the upper aqueous phase containing the RNA was transferred to a new tube containing 0.5 mL of ice-cold isopropyl alcohol to precipitate the RNA. The samples were incubated for 10 min at room temperature and RNA collected by centrifugation at 12,000 × *g* for 10 min at 4 °C. The RNA pellet was washed twice with 0.5 mL of 75 % (v/v) ethanol in DEPC-treated water followed by centrifugation at 7, 500 × *g* for 5 min at 4 °C. The pellet was air dried and the RNA was dissolved in RNAase-free (DEPC-treated) water.

2.3 Molecular manipulation of DNA

2.3.1 Polymerase chain reaction (PCR)

2.3.1.1 Standard polymerase chain reaction

To isolate the genes of interest PCR was used for *in vitro* amplification of the *D. discoideum* genes from AX2 $CsCl_2$ isolated gDNA using the primers outlined in Table 2.6. The reactions were carried out using 5 U of *Taq* DNA polymerase in 0.5 mL Eppendorf tubes containing 100 µl of reaction mixture with gene specific oligonucleotide primers. The PCR was carried out in a Minicycler apparatus (M. J. Research PTC-150). Conditions for each reaction mixture are shown in Table 2.7 and reaction protocol in Table 2.8.

2.3.1.1.1 Amplification of *Ddmucolipin* overexpression construct

To create a *Ddmucolipin* overexpression construct, the 2774 bp *Ddmucolipin* gDNA (dictyBase gene no. DDB_G0291275) was amplified in two sections from parental strain AX2 $CsCl_2$ isolated gDNA using the primers MUF and MuMR for the 1371 bp 5' fragment, and MuMF and MUR2 for the 1408 bp 3' fragment. Fragments were amplified using gene-specific primers incorporating restriction sites at the 5'end for cloning purposes.

2.3.1.1.2 Amplification of *Ddmucolipin* antisense inhibition construct

To create the *Ddmucolipin* antisense RNA (asRNA) 1411bp 3` fragment of the gene was amplified via PCR with the primers MuMF and MUR2 from AX2 gDNA.

2.3.1.1.3 Amplification of *Ddpolycystin* overexpression construct

To create a *Ddpolycystin* overexpression construct, the 2717 bp *Dictyostelium* polycystin homologue *Ddpolycystin* (dictyBase gene ID. DDB_G0272999), was amplified in two sections from AX2 gDNA with primers POLYF and PolyMR for the 1089 bp 5' fragment and using the primers PolyMF and POLYR for the 1628 bp 3' fragment.

2.3.1.1.4 Amplification of *Ddpolycystin* antisense inhibition construct

To create the *Ddpolycystin* asRNA an 803bp fragment cDNA was amplified via reverse transcription PCR with the primers POLYF and PolyMR from AX2 RNA.

2.3.1.1.5 Amplification of *pat3* antisense inhibition construct

To create the *pat3* asRNA a 1447 bp fragment of the gene was amplified via PCR with the primers SERCA2F and SE2MR from AX2 gDNA.

2.3.1.1.6 Amplification of *pat4* antisense inhibition construct

To create the *pat4* asRNA a1382 bp fragment of the gene was amplified via PCR with the primers SERCA1.AF and SE1MR from AX2 gDNA.

Table 2.6 Primer sequences for amplification of genes and gene fragments, shown in the 5' to 3' orientation. Primers included a short sequence CGC at the 5' end to provide "space" and a strongly annealed sequence for restriction endonucleases to bind and cut efficiently nearby. The restriction enzyme cut sites incorporated into the sequence and used for cloning are indicated in bold/bold underlined and listed below primer sequence.

Construct	**Primer name**	**Primer sequence**
Ddmucolipin overexpression/ *Ddmucolipin* antisense inhibition	MUF	CGC**GGATCCATCGAT***ATG*ACATCTTTTAAAGGTGACAG
		*Bam*HI *Cla*I
	MuMR	AACTAAC**GGTACC**AGGTACTTC
		*Kpn*I
	MuMF	GAAGTACCT**GGTACC**GTTAGTTC
		*Kpn*I
	MUR2	CGC**GGATCCCTCGAG**CATCATATC TCAATACCTGAATC
		*Bam*HI *Xho*I
Ddpolycystin overexpression/ *Ddpolycystin* antisense inhibition	POLYF	CGC**GGATCCATCGAT**ATGAATACATTAAAGAGGACAGT
		*Bam*HI *Cla*I
	PolyMR	CATATATAATT**GAATTC**TATAAGTTC
		*Eco*RI
	PolyMF	GAACTTATA**GAATTC**AATTATATATG
		*Eco*RI
	POLYR	CGC**GGATCCCTCGAG**TTAAGGTGTATTAGTACCACCA
		*Bam*HI *Xho*I
pat3 antisense inhibition	SERCA2F	GCG**GGATCC**ATCGATATGGTAAAATATCATTTTCAAGG
		*Bam*HI
	SE2MR	CCACTTAAT**GGTACC**TTTAATAATGC
		*Kpn*I
pat4 antisense inhibition	SERCA1.AF	GCG**GAATTC**TTCGAAATGAATAGAAATATTGATATAAATAAT
		*Eco*RI
	SE1MR	TAAGCGGTT**GAATTC**AAACTTATAC
		*Eco*RI

Table 2.7 PCR reaction mixtures for amplification of gene fragments

	***Ddmucolipin* antisense/ overexpression**	***Ddpolycystin* overexpression *pat3* and *pat4* antisense**	***Ddpolycystin* antisense**
Ingredients	**Volume (µl)**	**Volume(µl)**	**Volume(µl)**
MilliQ water	79	78	76.5
10 X PCR reaction buffer	10	10	10
$MgCl_2$ (50 mM)	4	6	5
dNTPs (10 mM)	2	1	1
Template DNA (~0.2 µg $µl^{-1}$)	2	2	5
Forward + Reverse primers (100 pmol $µl^{-1}$)	1+1	1+1	1+1
Taq polymerase (5 U $µl^{-1}$)	1	1	0.5
Total (µl)	100	100	100

Table 2.8 PCR reaction steps for PCR amplification

Step no.	**Reaction**	**Temperature(°C)/time**
1	Initial template denaturation	95/10 min
2	Template denaturation	95/1 min
3	Primer annealing	57/1 min
4	Primer elongation	72/1 min
5	Repeat cycle of step 2-4	40 X
6	Final primer elongation	72/10 min
7	Storage	4/24 h

2.3.1.2 Reverse transcription polymerase chain reaction (RT-PCR)

The DNA fragment used to create the *Ddpolycystin* asRNA plasmid construct was created by amplifying an 804 bp cDNA fragment of the gene via RT-PCR. The template was RNA extracted from vegetative AX2 cells using TRIzol® (Section 2.2.10) and cDNA synthesis was performed using the primer PolyMR. The RT reaction mixture and protocol is shown in Table 2.9. The cDNA produced from the RT reaction was used as a template for standard PCR with the primers POLYF and PolyMR (Table 2.6) as described in Section 2.3.1.1.

Table 2.9 Reverse transcription reaction mixture and protocol for cDNA synthesis of *Ddpolycystin* 5' fragment used to create asRNA construct.

	***Ddpolycystin* antisense**	***Reaction*** Denaturation and primer annealing	***Reaction*** cDNA synthesis	***Reaction*** Enzyme inactivation
Ingredients	**Volume (µl)**	**Temperature (°C)/time**	**Temperature (°C)/time**	**Temperature (°C)/time**
MilliQ water	2*	*heat components to 95 °C 5min cool gradually to room temperature and add remaining reaction components	42 °C 90 min	95 °C 5 min
Template RNA	2*			
3' primer (100 pmol μl^{-1})	2*			
dNTPs (10 mM)	4			
$MgCl_2$ (50 mM)	8			
5 X RT reaction buffer	5			
Reverse transcriptase (5 U μl^{-1})	1			
RNase inhibitor (2 U μl^{-1})	1			
Total (µl)	25			

2.3.1.3 Real time quantitative PCR (qPCR)

To determine the plasmid copy number of each transformant, DNA was extracted using DNAzol (Section 2.2.9) from approximately 10^7 cells, grown either axenically or on mass plates and washed free of bacteria. DNA was dissolved in MilliQ water containing 100 µg $µl^{-1}$ of RNaseA.

For each qPCR, two standard curves were made for which the nucleic acid concentrations of purified DNA was measured using absorbance at 260 nm in a spectrophotometer. The concentration was decided using the following formula:
Reading at 260 nm x dilution factor of DNA x 0.05 = X µg $µl^{-1}$.

The first standard curve was used as an internal control to enable absolute quantification of total genomic DNA in the reaction mixture. Six serial dilutions ranging from 100 ng-0.001 ng were made using purified AX2 gDNA. A portion of the filamin gene was used as the target amplicon for the internal control as it is a single copy gene in AX2 and has been successfully used in the laboratory for this purpose previously. The second standard curve was for the *Ddmucolipin* or *Ddpolycystin* genes, using maxi-preparations of construct pPROF646 for *Ddpolycystin* antisense, pPROF636 for *Ddpolycystin* overexpression, pPROF650 for *Ddmucolipin* antisense or pPROF638 for *Ddmucolipin* overexpression strains. The purified plasmid DNA was used to prepare serial dilutions of the target amplicon ranging from 100-0.001 ng. The primers used are outlined in Table 2.10.

Table 2.10 Primer sequences used in qPCR to amplify portions of the *filamin, Ddpolycystin* and *Ddmucolipin* genes respectively

	Primer	**Sequence 5' to 3'**
Ddpolycystin antisense and overexpression construct amplicon (fragment size 161bp)	PflagF POLY103R	CGCGGATCCAAGCTTATGAATACATTAAAGAGGACAGT CAACTGCTGCCAATAATGTTGC
Ddmucolipin antisense and overexpression construct amplicon (fragment size 135 bp)	MF1.1 MUR1.2	GATTGGTCTTGGTACTTTGTTA GGGAGACTTCCAGCCGAG
Filamin gene amplicon (fragment size 100 bp)	FIL1588F FIL1688R	CCCTCAATGATGAAGCC CCATCTAAACCTGGACC

For each reaction, 20 ng DNA was added to a 20 µl reaction mixture containing 1 x iQ SYBR Green Supermix (Bio-Rad) (containing dNTPs, 25 U mL^{-1} *iTaq*™ DNA polymerase, 3 mM $MgCl_2$, SYBR® Green I, 10 nM fluorescein, stabilizers and enhancers) and gene specific primers (10 pmol each). Duplicates were prepared for each sample and a negative control (no template) included by adding dH_20 instead of DNA. The qPCR was performed using an iCycler IQ Multicolor Real-Time PCR Detection System (Bio-Rad). The PCR protocol was carried out as stated in Table 2.8.

The calculation for copy number was based on the standard curves obtained for the filamin control and the gene of interest. The amount of DNA for each unknown sample was estimated using the average mean SQ (starting quantity) as duplicates were performed for each sample. Filamin estimated the total amount of DNA present and the

following formula was used to calculate copy numbers for target genes. This calculation yielded a primary, absolute estimate of the copy number.

Copy No. = (X/Y) x (60 x 10^6/F)

X= quantity of DNA fragment of interest (ng)

Y= quantity of total genomic DNA (ng)

F= fragment size of the amplified gene (bp)

60 x 10^6= approximate *Dictyostelium* genome size (bp)

2.3.1.4 Quantitative reverse transcription PCR (qRT-PCR)

RNA was extracted from 10^7 cells using Trizol reagent (Ambion, Life Technologies) (Section 2.2.10) and resuspended in 50 µl of DEPC treated MilliQ H_2O and treated with DNase I (Ambion) to remove any contaminating DNA in a reaction shown in Table 2.11.

Table 2.11 DNase I treatment of RNA sample

Ingredient	**Volume**
RNA	50 µl
DNase I (2U ul^{-1})	2 µl
10 X DNase I buffer1	6 µl
MilliQ H_2O	2 µl
Total	60 µl

RNA samples treated with DNase I were incubated at 37 °C for 1 h and the enzyme was inactivated by adding 0.1 vol of inactivation buffer and incubated at room temperature for 2 min. Samples were centrifuged at 10,000 × *g* for 2 min to pellet the inactivation reagent, the supernatant containing the RNA was transferred to a new tube and stored on ice. The qRT-PCR protocol provided by Bio-Rad was followed to measure mRNA expression levels in different strains. Iscript One Step RT-PCR kit with SyberGreen (Bio-Rad) was used to perform the qRT-PCR (Table 2.13). For each strain, duplicate reactions were prepared. An internal control was used to estimate total RNA in the sample by amplifying filamin in each RNA sample. To determine the relative expression of *Ddmucolipin*, *Ddpolycystin*, *pat3* and *pat4* in the transformants, portions of the target

genes were amplified using gene specific primers (For *Ddpolycystin* and *Ddmucolipin* see Table 2.10; For *pat3* and *pat4* see Table 2.12).

Table 2.12 Primer sequences used in qRT-PCR to amplify portions of *pat3* and *pat4* respectively

	Primer	**Sequence 5' to 3'**
pat3 (fragment 231 bp)	SERCA2F S2231R	GCGGGATCCATCGATATGGTAAAATATCATTTTCAAGG CCTCAAACCATTCCGCATATC
pat4 (fragment 135 bp)	SERCA1.AF S1135R	GCGGAATTCTTCGAAATGAATAGAAATATTGATATAAATAAT CCCTGATACACCTCCATATC

Table 2.13 Composition of master mix used in qRT-PCR reaction

Ingredient	**Volume**
MilliQ H_2O	17 µl
2 X SyberGreen Mix	25 µl
Forward primer (10 pmol)	2.5 µl
Reverse Primer (10 pmol)	2.5 µl
Iscript Reverse Transcriptase	1 µl
RNA	2 µl
Total	48 µl

A master mix was prepared and aliquoted into the wells of a 96 well plate which was kept on ice. For each reaction a negative control was included omitting the Iscript reverse transcriptase to ensure that sample did not contain gDNA contamination. 50-100 ng of RNA was added to each well and the reaction was performed in an iCycler IQ Multicolor Real-Time PCR Detection System (Bio-Rad) using the protocol (Table 2.14).

Table 2.14 qRT-PCR reaction steps

Step	Time/Temperature
1.cDNA synthesis	10 min/ 50 °C
2.iScript Reverse transcriptase inactivation	5 min/ 95 °C
3.PCR cycling and detection (35 cycles) a. Denaturation	 10 s / 95 °C
b. Primer annealing	30 s / 58 °C
c. Elongation	1 min/ 72 °C (data collection step)

2.3.1.5 Southern blotting to determine the plasmid copy number of *Ddmucolipin* overexpression strains

Genomic DNA was extracted from transformants using DNAzol® (Invitrogen). Quantitative Southern blot was used to estimate plasmid copy number of *mcln* overexpression strains (Fernando *et al.,* 2020). DNA loaded gels were stained with SYBR® Green I nucleic acid gel stain (Sigma-Aldrich®) and DNA was quantified using the Storm 860 Fluroimager (GE Healthcare, United Kingdom) in fluorescence mode. Southern blots of the same DNA samples were quantitated using fluorescein-labelled DNA probes, in conjunction with anti-fluorescein alkaline peroxidase conjugate antibody, and enhanced with the chemi-fluorescein substrate (GE Healthcare, United Kingdom). The Storm 860 Fluroimager fluorescence mode was used to quantitate Southern blots.

2.3.2 Dephosphorylation of linear plasmid vector DNA

Prior to vector/insert ligation during cloning experiments, linearized plasmid vectors were dephosphorylated to prevent circularization of vector DNA during cloning experiments. The 5′ phosphate groups were removed by incubation with thermosensitive alkaline phosphatase (Promega) at 37 °C for 1 h, and the enzyme inactivated at 70 °C for 10 min. The DNA was microdialysed before ligation to reduce the concentration of electrolytes (Section 2.3.4).

2.3.3 Ligation of vector and insert DNA

Both vector and insert DNA were digested with appropriate restriction enzymes (Section 2.2.3), agarose gel purified when necessary (Section 2.2.5), the vector dephosphorylated (section 2.3.2) (except for pZErO™-2) and microdialised (section 2.3.4) before ligation. The

ligation mixture contained a 1:3 molar ratio of vector to insert DNA. Ligations were performed in a total volume of 30 µl containing ligation buffer (1 X) and 1 µl of T4 DNA ligase ON at 16 °C for pA15GFP of 45 mins for pZErO™-2. The ligation reaction mixture was microdialysed before the transformation of electrocompetent *E. coli* cells (Section 2.3.4).

2.3.4 Microdialysis

All ligation reaction mixtures were microdialysed prior to electroporation to reduce salt concentrations that may result in shorting of the electroporation apparatus. Reaction mixtures were pipetted onto a small piece of 0.025 µm filter paper (Millipore), floating in sterile dH_2O. Samples were covered and microdialysed undisturbed for 1 h.

2.4 Transformation of *E. coli* cells with plasmid DNA

2.4.1 Preparation of electrocompetent cells

E. coli was grown ON in 5 mL of LB and then inoculated into 1 L of LB, and this was incubated at 37 °C with rapid shaking to an OD_{600} of 0.5-0.6. Cells were harvested via centrifugation in Sorval GSA bottles at 4, 500 rpm for 10 min at 4 °C. The pellet was washed twice by resuspending in 1 L and then 500 mL of ice-cold sterile water and centrifuged as above. The pellet was then washed in 20 mL of sterile ice cold 10 % glycerol. The final pellet was resuspended in 3 mL of 10 % (v/v) glycerol to a final density of approximately 3×10^{10} cells mL^{-1}, divided into 100 µl aliquots and stored at –70 °C.

2.4.2 Electrotransformation of *E. coli* cells

Electroporation of the *E. coli* cells was performed using a Bio-Rad Gene Pulser and Bio-Rad Gene Pulser *E. coli* Pulser cuvettes with a 0.2 cm gap. A 100 µl aliquot of electrocompetent cells was thawed on ice and 1 µg of plasmid DNA was added, this was placed into a pre-chilled electroporation cuvette. The moisture was removed from the cuvette which was then placed in the chamber of the Gene Pulser. The sample was pulsed at 2.5 kV, 25 µF and 200 Ω resistance. Immediately after electroporation, 1 mL of ice-cold SOC was added to the cells, which were then incubated with shaking at 37 °C for 1 h. Serial dilutions were prepared, and the cells plated onto LB agar plates containing either 25 µg mL^{-1} Kanamycin, or 100 µg mL^{-1} ampicillin, and incubated ON at 37 °C. Colonies were

picked and analysed by alkaline lysis mini prep (Section 2.2.2) and restriction enzyme analysis (Section 2.2.3)

2.5 Transformation of *D. discoideum* with plasmid DNA

A modified version of the calcium phosphate coprecipitation protocol developed by Nellen *et al.* (1984), was used for transformation of the *D. discoideum* strain AX2. A 50 mL culture of AX2 was grown axenically in HL5 medium at 21 °C with rapid shaking to a cell density of 1-3 x 10^6 mL^{-1}. Approximately 10^7 cells were dispensed onto a 9 cm tissue culture dish and allowed to settle for 1 h. The medium was then carefully replaced with 10 mL of MES-HL5, and the cells incubated for 1.5 h. Meanwhile, 50 µg of DNA, in 1.2 mL of 2 × *g* HBS, was precipitated by the drop-wise addition of 76 µl of 2 M $CaCl_2$ while vortexing, this mixture was incubated at room temperature for 25 min. The MES-HL5 medium was replaced by the precipitated DNA mixture and incubated for 30 min at which time 10 mL of MES-HL5 was added and the cells incubated for 6 h. The medium was removed and a glycerol shock was delivered to the cells by the addition of 2 mL of 18 % (v/v) glycerol in 1 × *g* HBS which was aspirated after 2-3 min before the addition of 10 mL HL5. The cells were allowed to recover in HL5 ON (~16 h) at 21 °C. Following recovery, the cells were resuspended and 1 mL was mixed onto each of 10, 2 day old *Micrococcus luteus* lawns on SM plates with 20 µg mL^{-1} G418 for selection of transformants. Transformants were observed, two weeks to one month later, as plaque like clearings in the lawns. Transformants were initially subcultured onto lawns of *E. aerogenes* with sterile toothpicks, and then purified to isolate single clonal colonies. Purified colonies were then inoculated into axenic medium HL5 with 100 µg mL^{-1} ampicillin, 100 µg mL^{-1} streptomycin and 15 µg mL^{-1} G418. These cultures were subcultured every four days to remove contaminating bacteria.

2.6 Phenotypic characterization

2.6.1 Growth on bacterial lawns

Lawns of *E. coli* B2 were prepared on normal agar (NA). 20 µl of *Dictyostelium* culture at a density of 1×10^6 cells mL^{-1}, was inoculated onto the center of each lawn and incubated at 21 °C for 100 h, during which time the plaque diameter (mm) was measured at intervals of 8-12 h. The recorded values were analyzed by linear regression using the "R" environment for statistical computing and graphics (http://www.R-project.org) to determine the plaque expansion rate (mm/h).

2.6.2 Growth in axenic medium

Dictyostelium cultures grown to exponential phase (`1-2 $\times 10^6$ cells mL^{-1}) in HL5 medium were used to inoculate 50 mL of fresh HL5 medium (no antibiotics) to an initial density of 1×10^4 cells mL^{-1}. Cultures were incubated at 21 °C on an orbital shaker at 150 rpm for 100 h, during which time cell densities were determined at 8-12 h intervals, by counting 10 µl aliquots using a hemocytometer. The cell densities were then analyzed by log-linear regression using the "R" programming environment computer software to determine the generation time from the exponential growth curve.

2.6.3 Morphology

Mature fruiting body morphology, after multicellular development, was scored as described previously (Kotsifas *et al.*, 2002). Transformants were cultured on lawns of *K. aerogenes* grown on SM agar plates, which were prepared by spreading 0.2 mL of a dense suspension in sterile saline, onto the surface of the plates. Once dry, amoebae were inoculated by picking and streaking a single plaque onto the lawns, and plates incubated at 21 °C for 4 – 6 d to allow growth and multicellular development. Photographs were taken from above and slices of agar were excised using a razor blade to observe fruiting bodies side on. Photographs were taken using Olympus SZ61 2300 steriomicroscope.

2.6.4 Measurement of LysoSensor™ Blue DND-167 stained cells

Cells were grown in HL5 medium to a density of 1-3 $\times 10^6$ cells mL^{-1}. An aliquot of 1×10^7 cells were harvested (700 $\times$ g for 2 min) and diluted 1:10 in Lo-Flo-HL5 containing 500 nM LysoSensor™ Blue DND-167 (Invitrogen) and incubated at 21°C shaking for 30 min. Cells were washed 2 times in 1 $\times$ PBS and resuspended to a density of 1×10^6 cells mL^{-1}. One mL of cells was diluted 1:2 in PBS and the fluorescence of the 2 mL sample measured in a

Modulus™ 9200-003 fluorometer (Turner BioSystems, Sunnyvale, CA) using the UV module kit 9200-041 (Ex. 365 nm, Em. 410-460 nm). For microscopy, the cells were washed twice with 1 X PBS, mounted in 80% glycerol and observed on an Olympus BX 61 microscope using a 100 X objective lens and the UV channel and images were captured using an Olympus U-CMAD3 camera.

2.6.5 Measurement of accumulation of autofluorescence medium and cellular autofluorescence

Cells were harvested and processed in the same manner as Section 2.6.4, however omitting the treatment with LysoSensor. Fluorescent readings of 1×10^6 cells were recorded immediately after 2 washes in $1 \times$ PBS with the UV module kit 9200-041. For readings of Lo-Flo-HL5 incubated cells, samples were incubated in Lo-Flo-HL5 for 30 min prior to washing and measurement.

2.6.6 Pinocytosis

Measurements of pinocytosis rates as described by Klein and Satre, 1986, were performed using fluorescein isothiocyanate (FITC)-dextran (Sigma-Aldrich; average mol. mass, 70 kDa; working concentration, 2 mg mL^{-1} in HL5 growth medium). Cultures of axenically growing *Dictyostelium* cells were harvested and resuspended in fresh HL5 medium at a density of $1.5–20 \times 10^6$ cells ml^{-1}. Cultures were shaken at 150 rpm for 30 min at 21 °C , and after the addition of FITC-dextran, 200 µl aliquots were transferred to 3 mL of ice-cold phosphate buffer (2 mM $Na_2HPO_42H_2O$ and 15 mM KH_2PO_4, pH 6.0) at the time points 0 and 70 min. Each sample was washed twice with ice-cold phosphate buffer, and just prior to measurement samples were lysed by addition of 2 mL of 0.25% (vol/vol) Triton X-100 in 100 mM Na_2HPO_4, pH 9.2. The fluorescence of the lysate, from duplicate samples at each time point, was measured in a Modulus fluorometer (9200-003 Turner Bio systems Turner BioSystems) using the green module. The cell density, increase in fluorescence over 70 min, and a separate calibration curve relating fluorescence signal to the volume of fluorescent medium, were used to calculate the hourly rate of uptake of medium per 10^7 cells.

ΔF = Difference in fluorescence over the course of the assay (fluorescence at $T_{70} – T_0$)

Uptake per cell ($nl\ h^{-1}$) = (ΔF x 10) / Total cell count ($cells\ mL^{-1}$) / time (h).

This number was multiplied by 10^7 to determine the volume (nl) of FITC-dextran-containing medium taken up by 10^7 cells per hour.

2.6.7 Phagocytosis

The rate of uptake of *E. coli* expressing the fluorescent protein DsRed (Maselli *et al*., 2002) was used to measure phagocytosis rates in *Dictyostelium* strains. DsRed-expressing *E*. *coli* (DsRed-Ec) cells were harvested from NB cultures (containing 75 µg mL^{-1} ampicillin and 1 mM IPTG), grown at 37 °C shaking for 24 h and resuspended to a density of $2 – 4 \times 10^{10}$ bacteria mL^{-1} in 20 mM Sorenson's buffer (2.353 mM $Na_2HPO_42H_2O$ and 17.65 mM KH_2PO_4, pH 6.3). The density and fluorescence of the bacterial culture in a given experiment, were used to determine the fluorescence signal per million bacteria. A separate calibration curve was used to determine the relationship between OD_{600} and the density of the bacterial suspension.

Cultures of *Dictyostelium* were harvested, washed, and resuspended in Sorenson's buffer at 1×10^6 cells mL^{-1} and starved for 30 min at 21 °C shaking. Duplicate 10 mL Falcon tubes (Sarstedt) containing 3 mL of 20 mM phosphate buffer and 5 mM sodium azide were set up for T_0 and T_{30} time points on ice. Following the 30 min incubation of the amoebae 1 mL of the prepared bacterial suspension was added and immediately two aliquots of 500 µl were removed and added to preprepared T_0 tubes. The vials were returned to the shaker and the DsRed-Ec uptake was allowed for 30 min. Amoebae in the T_0 samples were collected by centrifugation at 1, 000 × *g* for 30 s and cells washed with 20 mM phosphate buffer containing 5 mM sodium azide, resuspended in 3 mL of 20 mM phosphate buffer and counted using a hemocytometer. After 30 min of uptake duplicate aliquots of 500 µl were added to previously prepared T_{30} tubes. The T_{30} tubes were processed as T_0 tubes without the counting. A Modulus fluorometer 9200-003 (Turner Bio-Systems, Sunnyvale, CA, USA) fitted with a specially constructed module designed for DsRed-Ec (530-nm excitation and 580-nm emission) was used to measure fluorescence. Two mL of 0.25 % (v/v) Triton X-100 in Na_2HPO_4 was added to each tube, vortexed and fluorescence was measured. The increase in fluorescence over 30 min was used to calculate ingestion of DsRed-Ec cells per hour by a single amoeba.

ΔF (bacteria mL^{-1}) = difference in fluorescence over the course of the assay (fluorescence at $T_{30} - T_0$)

Uptake (bacteria $amoeba^{-1}$ h^{-1}) = ΔF x 10^6/ Total cell count (amoebae mL^{-1}) / time (h)

2.6.8 Spore germination assay

Dictyostelium strains were grown to a density of 1-2 x 10^6 cells mL^{-1} in HL5 medium. 10^7 cells were harvested (500 × g for 5 min) and washed 2 X in PBS. The cell pellet was resuspended in 50 µl PBS and pipetted in a 1 cm^2 area on non-nutrient agar and incubated at 21 °C until fruiting bodies had formed. The fruiting bodies were scraped using a sterile tip and resuspended in 1 mL PBS and washed 2 X in PBS (1, 000 × *g* 2 min) and then resuspended in PBS (0.1 % NP40 v/v) and incubated at 42 °C for 30 min to kill amoebae and activate spores. The spores were washed in 2 X in PBS and counted using a hemocytometer. Duplicate plates of 300 and 100 spores were plated onto SM agar by mixing with a thick slurry of *E. aerogenes* and evenly spreading onto the agar. Plates were incubated at 21 °C for ~ 3 days until spores had germinated and plaques had formed. Each plaque was assumed to have arisen from an individual spore. The number of plaques were counted, and the spore germination efficiency calculated.

2.6.9 Calcium experiments

2.6.9.1 *Dictyostelium* culture and development

Expression of the Ca^{2+}-sensitive luminescent protein apoaequorin, in each *Dictyostelium*, strain was used to measure cytosolic Ca^{2+} concentration ($[Ca^{2+}]_{cyt}$). *Dictyostelium* cultures were grown and allowed to develop as described by Nebl and Fisher (1997). Axenic cultures in HL5 medium were grown to a density of 1-2 × 10^6 cells mL^{-1}, and 1 × 10^8 cells were harvested, washed twice in 20 mL of MES development buffer (MES-DB) (10 mM MES/NaOH, pH 6.2, 10 mM KCl, 0.25 mM $CaCl_2$), and resuspended in either HL5 or MES-DB to a final density of 2 × 10^7 cells mL^{-1}. Cells were loaded with 5 µM coelenterazine-*h* (Invitrogen), a cofactor of aequorin, which had been prepared by dissolving 10 µg of lyophilized aequorin in 20 µl of the dispersing agent Pluronic F-127 (20 % (w/v) in methanol), and 200 µl H_2O. For *in vivo* reconstitution of aequorin 55 µl of prepared coelenterazine was used to load 10^8 cells, and 5 mL samples were incubated at 21 °C shaking at 150 rpm for 4 h (vegetative cells) or 6-7 h (aggregation competent cells).

2.6.9.2 Aequorin consumption and *in vivo* Ca^{2+} Measurements

All measurements were taken inside a Lumitran® model L-3000 photometer (New Brunswick Scientific). During all measurements, the cells were stirred at 100 rpm in 20 mL sample vessels placed in front of a photomultiplier. Dilutions of 1×10^{-2} and 1×10^{-3} were prepared in sterile saline from 5 mL cell aliquots. 500 µl of the 1×10^{-3} cell dilution was lysed by injection into 5 mL lysis solution (10 mM MOPS, 10 mM Ca-acetate, 1% Triton X-100, pH 7.0) causing a discharge of the total amount of aequorin, and therefore the total amount of light able to be produced by the cells. In the proceeding experiments, the amount of light emitted *in vivo* was processed as a fraction of the total amount that could be emitted. Luminescence signals were recorded from 5 mL cell suspensions stimulated with chemotactic stimuli delivered via injection of 50 µl of chemoattractant working stock solutions (cAMP, Folic Acid, Sigma Aldrich), to give a final concentration of 1 µm. The signal was captured by a model PCI-20428 multifunction I/O data acquisition board (Intelligent Instruments Pty. Ltd.). The signal was then converted into values of $[Ca^{2+}]_{cyt}$ on a PC using purpose designed software (Pr. P. R. Fisher), then analysed using software written in the 'R' programming language, a derivative of the 'S'-programming language for data analysis and graphical display (R Core Team, 2020).

2.7 Protein Analysis

2.7.1 Antibody production

To produce an antibody directed against Ddpolycystin a 134 aa portion of Ddpolycystin predicted to be located within the large loop between transmembrane one and two (aa66-aa199)
(PQSLFIINTSLKNQILFSQDSQYLEINNPSDFITYLNSTFCESISDMSLENNDAMNIIGNVIRIRTARVKP
DSCSNNGFNLTCYSNNYDKDTKDRSPFGPNDMYTYTSNSHGSYVFGHNQYVWDRSGYYIDIP),
called POECD, was expressed in *E. coli* and purified by GenScript®. To produce an antibody directed against Ddmucolipin a 200 aa portion of Ddmucolipin (aa101-aa301) (IFLQTGDLTVYSVGIEATWYNIFFPTDFQYEGDYGANIMYLYTINETISMIKDNLEAYNSLEDTSVNRF
QVYSPTNGDFSPPYNATMTIASYKHCDQVFDTSLVNANTATETIAYTISSDNLGPFQSYIDSGSGND
NDNDSNSNSNSGNHNSETIQQLFYCMSEMKVKYSFTNVHLQYEHPVAYLWDVYVIFNNIEQAGR),
called MUECD, was expressed in *E. coli* and purified by Genscript®. The peptides were

used to raise the anti-POECD and anti-MUECD antibodies in rabbits by the Institute of Medical and Veterinary Science (Adelaide, South Australia, Australia). Serum was affinity purified against purified protein as described previously (Smith *et al*., 1984). 500 µg of protein (POECD or MUECD) was diluted in 5000 µl PBS and used to coat small pieces of nitrocellulose membrane 0.45µm pore size (Thermo scientific) by incubation at 4 ˚C ON. The membrane was then incubated in PBS (3 % BSA) for 1 h and washed 6 X in PBS (0.1 % BSA). Eight mL of rabbit serum diluted in 2 mL PBS was added to the membrane and incubated at 4 °C ON. The membrane was washed 3 X in TBS (0.1 % BSA) and then 2 X in TBS (0.1 % BSA, 0.1 % NP40) and then 3 X in TBS (0.1 % BSA). The membranes were incubated with 600 µl 0.2 M glycine-HCl pH 2.5 for 1 min and immediately after neutralized by transferring to 300 µl 1M Tris pH 8 (5 % BSA) on ice. The purified antibody was preserved by adding 5 mM Na-azide.

2.7.2 Western blot

2.7.2.1 Protein extraction and estimation of total protein concentration

Dictyostelium strains were grown to a density of 1-2 x 10^6 cells mL^{-1} in HL5 medium. Cells were harvested (1500 × g for 2 min), washed 2 X in PBS and the cell pellet diluted in 1 X SDS lysis buffer (0.125 M Tris hydrochloride, 10 % glycerol, 4 % SDS) with a protease inhibitor cocktail (Complete-EDTA free, Roche) at a concentration of 2 x 10^5 cells $µl^{-1}$. The protein lysates were centrifuged at 13, 000 × *g* for 5 min and quantified using the Qubit™ Protein Assay Kit and Qubit 2.0 Fluorometer (Thermo Scientific).

2.7.2.2 SDS page gel electrophoresis and Western blotting

2.7.2.2.1 Ddpolycystin Western blots

Protein lysate of 30 µg were prepared by the addition of 5 % 2-mercaptoethanol and 0.001 % bromophenol blue. Samples were incubated at 37 °C for 1 h in order to reduce aggregation of the integral membrane proteins and prevent them adhering to the plastic tube, and then centrifuged at 13, 000 × *g* for 5 min. Proteins were separated by SDS-PAGE using the TGX Stain-Free, Fast Cast, Acrylamide Kit- 12 % (Bio-Rad, 161-0185) gel at 200 V for ~ 1.5 h in cold 1 X TGS running buffer (Bio-Rad). Band sizing was achieved by running the Precision-Plus Protein™ Dual-Colour Standards (Bio-Rad, 161 0374). Gels were imaged and activated on the Bio-Rad GelDoc™ EZ Imager and band analysis performed with Image-Lab 6.0 software (Bio-Rad). Proteins were transferred to PVDF-membrane (0.45 µm

pore, Amersham Hybond™-P, GE 7 Healthcare) preactivated in methanol using the Bio-Rad Trans-Blot® Turbo™ Semi Dry Transfer System using transfer buffer (25 mM Tris, 192 mM glycine, 20 % (v/v) methanol, 0.1 % SDS (pH 8.3)) at 25 V, 1.0 A for 30 min. The membrane was then rinsed in methanol and blocked in 1 X TBS (1 % BSA) ON at 4 °C. The membrane was then incubated with primary antibody, (rabbit) anti-POECD 1:100 ON at 4 °C. Unbound antibody was removed by washing the membrane 4 X in TBS (0.1% Tween-20) for 10 min, and then incubated at room temperature for 1 h with the secondary antibody, either (goat) anti-rabbit Alexa-Fluor 800 labelled secondary antibody (Invitrogen) 1:5000, or anti-rabbit alkaline phosphatase conjugate (1:5000) (GE Healthcare). Unbound secondary antibody was removed by washing the membrane 4 X in TBS (0.1% Tween-20) for 10 min. Membranes were imaged using the Bio-Rad ChemiDoc™ MP to visualise Alexa-Fluor 800. Membranes incubated with anti-rabbit alkaline phosphatase conjugate were then incubated with ECF™ substrate (GE Healthcare) for 5 min prior to imaging on a Storm 860 Gel and Blot Imaging System (Amersham) for detection of chemifluorescence. Gel analysis and band quantification was achieved using Image-Lab 6.0 software (Bio-Rad).

2.7.2.3.2 Ddmucolipin Western blots

Cells were grown in HL5 medium and 1 x 10^6 cells were lysed in 100 µl 1 x Bolt LDS sample buffer (Thermo Fisher Scientific) with a protease inhibitor 1 cocktail (Complete-EDTA free, Roche) on ice for 30 min then centrifuged at 1000 × *g* for 2 mins. 10 µl of lysate was with 1 % Bolt sample reducing agent (Thermo Fisher Scientific) was incubated at 70 °C for 10 min then loaded onto a Bolt™ 4 to 12 %, Bis-Tris-Plus, 1.0 mm, Protein Gel, 12-well (Invitrogen) alongside the Broad Multi Color Pre-Stained Protein Standard (GenScript®) and subject to electrophoresis. The gel containing protein was either stained with 0.25 % Coomassie brilliant blue (Bio Rad) for 1 h and subsequently destained (5% MeOH, 7.5% Acetic Acid) to visualise the protein bands, or protein was transferred to PVDF membrane (Amersham Hybond™-P, GE Healthcare) at 100 V, 4 °C for 1 h. Protein was visualised on the membrane by staining with No Stain Protein Labelling Reagent (Invitrogen) as per the manufacturer's instructions, and visualised on a Bio Rad Chemidoc MP imaging system. Membranes were then blocked with 1 % casein in 1 X TBS-T for 3 h at room temperature and probed with the primary antibodies 1:500 in blocking buffer, either polyclonal rabbit anti-MUECD or polyclonal rabbit anti-100310-1-PACDdmucolipin for 2 h at room

temperature. The SNAP i.d.® 2.0 Protein Detection System was used for application of anti-rabbit HRP conjugate (Life Technologies) 1: 10,000 in TBS-T as per manufacturer's instructions. Bands were detected with Clarity Western ECL substrate (Bio-Rad), with chemiluminescence imaged on Amersham Imager 600 (GE healthcare). The intensities of the total loaded protein and specific antigen bands were quantified digitally using the Image Quant TL 1D v 8.1 software 19 (GE Healthcare Life Sciences).

2.7.3 Immunofluorescence microscopy

2.7.3.1 Ddpolycystin Immunofluorescence microscopy

The two-step labelling method described by Vernary and Cosson (2013) was used to visualise Ddpolycystin, H36 and calnexin in AX2 cells. AX2 cells were grown in HL5 medium and ~1 x 10^6 cells were harvested, washed and transferred onto sterile cover slips in six-well costar plates (Nunc™) and allowed to attach at 21 °C for 1 h. The medium then was replaced with Lo-Flo-HL5 at 21 °C for 1 h. The Lo-Flo-HL5 was removed by washing 2 X with PBS (0.05 % BSA) and cells fixed by adding 4 % liquid paraformaldehyde for 10 min at room temperature. The cells fixed to the cover slips were washed 2 X with 20mM NH_4Cl in PBS and then 2 X with PBS. To label the surface antigens the coverslips were incubated with (rabbit) anti-POECD and/or (mouse) H36 diluted 1:100 (~2 µg mL^{-1}) in blocking buffer at 4 °C ON. Unbound antibody was removed by washing washed 2 X with PBS (0.05 % BSA). Cells were fixed again with 4 % liquid paraformaldehyde for 10 min at room temperature and then washed 2 X with 20 mM NH_4Cl in PBS and then 2 X with PBS. To enable labelling of internal cellular structures cells were then permeabilised with pre-chilled (-20 °C) methanol for 2 min and washed again 4 X with PBS (0.05 % BSA). The coverslips were incubated with (rabbit) anti-POECD, and/or (mouse) H36 diluted, and/or (mouse) anti-calnexin (270-390-2 was deposited to the DSHB by Gerisch, G., DSHB Hybridoma Product 270-390-2) 1:100 (~2 µg mL^{-1}) in blocking buffer at 4 °C ON. Coverslips were washed 2 X with PBS (0.05 % BSA) and then incubated with secondary antibodies (goat) anti-rabbit Alexa-Fluor®594 (Invitrogen, A11012) and (donkey) anti-mouse Alexa-Fluor®488 (Invitrogen, A21202) 1:1000 in blocking buffer at room temperature for 1 h. Coverslips were washed 2 X with PBS (0.05 % BSA) and then 1 X in milliQ H_20 and mounted and visualised as stated above.

2.7.4 Mass spectrometry identification of proteins in Bis-Tris-Plus gel slices.

Cells were grown in HL5 medium and 1×10^6 cells harvested and lysed in 100 µl 1 × Bolt LDS sample buffer (Thermo Fisher Scientific) with a protease inhibitor 1 cocktail (Complete-EDTA free, Roche) on ice from 30 min then centrifuged at 1200 rpm for 2 mins. 10 µl of lysate was with 1% Bolt sample reducing agent (Thermo Fisher Scientific) was incubated at 70°C for 10 min then loaded onto a Bolt™ 4 to 12%, Bis-Tris-Plus, 1.0 mm, Protein Gel, 12-well (Invitrogen) with the Broad Multi Color Pre-Stained Protein Standard (Genscript) and subject to electrophoresis. The gel containing protein was stained with 0.25 % Coomassie brilliant (Bio Rad) blue for 1 h and subsequently destained (5% MeOH, 7.5% Acetic Acid) to visualise the protein bands. Protein bands at ~120 and ~95 kDa were excised using a sterile scalpel and placed in 100 µl of sterile milliQH_2O. The proteins contained in the bands were identified by mass spectrometry at the La Trobe University-Proteomics and Metabolomics Platform according to the protocol described in Appendix 7.

Chapter three

Ddpolycystin and its role in *Dictyostelium*

3.1. Introduction

3.1.1 Polycystin-2

Polycystin-2 (PC2) is a member of the superfamily of TRP channels of which homologues have been studied in *Caenorhabditis elegans*, *Drosophila*, mice and human models. In mammals PC2 localises to the plasma membrane (Luo *et al*., 2003, Ma *et al*., 2005), primary cilium of kidney cells (Nauli *et al*., 2003, Pazour *et al*., 2003) and ER (Cai *et al*., 1999, Koulen *et al*., 2002), and is responsible for Ca^{2+} release, both intracellular and from the extracellular, as a mediator of sensory signalling. PC2 is an integral membrane protein comprising 6 TMD with cytoplasmic amino- and carboxyl-termini (Mochizuki *et al*., 1996). Patch clamping experiments have revealed that the channel is a non-selective cation channel with high permeability to Ca^{2+} (Hanaoka *et al*., 2000; González-Perrett *et al*., 2001;). PC2 contains an ER retention signal (Cai *et al*., 1999) and an EF-hand Ca^{2+} binding motif in the C terminal (Qian *et al*., 1997) which is thought to play a role in Ca^{2+} dependent activation of the channel (Schumann *et al*., 2009; Petri *et al*., 2010; Celic *et al*., 2012). Cytoplasmic Ca^{2+} concentration regulates the open probability of the channel and phosphorylation at Ser^{812} is important for Ca^{2+} stimulated activation (Cai *et al*., 2004).

PC2 complexes with polycystin-1 (PC1), an integral membrane mechanosensitive receptor that responds to fluid stress in the primary cilium and induces Ca^{2+} influx into the cytoplasm through PC2 (Hanaoka *et al*., 2000). This Ca^{2+} signal is then enhanced by release from the ER via PC2 (Liu *et al*., 2003, Nauli *et al*., 2003) to control Ca^{2+} regulated signaling processes. Furthermore, PC2 also interacts with other intracellular Ca^{2+} channels such as the InsP3 receptor of the ER and ryanodine receptor of the SR (Li *et al*., 2005; Anyatonwu

et al., 2007; Sammels *et al*., 2010) to regulate Ca^{2+} signaling. Both PC1 and PC2 are implicated in autosomal dominant polycystic kidney disease (ADPKD), a common high mortality inherited disorder, characterized by renal and hepatic cysts which in 50 % of patients leads to end stage renal disease (Wu *et al*., 1998). More than 95% of cases are linked to mutations in PC1 (Roitbak *et al*., 2004), however mutations in PC2 also cause the disease (Wu *et al*., 1998). Many ADPKD cells have reduced intracellular Ca^{2+} concentrations (Qian *et al*., 2003; Yamaguchi *et al*., 2006; Morel *et al*., 2009; Spirli *et al*., 2012; Zaika *et al*., 2013), which is thought to be linked to increased cAMP levels that induce fluid secretion and stimulate MAPK/ERK signaling pathways to enhance cell proliferation (Yamaguchi *et al*., 2004). The result is uncontrolled cell proliferation and accumulation of fluid filled cysts (Ye and Grantham, 1993). Wilczynska *et al*. (2005) reported a homologue of PC2 in *Dictyostelium* (Ddpolycystin), since then limited studies have begun to investigate the function of Ddpolycystin in this model organism, however much more work needs to be done to determine its physiological role and particularly Ca^{2+} channeling properties.

3.1.2 Calcium signalling and Ddpolycystin in *Dictyostelium*

Dictyostelium is a simple and useful model for studying the molecular mechanisms behind disease pathogenesis and protein function, therefore could be used to further knowledge into the molecular functions of PC2. Ddpolycystin, shares 46% protein similarity to the human PC2, is predicted to have 6 TMD, conserved pore region between TM 5 and 6, and the conserved c-terminal coiled-coil domain. Ddpolycystin lacks the EF-hand motif and ER retention signal seen in mammalian PC2 (Lima *et al*., 2014). FLAG-tagged Ddpolycystin localized the protein primarily to the plasma membrane where it colocalised with the plasma membrane marker H-36, and some colocalization was observed with recycling and early endocytic compartments (Lima *et al*., 2014). ER localisation has not been determined-no marker for the ER was used to check for colocalization- therefore it is yet to be determined if Ddpolycystin is also present at the ER, however lack of an ER retention signal suggests not likely. It is evident that the role of Ddpolycystin in *Dictyostelium* is related to Ca^{2+} regulation. Ddpolycystin KO strains are defective in Ca^{2+} induced lysosomal

exocytosis suggesting that it contributes to the cytosolic calcium release that regulates this process (Lima *et al*., 2014). Additionally, Ddpolycystin may be associated with Ca^{2+} signalling associated with rheotaxis (Lima *et al*., 2014), although this phenotype was not reproducible (Artemenko *et al*., 2016; Traynor and Kay 2017). Ddpolycystin KO strains are defective in cytosolic Ca^{2+} influx in response to ATP and ADP, however these KO strains still retained responses to cAMP and folic acid (Traynor and Kay 2017). It is unknown how Ddpolycystin function is regulated, it might be gated by the putative PC1 homologue encoded in the *Dictyostelium* genome (dictyBase gene ID: DDB_G0289409), however this has not been studied. It could also potentially interact with IplA to contribute to Ca^{2+} signalling events, as PC2-$InsP_3$ interactions have been reported in mammalian cells (Li *et al*., 2005; Sammels *et al*., 2010). Obviously further studies will need to be conducted to clarify the role of Ddpolycystin in Ca^{2+} signalling and its mode of action.

In this chapter the role of Ddpolycystin was investigated by analysis of phenotypic readouts in knockdown (KD) (asRNA inhibited) and overexpressing Ddpolycystin strains with a focus on characterizing the role of Ddpolycystin in chemotactic Ca^{2+} signaling. While it has been reported that Ddpolycystin KO cells still retain calcium responses to cAMP and folic acid (Traynor and Kay, 2017), this does not exclude the possibility of Ddpolycystin contributing to these Ca^{2+} responses given the overlapping and redundant functions of many calcium channels and pumps. It is also pertinent to attempt to confirm these results using a different experimental technique. This is of particular importance given the discrepancies surrounding phenotypes in Ddpolycystin KO strains between laboratories. Furthermore, I have used a knockdown and overexpression system, rather than KO cells, to assess the phenotypes. This allowed me to correlate phenotypic readouts with copy number of the constructs. This approach involves larger samples of independently isolated mutant strains, offers the possibility of regression analysis of phenotype versus copy number, and the reduced likelihood of off-target unknown genetic events influencing the outcome. For these reasons, it can be more sensitive in detecting any small phenotypic abnormalities, that may not be detected in analysis of knockout strains.

My work has confirmed the subcellular localisation of Ddpolycystin at the plasma membrane, as previously reported (Lima *et al*., 2014) and discovered that, in my strains, Ca^{2+} homeostasis is perturbed when Ddpolycystin is knockdown and overexpressed, as

are the Ca^{2+} responses to the attractants, cAMP and folic acid. These alterations in Ca^{2+} signaling also impacted on other downstream Ca^{2+}-sensitive processes such as stalk cell differentiation, growth, endocytosis and sporulation. My results show that Ddpolycystin functions as a plasma membrane-resident Ca^{2+} channel, and provides evidence that this channel contributes to cytosolic Ca^{2+} signaling in response to chemotactic stimuli. The following describes the results of the phenotypic characterization.

3.2 Results

3.2.1 Creation of Ddpolycystin constructs

In order to achieve knockdown and overexpression of the Ddpolycystin protein, plasmid constructs for asRNA inhibition and overexpression of *Ddpolycystin* were created using the two-phase cloning method. This two-phase cloning strategy involved firstly cloning the gene of interest into a small bacterial vector, and subsequently excising the gene and subcloning it into the larger *D. discoideum* expression vector. This method was adopted to increase cloning efficiency because attempting to clone PCR fragments that may not have been efficiently digested at restriction sites close to the ends of the fragments is often difficult. Excision of the fragment from the bacterial vector will produce an abundance of cut ends, and therefore increased cloning efficiency when ligating with large AT-rich *D. discoideum* expression vectors.

3.2.1.1 *Ddpolycystin* antisense inhibition construct

3.2.1.1.1 First phase cloning into an *E. coli* vector

To facilitate inhibition of protein expression, a fragment of the target gene is cloned into a *D. discoideum* expression vector in the antisense orientation. This vector is then introduced into the cells via transformation where it will randomly insert into the genome. Multiple copies of the construct are generated in tandem during the process of co-insertional rolling circle replication (Barth *et al.*, 1998). This will result in each individual transformant expressing different numbers of the plasmid insert, which can range dramatically from, less than 10 to more than 1000, and are stably expressed in the transformant under antibiotic selection. When expressed, the asRNA will bind to the

complementary mRNA expressed from the endogenous gene and target the double stranded RNA for degradation by RNases in the asRNA pathway. Therefore there is a reduction in the amount of mRNA that is able to be expressed as protein, thus reduction in protein levels (Kuhlmann *et al*., 2006).

To produce an asRNA inhibition construct that will decrease expression of *Ddpolycystin*, an 803bp fragment of *Ddpolycystin* cDNA was amplified via RT-PCR with the primers POLYF and PolyMR (Section 2.3.1.2), using RNA extracted from vegetative AX2 cells as a template. The product was then cloned into the *E. coli* vector pZErO2 using the endonuclease restriction cut sites *Bam*HI and *Eco*RI to create the construct pPROF645, which was verified by sequencing. The schematic representation of the cloning strategy is shown in Figure 3.1.

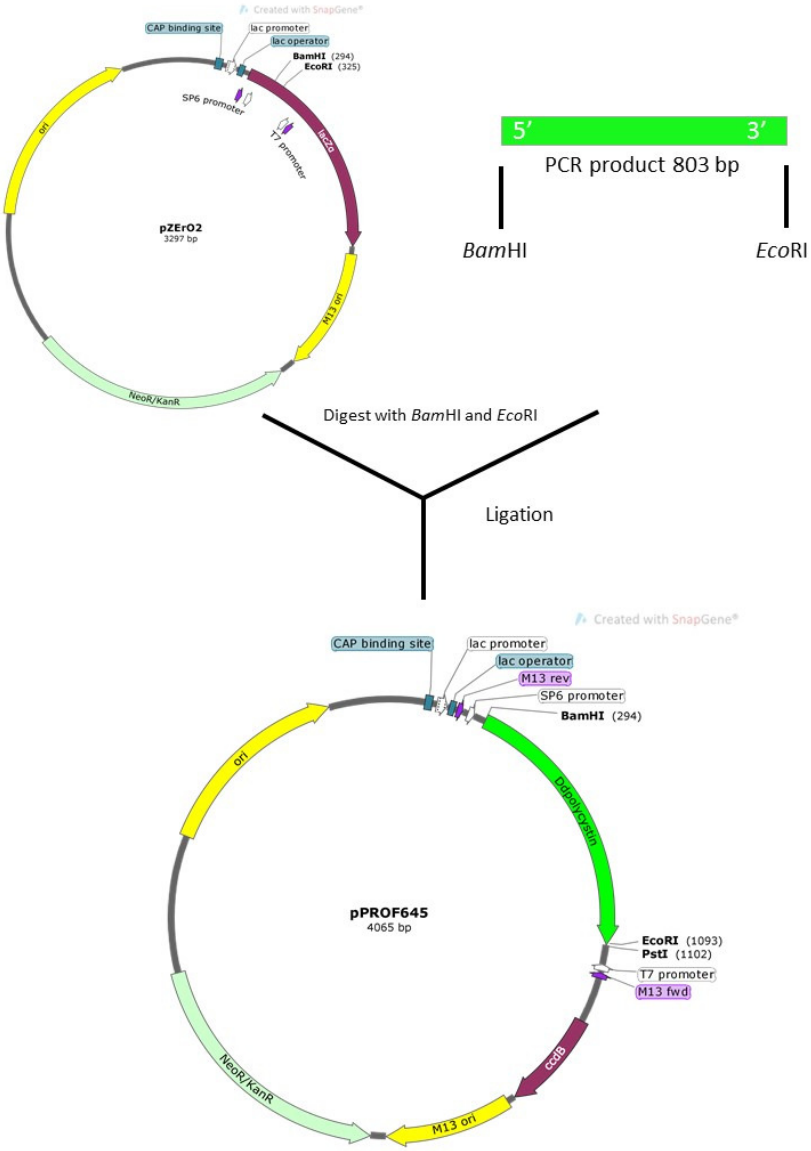

Figure 3.1 Cloning strategy phase one – *Ddpolycystin* antisense construct.

The *Ddpolycystin* cDNA fragment (803 bp) was RT-PCR amplified from AX2 RNA using primers POLYF and PolyMR. The amplified fragment was inserted into the *Bam*HI/ *Eco*RI sites of the *E. coli* vector pZErO™-2. The ligation product was electroporated into *E. coli* Top10 cells and colonies were selected for using kanamycin resistance. Colonies were further screened using restriction analysis of miniprep DNA from cultures grown from individual colonies. The resulting construct pPROF645 was confirmed via sequencing.

3.2.1.1.2 Subcloning of the *Ddpolycystin* antisense fragment into a *D. discoideum* expression vector

The 803 bp fragment of *Ddpolycystin* cDNA was excised from pPROF645 using the restriction endonuclease cut sites *Bam*HI and *Pst*I and subcloned in the antisense orientation into the *Dictyostelium* expression vector pDNeo2. The resulting construct, pPROF646, was verified by restriction enzyme digest. The schematic representation of the cloning strategy and restriction enzyme analysis is shown in Figure 3.2.

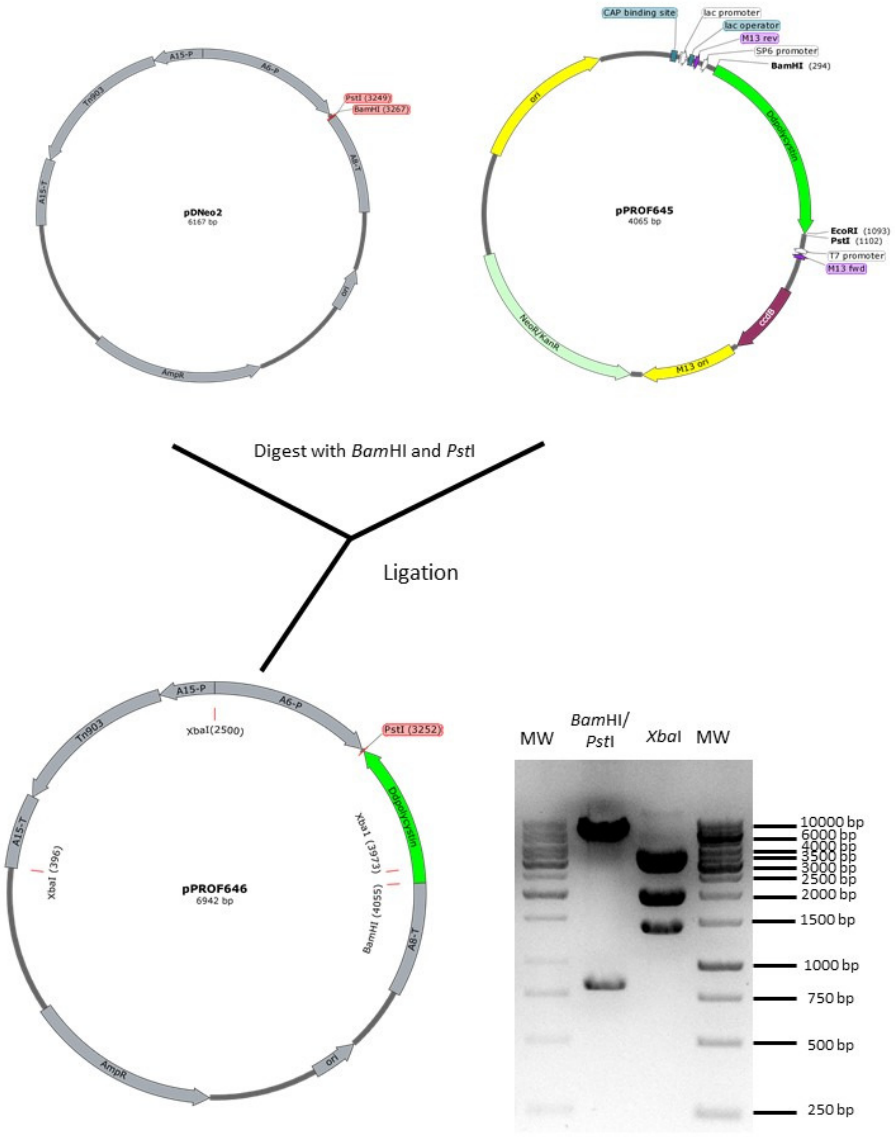

Restriction enzyme analysis – *Ddpolycystin* antisense construct pRPOF646

Construct name	Restriction enzymes	Expected fragments size (bp)
pPROF646	BamHI/PstI	6139 bp + 803 bp
	XbaI	3365 bp + 2014 bp + 1473 bp

Figure 3.2 Cloning strategy phase two – *Ddpolycystin* antisense inhibition construct.

The 803 bp *Ddpolycystin* fragment from pPROF645 was excised and subcloned in the antisense orientation into the *D. discoideum* expression vector pDNeo2 using the endonuclease cut sites *Bam*HI and *Pst*I. The ligation product was electroporated into *E. coli* DH5α cells, and colonies were selected on ampicillin. Plasmid miniprep DNA from individual colonies was extracted and screened by restriction analysis. The resulting construct pPROF646, was verified by restriction enzyme analysis as shown in the gel Image, the expected band sizes are indicated in the table.

3.2.1.2 *Ddpolycystin* overexpression construct

3.2.1.2.1 First phase cloning into an *E. coli* vector pZErO-2

To create a construct that will increase expression of *Ddpolycystin,* the gene was cloned into a *D. discoideum* overexpression vector. The 2717 bp gDNA fragment was amplified by PCR in two sections using AX2 genomic DNA as a template using the primers POLYF and PolyMR for the 1089 bp 5'section and PolyMF and POLYR for the 1628 bp 3'section. A three fragment ligation allowed the full length gDNA to be cloned into the bacterial vector pZErO-2 (Invitrogen, Carlsbad, CA) using the 5' and 3' restriction site *Bam*HI introduced into the sequence through the primers, and utilization of a resident *Eco*R1 restriction site within the gene sequence to allowed in-frame ligation of the 5' and 3' gene fragments. The resultant construct pPROF635, was verified by sequencing. The schematic representation of the cloning strategy is shown in Figure 3.3.

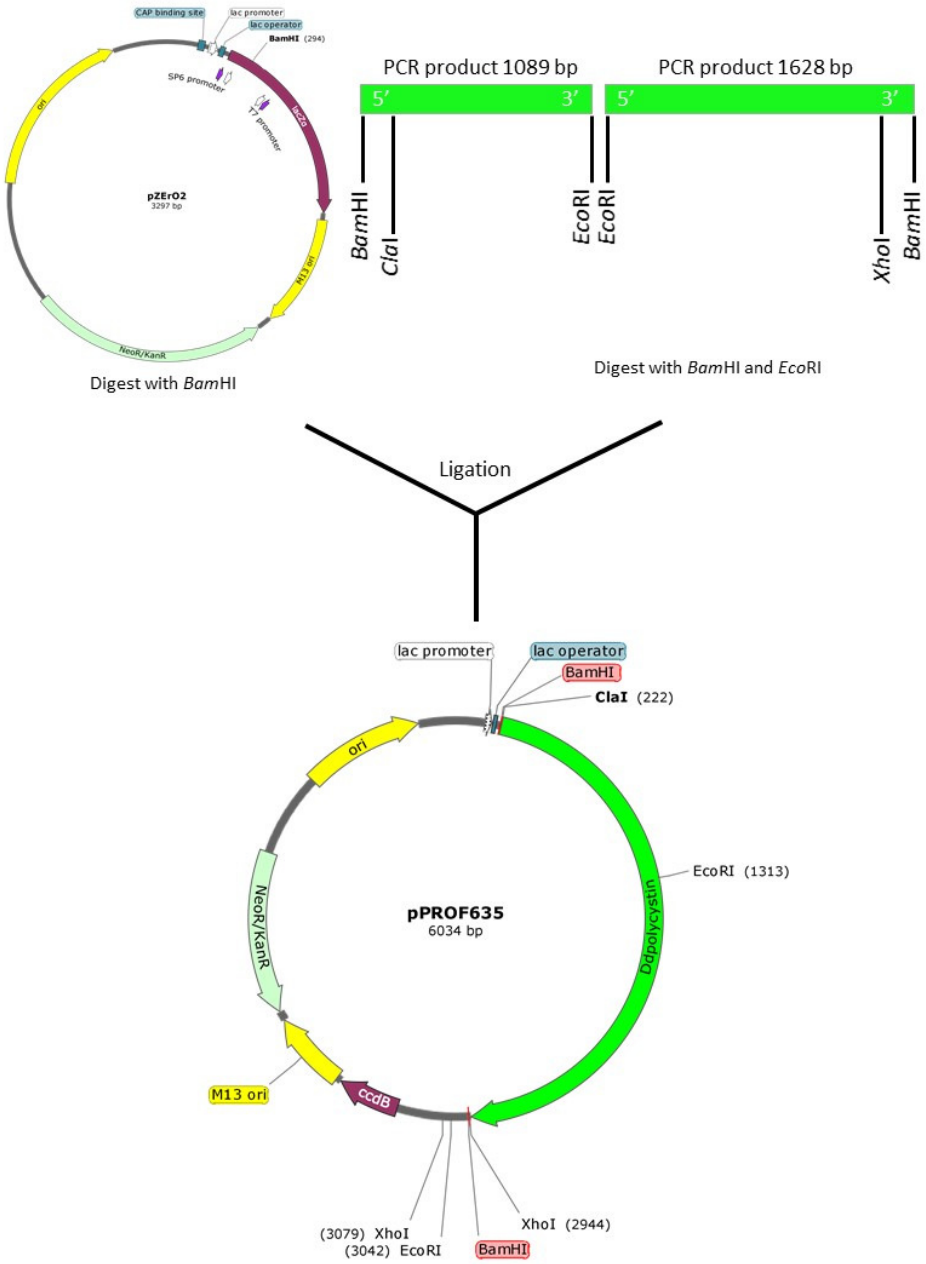

Figure 3.3 Cloning strategy phase one–- *Ddpolycystin* overexpression construct.

Two sections of *Ddpolycystin* gDNA were amplified from AX2 gDNA in two sections using primers POLYF and PolyMR for the 5'section and PolyMF and POLYR for the 3'section. A three fragment ligation allowed the full length gDNA to be and cloned into the bacterial vector pZErO-2 using the restriction site *Bam*HI, and utilization of a resident *Eco*RI restriction site within the gene. The *Cla*I and *Xho*I restriction enzyme cut sites were introduced in the primers to facilitate subcloning of the gene. The ligation product was electroporated into *E. coli* Top-10 cells and colonies were selected on kanamycin resistance. Individual colonies were screened further via restriction analysis of miniprep DNA. The resulting construct pPROF635 was confirmed via sequencing.

3.2.1.2.2 Subcloning *Ddpolycystin* into a *D. discoideum* expression vector

The full length *Ddpolycystin* gene was excised from pPROF635, subcloned into the *D. discoideum* expression vector pA15GFP using the *Xho*I and *Cla*I restriction enzyme sites and named pPROF636. The construct was verified by restriction enzyme digestion. The schematic representation of the cloning strategy is shown in Figure 3.4.

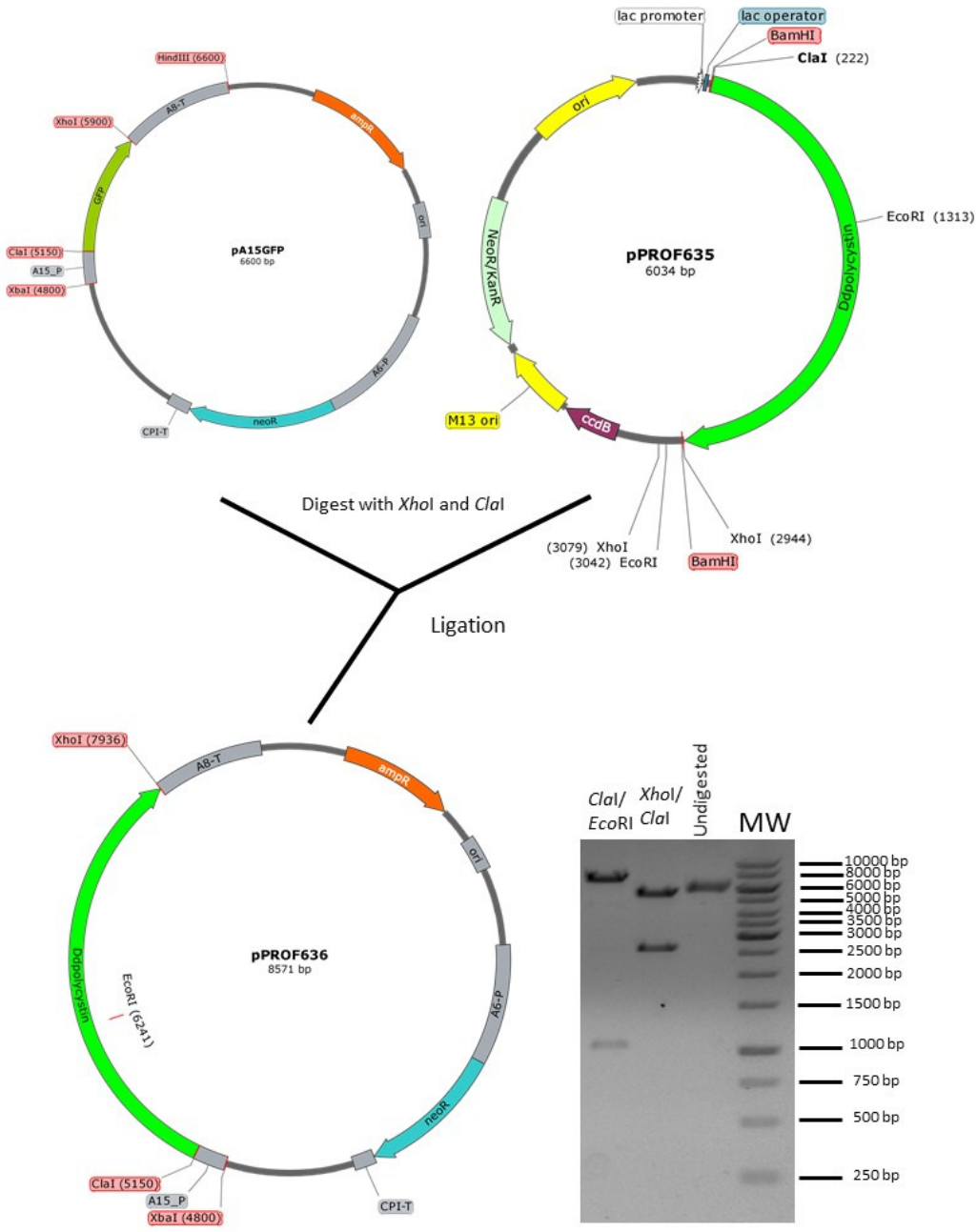

Restriction enzyme analysis – *Ddpolycystin* overexpression construct pRPOF636

Construct name	Restriction enzymes	Expected fragments size (bp)
pPROF636	XhoI/ClaI	5849 bp+2722 bp
	ClaI/EcoRI	7480 bp + 1091 bp

Figure 3.4 Cloning strategy phase two–- *Ddpolycystin* overexpression construct.

The cloned full length *Ddpolycystin* gene from pPROF635 was excised and subcloned into *D. discoideum* expression vector pA15GFP using *Xho*I and *Cla*I sites in sense orientation. The ligation product was electroporated into *E. coli* JC11451 cells and colonies were selected on ampicillin. Plasmid DNA was extracted from individual colonies and screened using restriction enzyme analysis. The resulting construct pPROF636 was verified with restriction enzyme digest depicted in the gel image, the expected DNA fragment sizes are indicated in the table.

3.2.2 Genetic manipulation of *Ddpolycystin* expression by transformation of *D. discoideum* with plasmid constructs

Antisense and overexpression constructs were introduced into wild type AX2 cells by the calcium phosphate coprecipitation method in order to knockdown and increase expression of *Ddpolycystin* respectively. Multiple copies of the construct are generated in tandem during the process of co-insertional rolling circle replication (Barth *et al.*, 1998). This will result in each individual transformant expressing different numbers of the plasmid insert, which can range dramatically from, less than 10 to more than 1000, and are stably expressed in the transformant under antibiotic selection. When expressed, the asRNA will bind to the complementary mRNA expressed from the endogenous gene and target the double standed RNA for degradation by RNases in the asRNA pathway. Therefore there is a reduction in the amount of mRNA that is able to be expressed as protein, thus reduction in protein levels (Kuhlmann *et al*., 2006). Because the number of copies of the integrated plasmid can vary between strains, real time quantitative PCR (RT-qPCR) was used to determine the plasmid copy number in each strain (Table 3.1).

Table 3.1 Copy number of *D. discoideum* transformants expressing the *Ddpolycystin* antisense-inhibition and overexpression constructs.

Group	Construct	Strain HPF number	Plasmid copy number
Antisense Inhibition	**pPROF646**	**HPF642**	**25**
Antisense Inhibition	**pPROF646**	**HPF831**	**133**
Antisense Inhibition	**pPROF646**	**HPF643**	**7**
Antisense Inhibition	**pPROF646**	**HPF833**	**22**
Antisense Inhibition	**pPROF646**	**HPF644**	**13**
Antisense Inhibition	**pPROF646**	**HPF835**	**8**
Antisense Inhibition	**pPROF646**	**HPF859**	**8**
Antisense Inhibition	**pPROF646**	**HPF838**	**22**
Overexpression	**pPROF636**	**HPF841**	**30**
Overexpression	**pPROF636**	**HPF651**	**188**
Overexpression	**pPROF636**	**HPF652**	**66**
Overexpression	**pPROF636**	**HPF845**	**149**

Overexpression	**pPROF636**	**HPF846**	**20**
Overexpression	**pPROF636**	**HPF653**	**46**
Overexpression	**pPROF636**	**HPF839**	**311**

In each strain, varying copies of plasmid are integrated into the genome, therefore each will express different levels of protein. This allowed me to create a *Ddpolycystin* expression index for phenotypic analysis, following the previously established convention of using negative values for the number of copies of the antisense inhibition construct and positive numbers for the overexpression construct (Bokko *et al*., 2007). This allowed gene dose-response relationships to be determined and reveal correlations between the construct copy number and severity of phenotypes. Semiquantitative real-time RT-PCR was used to determine the expression level of *Ddpolycystin* mRNA. As expected, antisense inhibition of *Ddpolycystin* caused a measurable decrease in mRNA transcripts and overexpression caused an increase in mRNA transcripts. *Ddpolycystin* mRNA expression correlated with the copy numbers of the antisense and overexpression constructs, being reduced in the antisense-inhibited strains and increased in the overexpression strains (Figure 3.5).

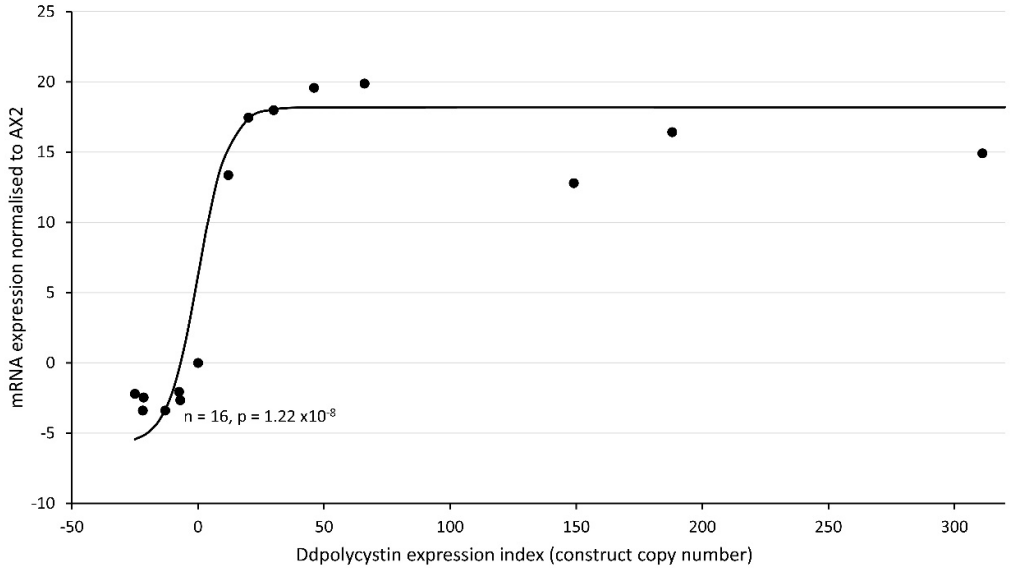

Figure 3.5 Expression of *Ddpolycystin* was altered in the isolated transformants.

Semiquantitative RT-PCR was performed to show altered levels of expression of *Ddpolycystin* in individual transformants compared to AX2. Expression correlates with plasmid copy number showing that asRNA decreases expression and overexpression increases *Ddpolycystin* expression. Each point represents mean data for a single strain for 3 experiments. Negative values refer to copy numbers of antisense constructs and positive values to copy numbers of overexpression constructs, AX2 has a copy number of 0 as contains neither construct. Expression levels were normalized against filamin to adjust for loading and then measured relative to AX2 expression. The curve was fitted by the least squares method to a sigmoidal (hyperbolic tangent) function. The regression was highly significant as indicated (F test). Negative values refer to copy numbers of antisense constructs and positive values to copy numbers of overexpression constructs, according to previously established convention (Bokko *et al*., 2007).

3.2.2.1 Protein quantification

To determine if the protein levels of Ddpolycystin were altered in the isolated transformants, a rabbit antibody was generated against a 134aa portion of Ddpolycystin (aa66-aa199), termed anti-POECD. The anti-POECD whole rabbit serum was affinity purified and used to detect Ddpolycystin in protein extracted from AX2 cells and two Ddpolycystin overexpressing strains. Three bands were detected, one at ~80 kDa corresponding to the predicted protein size of Ddpolycystin of 82,205.9 Da (dictyBase.org), one at ~180 kDa which could represent SDS stable protein aggregate dimers or post-translationally modified version of the protein, and one at ~70 kDa which

could reflect a breakdown product (Figure 3.6). The other possibility is that the other bands represent unidentified proteins that cross-react with the antibody. Therefore, it is important to note that these current results are preliminary because importantly the specificity of the anti-POECD antibody does need to be confirmed to ensure that all three bands represent Ddpolycystin. This could be done for example by Western blot using lysate from Ddpolycystin KO cells. This was not within the scope of this thesis, so it is important that this is tested in future studies. In assuming that the 80 kDa band represented Ddpolycystin, I then used the anti-POECD antibody to quantify the protein expression level of Ddpolycystin in a subset of transformants. The functional 80 kDa band was quantified in three knockdown strains and three overexpression strains and revealed a clear increase in Ddpolycystin overexpression and decreased protein expression in knockdown strains compared to AX2 (Figure 3.7).

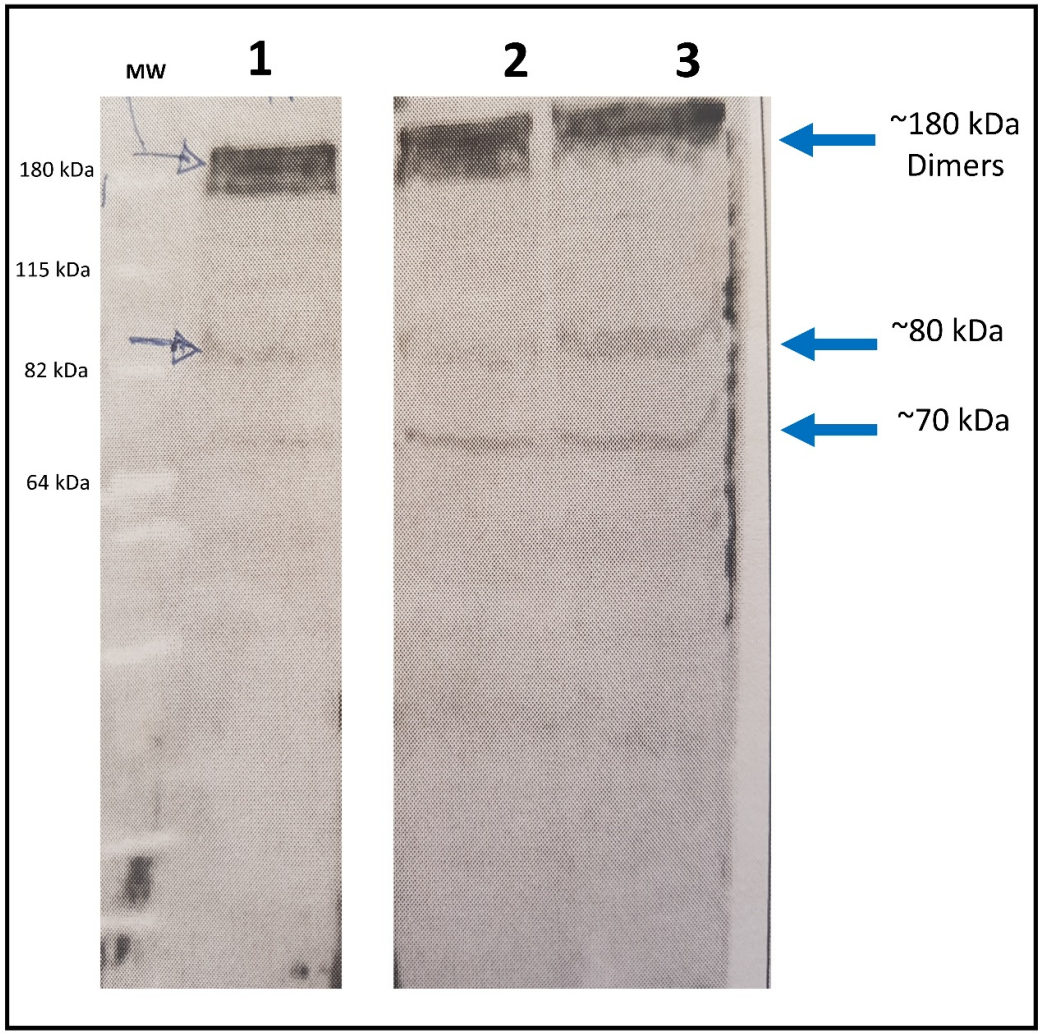

Figure 3.6 Western blot of crude protein extracts using rabbit anti-POECD antibody detects Ddpolycystin in AX2 and Ddpolycystin overexpressing strains.

A rabbit antibody was generated against a 134aa portion of Ddpolycystin (aa66-aa199), and termed anti-POECD. The anti-POECD whole rabbit serum was affinity purified and used to detect Ddpolycystin in crude protein extracts separated on SDS-PAGE. Band detection was achieved using chemifluorescence with the ECF Western blotting detection system (GE Healthcare Amersham) Lane 1: AX2 Lane2: Ddpolycystin overexpressing strain (HPF839), Lane 3: Ddpolycystin overexpressing strain (HPF653). Three bands were detected, one at ~80 kDa corresponding to the predicted protein size of Ddpolycystin of 82,205.9 Da (dictybase.org), one at ~180 kDa possibly to correspond to protein aggregate dimers or a modified version of the protein and one at ~70 kDa which could reflect breakdown products. The other possibility is that the other bands represent unidentified proteins that cross-react with the antibody, so the antibody needs to be verified.

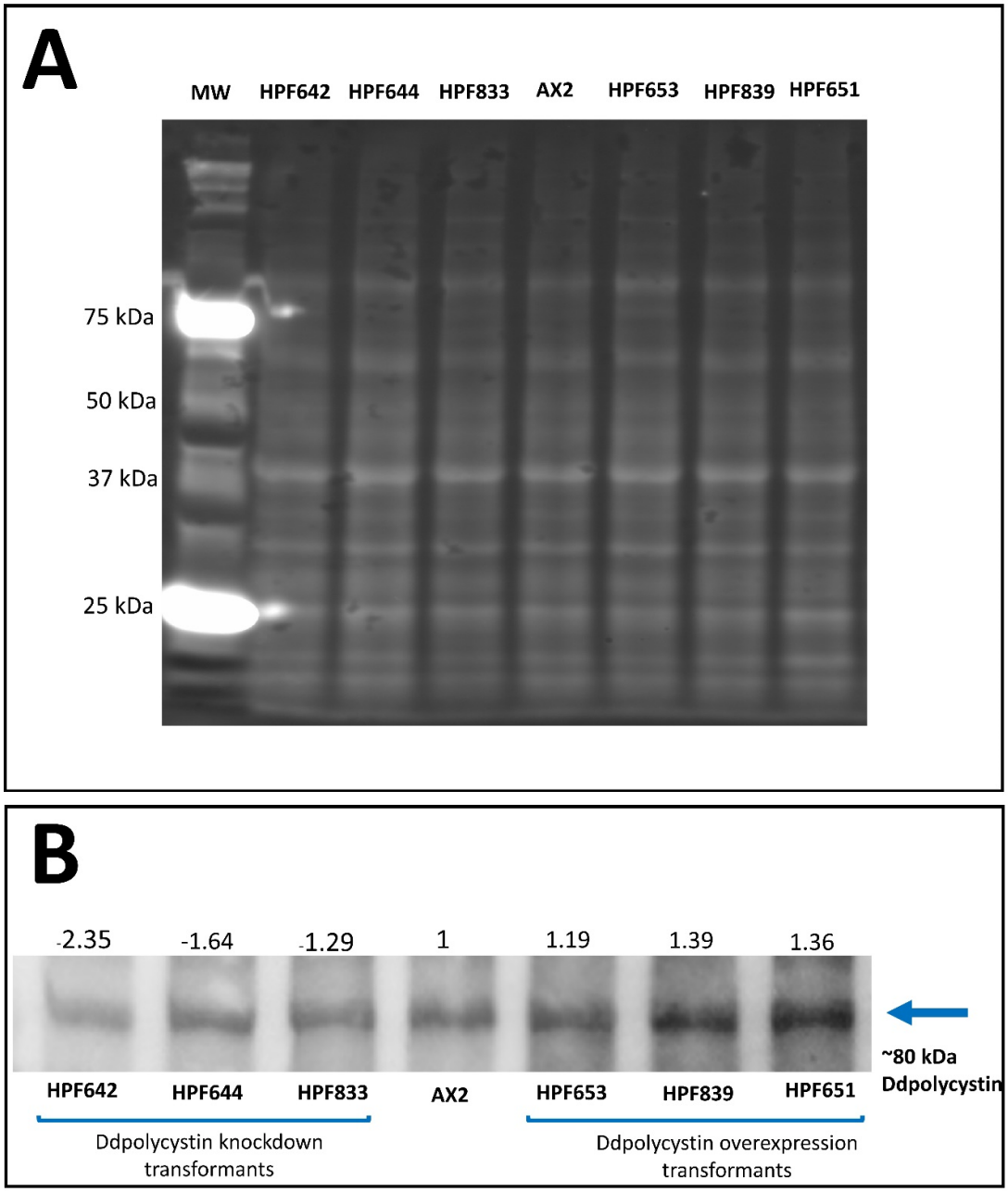

Figure 3.7 Quantification of Ddpolycystin protein expression in transformants.

Protein was extracted from vegetative cells from AX2, KD strains (HPF642, HPF644, HPF833) and overexpression strains (HPF653, HPF839, HPF651) and quantified. **(A)** 15µg of protein from each transformant was separated by SDS-PAGE on a stain free gel (Bio-Rad) and imaged on a Bio-Rad GelDoc™ EZ Imager. **(B)** Western blotting was used to probe Ddpolycystin using the rabbit anti-POECD antibody, and the signal detected using (goat) anti rabbit Alexa-Fluor 800 labelled secondary antibody (Invitrogen). The band intensity was quantified and the stain free gel allowed for normalization against the total protein loading for each lane. The band intensity normalized to total protein loading and then represented as a fold change below of above AX2 expression, indicated above each band.

After successfully obtaining Ddpolycystin transformants, phenotypic analysis was performed in order to characterize the function of the protein in *Dictyostelium*. The main focus of the project was to determine whether Ddpolycystin functions as a Ca^{2+} channel as has been described in other organisms. This was achieved by *in vivo* measurements of cytosolic Ca^{2+} in resting and chemotactically stimulated cells. The subcellular localisation of Ddpolycystin was determined using immunofluorescence, revealing that the protein localised to the plasma membrane. Additionally, characterization of phagocytosis, macropinocytosis and growth rates on bacterial lawns and axenically was performed. The following sections describe the results of phenotypic characterization.

3.2.3 Developmental expression of *Ddpolycystin*

Upon starvation, *Dictyostelium* cells begin a developmental program which involves various stages leading to multicellular morphogenesis and culmination into mature fruiting bodies (Kessin, 2001). Gene expression begins to change immediately upon starvation and can vary over the developmental period (Van Driessche *et al*., 2002). To investigate the expression of *Ddpolycystin* during development, AX2 cells were starved and allowed to develop on water agar plates for 24 hours. RNA samples were harvested at 2 hour intervals, and semiquantitative RT-PCR was used to assess the relative expression. *Ddpolycystin* was expressed throughout development, rising rapidly to a peak during early differentiation in response to the onset of starvation, falling to a trough at 8 hours, but then increasing rapidly again to a maximum at 10 hours during aggregation. Expression remained at high levels during subsequent multicellular development (Figure 3.8A). This expression data is similar to the RNAseq derived mRNA expression time course of *Ddpolycystin* in AX4 (Parikh *et al*., 2010) (Figure 3.8B) and the mRNA developmental time course determined by Traynor and Kay (2017). This expression pattern suggests important roles for polycystin-dependent calcium signalling in early starvation-induced differentiation, in chemotactic aggregation and subsequently during the multicellular stages of the life cycle.

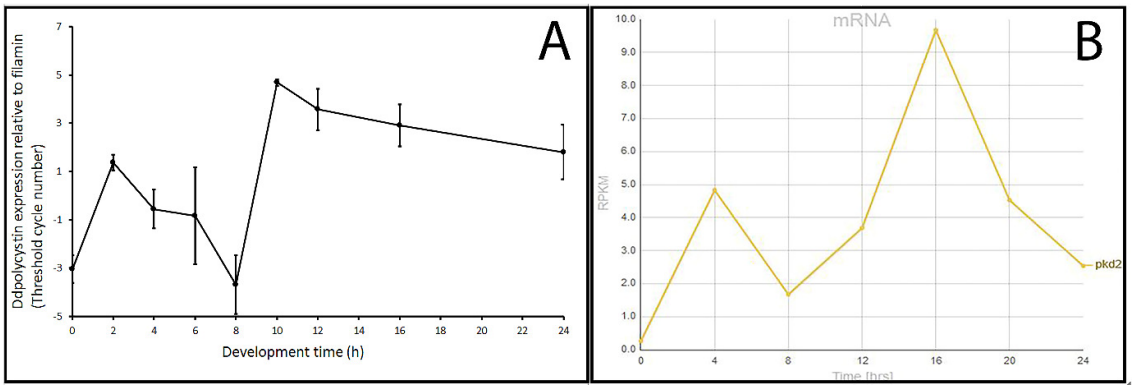

Figure 3.8 *Ddpolycystin* mRNA expression increases throughout development in *Dictyostelium* AX2 and AX4.

(A) Semiquantitative RT-PCR was used to determine the *Ddpolycystin* expression in AX2 throughout development. *Ddpolycystin* expression is normalized to filamin expression. Measurements were taken using RNA extracted from cells developing on water agar every two hours for 24 hours in two separate experiments. Error bars are standard errors of the mean. **(B)** Image reproduced from dictyexpress.org (Stajdohar *et al*., 2015) Developmental timing of expression of *Ddpolycystin* (*pkd2)* in AX4 as measured by RNA-Seq. Reads per kilobase per million (RPKM) over 24 hours. Published on dictyBase (Parikh *et al*., 2010; Stajdohar *et al*., 2017).

3.2.4 Ddpolycystin is localized to the plasma membrane but not the ER in *Dictyostelium*.

Mammalian PC2 functions at both the plasma membrane (Luo *et al*., 2003; Ma *et al*., 2005) and ER (Koulen *et al*., 2002; Pazour *et al*., 2002), and a 34 amino acid ER retention domain in the cytoplasmic C-terminal has been identified (Pazour *et al*., 2002). In *Dictyostelium*, FLAG-tagged Ddpolycystin colocalized with the cell surface marker H36 that detects the cell surface protein p46 which is excreted from macropinocytic cup (Cosson 2006; Lima *et al*., 2014) (DSHB Hybridoma Product H36), and also with recycling and newly formed endosomes (Lima *et al*., 2014). Performing immunofluorescence with a rabbit antibody generated against a 134aa portion of Ddpolycystin (aa66-aa199) (anti-POECD) enabled subcellular localisation of wild type Ddpolycystin. Initial IF staining only with the anti-POECD antibody revealed staining that appeared to accumulate around the plasma membrane, and also intracellular granulation (Figure 3.9A). Further analysis revealed that Ddpolycystin indeed co-localized with H36 at the plasma membrane in AX2 cells, confirming previous observations (Figure 3.9B). Considering the possibility that

Ddpolycystin might also be expressed at the ER, I decided to determine whether Ddpolycystin also colocalized with the ER marker calnexin. Immunofluorescence in AX2 cells using the anti-POECD and anti-calnexin (DSHB Hybridoma Product 270-390-2) antibodies revealed that Ddpolycystin does not show co-localisation with the ER (Figure 3.10). These results are preliminary as stated earlier as the antibody needs to be confirmed that it is specific for Ddpolycystin, however the localisation pattern does match with the previously published localisation.

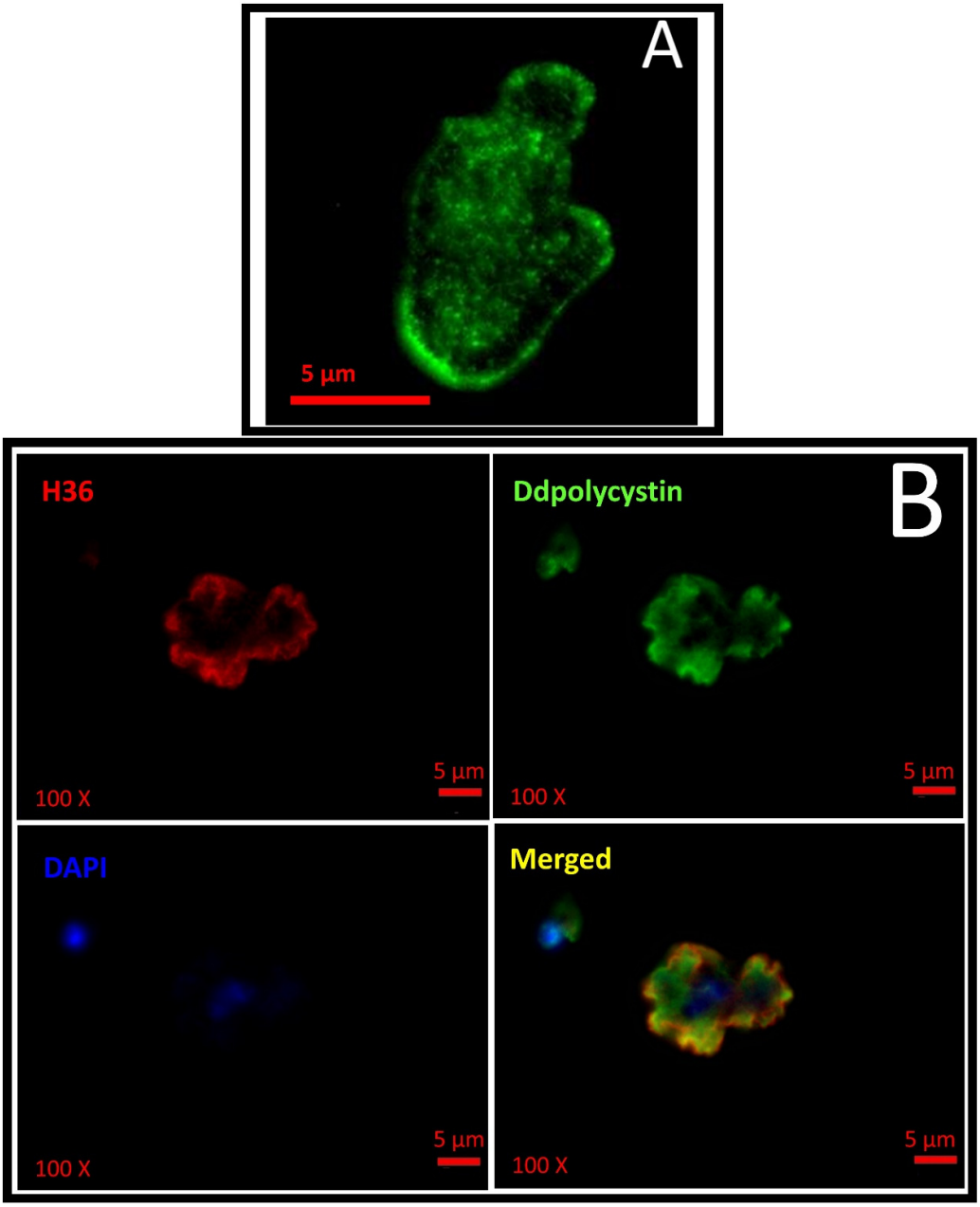

Figure 3.9 Co-ocalization of Ddpolycystin with the plasma membrane**.**

(A) Immunofluorescent image of AX2 cell labelled with anti-POECD rabbit antibody to detect Ddpolycystin. The protein can be seen in what appears to be the plasma membrane and also intracellular structures. **(B)** AX2 was labelled with anti-POECD rabbit antibody to detect Ddpolycystin, and the plasma membrane was localized using the marker H36, the nuclear DNA was marked with DAPI. The merged image shows co-localisation of Ddpolycystin with the plasma membrane marker H36 indicated by yellow.

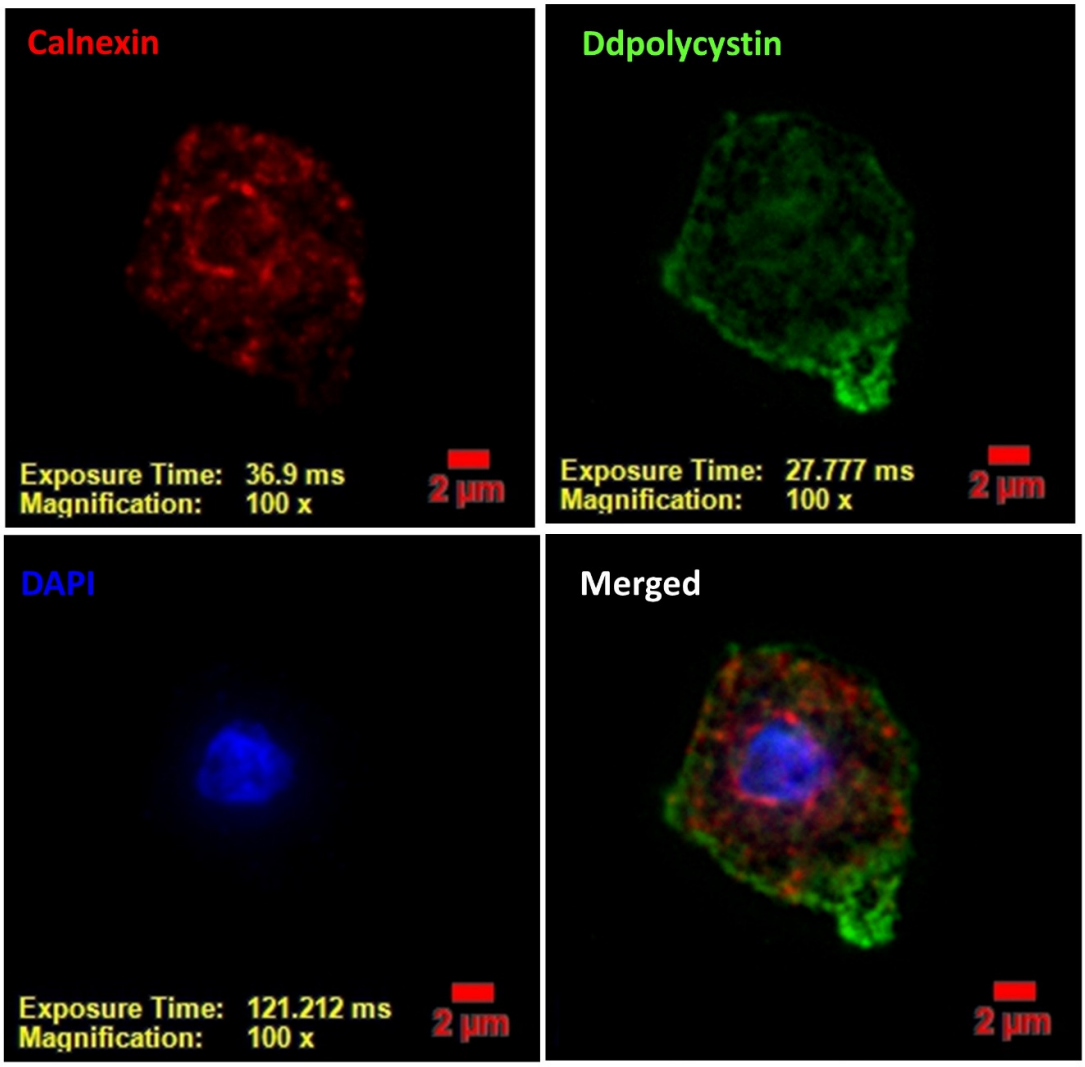

Figure 3.10 Ddpolycystin does not co -ocalize with the ER**.**

Immunofluorescent images of AX2 cell. The ER was localized using the anti-calnexin antibody, Ddpolycystin was localized using the anti-POECD rabbit antibody and the nuclear DNA was marked with DAPI. The merged image shows no co-localisation of Ddpolycystin with the ER.

3.2.5 Ddpolycystin functions as a calcium channel in *Dictyostelium*.

In mammals, PC2 functions as a high conductance Ca^{2+} channel (Koulen *et al*., 2002; Luo *et al*., 2003; AbouAlaiwi *et al*., 2009). To further investigate the role of Ddpolycystin in Ca^{2+} signaling, the $[Ca^{2+}]_{cyt}$ transients in response to cAMP and folic acid stimulation in knockdown and overexpressing strains were measured. Strains were cytoplasmically expressing the Ca^{2+} sensitive luminescent protein aequorin, to allow real time recordings of cytosolic Ca^{2+} responses. These chemotactic Ca^{2+} responses have been well characterized in wild type cells AX2 expressing aequorin (HPF401) therefore comparisons between the chemotactic responses in mutant cell lines with wild type responses provides information on the molecular mechanisms involved in the responses. The strain HPF401 is used as the control for the calcium experiments throughout this thesis, it has been shown that the aequorin expression construct has no other phenotypic effect (Nebl and Fisher, 1997). These cytosolic Ca^{2+} transients in response to 1µM of either cAMP of folic acid have been characterized using expression of the luminescent Ca^{2+}-indicator apoaequorin. This method provides sensitive and accurate readings with a temporal resolution of 20 ms and can detect changes in cytosolic Ca^{2+} concentrations with a sensitivity of 2 to 3 nM (Wilczynska *et al*., 2005). The Ca^{2+} responses last ~60 seconds, during which time basal cytosolic $[Ca^{2+}]_{cyt}$ levels of ~70 nM rise to ~150nM for folic acid responses and ~200 nM for cAMP responses. The responses are terminated via sequestration by Ca^{2+}-ATPases back into intracellular stores and across the plasma membrane to return cytosolic Ca^{2+} to basal (Nebl and Fisher, 1997; Wilczynska *et al*., 2005). Various parameters of the responses can be measured to determine response magnitude and kinetics, and comparisons made between wild type and mutant responses. Representative real-time recordings of $[Ca^{2+}]_{cyt}$ in wild type aequorin expressing (HPF401), Ddpolycystin asRNA strain HPF644 and overexpression strain HPF839 when stimulated with 1 µM chemoattractant are shown in Figure 3.11. Larger and smaller response magnitudes, compared to control, were observed in overexpression and antisense strains respectively for both cAMP and folate stimulation. In vegetative cells response magnitudes were decreased by an average of 45.5% in knockdown strains and increased by 48% in overexpression strains compared to control average. In differentiated cells response magnitudes were decreased by an average of 35.8% in knockdown strains and increased by 42.8% in overexpression strains compared to control average. This indicates

that Ddpolycystin contributes to chemotactic Ca^{2+} responses by facilitating Ca^{2+} release into the cytoplasm. The magnitude of the Ca^{2+} responses, to both chemoattractants, is positively correlated with the Ddpolycystin expression index (Figure 3.12A,B). The observation of similar copy number-dependent phenotypes in multiple, independently isolated clonal cell lines excludes the possibility that the altered Ca^{2+} responses might be due to additional, random and unknown genetic events elsewhere in the genomes of the mutant strains.

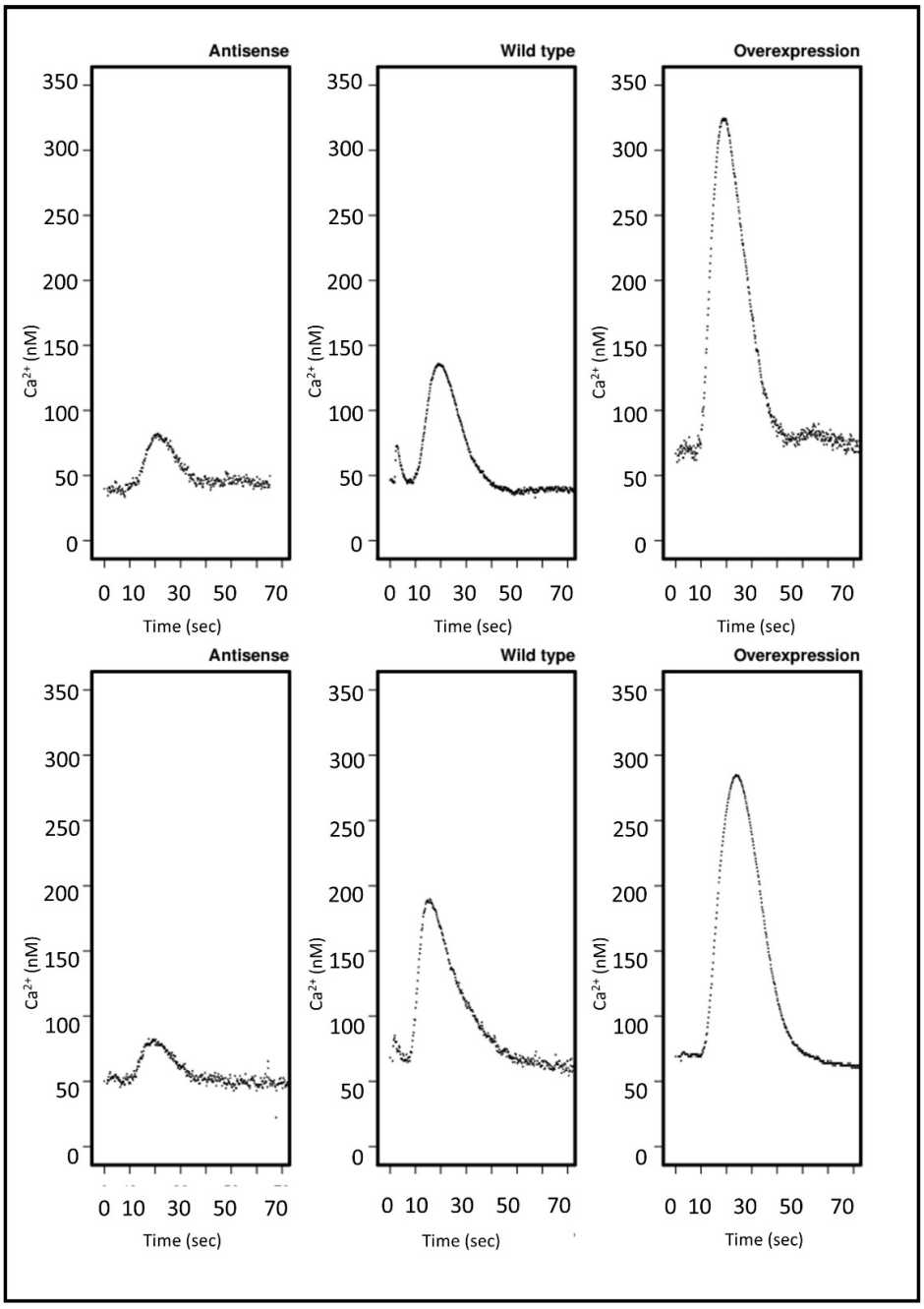

Figure 3.11 Cytoplasmic Ca^{2+} responses are larger in Ddpolycystin overexpressing strains and smaller in KD strains.

Real time recordings of calcium responses to folic acid (upper panel) and cAMP (lower panel) in, KD strain HPF644 (copy number 13), wild type (HPF401) and overexpression HPF839 (copy number 311). Cells were stimulated with 1 µM folate in vegetative cells, or 1 µM cAMP in cells starved for 7 h in MES-DB. Recordings began a 0 sec and the stimulus was injected immediately. The small peak preceding the Ca^{2+} response is due to mechanical force of stimulant injection, this has no effect on response magnitude.

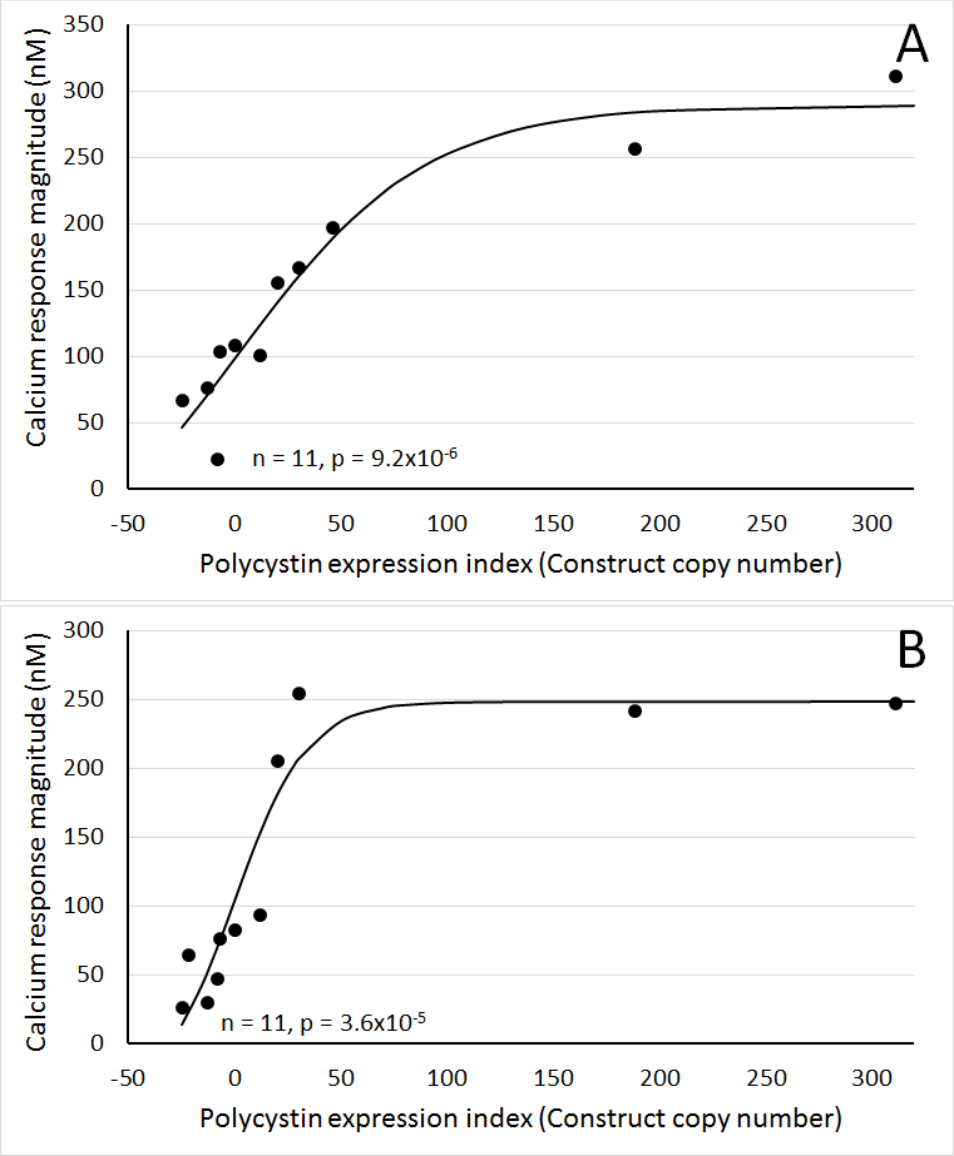

Figure 3.12 Calcium response magnitudes correlate with plasmid copy number.

Cytosolic response magnitudes (Ca^{2+} nM) in strains with different copy numbers for either *Ddpolycystin* overexpression of antisense constructs. Stimulation was with **(A)** 1µM cAMP and **(B)** 1µM folic acid, measured from real time recordings. Response magnitudes positively correlate with the *Ddpolycystin* expression index. Each point is the mean of 2-5 independent recordings for each transformant. Regression lines were fitted to a sigmoidal (hyperbolic tangent) function. The regressions were highly significant with the indicated probabilities (F test).

3.2.5.1 Analysis of chemotactic response kinetics

The kinetics of these chemotactic Ca^{2+} responses are known to be partly dependent on the response magnitude itself, in that larger responses start earlier and peak earlier due to faster entry of Ca^{2+} into the cytosol, and there is a correlation between the maximum rise and fall rates of Ca^{2+} into and out of the cytoplasm (Wilczynska *et al*., 2005). This confirms that the responses are autocatalytic in the rising phase of the response, implying a Ca^{2+}-induced Ca^{2+} entry to the cytosol with more channels opening earlier and allowing more rapid increases in cytosolic Ca^{2+}. The responses are also self-limiting in the falling phase of the response, larger responses being terminated more quickly because the Ca^{2+} itself homeostatically activates the mechanisms that clear Ca^{2+} from the cytoplasm, such as closure of Ca^{2+} channels or activation of Ca^{2+} pumps (Wilczynska *et al*., 2005).

To explore these relationships further, I measured the maximum rise and fall rates of cytosolic Ca^{2+} in Ddpolycystin mutants and observed the same relationship in response kinetics to both cAMP and folic acid (Figure 3.13A). This shows that the Ca^{2+}-regulated Ca^{2+} channels and pumps are the same for the two attractants, since responses to them exhibit the same kinetic properties. I also plotted the relationship between the response onset time and response magnitude. The relationship is negative for Ddpolycystin protein overexpression, knockdown and control strains, and in this respect is similar to the relationship previously reported for wild type, calnexin-deficient and calreticulin-deficient strains (Wilczynska *et al*., 2005). Calnexin and calreticulin are avid Ca^{2+}-binding proteins in the endoplasmic reticulum that contribute to sequestration of Ca^{2+} in the lumen of the ER. The data for all three of those strains fell onto the same regression line, the strains differing only in their position on the line. This was in keeping with differences in the steepness of the free Ca^{2+} gradients resulting from loss of Ca^{2}-sequestering capacity. In this present work however, each set of strains falls on a different line in what appears to be a family of similar log-linear regressions. In overexpression strains the response magnitude is greater than the controls by a constant amount (regression intercept increased but slope unchanged) at all response times. Conversely the response magnitude is reduced by a constant amount, independent of response times, compared to controls (intercept lower, but slope unchanged) (Figure 3.13B). The simplest explanation is that Ddpolycystin is itself a significant contributor to the Ca^{2+} responses at all response times

and magnitudes, but that the mechanism by which the response time and magnitude are coupled is unchanged eg. in the form of Ca^{2+}-induced Ca^{2+} release.

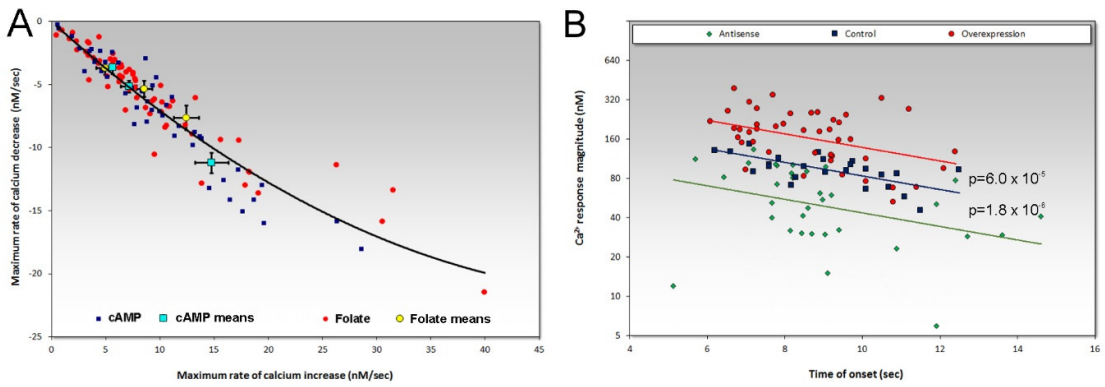

Figure 3.13 Kinetics of chemotactic Ca^{2+} responses in Ddpolycystin strains.

(A) Negative relationship between maximum rise and fall rates in control, *Ddpolycystin* overexpressing and KD strains. Each point represents an individual experiment. Blue squares indicate responses to 1µM cAMP and red circles indicate responses to 1µM folic acid. Aqua squares are means for cAMP responses, yellow circles are means for folic acid responses from left to right, KD, control and overexpression strains. Rise and fall rates at all stages in the responses were calculated from the Ca^{2+} concentrations at successive time points and the maximum rates of Ca^{2+} increase and decrease then determined graphically using features of the R statistics and graphics package. Multiple regression analysis showed that neither the attractant (folate or cAMP) nor the strain type (overexpression or KD or control) made a difference to the regression relationship ($p > 0.05$). **(B)** Relationship between the response onset time and magnitude. The relationship is log-linear and negative for Ddpolycystin overexpression, KD and control strains, however each set of strains falls on a different line. Multiple regression analysis showed that the intercepts (significance probabilities shown) but not the slopes ($p > 0.05$) differed significantly from the line for the control strain.

3.2.5.2 Resting Ca^{2+} levels are altered by changing Ddpolycystin expression

The ability of cells to maintain appropriate $[Ca^{2+}]_{cyt}$ is crucial for tight regulation of the many Ca^{2+}-regulated cellular processes. Assessment of the basal $[Ca^{2+}]_{cyt}$ in the Ddpolycystin strains showed significant differences between the basal $[Ca^{2+}]_{cyt}$ of knockdown strains compared to control, both in the vegetative ($P < 0.01$) and developed states ($P < 0.05$). However, no significant difference in the basal $[Ca^{2+}]_{cyt}$ of Ddpolycystin overexpressing strains compared to control. Analysis revealed that there was no

correlation between copy number and resting Ca^{2+} levels, therefore data from all transformants within each group was pooled to calculate the mean (Figure 3.14A,B). These results show that Ddpolycystin channels not only contribute to cytosolic Ca^{2+} transients in chemoattractant responses, but also contribute to basal Ca^{2+} homeostasis in unstimulated cells.

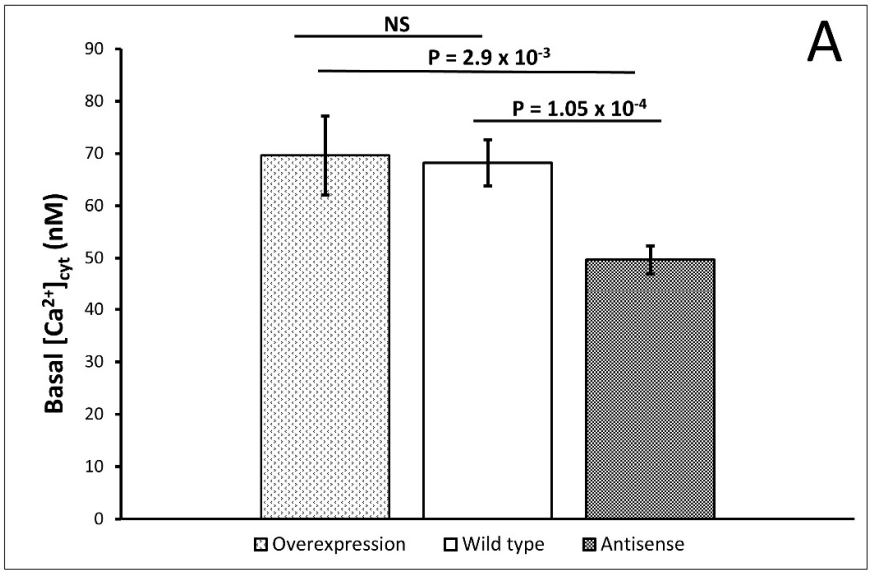

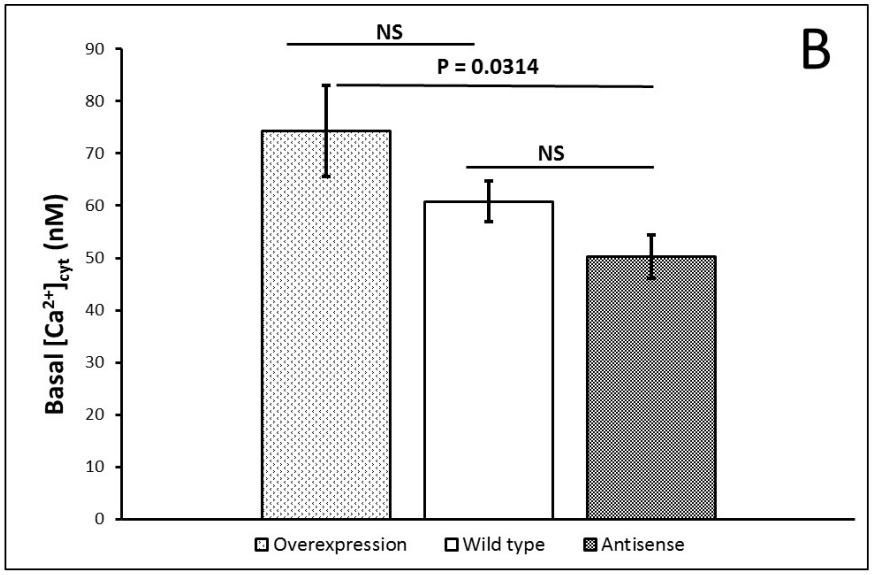

Figure 3.14 Basal cytosolic calcium concentration is reduced in Ddpolycystin KD transformants. **(A)** Basal $[Ca^{2+}]_{cyt}$ in cells starved and developed for 7 hours in MES-DB. There was a significant difference in the basal cytosolic Ca^{2+} levels between the wild type and KD strains, and the overexpression and KD strains ($p < 0.05$, One-Way ANOVA, with pairwise comparisons made by

the Least Squares Difference method). Error bars are standard errors of the mean. *Ddpolycystin* KD six strains (n=15), *Ddpolycystin* overexpression eight strains (n=19) control HPF401 one strain (n=12). **(B)** Basal $[Ca^{2+}]_{cyt}$ of vegetative cells growing in HL5 medium. The differences were not significant between wild type and overexpression transformants, or wild type and KD transformants. However, the difference between the overexpression and KD transformants was significant ($p < 0.05$), One-Way ANOVA, with pairwise comparisons made by the Least Squares Difference method). Error bars are standard errors of the mean. Ddpolycystin KD six strains (n=18), Ddpolycystin overexpression eight strains (n=26) control HPF401 one strain (n=13).

3.2.6 Ca^{2+}-ATPase mRNA expression is increased in *Ddpolycystin* overexpressing strains

The finding that resting Ca^{2+} levels are not affected in the Ddpolycystin overexpression strains suggests that the cells have employed mechanisms to maintain low resting cytosolic Ca^{2+} levels. One of these mechanisms may be upregulation of Ca^{2+} sequestering proteins as a response to the increase in abundance of Ca^{2+} channels. To explore this hypothesis, semiquantitative RT-PCR was used to determine the level of mRNA expression of putative Ca^{2+}-ATPase *pat4* (DDB_G0289473) in Ddpolycystin overexpression strains. Indeed, it was found that *pat4* mRNA expression was increased in all transformants compared to AX2 (Figure 3.15). This indicates that the cells are able to apply compensatory mechanisms in response to irregular protein expression in order to maintain low cytosolic Ca^{2+} levels required for biological function.

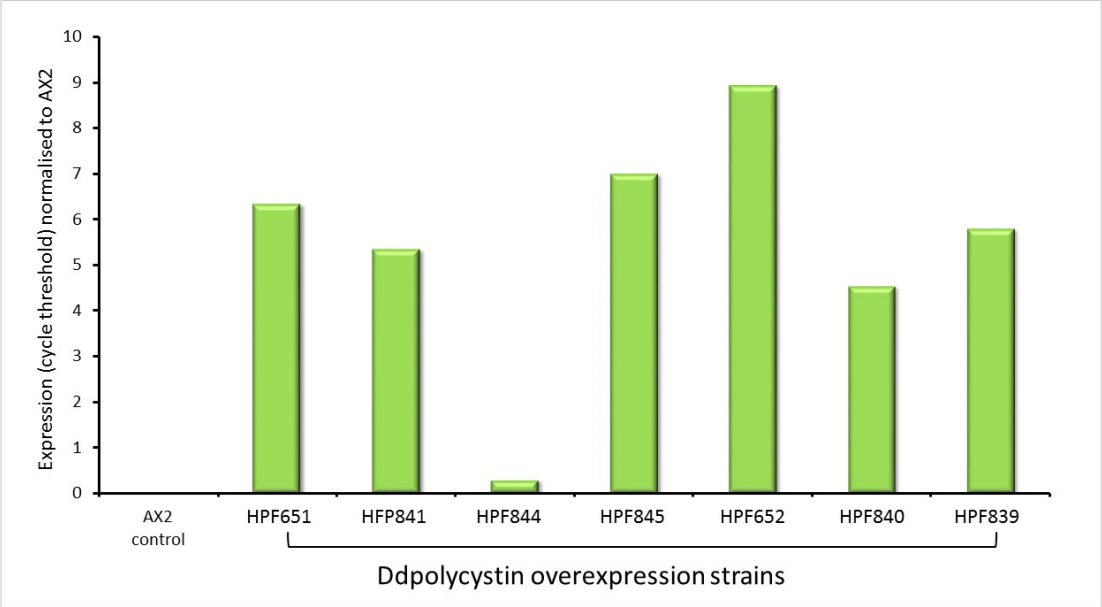

Figure 3.15 Expression of Ca^{2+}-ATPase mRNA is increased in Ddpolycystin overexpression strains. Semiquantitative RT-PCR was used to determine the level of mRNA expression of putative Ca^{2+}-ATPase (DDB_G0289473, PAT4) in Ddpolycystin overexpression strains. Expression was normalized to filamin expression and then normalized to AX2. RNA was extracted from vegetative cells in one biological replicate. mRNA expression was increased all transformants compared to AX2.

3.2.7 Ddpolycystin expression levels affect fruiting body morphologies

Multicellular development in *Dictyostelium* is initiated by starvation where cells undergo developmental program which involves various stages leading to multicellular morphogenesis and culmination into mature fruiting bodies consisting of a spore head, stalk and basal disc. In the fruiting body, the spore head (sorus) contains around 80 % of the cells, and the stalk and basal disc around 20 %. The spores are able to then be dispersed when conditions are favorable and germinate to give rise to amoebae. The stalk cells are formed as a result of autophagic cell death and therefore are non-viable. Downstream Ca^{2+} regulated processes such as multicellular morphogenesis are affect by aberrant Ca^{2+} signaling (Poloz and O'Day, 2012). When I overexpressed Ddpolycystin, cytosolic Ca^{2+} signaling was enhanced and the transformants developed fruiting bodies with very thick stalks presumably as a consequence of excess stalk cell differentiation (Figure 3.16C) compared to AX2 (Figure 3.16A). Conversely, knockdown transformants

developed into fruiting bodies with very thin fragile stalks, that were often unable to support the sorus (Figure 3.16B). This implicates Ddpolycystin dependent Ca^{2+} signaling in cell type specific differentiation into prespore and prestalk cells. Differentiation is controlled partly by Ca^{2+}, where higher Ca^{2+} levels tend to direct cells to the prestalk pathway, and lower Ca^{2+} to the prespore pathway (Saran *et al*., 1994a; Cubitt *et al*., 1995; Azhar *et al*., 1996; Schaap *et al*., 1996; Poloz and O'Day, 2012; Poloz and O'Day, 2012a). Stalk and disk cell differentiation is an endpoint of a form of autophagic cell death in *Dictyostelium* (Giusti *et al*., 2009; Giusti *et al*., 2010), and previous work has shown that shorter thicker stalks have been associated with increased numbers of cells entering the stalk differentiation (autophagic cell death) pathway (Bokko *et al.*, 2007). These results thus indicate that Ddpolycystin activity is involved Ca^{2+} signaling in processes involving entry into the autophagic cell death pathway.

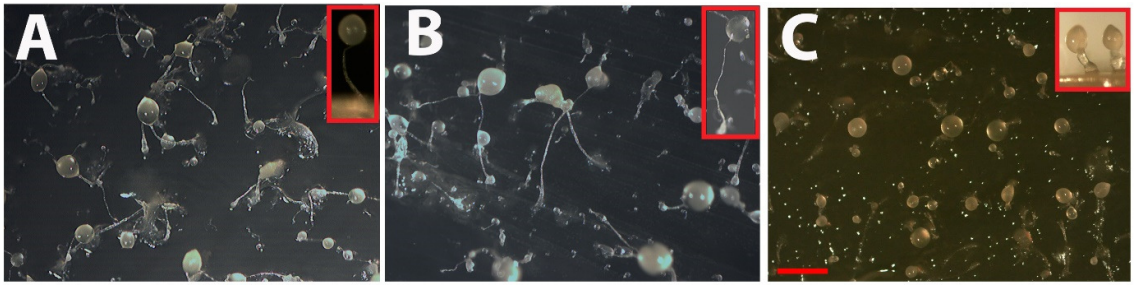

Figure 3.16 Ddpolycystin expression affects differentiation and multicellular morphogenesis. Effects of Ddpolycystin expression levels on multicellular morphogenesis in *Dictyostelium*. Cells were grown on lawns of *Enterobacter* at 21°C for ~ 24 h until mature fruiting bodies had formed. Photographs were captured using an Olympus SZ61 Moticam 2300 camera attached to a dissection microscope from above and from the side (Inserts). **(A)** Wildtype AX2. **(B)** Ddpolycystin KD strain HPF833 (copy number -22) exhibits very thin weak stalks, often unable to support the sorus. Insert shows side on image of typical thin fragile stalks. **(C)** Overexpression strain HPF845 (copy number 149) has short thick stalks, suggesting increased stalk cell differentiation. Insert shows side view of typical fruiting bodies with short thickened stalks. Scale bar = 1mm.

3.2.8 Ddpolycystin positively regulates growth rates and nutrient uptake via phagocytosis and macropinocytosis

The aberrant Ca^{2+} signaling in mutant strains with both reduced and increased Ddpolycystin expression affects nutrient uptake via phagocytosis and macropinocytosis. This was achieved by measuring the uptake of FITC-dextran over a 70 min period in wildtype AX2 and the Ddpolycystin transformants. The rates of phagocytosis were assayed

by measuring the uptake of fluorescently labelled live *E. coli* cells over 30 mins. Uptake of DS-red labelled *E. coli* and FITC-dextran HL5 is positively regulated by Ddpolycystin, and is correlated with the *Ddpolycystin* expression index (Figure 3.17A,B). To measure the growth rates of cells grown in HL5 medium, a growth experiment was conducted using wildtype AX2 and the Ddpolycystin transformants and the generation times of were measured during exponential growth in HL5 medium. The generation time in hours was calculated using log-linear regression in the "R" statistics and graphics environment. The plaque expansion rates (growth velocity) of AX2 control and Ddpolycystin transformants were measured from linear regressions of plaque diameters *vs* time during growth at 21°C on an *E. coli* B2 lawn. It was found that the increased rate of pinocytosis and phagocytosis in turn increased axenic and growth rates on lawns of bacteria (Figure 3.18A,B). These findings are consistent with previously reported decreased axenic growth rates in Ddpolycystin KO mutants (Waheed *et al*., 2014) however other studies found KO cells grow normally (Traynor and Kay, 2017), and also the known requirement for Ca^{2+} by phagocytosis (Yuan *et al*., 2001), particularly during phagocytic cup formation (Muller-Taubenberger *et al*., 2001).

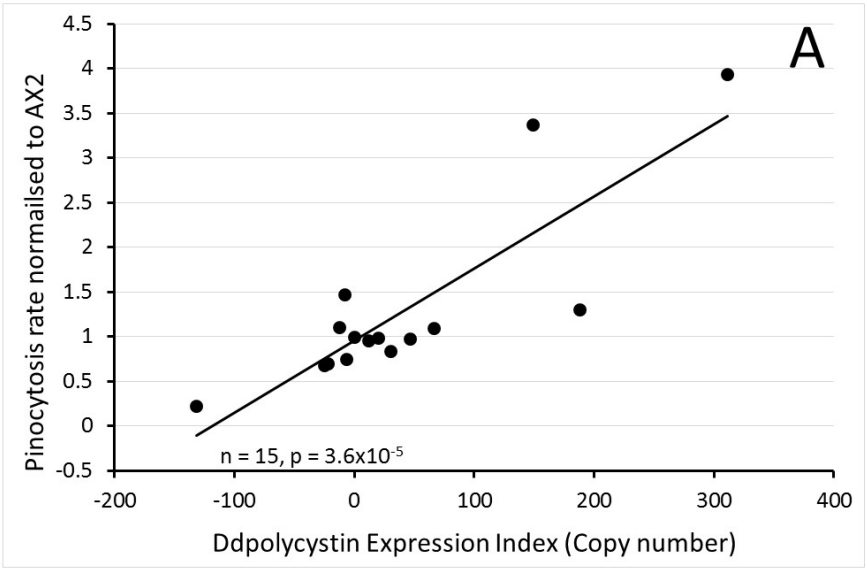

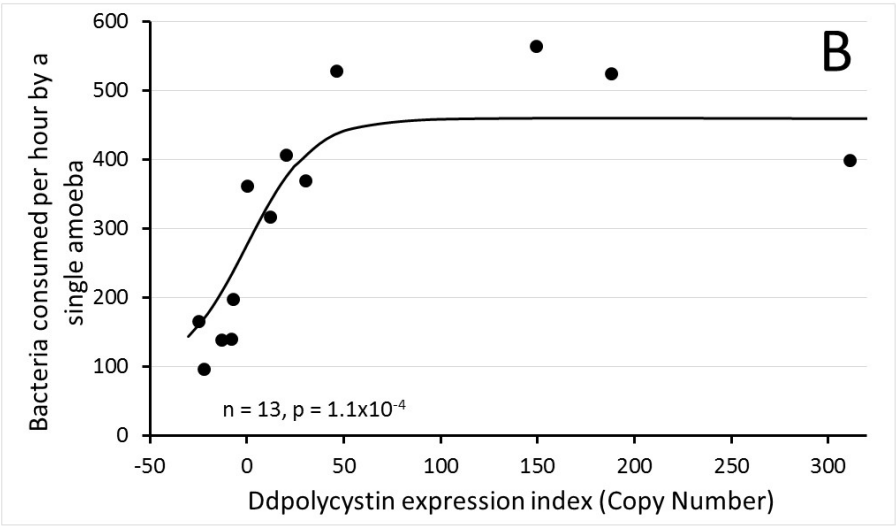

Figure 3.17 Ddpolycystin positively regulates pinocytosis and phagocytosis. **(A)** Pinocytosis was positively regulated by Ddpolycystin. The rate of consumption of HL5 medium containing FITC dextran was measured in Ddpolycystin KD and overexpression strains. As per previously established convention (Bokko *et al*., 2007), negative values represent the number of copies of the antisense-RNA construct and positive values are the number of copies of the overexpression constructs. **(B)** Phagocytosis was measured as consumption of *E. coli* cells expressing the fluorescent red protein Ds-Red. Phagocytosis and pinocytosis rates increased as Ddpolycystin expression increased. Regression lines were fitted by least squares to a linear function (A) or to a sigmoidal (hyperbolic tangent) function (B). The regressions were highly significant with the indicated probabilities (F test).

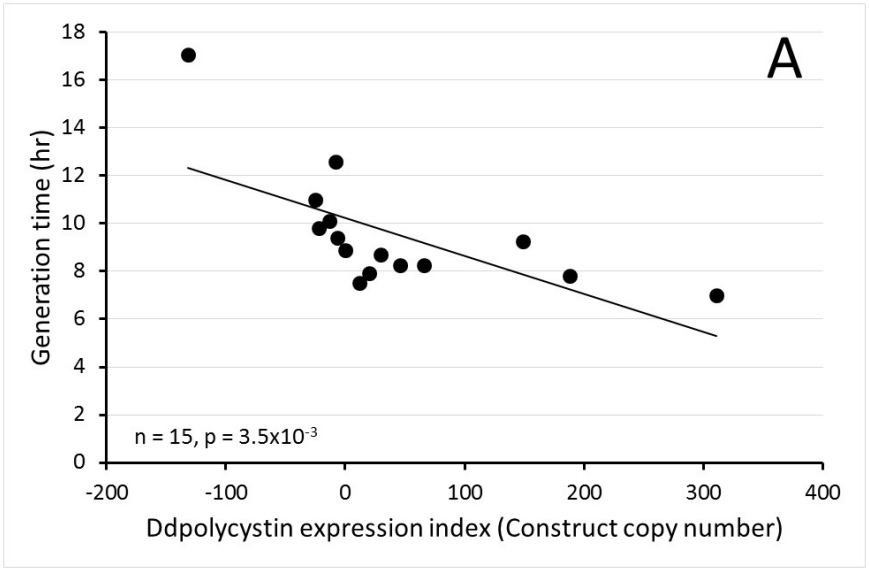

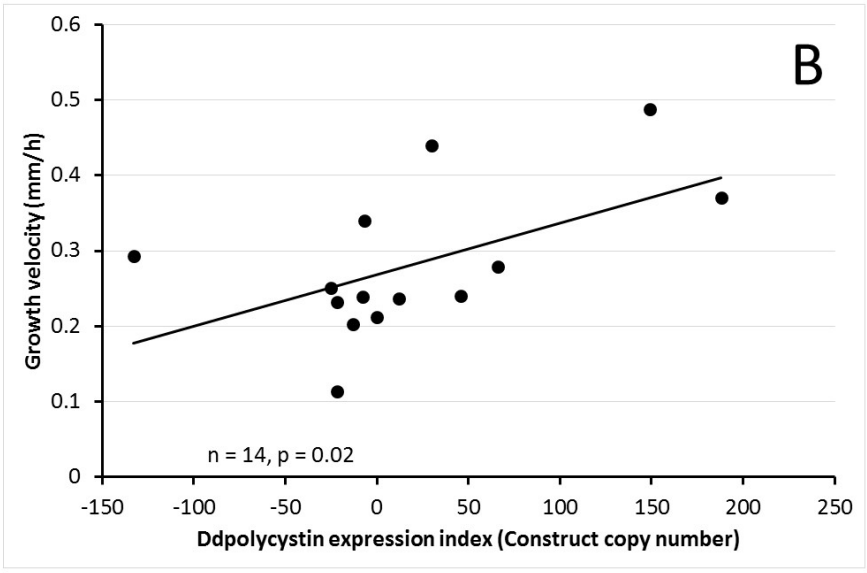

Figure 3.18 Ddpolycystin positively regulates *Dictyostelium* growth rates in HL5 medium and on lawns of *E. coli*.

(A) Expression of Ddpolycystin is significantly correlated with generation times in liquid medium. Strains were grown exponentially in HL5 medium, shaken at 150 rpm and generation times determined by log-linear regression of the relationship between cell density and time. **(B)** Expression of Ddpolycystin is significantly correlated with growth rates on bacterial lawns. Plaque expansion rates (growth velocity) were measured from linear regressions of plaque diameters *vs* time during growth at 21°C on an *E. coli* B lawn. The regressions were highly significant with the indicated probabilities (F test).

3.2.9 Ddpolycystin restricts spore germination

The spores of *Dictyostelium* are in a quiescent stage until they are activated to initiate germination (Cotter and Raper 1966; Cotter *et al.,* 1992) and Ca^{2+} signaling is involved in spore activation and germination. During spore activation Ca^{2+} is released from spores after receptor activated IP_3 dependent Ca^{2+} release from internal stores, and subsequent CaM dependent efflux of Ca^{2+} from the cells. Subsequently during amoebal emergence Ca^{2+} begins to be taken up by the cells which is thought to be necessary for production and secretion of emergence specific proteins (Lydan and Cotter, 1995). Therefore, the efficiency of germination of spores from the Ddpolycystin mutant strains was assessed. Spores were harvested from fruiting bodies and heat activated, the activated spores were then plated on lawns of *Enterobacter* an allowed to germinate so that the germination efficiency could be calculated. The results indicated that while there was no significant difference between the knockdown and control and overexpression and control, there was a significant an increased efficiency of germination in the knockdown strains compared to the overexpression strains (Figure 3.19). This indicated that Ddpolycystin plays a role in restricting spore germination, presumably by regulating Ca^{2+} fluxes during the activation and germination process.

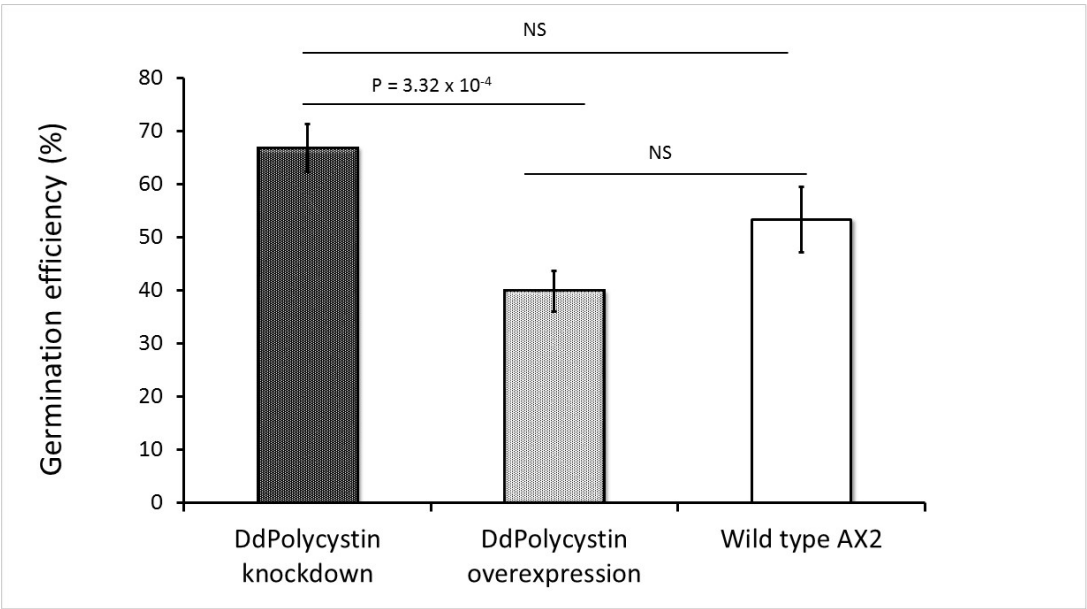

Figure 3.19 Ddpolycystin restricts spore germination.

Spores from three Ddpolycystin KD strains and three overexpression strains were harvested from fruiting bodies and heat activated. A known number of activated spores were then plated on lawns of *Enterobacter* an allowed to germinate. The germination efficiency was calculated by determining the number of germinated spores as a percentage of the number of plated spores. The means are calculated from pooled data from all strains within each group over three individual experiments. Error bars are standard errors of the mean. There was a significant difference in the germination efficiencies between the KD strains and overexpression strains, KD n= 9, overexpression n= 9, control n =3 ($p = 0.000331716$, One-Way ANOVA, with pairwise comparisons made by the Least Squares Difference method).

3.3 Discussion

Calcium signaling is central to many cellular functions, therefore control over cellular Ca^{2+} concentrations is essential. The movement of Ca^{2+} ions across cellular membranes is achieved by the actions of various Ca^{2+} channels and pumps to maintain homeostasis and propagate Ca^{2+} signals. The model organism *Dictyostelium* is an ideal system for studying Ca^{2+} signalling as its genome encodes a small collection of Ca^{2+} channels and pumps (Wilczynska *et al*., 2005), and amoebae exhibit robust cytosolic Ca^{2+} signals in response to various extracellular stimuli. These stimuli include the chemoattractants folic acid and cAMP, to which the cells are chemotactically responsive during their vegetative state and differentiated state respectively (Wick *et al*., 1978; Milne and Coukell 1991; Malchow *et al*., 1996; Malchow *et al*., 1996a; Yumura *et al*., 1996; Nebl and Fisher, 1997; Nebl *et al*., 2002; Wilczynska *et al*., 2005; Malchow *et al*., 2006; Fisher and Wilczynska, 2006).

Chemotaxis is essential in the vegetative growth phase, for hunting prey, and for post starvation aggregation and progress through to multicellularity (Cai *et al*., 2012, Dilão and Hauser, 2013). Many studies have implicated Ca^{2+} signaling in chemotaxis, however the specific roles that the second messenger plays remain unclear as Ca^{2+} signaling is not essential for chemotaxis to occur (Tyarnor *et al*., 2000). Stimulation of both chemoreceptors cAR1 (Klein *et al*., 1988) and fAR1 (Pan *et al*., 2016) with their activating ligands, cAMP and folic acid, respectively, initiates intracellular signaling cascades that induce a rapid Ca^{2+} influx across the plasma membrane and release from the ER (Nebl and Fisher, 1997; Wilczynska *et al*., 2005; Wilczynska *et al*., 2006). Importantly, the Ca^{2+} channel responsible for Ca^{2+} influx across the plasma membrane has not been identified. Conflicting evidence indicates that IplA, a homologue of mammalian ER Ca^{2+} channel the InsP3R, is a candidate protein as it has some localisation at the plasma membrane (Lusche *et al*., 2012). IplA null amoebae have been shown to lack both cAMP and folic acid Ca^{2+} responses measured by cytosolic $^{45}Ca^{2+}$ uptake (Traynor *et al*., 2000), and using a fluorescent Ca^{2+} indicator (Traynor and Kay, 2017). However, another study found IplA null strains retained a reduced cAMP Ca^{2+} response (Schaloske *et al*., 2005). Therefore, the role IplA plays in these chemotactic Ca^{2+} responses remains to be clarified. Another potential Ca^{2+} channel that could facilitate chemotactic Ca^{2+} uptake is Ddpolycystin, a homologue of the mammalian Ca^{2+} channel PC2, mutations in which are linked to ADPKD.

Expression of Ddpolycystin has been observed at the plasma membrane (Lima *et al*., 2014) so may play a role in chemotactic Ca^{2+} influx.

In this study Ddpolycystin function in *Dictyostelium* was investigated by knocking down and overexpressing the protein and assaying a variety of phenotypic readouts in transformants. Ddpolycystin's role in chemotactic Ca^{2+} signaling was assessed by using *in vivo* expression of the Ca^{2+} sensitive luminescent protein, aop-aequorin, the chemotactic Ca^{2+} responses in these transformants were characterized. As *Dictyostelium* is an excellent model organism for analysis of pathophysiology behind many diseases, the potential use as a model for ADPKD was assessed.

Immunofluorescence microscopy revealed that wild type Ddpolycystin in AX2 cells co-localised with the plasma membrane marker H36, confirming this subcellular location which has previously been reported (Lima *et al*., 2014; Traynor and Kay, 2017). The fluorescence images also revealed areas of Ddpolycystin corresponding with intracellular localization. Considering that PC2 in mammals has also been identified to function at the ER (Cai *et al*., 1999; Koulen *et al*., 2002), I decided to determine if Ddpolycystin is also expressed at the ER in *Dictyostelium*. Immunofluorescence microscopy revealed no colocalization of Ddpolycystin with the ER marker calnexin. This was not surprising it lacks the COOH- terminal ER retention signal present in mammalian PC2 (Lima *et al*., 2014), which has been attributed to a 34-amino acid region ^{Glu}787-^{Ser}820 in the COOH- terminal (Cai *et al*., 1999). It is important to note however, that the specificity of the anti-Ddpolycystin antibody does need to be confirmed, for example by Western blot using lysate from Ddpolycystin KO cells, this was not within the scope of this thesis, so it is important that this is tested in future studies.

The conformation that Ddpolycystin is localized to the plasma membrane in AX2 cells suggests that it may indeed be a Ca^{2+} channel facilitating extracellular Ca^{2+} influx. To investigate whether Ddpolycystin can function as a Ca^{2+} channel, chemotactic Ca^{2+} responses in knockdown and overexpression transformants were measured and analysed. If Ddpolycystin was capable of Ca^{2+} channeling, it was expected that overexpressing and knocking down expression of the protein would increase and decrease the Ca^{2+} responses respectively. Indeed, analysis of chemotactic Ca^{2+} responses revealed that they were

significantly altered. Overexpressing Ddpolycystin significantly amplified the magnitude of the Ca^{2+} responses to 1µM cAMP and 1µM folic acid compared to wild type. Furthermore, in knockdown transformants the Ca^{2+} responses were reduced, as were the basal cytosolic Ca^{2+} levels. These results infer not only that Ddpolycystin contributes to the responses, but also to maintaining the cells resting Ca^{2+} levels.

Analysis of the maximum rise and fall rates of cytosolic Ca^{2+} in Ddpolycystin mutants revealed the same relationship in response kinetics to both cAMP and folic acid and shows that the Ca^{2+}-regulated Ca^{2+} channels and pumps are the same for the two attractants, since responses to them exhibit the same kinetic properties. The relationship between the response onset time and response magnitude was negative for Ddpolycystin overexpression, knockdown and control strains, and in this respect is similar to the relationship previously reported for wild type, calnexin-deficient and calreticulin-deficient strains (Wilczynska *et al*., 2005). However, in my work, each set of strains falls on a different line so that in overexpression strains the response magnitude is greater than the controls by a constant amount at all response times. Conversely in the knockdown strains, the response magnitude is reduced by a constant amount, independent of response times, compared to controls. The simplest explanation is that Ddpolycystin is itself a significant contributor to the Ca^{2+} responses at all response times and magnitudes, but that the mechanism by which the response time and magnitude are coupled is unchanged eg. in the form of Ca^{2+}-induced Ca^{2+} release. This makes sense, given that these strains differ only in the level of expression of the Ddpolycystin channels, each of which however is wild type and functionally unchanged. These results provide compelling evidence for Ddpolycystin as a Ca^{2+} channel. I therefore suggest that after ligand binding of the plasma membrane GPCRs cAR1 and fAR1, intracellular signaling activates Ddpolycystin which contributes to the initial influx of Ca^{2+} over the plasma membrane from the extracellular medium into the cytosol. The response is then further amplified by release from the ER, and other intracellular Ca^{2+} pools such as the CV, acidic vesicles and mitochondrion which probably also contribute to this response, however this is yet to be measured.

Regulation of Ddpolycystin channeling activity is unknown, in other organisms modulation of PC2 channel activity includes regulation by Ca^{2+} itself through the C-terminal EF-hand motifs (Schumann *et al*., 2009; Petri *et al*., 2010; Celic *et al*., 2012), and interactions with

PC1 (Hanaoka *et al*., 2000) and the InsP3 receptor (Sammels *et al*., 2010). In *Xenopus* oocytes PC2 interacts via its COOH terminus with the InsP3 receptor to form a functional complex that facilitates intracellular Ca^{2+} release (Li *et al*., 2005). In mouse renal epithelial cells, the InsP3 receptor directly gated PC2 channel activity by interactions of the two channels through acidic residues in the N-terminal ligand binding domain of the InsP3 receptor and the C-terminal ER retention signal of PC2 (Sammels *et al*., 2010). Given this, and the distribution patterns of Ddpolycystin and IplA in *Dictyostelium*, it is possible that Ddpolycystin and IplA are potential interaction partners, and when together in the same sub cellular compartment both contribute to the chemotactic Ca^{2+} response. Evidence that both channels are involved in the Ca^{2+} response to chemoattractants comes from a combination of a report published by Traynor and Kay (2017), who found that Ddpolycystin KO strains retained normal responses to cAMP and folic acid, and my results that show differences in chemoattractant Ca^{2+} signaling in the overexpression and knockdown strains. Together these results suggest that Ddpolycystin *is* able to contribute to these responses, however the case may be that in the wild type situation both IplA and Ddpolycystin reside at the plasma membrane and facilitate Ca^{2+} influx. When Ddpolycystin is knocked out, IplA expression is up regulated so that normal Ca^{2+} homeostasis remains and Ca^{2+} responses are not altered. When IplA is knocked out, the Ca^{2+} responses are either abolished or reduced, suggesting that IplA itself may be responsible for gating Ddpolycystin. Indeed, Traynor and Kay (2017) found that a Ddpolycystin/IplA double KO completely lacked cAMP calcium responses. Coimmunoprecipitations of IplA and Ddpolycystin would also uncover whether the channels indeed interact. Another potential interaction partner of Ddpolycystin is the putative PC1 homologue that is encoded in the *Dictyostelium* genome (dictyBase gene ID: DDB_G0289409). Characterization of this protein is needed to reveal whether it functions as a PC1 like protein and interacts with Ddpolycystin-2, and determine its involvement in Ca^{2+} signalling.

Aberrant Ca^{2+} signaling can impact on the plethora of cellular processes that are Ca^{2+}-dependent. Previous reports have been somewhat conflicting in respect to phenotypic effects of knocking out Ddpolycystin in different laboratories. Some KO strains had rheotaxis defects (Lima *et al*., 2014) while others did not (Artemenko *et al*., 2016; Traynor and Kay, 2017), similarly some KO strains had growth defects (Waheed *et al*., 2014) and not others (Traynor and Kay, 2017). It may be that the phenotypes are only subtle

therefore not always detectable in an all or nothing system comparing KO cells to wildtype cells. Therefore, in my experiments, the use of knockdown and overexpression strains and correlating the phenotypic severity to an expression index may highlight subtle phenotypes. My results show that Ddpolycystin positively regulates growth rates and the nutrient uptake processes of macropinocytosis and phagocytosis. While the defects were only mild in knockdown strains, they were more pronounced in the overexpression strains. Therefore, strong correlations between the Ddpolycystin expression index and the phenotypic defects did indeed highlight that Ddpolycystin does help to regulate these processes, presumably through modulation of Ca^{2+} signaling as many steps of the endocytic pathway are known to be Ca^{2+} regulated in mammalian cells (Luzio *et al*., 2007; Patel and Cai, 2015). Lima *et al*. (2014) reported that in DH1-10 cells, some Ddpolycystin colocalizes with p25 marker for recycling endosomes. As I did not label endocytic vesicles in my experiments, I cannot rule out this possible subcellular location in my strains. In favour of a regulatory role for Ddpolycystin dependent Ca^{2+} signaling in endosomal trafficking, KO cells had reduced Ca^{2+} stimulated lysosome exocytosis (Lima *et al.,* 2014). Evidence suggests that Ca^{2+} signaling is involved in endocytic process in *Dictyostelium.* For example, KO mutants of fAR1, upon binding to bacteria, have a greatly reduced ability to induce actin polymerization or produce phagocytic cups, potentially due to the absence of fAR1 associated chemotactic signaling which likely involves Ca^{2+} (Pan *et al*., 2016). Furthermore, the calcium regulated actin bundling protein, fibrin, is associated with both the macrophagosome and macropinosome during formation (Pikzack *et al*., 2005). Biochemical studies have shown that disrupted Ca^{2+} homeostasis due to caffeine treatment inhibited axenic growth and fluid phase pinocytosis, results that were mimicked by treatment with the calcium transport inhibitor La^{3+} (Gonzalez *et al*., 1990). Since Ddpolycystin was observed at the plasma membrane and recycling endosomes (Lima *et al.,* 2014) it is possible that Ddpolycystin contributes to Ca^{2+} release from endocytic compartments to aide with membrane fusion/fission events.

The autophagic pathway in *Dictyostelium* plays an important role in multicellularity leading to the development of stalk cells. Ddpolycystin dependent Ca^{2+} signaling was evident in cell type specific differentiation and spore germination. Knockdown and overexpression strains exhibited abnormal stalk cell differentiation because knockdown strains had thin weak stalks and overexpression strains had thick stalks. Fragile fruiting

bodies that often collapse have been reported in Ddpolycystin KO cells (Traynor and Kay, 2017) which may be the result of thin stalks similar to what I observed in my knockdown strains. These phenotypes may reflect aberrant Ca^{2+} signaling and suggest that precise control of Ca^{2+} release by Ddpolycystin is necessary to maintain normal stalk/spore proportions within the population. This process is known to be Ca^{2+} regulated as cell type specific differentiation into prespore and prestalk cells is controlled partly by Ca^{2+}, where higher Ca^{2+} levels tend to direct cells to the prestalk pathway, and lower Ca^{2+} to the prespore pathway (Saran *et al*., 1994; Azhar *et al*., 1996; Schaap *et al*., 1996; Poloz and O'Day, 2012). Furthermore, stimulation with Differentiation Inducing Factor (DIF) causes intracellular Ca^{2+} concentrations to increase, which induces some pre-stalk specific genes (Schaap *et al*., 1996; Azhar *et al*., 1997). Defective autophagy is reported in ADPKD (Aguilar, 2017) but only recently a role for PC2 dependent Ca^{2+} signaling in autophagy is emerging. Impaired Ca^{2+} handling in PC2 deficient cells and KO mice impairs autophagic flux in response to nutrient deprivation. Conversely overexpression of PC2 enhanced autophagic flux. The PC2 regulation of autophagy appeared to be through regulation of intracellular Ca^{2+} because autophagy was attenuated after chelation of intracellular Ca^{2+} (Criollo *et al*., 2018). Similarly, knockdown of PC2 in human embryonic stem cell-derived cardiomyocytes reduced caffeine induced cytosolic Ca^{2+} rise and autophagic flux under glucose starvation. In these cell lines two stress sensor proteins that modulate autophagy were dysregulated. Starvation-induced activation of AMP-activated protein kinase (AMPK) was reduced, as was inactivation of mammalian target of rapamycin (mTOR) (Lu *et al*., 2018). Furthermore, PC2 activity has been found to be necessary to induce autophagy from hyperosmotic stress in HeLa and HCT116 cells via the mTOR pathway (Peña-Oyarzun *et al*., 2017). Because *Dictyostelium* is an ideal model for studying autophagy and autophagic cell death (Tresse *et al*., 2008; Calvo-Garrido *et al*., 2010) and much is already known about the AMPK (Bokko *et al.*, 2007) and DdTOR signalling (Swer *et al*., 2016), the model provides an invaluable system for investigating Ddpolycystin regulated autophagy and the signaling pathways involved.

Concluding remarks

This study has provided evidence that Ddpolycystin functions as a Ca^{2+}-conductive channel located at the plasma membrane in *Dictyostelium*, Ddpolycystin contributes to cytosolic Ca^{2+} signaling in response to chemotactic stimuli and its function may be regulated by IplA.

Further, Ddpolycystin dependent Ca^{2+}-signalling must be tightly controlled to regulate down-stream Ca^{2+} sensitive processes such as endocytosis, growth and autophagic cell death. Importantly, this study has also highlighted the potential to use *Dictyostelium* as a model to study the underlying molecular functioning behind ADPKD.

Chapter four

Ddmucolipin and its role in *Dictyostelium*

The information in this chapter has been accepted for publication. This chapter is based on the published work, but is not an exact replication. A full copy of the published manuscript and statement of contributions of joint authorship can be viewed in appendix 8.

Manuscript details:

Allan, C.Y. and Fisher P.F. (2022). The *Dictyostelium* model for Mucolipidosis Type IV. *Front. Cell Dev. Biol.* **(10)** doi: 10.3389/fcell.2022.741967

4.1 Introduction

4.1.1 Transient Receptor Potential Mucolipin (TRPML)

Transient receptor potential mucolipins (TRPMLs) belong to a conserved family of ion channels (Dong *et al.,* 2010), which localize to the membranes of components of the endocytic pathway. The three mammalian mucolipin homologues, TRPML1, TRPML2 and TRPML3, are encoded by the genes *MCOLN 1-3* (Cheng *et al.,* 2010; Grimm *et al.,* 2012). TRPML channels are non-selective cation channels permeable to a range of cations including Na^{+}, Ca^{2+}, Fe^{2+}, and Zn^{2+}, and are predicted to have six TMDs and cytosolic amino and carboxyl-terminus regions, and a pore region between TM5-TM6 (Grimm *et al*., 2007; Kim *et al*., 2010; Grimm *et al*., 2012). TRPMLs are localised to the membranes of components of the endocytic pathway, with TRPML2 and TRPML3 also localized to the plasma membrane (Kim *et al*., 2007; Dong *et al*., 2010). The cellular functions of the TRPMLs are associated with trafficking and sorting of membranes along the endocytic pathway (Cheng *et al*., 2010; Chen *et al.*, 2017; Plesch *et al*., 2018). TRPML-mediated Ca^{2+} release is involved in Ca^{2+} dependent fusion/fission events of membranes along the endocytic pathway (LaPlante *et al*., 2004), the importance of Ca^{2+} for such events being well established (Luzio *et al*., 2007; Brailoiu and Brailoiu, 2016). Additionally, TRPML1 is implicated in regulation of autophagy, mechanistic target of rapamycin (mTOR) and transcription factor EB (TFEB) signalling (Sun *et al*., 2018; Boudewyn and Walkley, 2019).

4.1.2 Ca^{2+} signaling at the endocytic pathway

The vesicles of the endolysosomal system are essential to maintenance of cellular homeostasis through macromolecule recycling and are important Ca^{2+} storage organelles which are integral to cellular Ca^{2+} signalling (Patel and Docampo, 2010; Patel and Cai, 2015) and can help regulate ER calcium signals by sequestering calcium (López-Sanjurjo *et al.,* 2013; López-Sanjurjo *et al.,* 2014). While there have been many advances in knowledge into the mechanisms associated with plasma membrane and ER Ca^{2+} signaling, the mechanisms associated with Ca^{2+} signaling by the acidic Ca^{2+} stores are only beginning to be expounded. In mammalian cells, luminal free Ca^{2+} concentrations estimations have varied from approximately 3-600 µM (Christensen *et al*., 2002, Luzio *et al*., 2007), substantially higher than cytosolic Ca^{2+} of around 100nM. Ca^{2+} release from vesicles regulates organelle homeostasis, compartmental acidification (Gerasimenko *et al*., 1998;

Dong, 2010; Morgan *et al*., 2011) and homotypic and heterotypic fusion of endosomal vesicles (Pryor *et al.*, 2000; Hay, 2007), as well as reformation of discrete compartments (Pryor *et al.*, 2000; Luizo *et al*., 2007a). Local Ca^{2+} bursts released from endosomal compartments can facilitate membrane fusion approximately 20-100 nm from the site of release (Neher, 1998; Burgoyne and Clague, 2003), Ca^{2+} signals are then dissipated by sequestering back to the lumen. This Ca^{2+} release from and sequestration back into the acidic stores is facilitated by the TPC, TRPMLs (Grimm *et al*., 2012b), and the resident Ca^{2+}-H^{+} exchangers (Melchionda *et al*., 2016). Ca^{2+}-dependent signalling is thought to regulate the soluble *N*-ethylmaleimide-sensitive-factor attachment protein receptors (SNARE) complex proteins, which are proteins involved in the fusion of vesicle membranes (Bharat *et al.,* 2014; Han *et al.,* 2017). Alongside SNAREs, the protein early endosome antigen-1 (EEA1) is necessary for vesicle tethering prior to fusion, and is regulated by Ca^{2+}/calmodulin dependent signalling through its IQ domain (Mills *et al.,* 1998; Christoforidis *et al.,* 1999; Lal*et al.,* 2003).

Acidic stores have also been implicated in global Ca^{2+} signal initiation and propagation through close associations between the lysosomes and ER. The second messenger NAADP is believed to stimulate lysosomal Ca^{2+} release which in turn activate neighboring ER Ca^{2+} channels resulting in propagation of global signalling (Kilpatrick *et al*., 2013; Kilpatrick *et al*., 2016). The ER might also supply Ca^{2+} to refill the lysosomal luminal stores after release (López-Sanjurjo *et al*., 2013; López-Sanjurjo *et al*., 2014). TRPML specific peri-lysosomal calcium signals have been notoriously difficult to measure due to the localised nature of the signals which are often clouded by larger global calcium signals. In an attempt to resolve the local calcium signals genetically encoded calcium sensors directly tagged to TRPML1 have been used to measure local calcium transients (Shen *et al*., 2012; Cao *et al*., 2015; Medina *et al*., 2015). The TRPML agonist ML-SA1 stimulates calcium release into the cytoplasm (Shen *et al*., 2012), which in some cell types is independent of extracellular and ER calcium pools (Gómez *et al*., 2018). However, some evidence shows that TRPML channels can affect ER calcium release and activate influx of calcium across the plasma membrane to contribute to global calcium signals (Kilpatrick *et al.,* 2016), and small calcium release from the acidic stores can prime and amplify calcium release from the ER (Ronco *et al*., 2015).

4.1.3 Channeling properties of TRPML

Historically there has been some uncertainty around the channeling properties of TRPMLs. Inward and outward rectifying currents have been measured in different systems leading to a lack of consensus as to whether the channels release Ca^{2+} or facilitate its uptake. Outward rectification of TRPML1 has been reported in in human fibroblasts (Kiselyov *et al*., 2005), and a study using planar lipid bilayers reported TRPML1 to be an outwardly rectifying cation channel which moves cations into the lysosomal lumen and is blocked by Ca^{2+} (Cantiello *et al*., 2005). Soyombo *et al*. (2006) reported findings that TRPML1 has no effect on cellular Ca^{2+} signalling or lysosomal luminal Ca^{2+} content, but in fact is a regulator lysosomal pH, and consequently lipid hydrolysis and metabolism. More recently, the role of TRPML1 in lysosomal Ca^{2+} release has been reported from a number of studies (Zhang *et al*., 2009; Feng *et al*., 2014; Kilpatrick *et al*., 2016; Cao *et al*., 2017; Wu *et al*., 2018a), and appears to be an important functional attribute. TRPML2 has been shown to act as an inwardly rectifying lysosome Ca^{2+} release channel (Lange *et al*., 2008; Lange *et al*., 2009) whose expression is influenced by TRPML1 expression (Samie *et al*., 2009). The Ca^{2+} channeling properties of TRPML3, shown through whole cell patch clamp techniques, have indicated that it is an inwardly rectifying Ca^{2+} permeable cation channel in HEK-293 cells where the protein was localised in intracellular vesicles and the plasma membrane (Di Palma *et al*., 2002; Kim *et al*., 2007). An activating mutation in the TRPML3 pore region (A419P), locks the channel open to induce large amounts of Ca^{2+} flow from the extracellular into the cytoplasm inducing apoptosis and cell death (Kim *et al*., 2007; Xu *et al*., 2007). Interestingly, TRPML control over ER Ca^{2+} release and uptake has been identified (Kilpatrick *et al*., 2016). Reported mechanisms of activation have included regulation by Ca^{2+} and pH, where TRPML1 has been found to have high conductance in low pH environments and low conductance in neutral pH environments. Therefore, the specific subcellular location, which impose different Ca^{2+} concentrations and pH, can affect function of the channel (Li *et al*., 2017). The second messenger nicotinic acid adenine dinucleotide phosphate (NAADP) has been shown to induce TRPML1 to release Ca^{2+} from lysosomal lumen (Zhang *et al*., 2009), as has the binding of $PI(3,5)P_2$, a phosphoinositide enriched in endolysosomes, which is thought to regulate juxta-organellar Ca^{2+} release via TRPML1 (Dong *et al*., 2010a, Feng *et al*., 2014).

4.1.4 Mucolipidosis type IV

Mucolipidosis type IV (MLIV) is a devastating neurological lysosomal disease (Berman *et al*., 1974) caused by loss of function mutations in TRPML1 (Sun *et al.,* 2000). MLIV is characterized by growth and psychomotor retardation, severe visual impairment attributed to corneal clouding (Berman *et al*., 1974; Smith *et al*., 2002; Goldin *et al*., 2008), and elevated blood gastrin levels caused by achlorhydria (Schiffmann *et al*., 1998). Defects in TRPML1 cause defective sorting of membranes along the late endocytic pathway which results in accumulation of phospholipids, sphingolipids, and acid mucopolysaccharides in lysosomes (Bargal and Bach, 1997). MLIV differs from other lysosomal diseases, as the lysosomal hydrolases in MLIV cells are not defective (Chen *et al*., 1998). The defective transport of lipids to the Golgi and plasma membrane causes accumulation of substrates in the lysosomes and disrupts transport pathways (Bargal and Bach, 1997; Chen *et al*., 1998; Pryor *et al.*, 2006; Miedel *et al*., 2008). Model studies have found that defective membrane trafficking can be caused by both KO and overexpression of TRPMLs causing accumulation of large hybrid late endosomes-lysosome (LEL) compartments (Lubensky *et al*., 1999; Berman *et al*., 1974) and enlargement and clustering of endosomes (Fares and Greenwald, 2001; Kim *et al*., 2007; Martina *et al*., 2009; Vergarajauregui *et al*., 2009). The exact nature of how loss of function of TRPML1 causes cellular storage and neuronal dysfunction is still not well understood. TRPML-associated dysfunction in the endolysosomal system is also implicated in other neurodegenerative diseases (Santoni *et al.,* 2020; Lee *et al.,* 2021). Therefore, TRPMLs may underpin the pathophysiology of neurodegenerative disease more generally and are suggested to be a therapeutic target.

A variety of model organisms have been used to study TRPML proteins including the mouse (Kim *et al.,* 2007; Micsenyi *et al.,* 2009; Curcio-Morelli *et al.,* 2010), zebrafish (Benini *et al.,* 2013), *Drosophila* (Venkatachalam *et al.,* 2008; Wong *et al.,* 2012; Feng *et al.,* 2014), *C. elegans* (Fares and Greenwald, 2001; Treusch *et al.,* 2004) and yeast (Denis and Cyert, 2002). One important cellular model, the eukaryotic social amoeba, *Dictyostelium*, encodes a single mucolipin homologue, *mcln* (Termed *Ddmucolipin* in this thesis) (Wilczynska *et al.,* 2005; Lima *et al.,* 2012) which has been the subject of only a limited number of studies. *Dictyostelium* is a well-established model to study neurodegenerative and lysosomal disease (Annesley and Fisher 2009; Maniak, 2011; Annesley *et al.,* 2014; Martín-González *et al.,* 2021). This model organism has been

extensively employed to study the function of proteins associated with neuronal ceroid lipofuscinosis (NCL) (Huber, 2020), a group of lysosomal diseases linked to mutations in the genes, *CLN1-CLN8* and *CLN10-CLN14* (Yap *et al*., 2021). Therefore, *Dictyostelium* is a promising model to study lysosomal disorders and Ddmucolipin function.

4.1.5 Studying Ddmucolipin function and creating a MLIV model in *Dictyostelium*

Ddmucolipin was first identified by Wilczynska *et al*. (2005) and shares homology to all three human TRPMLs. Protein alignments of a conserved TRPML similarity region (positions 385–541, TM3 to TM6) show that Ddmucolipin shares 55% similarity with the human protein in this region (Lima *et al*., 2012). Like the human homologues Ddmucolipin is predicted to have six TM domains (Fig 4.0), a conserved pore region at position 498–511, and a large extracellular loop between TM1 and TM2. However, unlike the human proteins, Ddmucolipin contains a predicted C-terminal Ca^{2+}-binding EF-hand (pos. 614–626) (Lima *et al*., 2012). In DH1-10 *Dictyostelium* cells Ddmucolipin has been localised to endosomal compartments rich in the endosomal marker p80, predominately to post lysosomes (Lima *et al*., 2012). Evidence suggests that Ddmucolipin is involved in Ca^{2+} homeostasis and signalling because knockout cells grew two times faster than wild type in Ca^{2+} depleted medium, they also had reduced Ca^{2+} concentrations in secretory post lysosomes, and accordingly controlled calcium induced lysosome exocytosis (Lima *et al.,* 2012) and are defective in rheotaxis, a calcium-regulated mechanosensing mechanism (Lima *et al.,* 2014). These results do indicate Ddmucolipin plays a role in both the endocytic cycle and Ca^{2+} signaling, however, the role of this putative channel in Ca^{2+} signalling has not been studied, therefore it was of particular interest to investigate the role of Ddmucolipin in chemotactic calcium signalling in *Dictyostelium*.

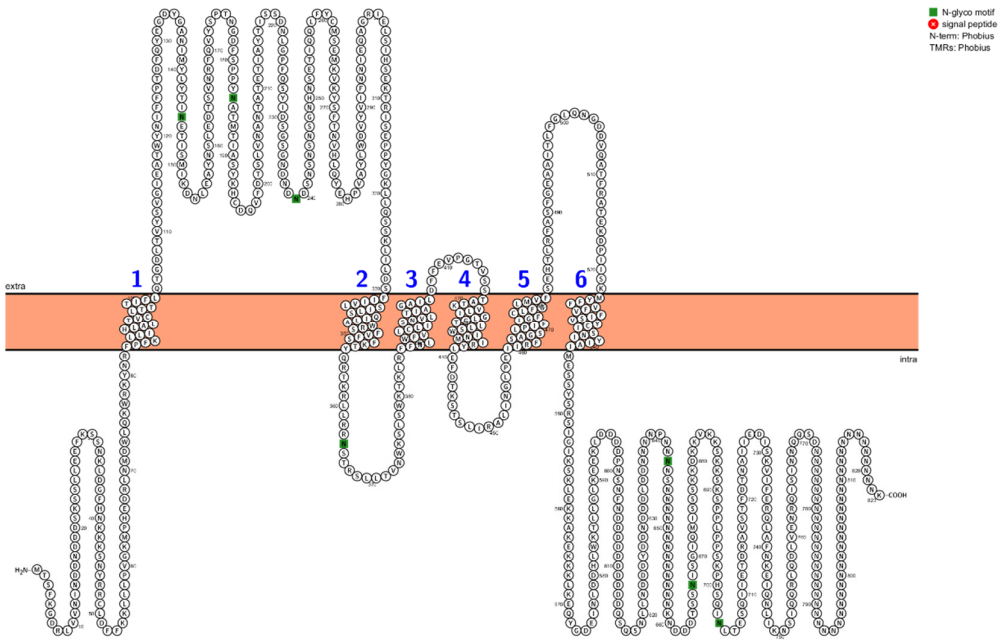

Figure 4.0 Predicted membrane topology of Ddmucolipin.

Ddmucolipin is predicted to comprise six TM domains with cytosolic NH_2 and COOH terminals. Topology predicted using: Protter (Omasits *et al*., 2014).

Dictyostelium is a well-established model to study calcium signalling (Nebl and Fisher, 1997; Traynor *et al*., 2000; Nebl *et al.,* 2002; Schaloske *et al*., 2005; Fisher and Wilczynska, 2006; Malchow *et al*., 2008). Given the localisation of Ddmucolipin at the post-lysosomes and potentially other vesicles of the endocytic pathway, I decided to determine if Ddmucolipin and these endocytic vesicles are involved in cytosolic Ca^{2+} responses to chemoattractants. To achieve this, I created Ddmucolipin overexpression and knockdown strains which coexpress the calcium-sensitive luminescent protein apoaequorin which allowed me to analyze real-time chemotactic induced cytoplasmic Ca^{2+} responses (Nebl and Fisher, 1997).

My experiments revealed that when overexpressed, Ddmucolipin is involved in chemoattractant-elicited Ca^{2+} responses because overexpression strains had enhanced responses to both cAMP and folic acid. Surprisingly, chemoattractant Ca^{2+} responses in knockdown strains were also enhanced, but only in vegetative cells. Responses in aggregation-competent cells were not affected in the knockdown strains, suggesting that, unless overexpressed, Ddmucolipin is not a major contributor to cAMP-mediated calcium

responses. However, it may be involved in local Ca^{2+} signalling associated with changes in the vesicle trafficking pathways throughout the developmental cycle, in particular aggregation center formation and autophagic cell death.

In other work, the cellular phenotypes of growth, endocytosis and multicellular development were found to be unaffected in Ddmucolipin knockout cells created from the parental strain DH1-10 (Lima *et al*., 2012). Therefore, I decided to analyze these phenotypes in my strains which were created from the parental strain AX2. I discovered that Ddmucolipin expression did affect growth rates and nutrient uptake via macropinocytosis and phagocytosis in AX2. Surprisingly however, the phenotypes were not linear in that both increasing and decreasing expression of Ddmucolipin often, but not always, resulted in the same phenotypic outcome. Both overexpression and knockdown strains had increased fluorescence in cells stained with Lysosensor blue, indicating either increased acidification of the vesicles or increased abundance of the vesicles. Phagocytosis and pinocytosis rates were upregulated, but this did not correlate with an increase in growth rates, which suggests defects in catabolism, in endocytic vesicle trafficking or in endolysosomal breakdown of macromolecular contents. Ddmucolipin is involved in the regulation of aggregation as both overexpression and knockdown strains formed smaller, more numerous slugs and fruiting bodies than AX2. Increased numbers of cells entering the autophagic cell death pathway were also evident in Ddmucolipin mutants because they had thickened stalks compared to AX2. My results suggest that normal growth and development of *Dictyostelium* is sensitive to Ddmucolipin expression, and my strains show similar phenotypes to other *Dictyostelium* lysosomal disease models further affirming that *Dictyostelium* is an ideal model to study lysosomal disease.

4.2 Results

4.2.1 Creation of *Ddmucolipin* constructs

In order to achieve knockdown and overexpression of Ddmucolipin, plasmid constructs for asRNA expression and overexpressing *Ddmucolipin* were created using the two phase cloning method.

4.2.1.1 *Ddmucolipin* antisense construct

4.2.1.1.1 First phase cloning into an *E. coli* vector

To facilitate inhibition of protein expression, a fragment of the *Ddmucolipin* gene was cloned into a *D. discoideum* expression vector in the antisense orientation. This vector is then introduced into *D. discoideum* cells via transformation where it will randomly insert into the genome.

To produce an asRNA inhibition construct that will decrease expression of *Ddmucolipin*, a 1411bp 3' fragment of *Ddmucolipin* gDNA was amplified via PCR with the primers MuMF and MUR2, using DNA extracted from vegetative AX2 cells as a template. The product was then cloned into the *E. coli* vector pZErO2 using the endonuclease restriction cut sites *Bam*HI and *Kpn*I to create the construct pPROF649, which was verified by sequencing. The schematic representation of the cloning strategy is shown in Figure 4.1.

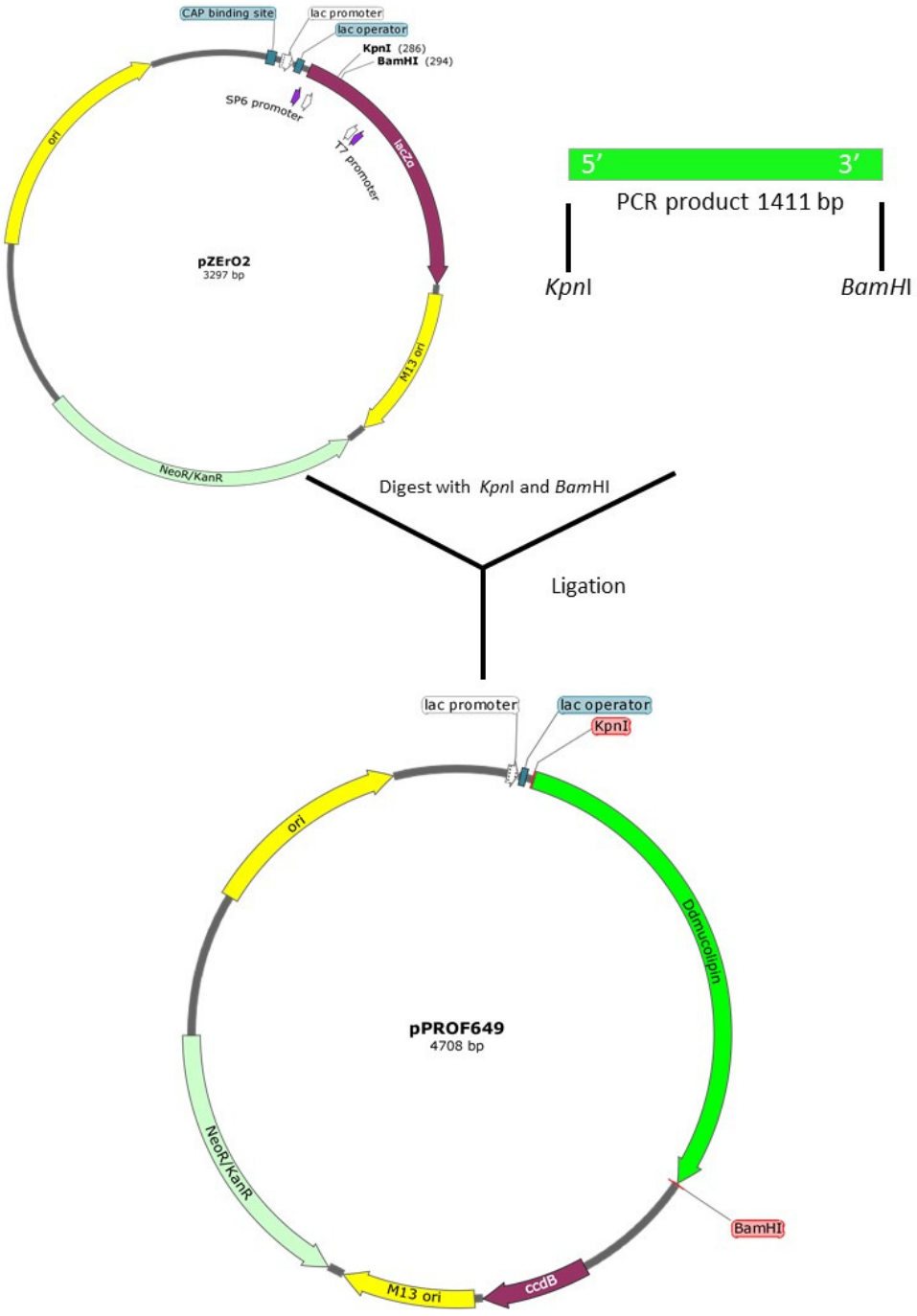

Figure 4.1 Cloning strategy phase one – *Ddmucolipin* antisense construct.

The *Ddmucolipin 3'* gDNA fragment (1411 bp) was PCR amplified from AX2 gDNA using primers MuMF and MUR2. The amplified fragment was inserted into the *Bam*HI/ *Kpn*I sites of the *E. coli* vector pZErO™-2. The ligation product was electroporated into *E. coli* Top10 cells and colonies were selected for using kanamycin resistance. Colonies were further screened using restriction analysis of miniprep DNA from cultures grown from individual colonies. The resulting construct pPROF649 was confirmed via sequencing.

4.2.1.1.2 Subcloning of the Ddmucolipin antisense fragment into a *D. discoideum* expression vector

The 1411 bp fragment of *Ddmucolipin* gDNA was excised from pPROF649 using the restriction endonuclease cut sites *Bam*HI and *Kpn*I and subcloned in the antisense orientation into the *Dictyostelium* expression vector pDNeo2. The resulting construct, pPROF650, was verified by restriction enzyme digest. The schematic representation of the cloning strategy is shown in Figure 4.2.

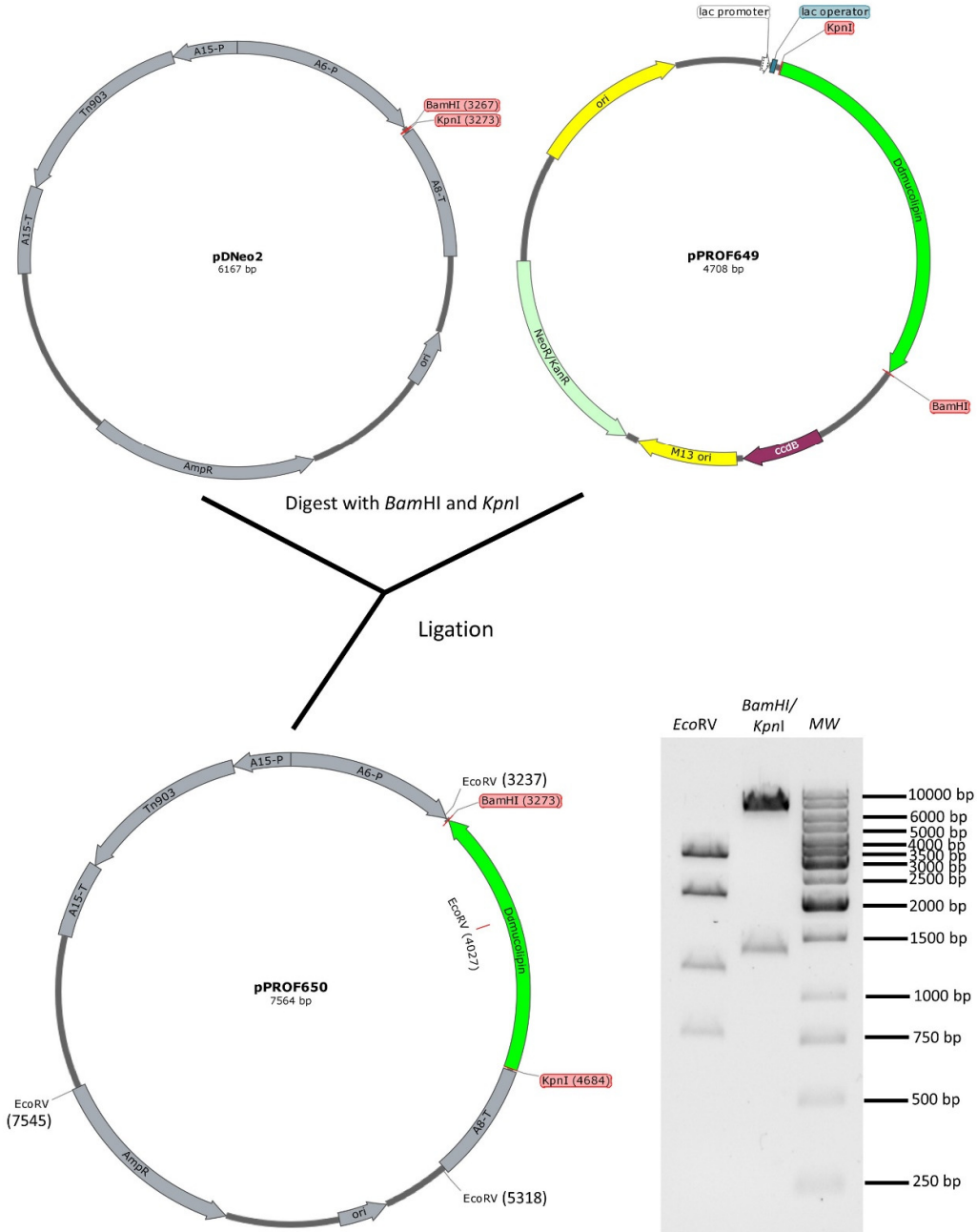

Restriction enzyme analysis – *Ddmucolipin* antisense inhibition construct pRPOF650

Construct name	Restriction enzymes	Expected fragments size (bp)
pPROF650	BamHI/KpnI	6153 bp + 1411 bp
	EcoRV	3256 + 2227 + 1291 + 790 bp

Figure 4.2 Cloning strategy phase two–- *Ddmucolipin* antisense construct.

The 1411 bp fragment from pPROF649 was excised and subcloned in the antisense orientation into the *D. discoideum* expression vector pDNeo2 using the endonuclease cut sites *Bam*HI and *Kpn*I. The ligation product was electroporated into *E. coli* DH5α cells, and colonies were selected on ampicillin. Plasmid miniprep DNA from individual colonies was extracted and screened by restriction analysis. The resulting construct pPROF650, was verified by restriction enzyme analysis.

4.2.1.2 Ddmucolipin overexpression construct

4.2.1.2.1 First phase cloning into an *E. coli* vector pZErO-2

To create a construct that will increase expression of *Ddmucolipin,* the gene was cloned. The full length gDNA *Ddmucolipin* gene was amplified by PCR in two sections using AX2 gDNA as a template using the primers MUF and MuMR for the 1371 bp 5' fragment, and MuMF and MUR2 for the 1408 bp 3' fragment (Table 2.3.1). A three-fragment ligation allowed the full length gDNA to be and cloned first into the bacterial vector pZErO-2 (Invitrogen, Carlsbad, CA) with the restriction enzyme *Bam*HI, and utilization of a resident *Kpn*I restriction site within the gene sequence allowed seamless ligation of the 5' and 3' gene fragments to produce the construct pPROF637. The schematic representation of the cloning strategy is shown in Figure 4.3.

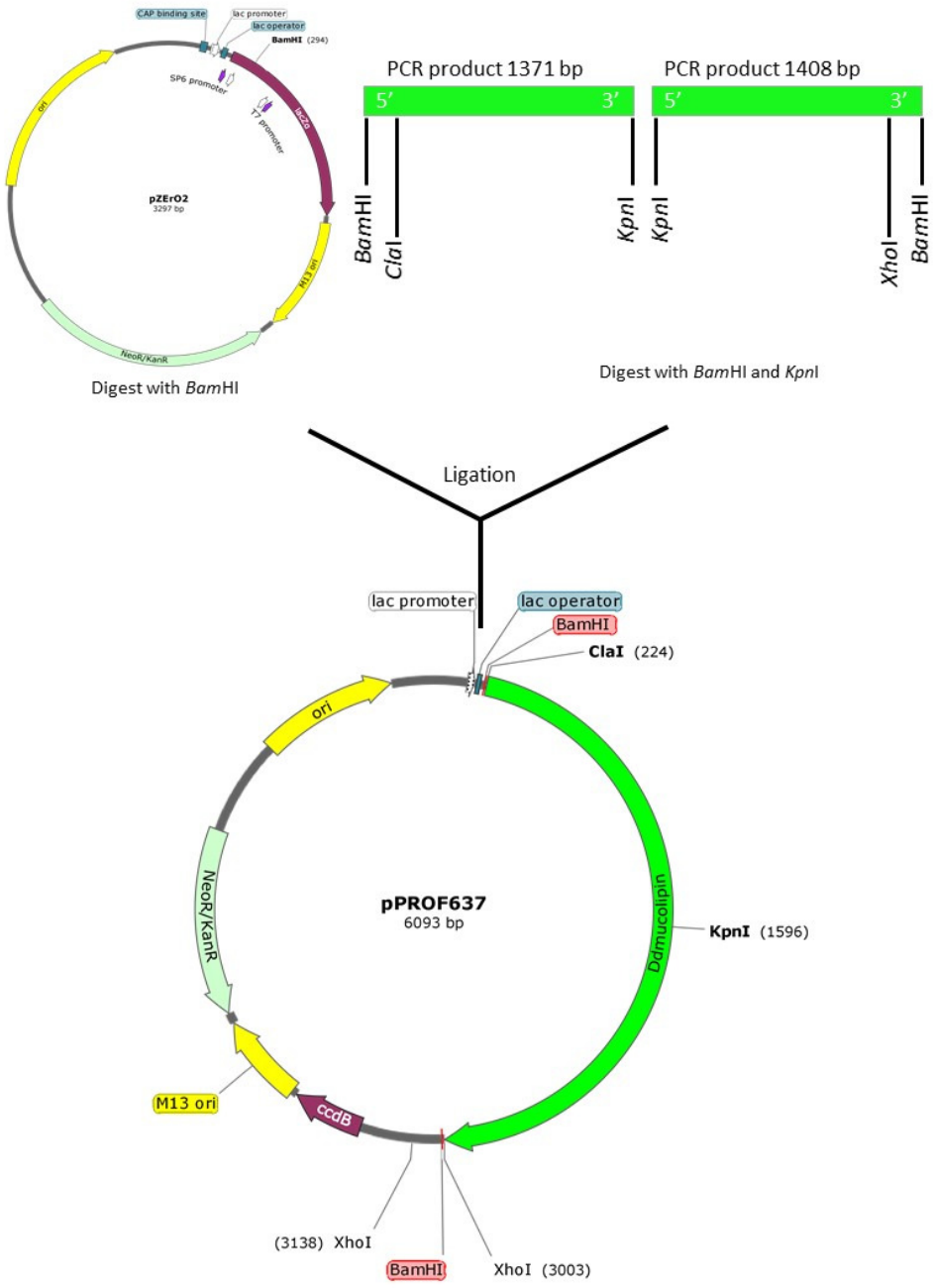

Figure 4.3 Cloning strategy phase one–- *Ddmucolipin* overexpression construct.

Two sections of *Ddmucolipin* gene gDNA were amplified from AX2 gDNA in two sections using primers MUF and MuMR for the 5' fragment, and MuMF and MUR2 for the 3' fragment. A three fragment ligation allowed the full length gDNA to be and cloned into the bacterial vector pZErO-2 using the restriction site *Bam*HI, and utilization of a resident *Kpn*I restriction site within the gene. The *Cla*I and *Xho*I restriction enzyme cut sites were included in the primers to facilitate subcloning of the gene. The ligation product was electroporated into *E. coli* Top-10 cells and colonies were selected on kanamycin resistance. Individual colonies were screened further via restriction analysis of miniprep DNA. The resulting construct pPROF637 was confirmed via sequencing.

4.2.1.2.2 Subcloning of the Ddmucolipin full length gene into a *D. discoideum* expression vector

The full length *Ddmucolipin* gene was excised from pPROF637, subcloned into the *D. discoideum* expression vector pA15GFP using the *Xho*I and *Cla*I restriction enzyme sites and named pPROF638. The construct was verified by restriction enzyme digestion. The schematic representation of the cloning strategy is shown in Figure 4.4.

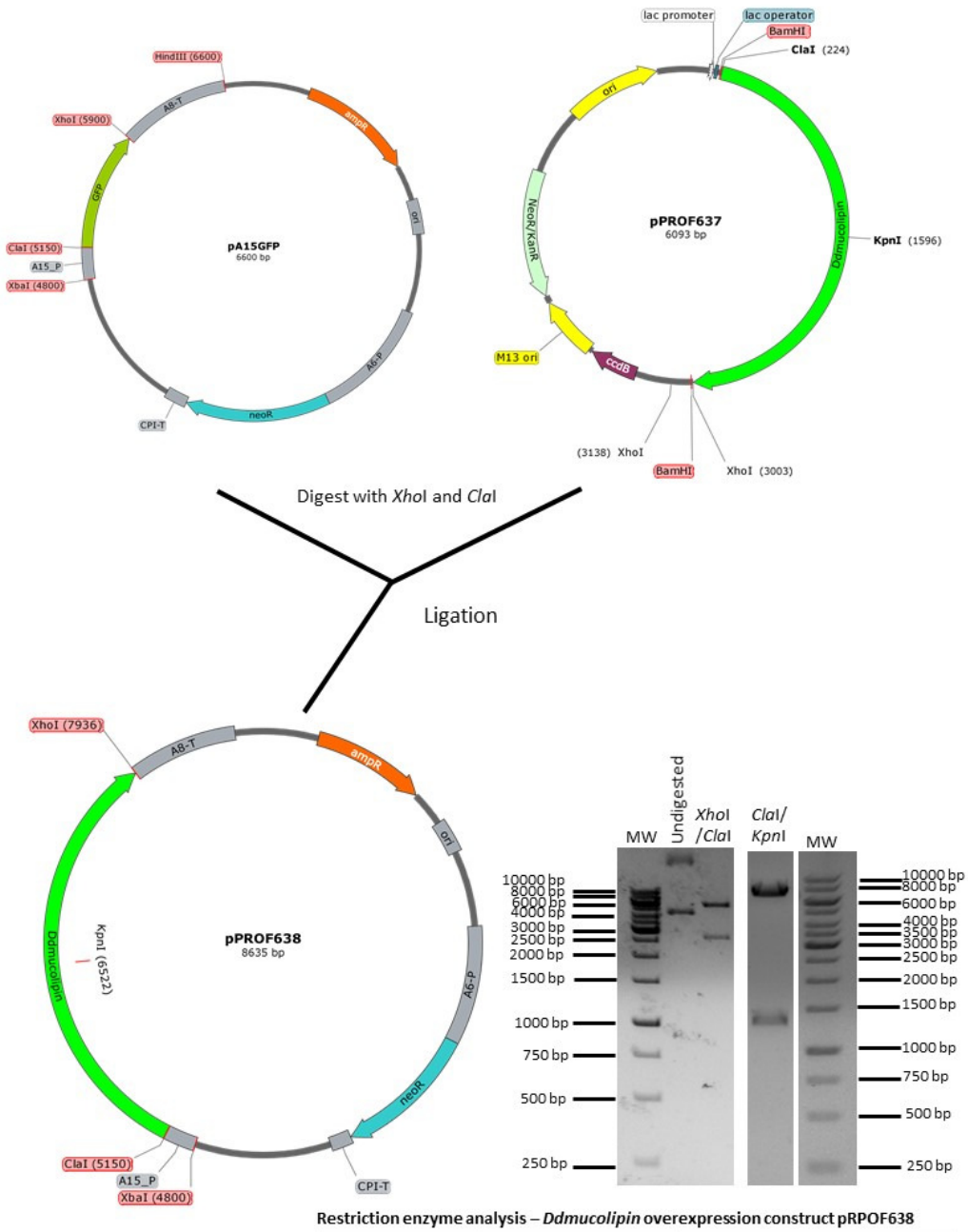

Restriction enzyme analysis – *Ddmucolipin* overexpression construct pRPOF638

Construct name	Restriction enzymes	Expected fragments size (bp)
pPROF638	XhoI/ClaI	5849 bp + 2786 bp
	ClaI/KpnI	7263 bp + 1372 bp

Figure 4.4 Cloning strategy phase two–- *Ddmucolipin* overexpression construct.

The cloned full length *Ddmucolipin* gene from pPROF637 was excised and subcloned into *D. discoideum* expression vector pA15GFP using *Xho*I and *Cla*I sites in sense orientation. The ligation product was electroporated into *E. coli* JC11451 cells and colonies were selected on ampicillin. Plasmid DNA was extracted from individual colonies and screened using restriction enzyme analysis. The resulting construct pPROF638 was verified with restriction enzyme digest analysis depicted in the gel image, the expected DNA fragment sizes are indicated in the table.

4.2.2 Genetic manipulation of *Ddmucolipin*

Antisense and overexpression constructs were introduced into wild type AX2 cells by the calcium phosphate coprecipitation method in order to reduce and increase expression of *Ddmucolipin* respectively. Because the number of copies of the integrated plasmid can vary between strains, southern blotting and quantitative real time PCR was used to determine the plasmid copy number in each strain (Table 4.1)

Table 4.1 Copy number of *D. discoideum* transformants with the *Ddmucolipin* antisense-inhibition and overexpression constructs.

Group	Construct	Strain HPF number	Plasmid copy number
Antisense Inhibition	**pPROF650**	**HPF812**	**274**
Antisense Inhibition	**pPROF650**	**HPF813**	**640**
Antisense Inhibition	**pPROF650**	**HPF640**	**116**
Antisense Inhibition	**pPROF650**	**HPF815**	**113**
Antisense Inhibition	**pPROF650**	**HPF655**	**133**
Antisense Inhibition	**pPROF650**	**HPF817**	**450**
Antisense Inhibition	**pPROF650**	**HPF818**	**260**
Overexpression	**pPROF638**	**HPF827**	**443**
Overexpression	**pPROF638**	**HPF654**	**214**
Overexpression	**pPROF638**	**HPF825**	**600**
Overexpression	**pPROF638**	**HPF829**	**225**
Overexpression	**pPROF638**	**HPF826**	**144**
Overexpression	**pPROF638**	**HPF820**	**68**
Overexpression	**pPROF638**	**HPF656**	**227**

Relative mRNA expression levels of *Ddmucolipin* in knockdown and overexpressing strains was determined by semiquantitative RT-PCR. As expected, antisense inhibition of *Ddmucolipin* caused a measurable decrease in mRNA transcripts and overexpression caused an increase in mRNA transcripts. The relative expression of *Ddmucolipin* mRNA was correlated with the copy number of the plasmid construct in the strains (Fig. 4.5).

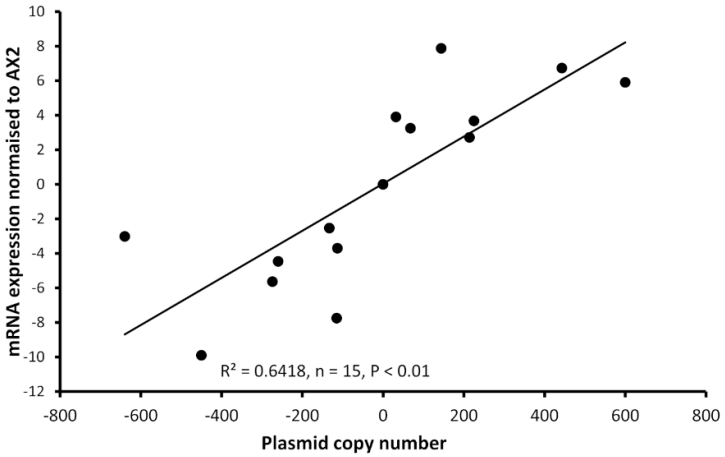

Figure 4.5 Plasmid copy number of *Ddmucolipin* strains was correlated with mRNA expression levels in the transformants.

Semiquantitative RT-PCR was performed to determine mRNA expression levels in each strain. Copy numbers of overexpressing strains were determined by quantitative southern blotting, and in antisense strains by quantitative real time PCR. Expression levels were normalized against the filamin mRNA to adjust for loading and then measured relative to AX2 expression. Expression correlates with plasmid copy number showing that the antisense RNA construct decreases *mcln* expression and the overexpression increases it. The correlation was highly significant, $p = 2.36 \times 10^{-5}$ (Pearson product-moment correlation coefficient, ρ) and similar results were also obtained using non-parametric methods (Spearman's rank $p = 1.195 \times 10^{-5}$ and Kendall's rank $p = 9.995 \times 10^{-5}$). Each point represents mean data for a single strain for 3 experiments. Negative values refer to copy numbers of antisense constructs and positive values to copy numbers of overexpression constructs, AX2 has a copy number of 0 as contains neither construct.

After successfully obtaining Ddmucolipin transformants, phenotypic analysis was performed in order to characterize the function of the protein in *Dictyostelium*. The main focus of the project was to determine whether Ddmucolipin contributes to chemotactic calcium signalling, and also to provide evidence that the acidic Ca^{2+} stores contribute to Ca^{2+} homeostasis and chemotactic Ca^{2+} responses. This was achieved by *in vivo* measurements of cytosolic Ca^{2+} in resting and chemotactically stimulated cells. Importantly, it was also pertinent to investigate the role of Ddmucolipin in the endocytic cycle, as disruptions in expression and mutations of TRPML homologues are known to cause defects in membrane trafficking and cargo degradation along the

endocytic/exocytic pathways. To investigate this, characterization of phagocytosis, macropinocytosis and growth rates on bacterial lawns and axenically was performed. The following sections describe the results of phenotypic characterization.

4.2.3 Phenotypic analysis

4.2.3.1 Developmental expression of *Ddmucolipin* over 24 hours

The expression profiles of many *Dictyostelium* genes change throughout development. To determine the *Ddmucolipin* mRNA expression levels throughout development, AX2 cells were developed on water agar plates for 24 hours, and RNA extracts were taken at 2-hour intervals. Semiquantitative RT-PCR was used to assess the relative expression of *Ddmucolipin* in cells at these time points. Expression changed throughout development, rising slightly during early differentiation in response to the onset of starvation, falling to a trough at 8 hours, but then increasing rapidly to a maximum at 10 hours during aggregation. Expression remained at high levels during subsequent multicellular development (Figure 4.6A). The measured developmental expression profile is similar to the RNA-Seq expression profile of *D. discoideum* AX4 published on dictyBase (Parikh *et al.,* 2010; Stajdohar *et al.,* 2017), which shows increased *Ddmucolipin* expression over the course of development (Figure 4.6B). Subtle differences in the patterns of expression in my experiments compared to those published on dictyBase (Parikh *et al.,* 2010) could arise from differences in the parental strain used (AX2 in my experiments and AX4 for dictyBase) and also from the fact that in my experiments the cells were developed on water agar, as opposed to filters. This expression pattern suggests important roles for Ddmucolipin-dependent calcium signalling in early starvation-induced differentiation, in chemotactic aggregation and subsequently during the multicellular stages of the life cycle.

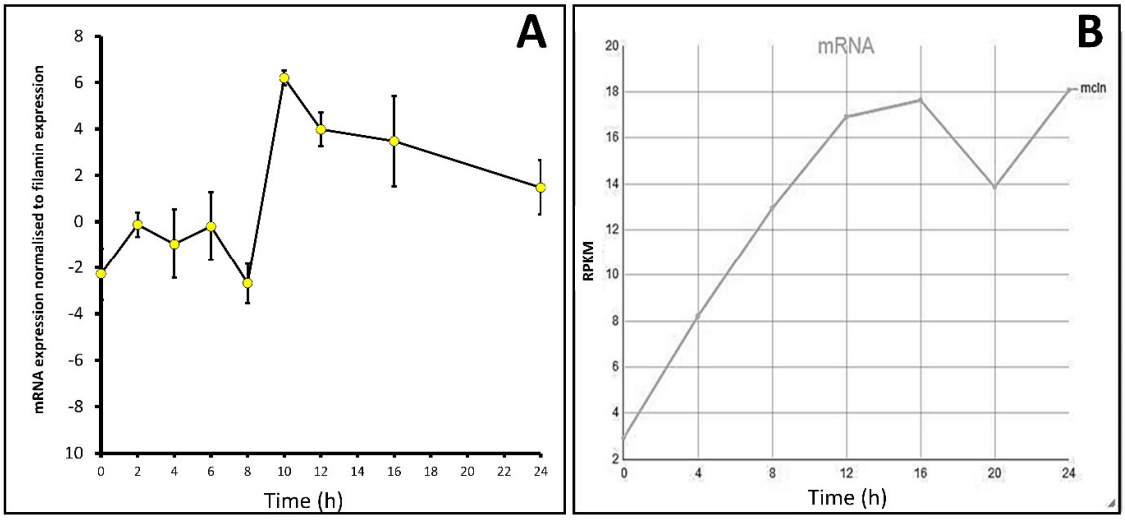

Figure 4.6. *Ddmucolipin* mRNA expression increases throughout development in *Dictyostelium* AX2 and AX4. **(A)** Semiquantitative RT-PCR was used to determine the *mcln* expression in AX2 throughout development presented normalized to filamin expression. RNA was extracted from cells developing on water agar every two hours for 24 hours in two separate experiments. Error bars are standard errors of the mean. **(B)** Developmental timing of expression of *Ddmucolipin (mcln)* in AX4 as measured by RNA-Seq. Reads per kilobase per million (RPKM) over 24 hours. Published on dictyBase (Parikh *et al.,* 2010; Stajdohar *et al.,* 2017).

4.2.3.2 Overexpressed Ddmucolipin can be detected in Western blot

I created a polyclonal antibody directed against a 200aa portion of *Dictyostelium* Ddmucolipin, anti-MUECD. In a Western blot this antibody detected multiple bands so was not suitable to be used for localisation studies. To determine if any of these bands did represent Ddmucolipin, I tested the antibody against Ddmucolipin knockout cell lysate (Lima *et al*., 2012) and ran these proteins alongside protein extracted from DH1-10 (the parental strain for the knockout cell line), AX2 and my Ddmucolipin overexpression and knockdown strains. Indeed, there were two bands absent in the Ddmucolipin knockout lysate but present in the Ddmucolipin overexpression strains which ran at approximately 95 kDa and 120 kDa. The 120 kDa band was also detected in DH1-10 (Figure 4.7A, B). It was not observed in the knockout strain derived from DH1-10, despite a similar protein loading in the gel. These bands were not detected in AX2 or my Ddmucolipin antisense strains, presumably because the wild type and knockdown expression levels for

Ddmucolipin were insufficient for detection by my antibody. Mass spectrometry analysis of bands excised from a Coomassie Blue-stained Bis-Tris-Plus gel confirmed the presence of Ddmucolipin in these two bands (indicated by the red stars in Figure 4.7B), but not the smaller molecular weight bands (Figure 4.8A,B). I thus confirmed that there are two genuine Ddmucolipin bands – one at the predicted MW position ~95kDa and one running at ~120kDa. There are two possible explanations for the presence of two bands. Firstly, the upper band could be a posttranslationally modified (glycosylated) form of the protein as is reported for human TRPML1 (Miedel *et al*., 2006), and the lower band could be the native nonglycosylated protein. Secondly, the upper band could be the native, full-length protein running a little more slowly than expected, and the lower band could be a cleavage product. The human TRPML1 has a proteolytic cleavage site in the intralumenal loop between transmembrane domains 1 and 2, and this cleavage is believed to be involved in regulation of channel activity (Kiselyov *et al*., 2005). Since I confirmed that these bands represented Ddmucolipin, I was able to confirm by quantification that Ddmucolipin expression is increased in my overexpression strains (Figure 4.7C), and the protein expression was significantly correlated with copy number of the overexpression plasmid construct (Figure 4.7D).

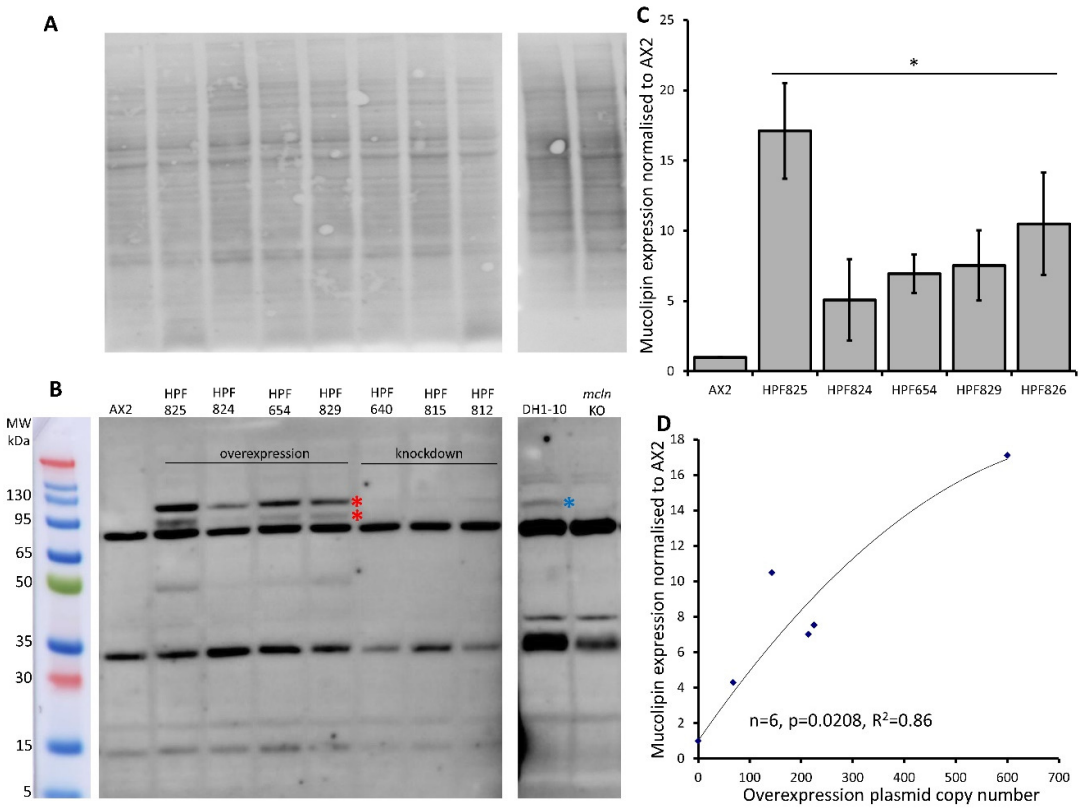

Figure 4.7 Ddmucolipin can be detected in protein extracted from overexpression strains.

(A) Total protein extracted from AX2, four representative Ddmucolipin overexpression strains, three representative Ddmucolipin knockdown strains, DH1-10 and Ddmucolipin knockout, were separated on a Bis-Tris-Plus gel by electrophoresis, transferred to PVDF membrane and stained with No Stain Protein Labelling Reagent (Invitrogen). Protein lysate for DH1-10 and *mcln* KO were kindly provided by Professor Pierre Cosson (Lima *et al*., 2012). **(B)** Western blot of the same membrane, the anti-MUECD antibody detects multiple bands. Markers were the Broad Multi Color Pre-Stained Protein Standard (Genscript). Two bands of ~95 kDa and ~120 kDa were absent in the Ddmucolipin knockout cells but present in the Ddmucolipin overexpression strains (Red stars) and the higher MW band also detected in DH1-10 (blue star). **(C)** Quantification of Ddmucolipin expression in overexpression strains. To quantify Ddmucolipin expression the combined intensity of the 120 kDa and 95 kDa bands was measured in Image Lab™ and normalized to the intensity of the total protein loaded in each lane (Fig 3A). Expression in each strain was then and normalized to AX2 expression. As no bands were visualised for AX2 at these sizes, AX2 expression was determined by measuring the intensity of a similar sized area on the blot where the bands would be located. Each strain was tested 2-4 times and data was pooled from each experiment and the means calculated (error bars are standard errors of the mean). Expression is relative to AX2 and is increased in overexpression strains (* = <0.05, One-Way ANOVA, with pairwise comparisons made by the Least Squares Difference method, AX2 vs. strain). **(D)** Protein expression in overexpression

strains correlates with overexpression construct copy number. AX2 had a construct copy number of 0 as does not contain an overexpression construct. The correlation was highly significant (Spearman's rank p = 0.0208 and Kendall's rank p = 0.0194).

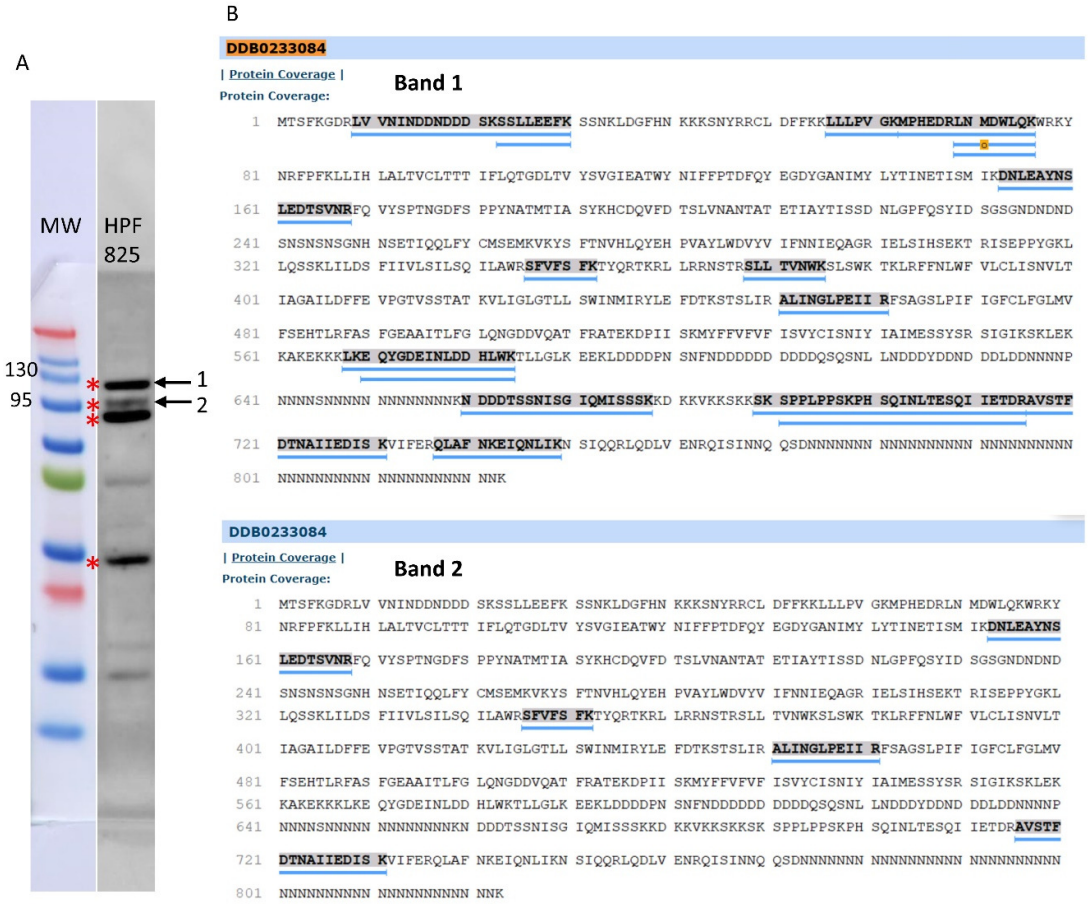

Figure 4.8 Ddmucolipin was detected in two gel bands by mass spectrometry.

(A) Representative Western blot indicating the position of the two bands where Ddmucolipin was detected by mass spectrometry in Ddmucolipin overexpression strain HPF825. **(B)** Mass spectrometry results. To identify Ddmucolipin in bands 1 and 2 whole cell protein was extracted from Ddmucolipin overexpression strain HPF825, separated on a Bis-Tris Plus gel and stained with Coomassie blue. Four bands (~120 kDa, ~90 kDa, ~95 kDa and ~32 kDa, indicated by stars) were excised from the gel and the proteins contained in the gel pieces were identified by mass spectrometry. The peptides underlined in blue represent the Ddmucolipin specific peptides identified in the gel slices corresponding to bands 1 and 2 in the Western blot. Upper sequence from band 1 and lower sequence from band 2. (Mucolipin dictyBase.org accession number DDB0233084).

4.2.3.3 Ddmucolipin contributes to chemotactic calcium signals in *Dictyostelium*.

TRPMLs are thought to be important for Ca^{2+} signalling events associated with Ca^{2+}-dependent fusion/fission events of membranes along the late endocytic pathway (LaPlante *et al.,* 2004; Luzio *et al.,* 2007; Brailoiu and Brailoiu 2016). In *Dictyostelium* DH1-10 cells, knockout of Ddmucolipin reduces Ca^{2+} concentrations in secretory post-lysosomes, measured using dextran-coupled fluorophores (Lima *et al.,* 2012) suggesting a role in regulation of calcium homeostasis/signalling. To further investigate the role of Ddmucolipin in Ca^{2+} signalling, and the possible contribution of the acidic stores to chemotactic Ca^{2+} responses, I measured the cytosolic Ca^{2+} transients in vegetative cells (folic acid responses), and in aggregation competent cells (cAMP responses) in Ddmucolipin knockdown and overexpressing strains. All strains also ectopically expressed a recombinant Ca^{2+}-sensitive luminescent protein, apoaequorin, to allow real time recordings of cytosolic Ca^{2+} responses. These chemotactic Ca^{2+} responses have been well characterized in wild type cells expressing apoaequorin (HPF401) (Nebl and Fisher, 1997). In this work I compared the mutants' Ca^{2+} responses with wild type responses to gain insight into the molecular mechanisms involved. Representative real-time recordings of cytosolic calcium concentration in wild type aequorin-expressing strain (HPF401), Ddmucolipin knockdown strain (HPF812) and Ddmucolipin overexpression strain (HPF825) when stimulated with 1 μM chemoattractant are shown in Figure 4.9A.

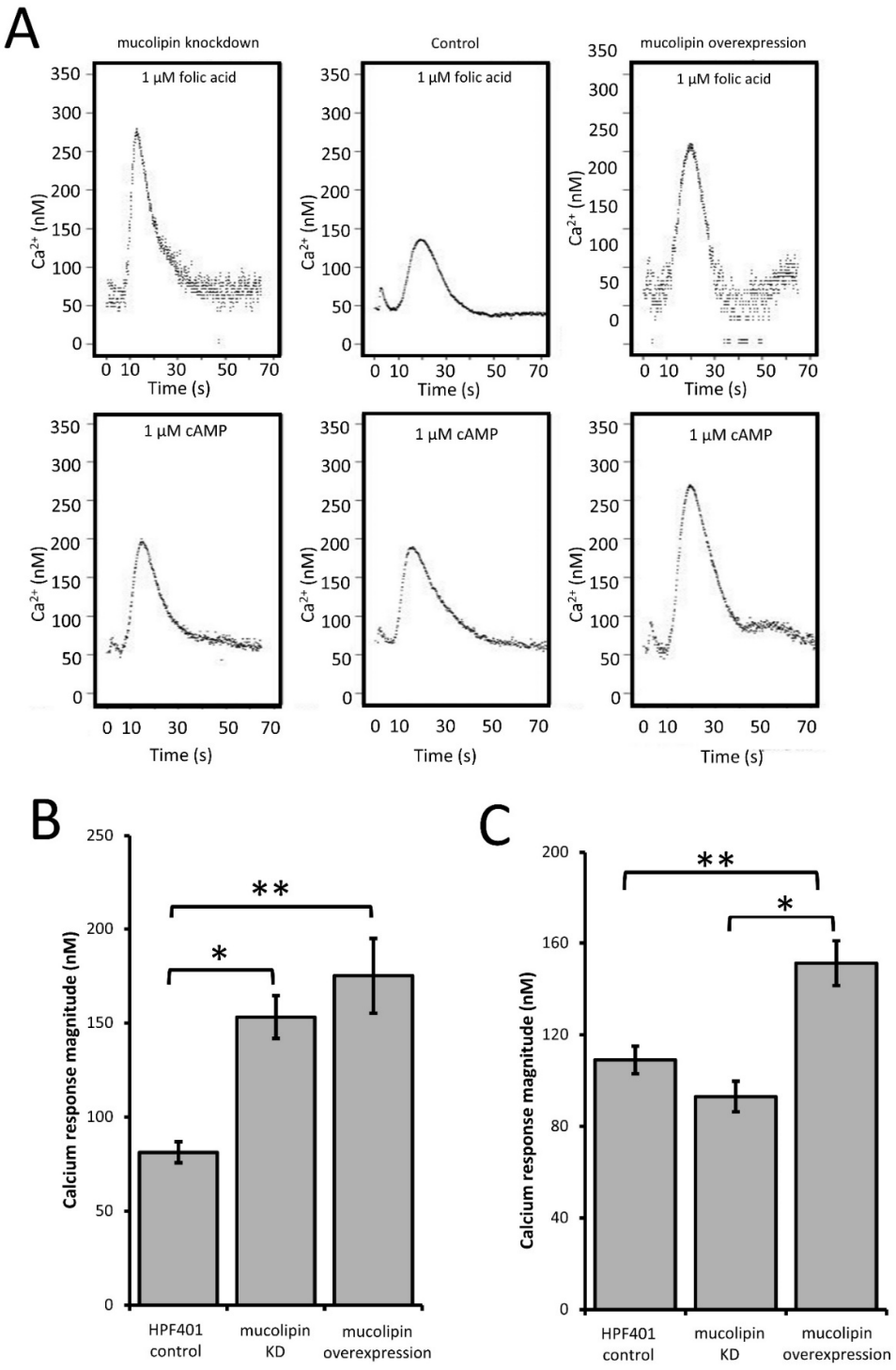

Figure 4.9 Cytosolic calcium responses to cAMP and folic acid stimulation.

(A) Representative real time recordings of cytoplasmic Ca^{2+} responses to chemoattractants. **Upper panel:** Real time recordings of Ca^{2+} responses to 1 µM folate in vegetative cells. Left to right: Ddmucolipin knockdown, HPF401 control strain and Ddmucolipin overexpression. **Lower panel:** Real time recordings of Ca^{2+} responses to 1 µM cAMP in cells at 7 h development. Left to right: as above. Recordings began at 0 s and the stimulus was injected immediately after. The small

peak preceding the Ca^{2+} response is due to a Ca^{2+} response to the mechanical stimulus of chemoattractant injection, which has no effect on the chemoattractant responses (Nebl and Fisher, 1997). **(B)** Mean calcium response magnitudes in vegetative cells stimulation with 1µM folic acid. Ca^{2+} response magnitudes (Ca^{2+} nM) were measured in Ddmucolipin KD, Ddmucolipin overexpression and control strain HPF401. There was no correlation with copy number so data from strain groups was pooled and the means compared. Both knockdown and overexpression of Ddmucolipin significantly enhances the magnitude of the response compared to the control strain HPF401 (* $p=3.15\times10^{-5}$, ** $p=4.7\times10^{-4}$). Means were compared using an independent one-tailed t-test. Errors are standard errors of the mean. Individual strains were tested in 3-9 independent experiments in 5 Ddmucolipin overexpression (n=13), 6 Ddmucolipin knockdown strains (n =30) and control strain HPF401 (n=12), and all experiments from each strain group were pooled to determine the mean. **(C)** Mean calcium response magnitudes (Ca^{2+} nM) in developed cells stimulated with 1µM cAMP. Ca^{2+} response magnitudes were measured in overexpression, knockdown and control strain HPF401. Cells were developed to 7 hours in MED-DB. Overexpression of Ddmucolipin increases the response magnitude significantly compared to both control HPF401 and knockdown strains (* $p=1.33\times10^{-6}$, **$p=5,928\times10^{-4}$). Knockdown of Ddmucolipin has no effect on response magnitude in developed cells when compared to wildtype ($p=0.083$). Means were compared using an independent one-tailed t-test. Errors are standard errors of the mean. Individual strains were tested in 2-9 independent experiments and all experiments were pooled to determine the mean. Ddmucolipin overexpression 8 strains (n=37), Ddmucolipin knockdown seven strains (n=33), control HPF401 (n=12).

4.2.3.3.1 Overexpression of Ddmucolipin enhances the Ca^{2+} responses to cAMP and folic acid.

Real time recordings of the Ca^{2+} responses for control, knockdown and overexpression strains to both cAMP and folic acid were recorded over multiple experiments and analysed. As there was no correlation between the various parameters and plasmid copy number, data was pooled for all transformants within each group for combined analysis. Overexpression of Ddmucolipin significantly enhanced Ca^{2+} response magnitudes to both folic acid (vegetative cells) and cAMP (aggregation competent cells) compared to the control (Figure 4.9B, C). The response magnitudes were increased compared to the control by an average of 46.4% and 28.0% for the folic acid responses and cAMP responses respectively. This result suggests, Ddmucolipin is involved in Ca^{2+} chemotactic calcium responses and because the channel localises to post-lysosomes and possibly other endocytic compartments (Lima *et al*., 2012) the results suggest that these vesicles are also involved in the calcium response.

4.2.3.3.2 Knockdown of Ddmucolipin increases Ca^{2+} response magnitudes in vegetative cells, but not in aggregation competent cells

Given that overexpression of Ddmucolipin enhances the responses to folic acid and cAMP, it was expected that knockdown of Ddmucolipin would reduce the magnitude of calcium responses. Surprisingly, the magnitude of the Ca^{2+} responses to 1µM folic acid was significantly increased in knockdown strains compared to the control (Figure 4.9B). Contrary to the folate responses, the magnitude of the cAMP Ca^{2+} responses in aggregation competent cells were slightly reduced in Ddmucolipin knockdown strains compared to the control (Figure 4.9C), but the difference did not reach statistical significance (p=0.083).

4.2.3.4 The role of Ddmucolipin in the endocytic pathway

Dictyostelium Ddmucolipin overexpression and knockdown strains both exhibit increased Ca^{2+} signalling in vegetative cells. As Ca^{2+} plays an important role in the endocytic pathways it was of interest to assess the role of Ddmucolipin in these processes. The endocytic pathway of *Dictyostelium* is well described. Shortly after endocytosis the internalized nascent endocytic compartment (NC) progresses through the endo-lysosomal pathway which involves a series of vesicle fusion and maturation events. The NC fuses with a H^+-ATPase containing vesicle and becomes acidified shortly after internalization (Clarke *et al*., 2002; Charette and Cosson, 2008). The acidified lysosomal like vesicles recycle the plasma membrane components likely by budding off small recycling endosomes (RE) that fuse with the plasma membrane. The early endosomes then go through a series of fission events where they are fragmented into many smaller vesicles (Maniak, 2001). The endosomes also go through dynamic and plastic fusion events, the so called “mixing stage”, which peaks at ~15 minutes after internalisation. During this stage vesicles readily undergo homotypic and heterotypic fusion events (Clarke *et al*., 2002b). During the mixing stage early endosomes can fuse with other early endosomes that were formed within minutes of each other. They can also fuse with older acidified endosomes mixing the cargo and delivering the vacuolar H^+-ATPase thus rapidly acidifying the vesicle. These mixing endosomes can go through extreme shape changes and extend tubular appendages to fuse with other vesicles and small vesicles have been seen to cluster around newly formed endosomes. Fusion is facilitated by vesicle transport along microtubules which increase the chance of encounters with other vesicles and fusion

events can even bridge the gaps between microtubules (Clarke *et al*., 2002b). The vesicles subsequently acquire lysosomal enzymes in order to catabolize the cargo and then gradually mature into neutralized post-lysosomes (PL) by removal of the H^+-ATPase, again by budding off from the membrane. The PL then fuse with the plasma membrane at an exocytic patch and expel contents (Fig. 4.10) (Jenne *et al*., 1998; Neuhaus and Soldati, 1999; Maniak, 2001; Maniak, 2003; Charette and Cosson, 2008). Similarly to mammalian cells, Ca^{2+} release from the endocytic compartments in *Dictyostelium* is likely to be integral to the entire process. Considering that Ddmucolipin localizes to these organelles it is likely that Ddmucolipin dependent Ca^{2+} signaling is involved as is described for other TRPMLs.

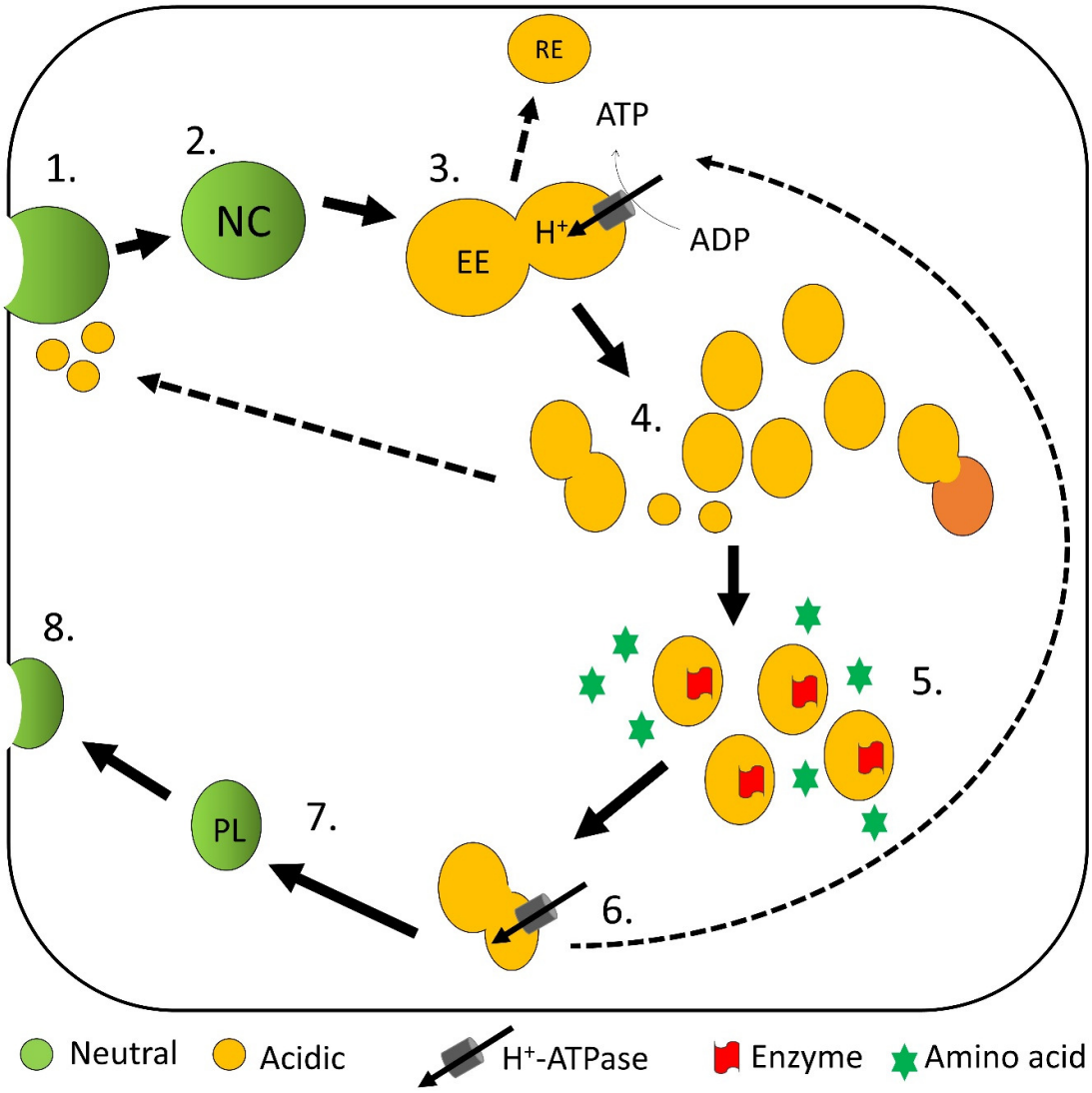

Figure 4.10 *Dictyostelium* endocytic pathway adapted and modified from (Clarke *et al*., 2002b; Maniak, 2003; Charette and Cosson 2008).

1. Extracellular material is internalised through internal budding into the cytoplasm forming a nascent endocytic compartment (NC). The process involves the actin system which results in the NC being coated in actin and other cytoskeletal proteins. **2.** The actin protective coat is lost from the NC and is primed for subsequent fusion processes. **3.** The NC acquire H^+-ATPases by fusion with other vesicles that contain the H^+-ATPases to produce an acidified early endosome (EE). Plasma membrane components are recycled by budding off of small recycling endosomes (RE). **4.** Early endosomes become fragmented into smaller vesicles (Maniak, 2003). During this 'mixing stage' the endosomes go through a series of dynamic and plastic fusion events that is facilitated by transport along microtubules to increase the chance of encounters with other vesicles. Early endosomes can fuse with other early endosomes that were formed within minutes of each other. They can also fuse with older endosomes (indicated by dark orange) and the contents mixed.

These mixing endosomes can go through extreme shape changes and extend tubular appendages to fuse with other vesicles and can even bridge the gaps between microtubules. Small vesicles have been seen to cluster around newly formed endosomes (Clarke *et al*., 2002b). **5.** The endosomes receive lysosomal enzymes which hydrolyse the cargo and amino acids are released into the cell. **6.** The H^+-ATPases are removed from the endosome by budding off of recycling endosomes which can then recycle the H^+-ATPases to newly formed vesicles that require acidification. **7.** The endosome neutralises into a post lysosome (PL) and becomes coated with actin, vacuolin and coronin. **8.** The PL fuses transiently with the plasma membrane at an exocytic patch, and expels undigested cargo and lysosomal enzymes such as alpha-mannosidase and beta-glucosidase.

4.2.3.4.1 Overexpression and knockdown of Ddmucolipin increases fluorescence of cells stained with LysoSensor™ Blue DND-167

One of the hallmarks of MLIV cells is an accumulation of hybrid late endosome-lysosome compartments (LELs) with defective exit of lipids from LELs to the trans-Golgi network (Chen *et al.,* 1998, LaPlante *et al.,* 2004). The connection between Ca^{2+} release via TRPMLs and build-up of hybrid LELs is somewhat undecided. To assess this phenotype in AX2 *Dictyostelium* cells, I stained vegetative Ddmucolipin knockdown and overexpressing cells with LysoSensor™ Blue DND-167 which has a pK_a of is ~5.1 and accumulates in acidic vesicles. There was a significant increase in fluorescence in the mutants compared to AX2 (Figure 4.11A) representative images of live stained cells are presented in Figure 4.11C. This could reflect an increase in lysosomal mass, or because the fluorescence of LysoSensor™ Blue DND-167 increases as the pH decreases, my results could reflect increased acidification of the lysosomes.

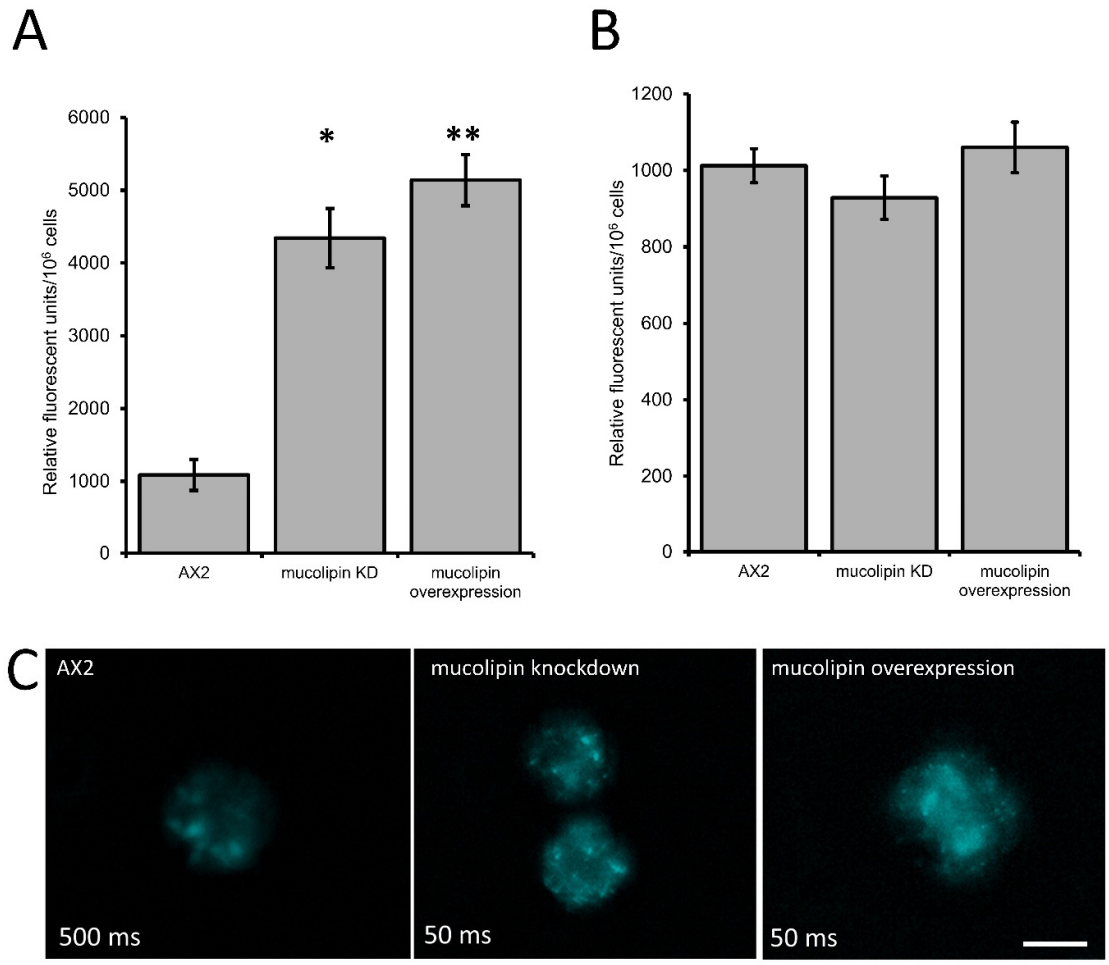

Figure 4.11 Altering Ddmucolipin expression causes accumulation or increased acidification of vesicles stained with LysoSensor™ Blue DND-167 but does not cause autofluorescence.

(A) Quantification of LysoSensor™ Blue DND-167 was performed by measuring the increase in fluorescence in 1×10^6 vegetative cells after incubation with 500 nM LysoSensor™ Blue DND-167. Data was collected from seven knockdown strains and six overexpression strains in three individual experiments and the mean calculated, error bars are standard errors of the mean. There was no correlation with copy number of the plasmid constructs, therefore data for strain groups was pooled. The mean fluorescence of AX2 (n=3) was significantly different to the means of either knockdown (n=21) or overexpression strains (n=18) (Pairwise comparisons, Independent t-test, * p = 0.00067, ** p = 0.01107312). **(B)** Fluorescence measured in *Dictyostelium* strains harvested from low fluorescence medium. The level of fluorescence in knockdown and overexpression strains was measured in 1×10^6 cells. Autofluorescence was measured in a fluorometer (Modulus 9200-003 Turner Bio systems) using the UV module (excitation 365 nm, emission 410-460 nm). Fluorescence displayed in relative fluorescent units, was measured in two independent experiments for AX2 (n = 2), six knockdown strains (n=12) and six overexpression strains (n = 12) and the mean within each group calculated. Error bars are standard errors of the mean. There was

no significant difference ($p > 0.05$, One-Way ANOVA, multiple comparisons made by the Least Squares Difference method). **(C)** Representative live cells stained with LysoSensor™ Blue DND-167. *Dictyostelium* AX2, Ddmucolipin knockdown (copy number 274) and overexpression (copy number 443) were incubated in the presence of 500 nM LysoSensor™ Blue DND-167 for 1 h and observed under fluorescence microscopy (Excitation- 373 nm, Emission- 425 nm). The AX2 image was taken at 500ms exposure, the knockdown and overexpression cells were overexposed at this exposure so were taken at 50ms. Scale bar = 5 µm

4.2.3.4.2 Altering Ddmucolipin expression does not cause autofluorescence

Accumulation of autofluorescent material has been observed in MLIV cell lines and is thought to be related to specific compounds stored in the lysosomes (Goldin *et al.,* 1995). Autofluorescence is also a hallmark of NCL (Dowson *et al*., 1982), and has been detected in some *Dictyostelium* NCL models. In the cln3 model, *cln3*$^{-}$ cells do not accumulate autofluorescent material during the growth stage (Huber *et al*., 2014), however in starved *cln3*$^{-}$ cells autofluorescent material was detected (Huber and Mathavarajah, 2019). In the cln2 lysosomal disease model, mutants with knockdown and knockout of the *tpp1/cln2* gene, which encodes the lysosomal protein tripeptidyl peptidase I (TPP-I), a soluble lysosomal aminopeptidase, accumulate cellular autofluorescent material (Phillips and Gomer, 2015; Smith *et al.,* 2019). Therefore, I measured autofluorescence in *Dictyostelium* Ddmucolipin knockdown and overexpression strains under UV light. No increase of autofluorescence was detected in any of my Ddmucolipin mutants (Figure 4.11B). This phenotype in *Dictyostelium* lysosomal disease models seems to be specific to the particular disease gene in question.

4.2.3.4.3 Knockdown of Ddmucolipin increases macropinocytic uptake, but decreases growth rates of cells in liquid medium, while overexpression does not affect growth or macropinocytosis.

An analysis of uptake of medium as compared to growth rates can indicate whether ingested nutrients are efficiently catabolised. The rate of fluid uptake by macropinocytosis was increased in Ddmucolipin knockdown strains and correlated with plasmid copy number, however overexpression had no affect (Figure 4.12A). Surprisingly the growth rates of Ddmucolipin knockdown strains were slower than AX2 (longer generation times) and similarly correlated with plasmid copy number, while overexpression had no affect (Figure 4.12B).

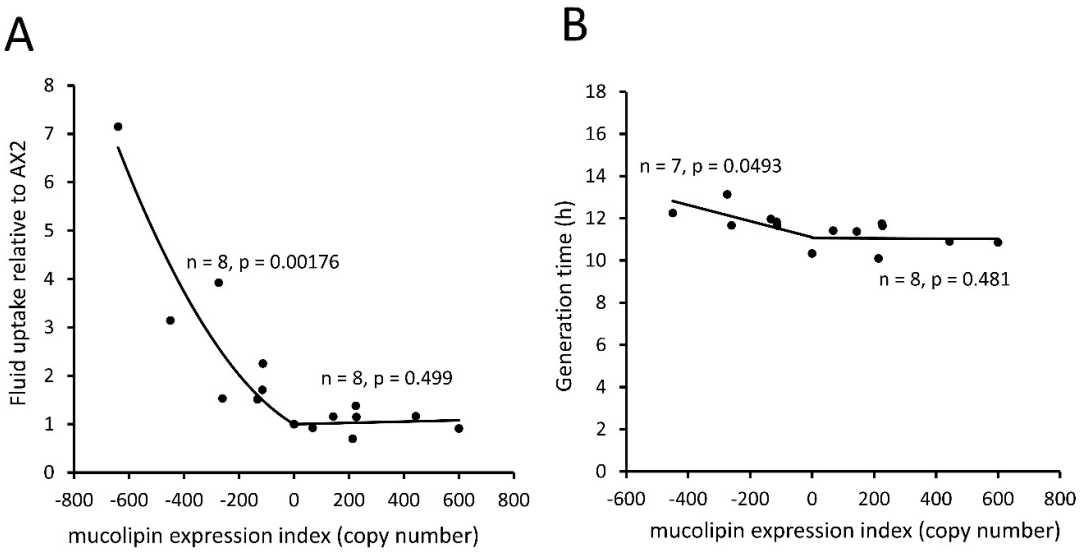

Figure 4.12 Ddmucolipin knockdown affects macropinocytic uptake and growth rates of cells in HL5 medium. **(A)** Consumption of HL-5 medium containing FITC dextran via macropinocytosis in knockdown strains (negative copy numbers), overexpression strains (positive copy numbers) and wild type normalized to AX2. In the antisense strains fluid uptake normalized to AX2 was increased and correlates with Ddmucolipin expression index (Pearson correlation coefficient, p = 0.00176), however there was no correlation in the overexpression strains (Pearson correlation coefficient, p = 0.499). Each point represents the mean uptake from a single strain. Duplicate samples were assayed for each strain in two to six separate experiments and data was normalized within each experiment to AX2. **(B)** Generation times (h) of Ddmucolipin strains and AX2 grown in HL5 medium. In the antisense strains generation time was increased and correlates with Ddmucolipin expression index (Pearson correlation coefficient, p = 0.0493), however there was no correlation in the overexpression strains (Pearson correlation coefficient, p = 0.481). AX2 has a copy number of 0.

4.2.3.4.4 Ddmucolipin knockdown and overexpression increase phagocytosis, but do not affect growth rates on lawns of bacteria

Dictyostelium consume bacteria by phagocytosis in their natural environment and can be cultured on lawns of bacteria where they grow as plaques which gradually expand as the amoebae consume bacteria. The plaque expansion rates (growth velocity) of Ddmucolipin transformants were slightly but not significantly elevated compared to AX2 (Figure 4.13A). The rates of phagocytosis in Ddmucolipin transformants and AX2 control were assayed by measuring the uptake of fluorescently labelled live *E. coli* cells. Surprisingly, unlike the plaque expansion rates on bacterial lawns, both overexpression and knockdown of Ddmucolipin significantly increased the rates of phagocytosis of *E.coli* (Figure 4.13B).

These results indicate although these transformants are engulfing bacteria at a faster rate than AX2, this does not significantly increase the growth rates.

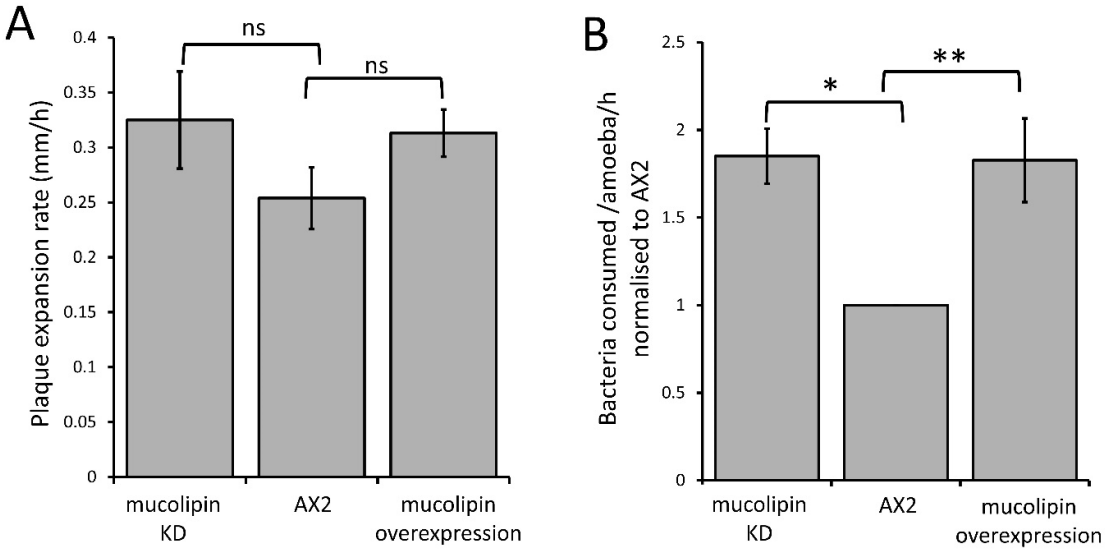

Figure 4.13 Ddmucolipin expression did not affect plaque expansion rates but increased phagocytosis rates. **(A)** Plaque expansion rates (growth velocity) were measured from linear regressions of plaque diameters *vs* time during growth at 21°C on an *E. coli* B lawn. Growth velocity was not significantly altered in Ddmucolipin knockdown compared to AX2 (p=0.278) or overexpression compared to AX2 (p=0.133) (One-Way ANOVA, with pairwise comparisons made by the Least Squares Difference method). Analysis revealed that there was no correlation between construct copy number and growth velocity of the Ddmucolipin overexpressing strains. Therefore, the growth velocities for different strains in each of the two sets of transformants were pooled to calculate the means for comparison with AX2. Individual strains were each tested in 2-4 independent experiments and the data pooled to calculate the mean. Eight overexpression strains (n=33), seven knockdown strains (n=20) and the control strain (n=4) were tested (n=total number of experiments in each strain group). Errors are standard errors of the mean. **(B)** Uptake of *E. coli* cells expressing the fluorescent red protein Ds-Red via phagocytosis was significantly increased in both knockdown and overexpression Ddmucolipin transformants when compared to AX2 (*$p=3.35\times10^{-5}$, **p=0.002, One-Way ANOVA, with pairwise comparisons made by the Least Squares Difference method). All of the Ddmucolipin overexpressing strains exhibited similarly elevated phagocytosis rates so that there was no correlation amongst them between construct copy number and phagocytosis rates (Pearson product-moment correlation coefficient, ρ, overexpression p= 0.15). The same was true of the Ddmucolipin knockdown strains (Pearson product-moment correlation coefficient, ρ, p = 0.48). Accordingly, the uptake rates obtained from different strains within each group were pooled and the means calculated. Individual strains were

tested in 2-4 independent experiments. Seven overexpression (n=24), seven knockdown strains (n=19) and the control strain (n=4) were tested (n= total number of experiments). Errors are standard errors of the mean.

4.2.3.4.5 Ddmucolipin expression affects *Dictyostelium* multicellular development

Multicellular development in *Dictyostelium* is initiated by starvation upon which the cells undergo a developmental program leading to multicellular morphogenesis and culmination into mature fruiting bodies consisting of a spore droplet (sorus), stalk and basal disc. The stalk cells undergo autophagic cell death and so are nonviable. The developmental timing of expression of Ddmucolipin suggests it is involved in chemotactic aggregation and progression through multicellular morphogenesis, likely through Ddmucolipin-dependent calcium signalling, and its effects on the endocytic system. Calcium signalling plays an important role during development, from chemotactic aggregation to cell type differentiation. To investigate how expression levels of Ddmucolipin affect multicellular morphogenesis in *Dictyostelium*, knockdown and overexpression strains were observed at the slug and fruiting body stage. Both knockdown and overexpression strains formed smaller fruiting bodies than AX2. In high copy number strains, the stalks and basal disks of the fruiting bodies appear thickened indicating increased stalk cell differentiation (Figure 4.14A,B) and formed more numerous fruting bodies(Figure 4.14C) with smaller sori (Figure 4.14D). I then determined if the smaller fruiting bodies were the result of small aggregate and slug formation in the mutants. Indeed, both knockdown and overexpression strains developed into smaller slugs containing fewer cells compared to AX2 (Figure 4.15A). The aggregate size was quantified by determining the number of cells per slug, revealing a dramatic copy number-dependent reduction in slug size in both overexpression and knockdown strains (Figure 4.15B). This phenotype is also present in *cln2* knockdown mutants (Smith *et al.,* 2019), and similarly *cln3*$^{-}$ and *cln5*$^{-}$ mutants have increased numbers of tipped mounds, fingers, slugs and fruiting bodies for the same density of cells (Huber *et al*., 2014; Huber *et al*., 2016; McLaren *et al*., 2021).

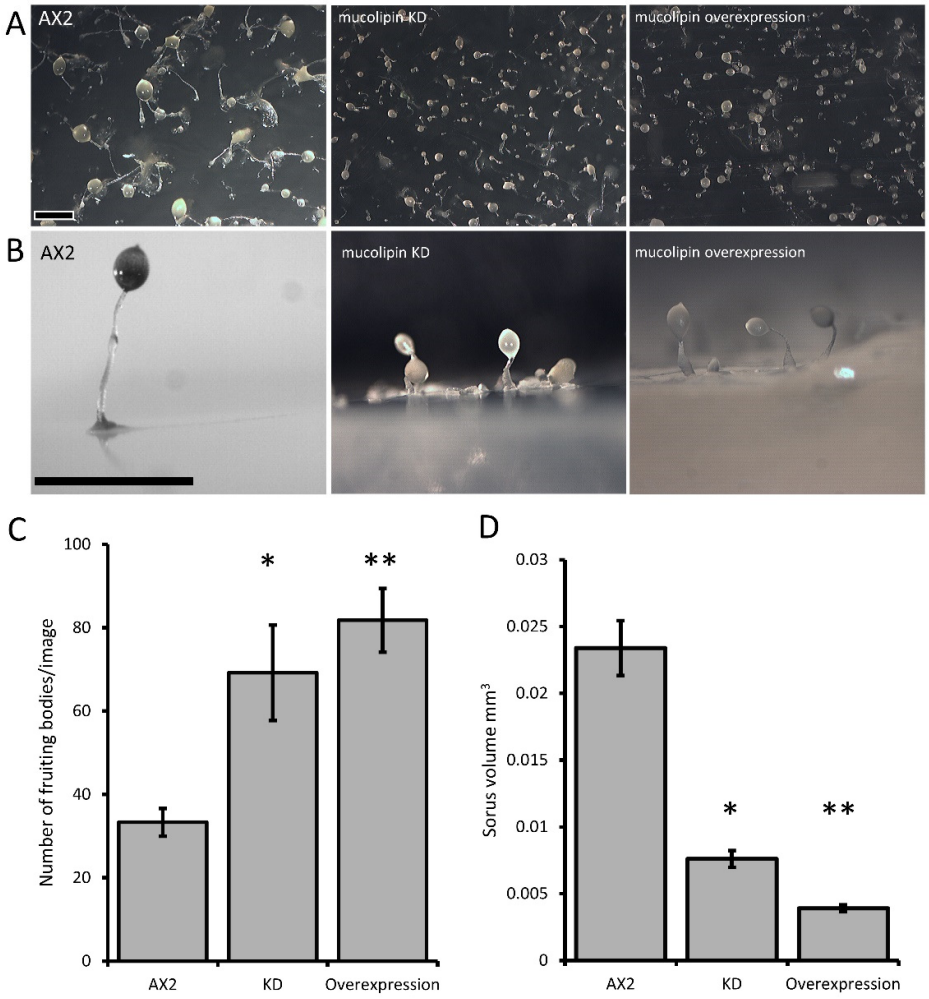

Figure 4.14 Ddmucolipin knockdown and overexpression strains form smaller more numerous fruiting bodies.

(A) AX2 wild type, Ddmucolipin knockdown strain HPF817 (copy number 450) and Ddmucolipin overexpression strain HPF825 (copy number 600). Cells grown on lawns of *E. aerogenes* at 21°C for ~ 24 h until fruiting bodies had formed which were photographed from above. **(B)** The same strains photographed from the side. Both increasing and decreasing Ddmucolipin expression results in very small fruiting bodies compared to that of AX2. In high copy number strains the stalks and basal disks are thickened and enlarged. Scale bar = 1mm. **(C)** The number of fruiting bodies were significantly increased in Ddmucolipin knockdown and overexpression strains. Images were taken from above at the same magnification for all strains and the number of fruiting bodies in the same area of photograph were counted and the means calculated. (AX2: n=3; KD: n=5, overexpression: n=5) (independent t-test * p= 0.0470 vs. AX2, **p= 0.00303 vs. AX2) **(D)** Sorus volume was smaller in the knockdown and overexpression strains than AX2. Sorus area was quantified from photographs of fruiting bodies from above using the ImageJ measurement tool and then converted to volume on the assumption that the sorus is approximately spherical using

the equation (V=4/3*A/sqrt(A/pi) (A=area) and presented as mm^3. For each strain 30-111 sori were measured. The sorus size was significantly reduced in knockdown ($p= 2.402\times10^{-20}$ vs. AX2) and overexpression strains (**$p= 1.8998\times10^{-56}$ vs. AX2). Sample sizes: AX2 – N=3 images, n = 97 sori; KD–- N=5 strains, n=349 sori; overexpression–- N=5 strains, n=298 sori) (independent t-test).

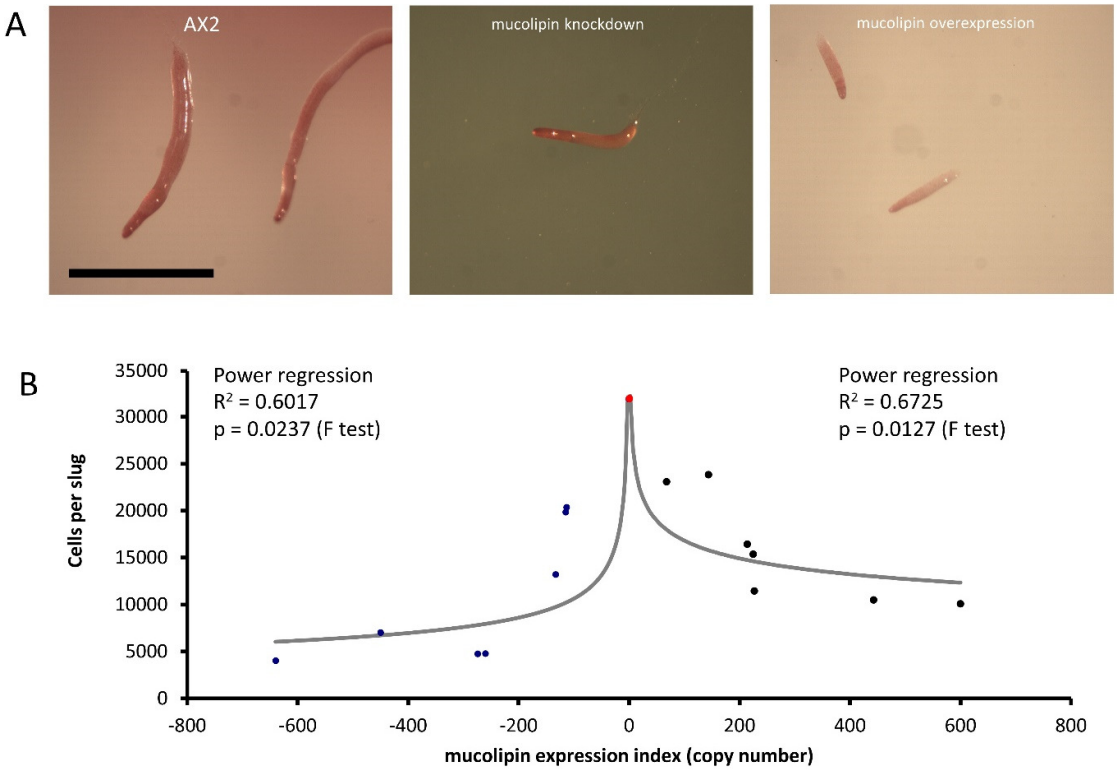

Figure 4.15 Slug sizes are smaller in Ddmucolipin knockdown and overexpression strains and is copy number dependent.

(A) Slugs formed after ~16 h of development on water agar. Mutants formed smaller slugs than AX2 Scale bars = 1mm. **(B)** Both increasing and decreasing Ddmucolipin expression reduces aggregate size. The aggregate size of overexpression and knockdown strains was quantified by determining the number of cells per slug. The mean aggregate size for each transformant was determined by isolating single slugs and counting the number of cells in each slug using a haemocytometer (n=30). The mean aggregate size was reduced in a copy number dependent manner, the regressions were significant indicated by the p values. Positive copy numbers represent overexpression strains and negative numbers knockdown strains, AX2 had a copy number of 0 as it contains neither plasmid (indicated as red circle).

4.3 Discussion

In this study I have used the model organism *Dictyostelium* to investigate if Ddmucolipin expression can affect global calcium signals during chemotactic calcium responses. Gross (2009) suggested that the *Dictyostelium* acidic stores, which includes the endolysosomal vesicles, the contractile vacuole system and the acidocalcisomes, can release Ca^{2+} and increase cytosolic Ca^{2+} during chemotaxis. A selection of calcium channels have been identified to be associated with the acidic stores including the P2X receptors of the contractile vacuole (Fountain *et al*., 2007), the two pore channel (TPC) (Wilczynska *et al*., 2005; Chang *et al*., 2020), and Ddmucolipin. Given that Ddmucolipin resides in late endosomes and other endocytic vesicles (Lima *et al*., 2012), I hypothesized that Ddmucolipin could contribute to calcium release from these stores. I measured cytosolic Ca^{2+} responses to chemoattractants in Ddmucolipin knockdown and overexpression transformants using the luminescence of the Ca^{2+}-sensitive luminescent protein, apoaequorin, which I ectopically expressed in the same cells (Nebl and Fisher 1997). I found that overexpression of Ddmucolipin significantly increased the magnitudes of the cytosolic Ca^{2+} responses to folic acid and cAMP. While I cannot determine if the increased calcium influx into the cytosol is the result of direct release of calcium from the endocytic compartments through Ddmucolipin itself, my results do implicate Ddmucolipin in cytosolic calcium signalling. Lima *et al*. (2012) provided evidence of Ddmucolipin involvement in calcium homeostasis because knockout cells grew faster in calcium-depleted medium and had reduced lumenal calcium concentrations in the post-lysosomes, below 0.2 µM, much lower than the 1-3 µM of the wild type control. In other cell types TRPML1 has been shown to affect lysosomal pH (Soyombo *et al*., 2006; Miedel *et al*., 2008), therefore, knocking out Ddmucolipin in *Dictyostelium* could affect the proton/Ca^{2+} exchange between the vesicle lumen and cytoplasm, thereby reducing steady state Ca^{2+} levels in the lumen as has been reported (Lima *et al*., 2012). This could in turn mean that overexpressing Ddmucolipin may result in elevated resting lumenal Ca^{2+}, again because of the disturbed pH gradient across the vesicle membrane. This, and the greater number of available channels could then facilitate the larger responses in my overexpressing strains. Lima *et al*. (2012) hypothesized that Ddmucolipin may be responsible for transfer of calcium from the cytosol to the lumen where the vesicles meet high local cytosolic calcium concentrations. My results suggest that, at least when

overexpressed, Ddmucolipin significantly contributes to cytosolic signals, thus could function as a calcium release channel. It is possible that the channel could work both ways depending on the particular cellular requirements.

As stated previously, in other cell types TRPML channels are known to regulate localised calcium signals, as well as global calcium waves via activation of ER and plasma membrane calcium flux (Kilpatrick *et al.,* 2016). The same may be true in *Dictyostelium* - if Ddmucolipin is capable of activating calcium release from ER and across the plasma membrane, then overexpressing the channel would enhance the cytosolic calcium responses as I observed in my experiments. It is also possible that overexpression of Ddmucolipin results in expression at the plasma membrane, as this has been reported for TRPML1 expression in HEK293 cells (Kiselyov *et al*., 2005), or it may be translocated there during exocytosis as TRPML1 is in *Xenopus* oocytes (LaPlante *et al*., 2002). Similar findings have been reported in *Drosophila* TRPML heterologously expressed in HEK293 cells, where TRPML was expressed and functional on both endolysosomes and plasma membrane (Feng *et al*., 2014). Interestingly endogenous TRPML translocated from plasma membrane to endolysosomal localization in response to the initiation of autophagy (Wong *et al*., 2012). Ddmucolipin may either be expressed and function as a Ca^{2+} channel integral to the plasma membrane, or be found there as a result membrane fusion during exocytosis.

The *Dictyostelium* channels responsible for plasma membrane and ER calcium release are still not confirmed. Contenders are IplA, a channel related to the mammalian ER IP_3 receptors (Taylor *et al*., 1999; Lusche *et al*., 2012) and pkd2 the *Dictyostelium* polycystin-2, another member of the TRP superfamily (Lima *et al*., 2014; Traynor and Kay, 2017). Both IplA and pkd2 have been localised to the plasma membrane (Lusche *et al.,* 2012; Lima *et al*., 2014). However, IplA localises primarily to unidentified cytoplasmic inclusions, and it has not been determined whether this includes the ER (Lusche *et al*., 2012). Some studies have found that knockout of IplA abolishes calcium responses to chemoattractants (Traynor *et al*., 2000; Traynor and Kay, 2017), however another reported that the Ca^{2+}response to high concentrations of cAMP is maintained but smaller (Schaloske *et al*., 2005). Calcium responses to cAMP and folic acid are retained in pkd2 knockout cells (Traynor and Kay, 2017). Therefore, clarification of which channels involved in ER and

plasma membrane calcium signalling is still necessary. Future work to investigate if Ddmucolipin contributes to calcium influx across the plasma membrane and release from the ER calcium could include measurement of the uptake of $^{45}Ca^{2+}$ from the extracellular milieu, treatment of overexpression cells with thapsigargin to reduce ER calcium content (Lytton *et al*., 1991), and with EGTA to chelate extracellular calcium.

I also analysed cytosolic calcium signals in Ddmucolipin knockdown strains, and was surprised to find that reducing Ddmucolipin expression resulted in larger, rather than smaller Ca^{2+} responses. However, this occurred only in vegetative cells, the magnitudes of the calcium responses in differentiated cells stimulated with cAMP were not significantly different from controls. The enhanced Ca^{2+} responses observed in my vegetative Ddmucolipin knockdown strains might be caused by a decrease in Ca^{2+} buffering capacity by the acidic stores. Lysosomes can shape calcium signals by tempering cytosolic calcium released from the ER (López-Sanjurjo *et al*., 2013). It has been reported that the ability of lysosomes to buffer Ca^{2+} in lysosomally diseased cells is greatly reduced, possibly because of the accumulation of undigested lysosomal cargo (Lloyd-Evans *et al*., 2008; Kiselyov *et al*., 2010). Furthermore, buffering of cytosolic calcium by the mitochondria is defective in MLIV cells (Jennings *et al*., 2006). Interactions between lysosomes and mitochondria have recently been described, and may be involved in lysosomal-mitochondrial Ca^{2+} cross talk (Todkar *et al*., 2017). As calcium buffering is a mechanism involved in tempering calcium responses, loss of buffering capacity could actually result in enhanced global calcium signals. A similar mechanism has been demonstrated in *Dictyostelium* cells lacking the ER calcium binding proteins calnexin and calreticulin, as these strains had much larger calcium responses to chemoattractants than control cells (Wilczynska *et al*., 2005).

Since my Ddmucolipin knockdown strains exhibited increased, as opposed to decreased, cytosolic Ca^{2+} signals during the vegetative phase of the lifecycle, it was surprising to find that when these strains were allowed to differentiate to aggregation-competence, their Ca^{2+} responses to cAMP were unaffected. Similarly, Chang *et al*. (2020) reported that in *Dictyostelium* TPC-null cells the magnitude of cAMP-mediated Ca^{2+} responses was comparable to that in wild type AX2 cells. Together these results suggest that Ddmucolipin-dependent calcium signalling is not a major contributor to cytosolic calcium responses at this stage of development. Instead, the role of Ddmucolipin in the differentiated cells may be restricted to regulating local calcium signalling. Accordingly,

the cAMP responses in the TPC null cells were slightly delayed in the time of onset, and this may be related to local calcium release from the acidic stores in 'priming' ER calcium release (Chang *et al*., 2020), but this will require further investigation.

In previous work, the cellular phenotypes of growth, endocytosis and multicellular development were unaffected in Ddmucolipin knockout cells created from the parental strain DH1-10 (Lima *et al*., 2012). Since my strains were made in the parental strain AX2, I wanted to also characterise these phenotypes in my strains. I found that surprisingly my strains did have abnormal phenotypes and many, but not all of these, presented similarly in the knockdown cells as overexpression cells. Furthermore, some of the phenotypes in my strains were similar to those reported in *Dictyostelium* NCL models.

Phagocytosis rates were increased in both Ddmucolipin knockdown and overexpression cells. This may be directly related to the increased calcium signalling in these strains as evidence suggests that calcium is involved in phagocytosis (Muller-Taubenberger *et al.,* 2001; Yuan *et al.,* 2001; Fajardo *et al.,* 2004; Pikzack *et al.,* 2005). Pinocytosis rates were increased in knockdown strains, but unaffected in overexpression strains which suggests the defect is not directly caused by the abnormal calcium signalling. The involvement of Ca^{2+} in macropinocytosis is unclear. Extracellular Ca^{2+} is not essential (Williams and Kay, 2018), but both liberation of intracellular Ca^{2+} by caffeine treatment and inhibition of Ca^{2+} transport by La^{3+} treatment reduces macropinocytosis (Gonzalez *et al.,* 1990). However, both caffeine and La^{2+} can affect other processes. My results suggest different roles for Ddmucolipin function in macropinocytosis and phagocytosis.

When measuring growth rates, I expected that the increase in phagocytosis rates would correlate with an increase in growth rates on bacterial lawns, however both knockdown and overexpression strains grew normally on *E. coli*. Furthermore, axenic growth rates were slightly reduced in knockdown strains, so again did not correlate with the increase in pinocytic uptake. This phenotype was also present in *cln2* knockdown mutants (Smith *et al.,* 2019) and together these results may represent the presence of compensatory feedback pathways that upregulate rates of endocytosis as a response to nutrient deprivation caused by defective endolysosomal trafficking. This kind of reverse coupling of growth and endocytosis rates has also been observed in relation to other *Dictyostelium*

lysosomal proteins. A *Dictyostelium* knockout of *alyA* (encoding the major lysozyme isoform) has 40% reduction in total lysozyme activity, exhibits slow growth on bacterial lawns but increased phagocytosis of fluorescently labelled yeast cells due to a compensatory pathway (Müller *et al*., 2005). Knocking down expression of lysosomal Tpp1 (tripeptidyl peptidase I encoded by *cln2/tpp1*) caused reductions in the growth rate in liquid medium, slower plaque expansion rates on bacterial lawns, but elevated rates of phagocytosis (Smith *et al*., 2019). These effects were mediated by reduced activity of the *Dictyostelium* TORC1 (homologue of the human mechanistic Target of Rapamycin Complex I) signalling pathway, being mimicked by rapamycin treatment (inhibitor of TORC1) and Rheb knockdown (upstream activator of TORC1), and rescued by Rheb overexpression (Smith *et al*., 2019). Other *Dictyostelium* NCL models have shown varying phenotypes in their growth and nutrient uptake phenotypes. Mutants lacking *cln3* and *cln5* displayed enhanced proliferation in HL5 medium, however pinocytic uptake was not significantly different from AX3, and the *cln3*$^{-}$ phenotype was rescued by overexpression of GFP-cln3 (Huber *et al*., 2014; McLaren *et al*., 2021). Combined these results indicate abnormalities in nutrient uptake and growth and the pathways that connect them in the different lysosomal disease models.

The defects in catabolism that I observed in my strains could also be caused by disruptions in Ddmucolipin-mediated Ca^{2+}-dependent vesicle fragmentation/fusion which is characteristic of MLIV and other MLIV models (Berman *et al.,* 1974; Bargal and Bach, 1997; Lubensky *et al.,* 1999). I observed that Ddmucolipin knockdown and overexpression strains had increased fluorescence when stained with Lysosensor Blue. This may be linked to accumulation of Lysosensor Blue-stained vesicles as a result of Ca^{2+}-dependent increases in homotypic or heterotypic vesicle fusion during the endosomal mixing stage and subsequent failure to progress through to exocytosis. Studies in other models reported that the defective membrane trafficking can be caused by both knockout and overexpression of TRPMLs causing accumulation of large hybrid late endosome-lysosomal compartments (Berman *et al.,* 1974; Lubensky *et al.,* 1999) as well as enlargement and clustering of endosomes (Fares and Greenwald, 2001; Kim *et al.,* 2007; Martina *et al.,* 2009; Vergarajauregui *et al.,* 2009). In *Dictyostelium* DH1-10 Ddmucolipin knockout cells, a significant increase in generation of post-lysosomes was reported, however as this was coupled with enhanced rate of post-lysosome fusion with the plasma membrane, and

subsequent exocytosis, so that there was no measurable build-up of vesicles (Lima *et al.,* 2012). I did not measure exocytosis rates in my strains, so further experiments could determine if exocytosis is blocked in my strains and account for the accumulation.

Alternatively, because Lysosensor Blue fluorescence increases as the pH becomes more acidic, the increased fluorescence in my knockdown and overexpression strains could also be caused by a decrease in the pH of the vesicles. Dysregulated lysosomal pH is common to lysosomal storage disease cells, however this is generally linked to increased pH as reported in MLIV fibroblasts type (Bach *et al*., 1999) and most NCLs (Holopainen *et al*., 2001). However, decreased lysosomal pH has been described in some MLIV fibroblasts (Soyombo *et al*., 2006). It is important to note that *Dictyostelium* cells lacking Ddmucolipin exhibited no change in the pH of endosomal compartments (Lima *et al*., 2012).

A further consequence of dysfunctional catabolism, retention of unprocessed nutrients and decreased release of amino acids from the vesicles, could be that the cells are in a state of partial starvation and this would favour the initiation of aggregation. In support of this, both Ddmucolipin knockdown and overexpression strains exhibited increased numbers of aggregation centers and accordingly formed slugs and fruiting bodies significantly smaller than those of AX2. This implicates Ddmucolipin in activation of aggregation center formation and could be linked to calcium-dependent regulation of developmental processes (Sakamoto *et al*., 2003; Poloz and O'Day, 2012). The same phenotype is present in *IplA*$^{-}$ cells which form smaller mounds and fruiting bodies due to fragmented aggregation streams (Traynor *et al*., 2000; Schaloske *et al*., 2005). Similar phenotypes are also present in other *Dictyostelium* lysosomal disease models. Mutants with knocked down *cln2*/*tpp1* form smaller aggregates and fruiting bodies (also mediated by reduced TORC1 signalling, Smith *et al*., 2019), and *cln2*/*tpp1*$^{-}$ mutants progress faster through development (Phillips and Gomer, 2015). Cells lacking *cln3* and *cln5* exhibit precocious development, increased numbers of tipped mounds, fingers and slugs, similar to my Ddmucolipin strains (Huber *et al*., 2014; Huber *et al*., 2016; McLaren *et al*., 2021). Interestingly, the precocious development in *cln3*$^{-}$ cells was rescued by chelation of calcium with EGTA. This implicates Cln3 in calcium regulation, likely due to its localisation at the contractile vacuole, a major calcium regulatory organelle (Malchow *et al*., 2006;

Huber *et al*., 2014), and suggests calcium dysregulation may be common to lysosomal disease cells.

In addition to the increased numbers of aggregates formed in my knockdown and overexpression mutants, an increased proportion of the cells in the aggregates appear to be entering the autophagic cell death pathway. This was suggested by the proportionately thicker stalks and enlarged basal disks, a phenotype associated with increased autophagic cell death (Bokko *et al.,* 2007). This is another phenotype common among *Dictyostelium* lysosomal disease mutants. It is also present in *tpp1* knockdown cells where it is mediated by reduced TORC1 signalling (Smith *et al.,* 2019). Furthermore, enhanced autophagy has been reported in *tpp1* knockout cells (Phillips and Gomer, 2015) and *cln5*$^{-}$ cells display aberrant autophagy (McLaren *et al*., 2021). TPC knockout cells also accumulate autophagosomes (Chang *et al*., 2020) which further implicates calcium signalling through the acidic stores in autophagic processes. As autophagic cell death occurs late in the developmental cycle during stalk formation, it is possible that during autophagy, Ddmucolipin together with other calcium channels in that location (TPC in particular) could play similar roles in generating a local Ca^{2+} cloud to facilitate fusion of the autophagosome and lysosome during formation of the stalk cell vacuole. Schaap *et al.* (1996) showed that a sustained elevation of resting cytoplasmic Ca^{2+} levels mediates late stalk gene (*ecmB*) induction by the morphogen DIF (Differentiation Inducing Factor) in *Dictyostelium.* Ddmucolipin could play a role in this process. In that case, as I have seen in the endolysosomal pathway, Ddmucolipin overexpression and knockdown would both cause increased Ca^{2+} signals and subsequent disturbances in autophagolysosome formation, possibly explaining the stalk phenotype. An increase in cellular autophagic vacuoles is a characteristic associated with MLIV (Vergarajauregui *et al.,* 2008) is observed both in mouse models (Curcio-Morelli *et al.,* 2010), and *Drosophila* Ddmucolipin knockout flies (Wong *et al.,* 2012). The underlying nature of the autophagic defect may be related to disruption in signalling by the nutrient stress sensor mTORC1, a key regulator of autophagy. One study has shown that mTORC1 can directly phosphorylate TRPML1 to negatively regulate channel activity and decrease autophagy (Onyenwoke *et al.,* 2015). To add further complexity, recent evidence has revealed that TRPML1 Ca^{2+} release can regulate mTORC1 autophagic pathways through a nutrient-sensitive negative feedback loop (Sun *et al*., 2018). Furthermore, TRPML1 is directly involved in the Ca^{2+}/calmodulin

dependent protein kinase β (CaMKKβ) activation of AMP-activated protein kinase (AMPK) (Scotto-Rosato *et al.,* 2019). AMPK in turn inhibits TORC1 and thereby activates autophagy.

The nature of these complex signalling pathways still needs to be unravelled, therefore my study supports the view that *Dictyostelium* offers a tractable, simple model for MLIV-like cytopathology. The results suggest it would be valuable in future experiments to investigate further the signalling pathways involved in Ddmucolipin Ca^{2+} signalling-dependent regulation of cellular growth and autophagy through *Dictyostelium* TORC1. This is of particular interest because the role of Ca^{2+} signalling in regulation of mTORC1 autophagy pathways is evident, but details are still unclear (Decuypere *et al.,* 2011), as are mTORC1-TRPML signalling pathways. Therefore, it would be relevant to explore whether the growth and developmental defects can be rescued by genetically altering *Dictyostelium* TORC1 and *Dictyostelium* AMPK expression in Ddmucolipin knockdown and overexpression backgrounds.

The results I have presented here highlight common phenotypes amongst *Dictyostelium* lysosomal disease models suggesting they may share common pathologies. I have also shown that both increasing and decreasing Ddmucolipin expression levels can cause the same phenotypic outcome. My results are similar to other studies where reports of both increased and decreased expression of Ddmucolipin proteins can cause problems along the endocytic pathways. For example, when TRPML3 is knocked down there are defects in endosomal acidification and also increased homotypic endosomal fusion (Lelouvier and Puertollano, 2011), while when TRPML3 is overexpressed, endosomes become enlarged (Martina *et al.,* 2009; Lelouvier and Puertollano, 2011). In *C. elegans*, both Ddmucolipin knockout and some overexpression coelomocytes, exhibited the formation of large vacuoles (Fares and Geenwald, 2001). Similarly, overexpression of TRPML1 results in accumulation of enlarged endosomes containing both early and late endocytic markers (Vergarajauregui *et al.,* 2009) and induces an aberrant distribution of these compartments within the cell (Manzoni *et al.,* 2004). These combined reports show that the endocytic pathway is clearly impacted by disturbances in both directions in the expression levels or activities of Ddmucolipin proteins and the resultant alterations in Ca^{2+} signalling.

Concluding remarks

In this study I show that in *Dictyostelium* Ddmucolipin overexpression contributes significantly to global chemotactic calcium responses in vegetative and differentiated cells. Knockdown of Ddmucolipin also enhances calcium responses in vegetative cells but does not affect responses in 6-7 hour developed cells, suggesting that in developed cells Ddmucolipin may help regulate local calcium signals rather than global calcium waves. I found that both knocking down and overexpressing Ddmucolipin often, but not always, presented the same phenotypes. Altering Ddmucolipin expression levels caused an accumulation or increased acidification of Lysosensor Blue stained vesicles in vegetative cells. Nutrient uptake by phagocytosis and macropinocytosis were increased but growth rates were not, suggesting defects in catabolism. Both increasing and decreasing Ddmucolipin expression caused the formation of smaller slugs and larger numbers of fruiting bodies during multicellular development, suggesting that Ddmucolipin is involved in initiation of aggregation centers. The fruiting bodies that formed from these smaller aggregates had proportionately larger basal discs and thickened stalks, consistent with a regulatory role for Ddmucolipin-dependent Ca^{2+} signalling in the autophagic cell death pathways involved in stalk and basal disk differentiation in *Dictyostelium*. Thus, I have provided evidence that Ddmucolipin contributes to chemotactic calcium signalling and that *Dictyostelium* is a useful model to study the molecular mechanisms involved in the cytopathogenesis of Mucolipidosis type IV.

Chapter five

Investigating the role of two putative Ca^{2+}-ATPase in *Dictyostelium,* a phenotypic characterization

5.1 Introduction

Eukaryotic Ca^{2+} translocating ATP-ases belong to a large family of P-type cation translocases which maintain basal Ca^{2+} levels and terminate Ca^{2+} signals by excreting Ca^{2+} out of the cytosol after influx events. They are classified according to their subcellular localisation and include plasma membrane Ca^{2+} ATPases (PMCA), secretory pathway Ca^{2+} ATPases (SPCA) of the Golgi and those located in the ER/SR membranes, the sarco(endo)plasmic reticulum Ca^{2+} ATP-ases (SERCA) which refill internal Ca^{2+} stores. These enzymatic pumps couple the energy provided by ATP hydrolysis to power uphill transport of cations across the membrane. As opposed to the high Ca^{2+} conductance of cation/Ca^{2+} exchangers, Ca^{2+}- ATPases have a high Ca^{2+} binding affinity but low conductance rate. This means that the proteins are particularly suited to maintaining the low basal cytosolic Ca^{2+} levels (Stammers *et al*., 2015; Brini *et al*., 2017; Wu *et al*., 2018). All three groups share the same basic topology, involving 10 hydrophobic transmembrane domains (TMDs) with cytosolic COOH and NH_2 terminals. A large cytoplasmic loop between TMD 4 and 5 contains the catalytic domain (Toyoshima *et al*., 2000; Di Leva *et al*., 2008; Chen *et al*., 2020). The reaction cycle of the pumps sees the enzyme go through a number of conformational changes on the cytosolic side and within the TMDs. These changes direct Ca^{2+} from the cytosol to the extracellular/luminal space. While similar in structure, the enzymes' diverse roles in Ca^{2+} signalling and homeostasis and cellular and biological function are attributed to differences in their subcellular and tissue distribution and regulatory mechanisms (Brini *et al*., 2012; Strehler, 2015; Brini *et al*., 2017).

Schatzmann (1966) provided the first report of an ATP- dependent Ca^{2+} transporter active at the PM of erythrocytes. Since then four isoforms have been identified in mammalian cells, PMCA1-4, encoded by four different genes (*ATP2B1-4*). Of these, PMCA1 and PMCA4 are ubiquitously expressed in the tissues while PMCA2 and PMCA3 are restricted to specific tissues including cells of the nervous system (Stauffer *et al*., 1993; Hammes *et al*.,

1994). Native PMCAs form functional heteromers composed of PMCA1–4 and the obligatory auxiliary subunits neuroplastin and basigin which are essential for stability, surface trafficking and proper Ca^{2+} pumping (Schmidt *et al*., 2017; Gong *et al*., 2018). The PMCA mRNA can be processed into many splice variants, expression of which are developmentally regulated and allow the enzymes to serve a diverse range of functions (Zacharias and Kappen, 1999; Strehler and Zacharias, 2001; Romero-Lorca *et al*., 2018). As the name suggests, the enzymes transport Ca^{2+} ions across the PM from the cytosol to the extracellular space at a rate of one Ca^{2+} ion for every one ATP molecule hydrolysed (Guerini *et al*., 2000). Within the catalytic domain reside a lysine residue essential for ATP binding as well as a highly conserved aspartate residue which upon phosphorylation changes the conformation of the protein into an intermediate state (Pedersen and Carafoli, 1987). The intracellular loop also contains an autoinhibitory domain, which interacts with a calmodulin binging domain in the COOH terminal (Falchetto *et al*., 1991). When not bound to calmodulin, the enzyme remains in a closed conformation, but upon binding calmodulin, the main regulatory element, the autoinhibition is released, the Ca^{2+} affinity is increased and the enzyme is activated (Falchetto *et al*., 1992; Mandal *et al*., 2008; Tidow *et al*., 2012). The local Ca^{2+} concentrations can regulate the autoinhibition such that when Ca^{2+} concentrations are low the enzyme is almost inactive and high local Ca^{2+} relieve autoinhibition (Mandal *et al*., 2008).

PMCAs are believed to be primarily involved in regulating resting Ca^{2+} levels and fine tuning cytosolic Ca^{2+} signals by modulation the amplitude and duration of the responses (Hegedus *et al*., 2020). When cytosolic Ca^{2+} levels rise transiently, PMCAs are believed to temper only about 1% of the global Ca^{2+} wave. Together, the PMCA and the mitochondrial Ca^{2+} uniporter, which is also responsible for uptake of ~1% of the Ca^{2+}, are referred to as the “slow systems”. The higher conductance Na^{+}/Ca^{2+} exchanger (NCX) of the PM, and sarco-endoplasmic reticulum Ca^{2+} ATPases (SERCAs) sequester the bulk, removing ~28% and ~70% respectively (Bers, 2000).

The SERCAs are exclusively responsible for uptake of Ca^{2+} ions into the ER/SR lumen (Rossi and Dirksen, 2006) which is the major Ca^{2+} storage organelle, harbouring Ca^{2+} concentrations of ~ 1mM, similar to the extracellular environment (Marchi *et al*., 2014). SERCAs have a higher capacity than PMCAs, binding and translocating two Ca^{2+} ions for

every one ATP molecule hydrolysed (Guerini *et al*., 2000; Strehler, 2015). Each of the mammalian SERCAs 1-3 exist in multiple splice variants, which differ in tissue specificity and serve different biological and physiological functions (Periasamy and Kalyanasundaram, 2007). Various interacting and regulatory proteins have been identified (Brini, 2009). The regulatory proteins phospholamban (PLB) and sarcolipin (SLN) interact with specific SERCA isoforms, such that binding of unphosphorylated PLB or SLN reduces the pump's Ca^{2+} affinity and inhibits its activity (James, 1989; Tada and Toyofuku, 1996; Smeazzetto *et al*., 2017; Glaves *et al*., 2020). When phosphorylated by PKA and or/ calmodulin-dependent kinase II (CaMKII), PLB dissociates and this relieves inhibition of the SERCA (Karczewski *et al*., 1997; Naraynan and Xu 1997). Other regulatory subunits are beginning to be uncovered including the dwarf open reading frame (DWORF) and myoregulin (MLN) (Xu and Van Remmen, 2021). The ER/SR luminal Ca^{2+}-binding proteins calnexin and calreticulin are also thought to regulate the activity of the SERCA2 isoforms (Roderick *et al*., 2000; John *et al*., 1998). The model suggests that when calnexin is phosphorylated in the cytosolic domain (S562) it interacts with and inhibits SERCA2b through the COOH terminal. Ca^{2+} release from the ER/SR through IP_3R promotes Ca^{2+}-dependent dephosphorylation at S562, and relieves SERCA2b inhibition and promotes refilling of luminal stores (Roderick *et al*., 2000). The large contribution to buffering cytosolic Ca^{2+} transients means that SERCA function is paramount to regulation of Ca^{2+} homeostasis and signaling.

The *Dictyostelium* genome encodes three P-type Ca^{2+}-ATPases, PAT1 (discussed in section 1.1.4.8) which localizes to the membrane of the CV (Moniakis *et al*., 1995; Moniakis *et al*., 1999), and two predicted homologues of PMCA/SERCA, dictyBase accession numbers DDB_G0284605 and DDB_G0289473 (Wilczynska *et al*., 2005). For this thesis, the homologues have been named PAT3 (DDB_G0284605) and PAT4 (DDB_G0289473). Both putative proteins encode predicted calmodulin-binding helical peptide IQ motifs, however the subcellular localization of both is unknown. Early experiments measuring ATP-dependent Ca^{2+} release over the plasma membrane at a rate of roughly 5×10^6 ions/cell/min, provided evidence for PMCA activity at this location (Böhme *et al*., 1987). Subsequently an ATP/Mg^{2+}-dependent, high-affinity Ca^{2+} pump at the plasma membrane was described (Milne and Coukell, 1988). Given the evidence that Ca^{2+} can be released from the ER during chemotactic Ca^{2+} responses (Wilczynska *et al*., 2005), one can assume

that an active SERCA-like pump also functions at this location and is responsible for refilling the ER Ca^{2+} store after Ca^{2+} release.

The PAT3 and PAT4 homologues have not previously been genetically studied, therefore the aim of this study was to investigate the role of the putative pumps in Ca^{2+} homeostasis and chemotactic signaling. The involvement of these pumps in growth and development was also explored. To achieve this, a collection of transformants with reduced expression of PAT3 and PAT4 were produced by antisense RNA inhibition. The mutants were then phenotypically characterized to investigate the role of PAT3 and PAT4 in growth, development and Ca^{2+} signaling. The following describes the results of the phenotypic characterization.

5.2 Results

5.2.1 Creation of *pat3* and *pat4* asRNA inhibition constructs

In order to achieve knockdown of *pat3* and *pat4*, plasmid constructs for asRNA expression were created using the two phase cloning method.

5.2.1.1 First phase cloning into an *E. coli* vector

To facilitate inhibition of protein expression, fragments of the *pat3* and *pat4* genes were cloned into a *D. discoideum* expression vector in the antisense orientation. The vectors were then introduced into *D. discoideum* cells via transformation where they will randomly insert into the genome. To produce the antisense RNA constructs, a 1447 bp fragment of *pat3* and 1382 bp fragment of *pat4* gDNA were amplified via PCR with the primers *pat3*: SERCA2F and SE2MR, and *pat4*: SERCA1.AF and SE1MR (Table 2.6), using DNA extracted from vegetative AX2 cells as a template. The gene fragments were cloned into the *E. coli* vector pZErO™-2 using endonuclease restriction cut sites incorporated into the PCR primers– *Bam*HI and *Kpn*I for *pat3* and *Eco*RI for *pat4.* The resulting constructs pPROF642 (for *pat3*) and pPROF639 (for *pat4*) were verified by sequencing. The schematic representation of the cloning strategy is shown in Figure 5.1 and Figure 5.2.

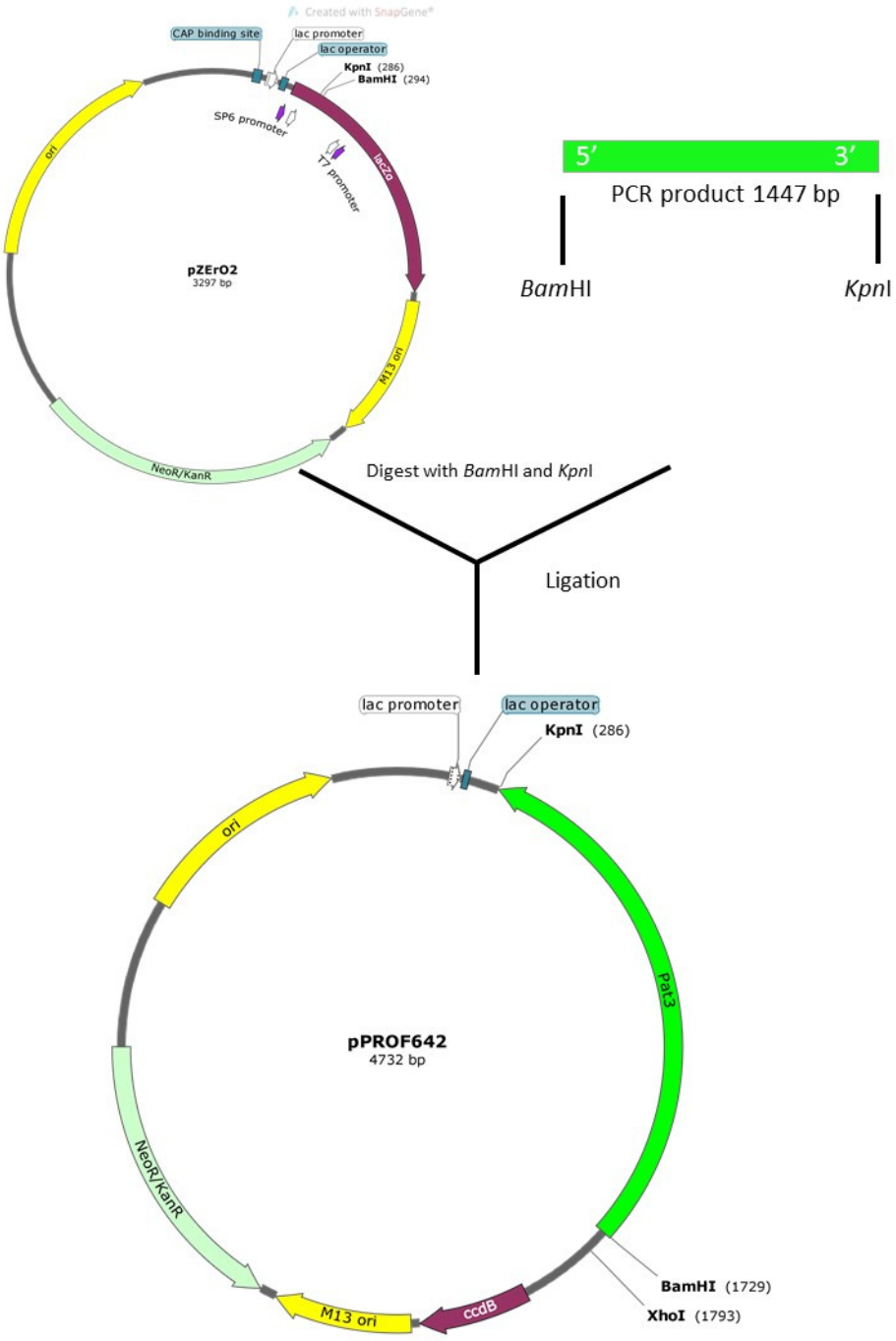

Figure 5.1 Cloning strategy phase one – *pat3* antisense construct.

The *pat3* gDNA fragment (1447 bp) was PCR amplified from AX2 gDNA using primers SERCA2F and SE2MR. The amplified fragment was inserted into the *Bam*HI/ *Kpn*I sites of the *E. coli* vector pZErO™-2. The ligation product was electroporated into *E. coli* Top10 cells and colonies were selected for using kanamycin resistance. Colonies were further screened using restriction analysis of miniprep DNA from cultures grown from individual colonies. The resulting construct pPROF642 was confirmed via sequencing.

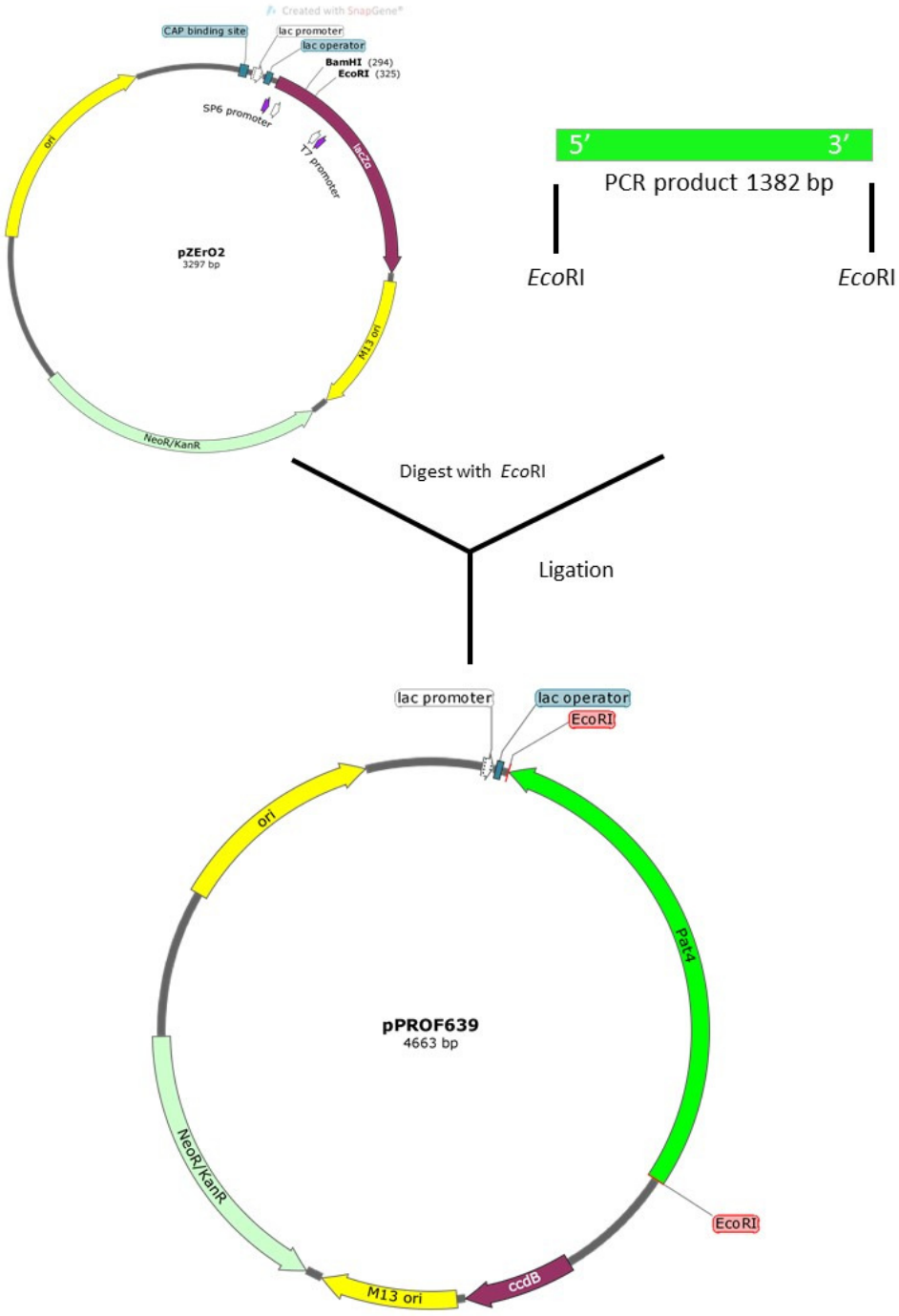

Figure 5.2 Cloning strategy phase one – *pat4* antisense construct.

The *pat4* gDNA fragment (1382 bp) was amplified by PCR from AX2 gDNA using primers SERCA1.AF and SE1MR. The amplified fragment was inserted into the *Eco*RI site of the *E. coli* vector pZErO™-2. The ligation product was electroporated into *E. coli* Top10 cells and colonies were selected for using kanamycin resistance. Colonies were further screened using restriction analysis of miniprep DNA from cultures grown from individual colonies. The resulting construct pPROF639 was confirmed via sequencing.

5.2.1.2 Subcloning of the *pat3* and *pat4* antisense fragments into a *D. discoideum* expression vector pDNeo2

The 1447 bp fragment of *pat3* and 1382bp fragment of *pat4* gDNA were excised from constructs pPROF642 and pPROF639 respectively and subcloned in the antisense orientation into the *Dictyostelium* expression vector pDNeo2. The resulting constructs, pPROF643 and pPROF640, were verified by restriction enzyme digest. The schematic representation of the cloning strategy is shown in Figure 5.3 and Figure 5.4.

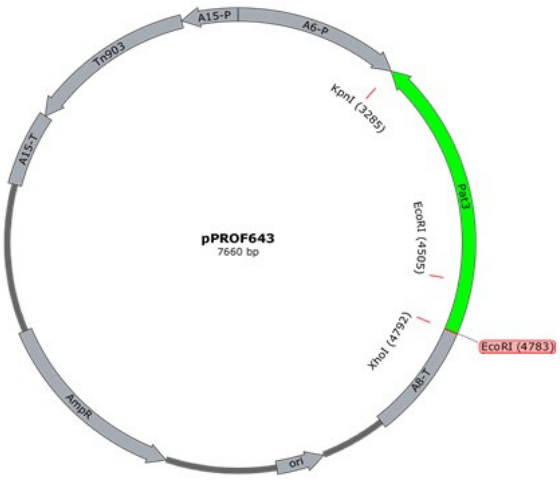

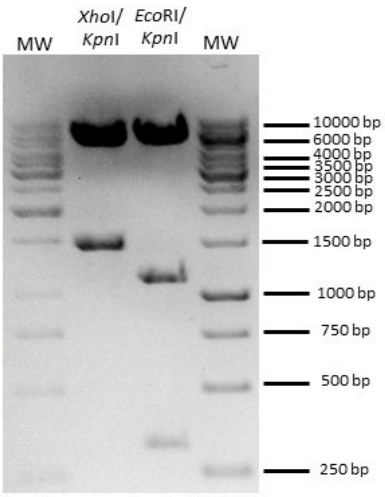

Restriction enzyme analysis – *Pat3* antisense construct pRPOF643

Construct name	Restriction enzymes	Expected fragments size (bp)
pPROF643	XhoI/KpnI	6153 bp + 1507 bp
	EcoRI/KpnI	6162 bp + 1220 bp + 278 bp

Figure 5.3 Cloning strategy phase two – *pat3* antisense inhibition construct.

The 1507 bp fragment from pPROF642 was excised and subcloned in the antisense orientation into the *D. discoideum* expression vector pDNeo2 using the endonuclease cut sites *Xho*I and *Kpn*I. The ligation product was electroporated into *E. coli* DH5α cells, and colonies were selected on ampicillin. Plasmid miniprep DNA from individual colonies was extracted and screened by restriction analysis. The resulting construct pPROF643, was verified by restriction enzyme analysis as depicted in the gel image, the expected DNA fragment sizes are indicated in the table.

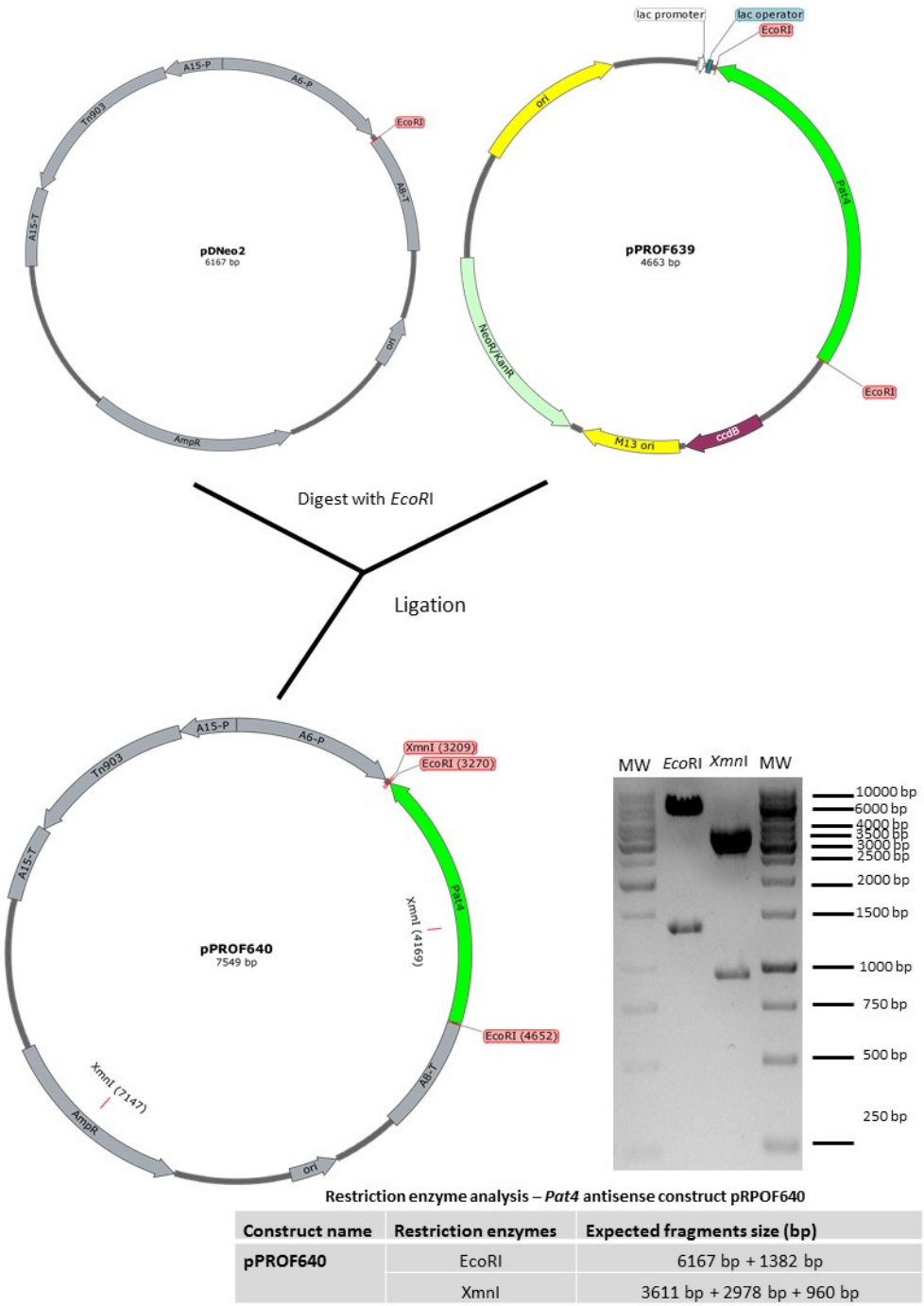

Restriction enzyme analysis – *Pat4* antisense construct pRPOF640

Construct name	Restriction enzymes	Expected fragments size (bp)
pPROF640	EcoRI	6167 bp + 1382 bp
	XmnI	3611 bp + 2978 bp + 960 bp

Figure 5.4 Cloning strategy phase two – *pat4* antisense inhibition construct.

The 1382 bp fragment from pPROF639 was excised and subcloned in the antisense orientation into the *D. discoideum* expression vector pDNeo2 using the endonuclease cut site *Eco*RI. The ligation product was electroporated into *E. coli* DH5α cells, and colonies were selected on ampicillin. Plasmid miniprep DNA from individual colonies was extracted and screened by restriction analysis. The resulting construct pPROF640, was verified by restriction enzyme analysis to ensure the insert was in the antisense orientation as depicted in the gel image, the expected DNA fragment sizes are indicated in the table.

5.2.2 **Genetic manipulation of *pat3* and *pat4***

Antisense inhibition constructs were introduced into wild type AX2 cells by the calcium phosphate coprecipitation method in order to knockdown expression of *pat3* and *pat4* respectively. Transformants were isolated and to confirm that the mRNA expression had been reduced in the transformants, semiquantitative RT-PCR was used to measure relative expression of *pat3* and *pat4* mRNA in a subset of transformants. As expected, antisense inhibition caused a measurable decrease in mRNA transcripts in all transformants tested except HPF862 and HPF649 (Table 5.1). In these two transformants a decrease in the level of mRNA expression might have been too small to be identified by RT-PCR, this may be due to low copy numbers of the integrated plasmid. These strains were included in the phenotypic characterization, and because they displayed phenotypes consistent with those of the other transformants they were included in data analysis. Similarly, as time did not permit further expression screening of the remaining transformants (indicated as N/A in Table 5.1), the phenotypes were characterized and because they displayed consistent phenotypes they were also included in analysis. Unfortunately, time did not allow copy number quantification for the transformants. There was not a significant correlation between any of the phenotypes with mRNA expression levels, therefore for phenotypic analysis, data from all transformants from each group was pooled.

Table 5.1 *pat3* and *pat4* knockdown transformants

Group	**Antisense inhibition construct**	**Strain HPF number**	**mRNA expression relative to AX2 (cycle threshold)**
PAT3	pPROF643	HPF866	-1.4
PAT3	pPROF643	HPF865	-1.3
PAT3	pPROF643	HPF648	-0.5
PAT3	pPROF643	HPF862	1*
PAT3	pPROF643	HPF649	0.8*
PAT3	pPROF643	HPF863	-1.8
PAT3	pPROF643	HPF868	-5.2
PAT3	pPROF643	HPF867	N/A

PAT3	pPROF643	HPF869	N/A
PAT3	pPROF643	HPF870	N/A
PAT3	pPROF643	HPF871	N/A
PAT3	pPROF643	HPF650	N/A
PAT4	pPROF640	HPF852	-9.2
PAT4	pPROF640	HPF646	-7
PAT4	pPROF640	HPF853	-4.9
PAT4	pPROF640	HPF851	-4.8
PAT4	pPROF640	HPF850	-4.1
PAT4	pPROF640	HPF849	N/A
PAT4	pPROF640	HPF658	N/A
PAT4	pPROF640	HPF856	N/A
PAT4	pPROF640	HPF645	N/A
PAT4	pPROF640	HPF659	N/A
PAT4	pPROF640	HPF647	N/A

After successfully obtaining *pat3* and *pat4* knockdown transformants, phenotypic analysis was performed in order to characterize the function of the proteins in *Dictyostelium*. The following sections describe the results of phenotypic characterization.

5.2.3 Phenotypic analysis

5.2.3.1 Developmental expression of *pat3* and *pat4* mRNA over 24 hours

The expression profiles of many *Dictyostelium* genes change throughout development. To determine the mRNA expression levels of *pat3* and *pat4* throughout development, AX2 cells were allowed to develop on water agar plates for 24 hours until mature fruiting bodies had formed, and RNA extracts were taken at 2 hour intervals. Semiquantitative RT-PCR was used to assess the relative expression in cells at these time points. Both genes were expressed throughout development, and their mRNA expression patterns were similar. Expression remained fairly constant during early differentiation in response to the onset of starvation, and then fell dramatically to a trough at 8 hours corresponding to the time the cells became aggregation competent, remaining low during subsequent multicellular development (Fig. 5.5A and Fig. 5.6A). In both cases the expression level in

differentiated cells was markedly lower than in vegetative cells. The measured expression profiles are similar to the RNA-Seq expression profiles of these genes in *D. discoideum* published on dictyBase (Parikh *et al*., 2010; Stajdohar *et al*., 2017) although the drop in expression of *pat4* occurred at 16 hours and even after the decrease in expression at 8 or 16 h, the expression levels remained higher than those observed in vegetative cells (Fig. 5.5B and Fig. 5.6B). The differences in the patterns of expression may relate to differences in the strain (AX2 or AX4), growth and development conditions for the dictyBase RNASeq data versus my experiments. The dictyBase RNA-Seq profile of *patA* (encoding PAT1) shows an initial drop in expression, and then a gradual increase in expression up until a peak at 12 hours, where expression gradually decreases again (Fig. 5.7). Together these results might suggest roles for all three pumps in calcium signalling in early starvation-induced differentiation. It is unknown if the levels of the encoded proteins also decline at the onset of aggregation, if the proteins are stable, there may not be a need for ongoing high levels of mRNA expression.

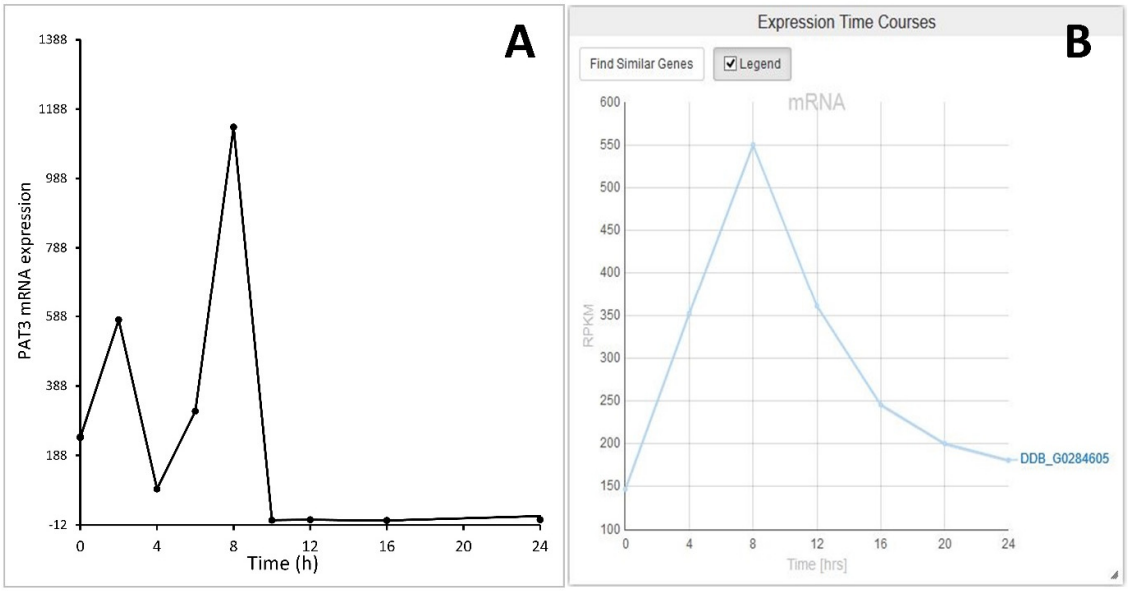

Figure 5.5 *pat3* mRNA expression changes throughout development in *D. discoideum.*

(A) Semiquantitative RT-PCR was used to determine the *pat3* mRNA expression in AX2 over 24 hours. *pat3 mRNA* expression is normalized to filamin expression and presented as nominal mRNA expression (2^{Qt}). Measurements were taken using RNA extracted from cells developing on water agar every two hours for 24 hours. Each data point represents the average expression from two separate experiments. **(B)** Image reproduced from dictyexpress.org. Developmental timing of expression of *pat3* in *D. discoideum* AX4 as measured by RNA-Seq. Reads per kilobase per million (RPKM) over 24 hours. Published on dictyBase (Parikh *et al*., 2010; Stajdohar *et al*., 2017).

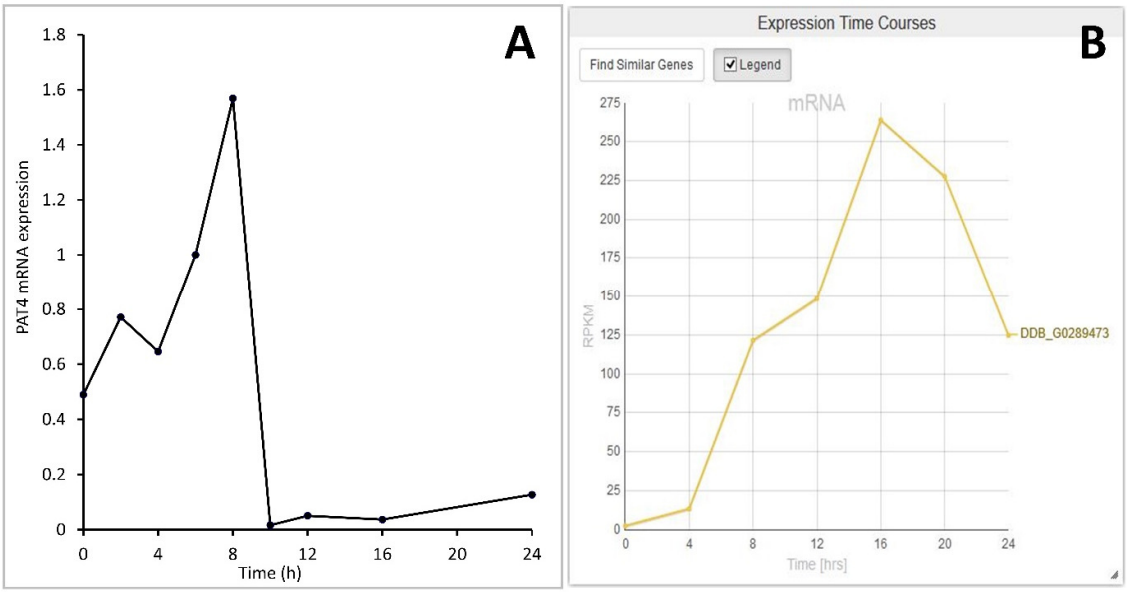

Figure 5.6 *pat4* mRNA expression changes throughout development in *D. discoideum.*

(A) Semiquantitative RT-PCR was used to determine the *pat4* expression in AX2 over 24 hours. *pat4* expression is normalized to filamin expression and presented as nominal mRNA expression (2^{Qt}). Measurements were taken using RNA extracted from cells developing on water agar every two hours for 24 hours. Each data point represents the average expression from two separate experiments. **(B)** Developmental timing of expression of *pat4* (DDB_G0289473) in *D. discoideum* AX4 as measured by RNA-Seq. Reads per kilobase per million (RPKM) over 24 hours. Published on dictyBase (Parikh *et al.*, 2010; Stajdohar *et al.*, 2017).

Figure 5.7 *patA* mRNA expression profile.

Developmental timing of expression of *patA* in *D. discoideum* AX4 as measured by RNA-Seq and published on dictyBase (Parikh *et al*., 2010; Stajdohar *et al*., 2017).

5.2.3.2 Knockdown of PAT3 and PAT4 had no effect on growth rates or rates of endocytosis

An analysis of nutrient uptake by phagocytosis and pinocytosis and growth rates on bacterial lawns and axenically was performed using the PAT3 and PAT4 knockdown strains. To measure the growth rates of cells grown in HL5 medium, a growth experiment was conducted using wildtype AX2 and the PAT3 and PAT4 transformants and the generation times of were measured during exponential growth in HL5 medium. Decreased expression of PAT3 and PAT4 had no effect on axenic growth (Fig. 5.8A). The rates of fluid uptake by macropinocytosis in these strains was determined by measuring the uptake of FITC-dextran over a 70 min period in wildtype AX2 and the knockdown transformants. Macropinocytosis rates of the transformants were not significantly different from AX2 (Fig. 5.8B). The plaque expansion rates (growth velocity) of AX2 control and PAT3 and PAT4 knockdown transformants were measured from linear regressions of plaque diameters *vs* time during growth at 21˚C on an *E. coli* B lawn. Neither knockdown

significantly altered the plaque expansion rate compared to the control AX2 (Fig. 5.9A). The rates of phagocytosis in the knockdown transformants and AX2 control were assayed by measuring the uptake of fluorescently labelled live *E. coli* cells over 30 mins. Similarly to the rates of growth, there was no significant difference in the rates of phagocytosis in the knockdown transformants compared to control AX2 (Fig. 5.9B). These results are consistent with *patA* antisense inhibition transformants which grow the same as wild type in MES/HL5 medium, and on lawns of *E. coli* on SM agar (Moniakis *et al*., 1999).

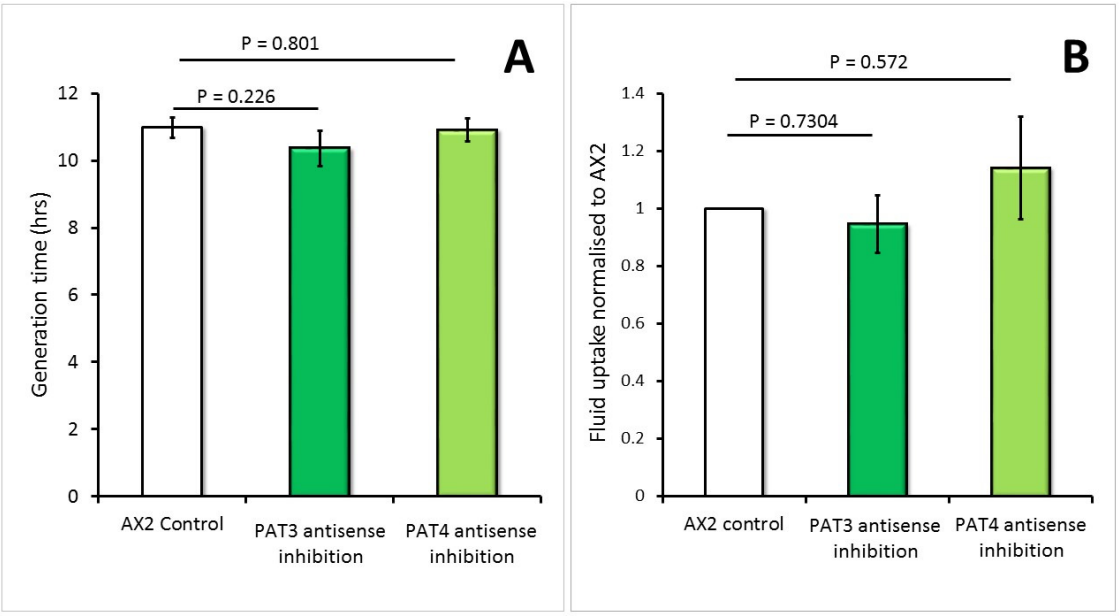

Figure 5.8 KD of PAT3 and PAT4 does not affect growth rates of cells grown HL5 medium or macropinocytic fluid uptake.

(A) Generation times of cells grown in HL5 medium were not affected in PAT3 and PAT4 antisense inhibition strains ($p > 0.05$, One-Way ANOVA, with pairwise comparisons made by the Least Squares Difference method). Error bars are standard errors of the mean. Each strain antisense inhibition strain was measured in two individual experiments and data from all groups of transformants pooled to determine the mean across groups. PAT3 11 strains (n= 22), PAT4 ten strains (n= 20) control AX2 one strain (n=6). The generation time in hours was calculated using log-linear regression in the "R" statistics and graphics environment. **(B)** Consumption of HL5 medium containing FITC dextran via macropinocytosis in KD, and AX2 control normalized to AX2. Fluid uptake was not affected by KD of PAT3 or PAT4. ($p > 0.05$, One-Way ANOVA, with pairwise comparisons made by the Least Squares Difference method). Error bars are standard errors of the mean. Each strain was measured in two to three separate experiments and data from all groups of transformants pooled to determine the mean across groups. PAT3 eight strains (n=19), PAT4 eight strains (n= 16) control AX2 one strain (n=8).

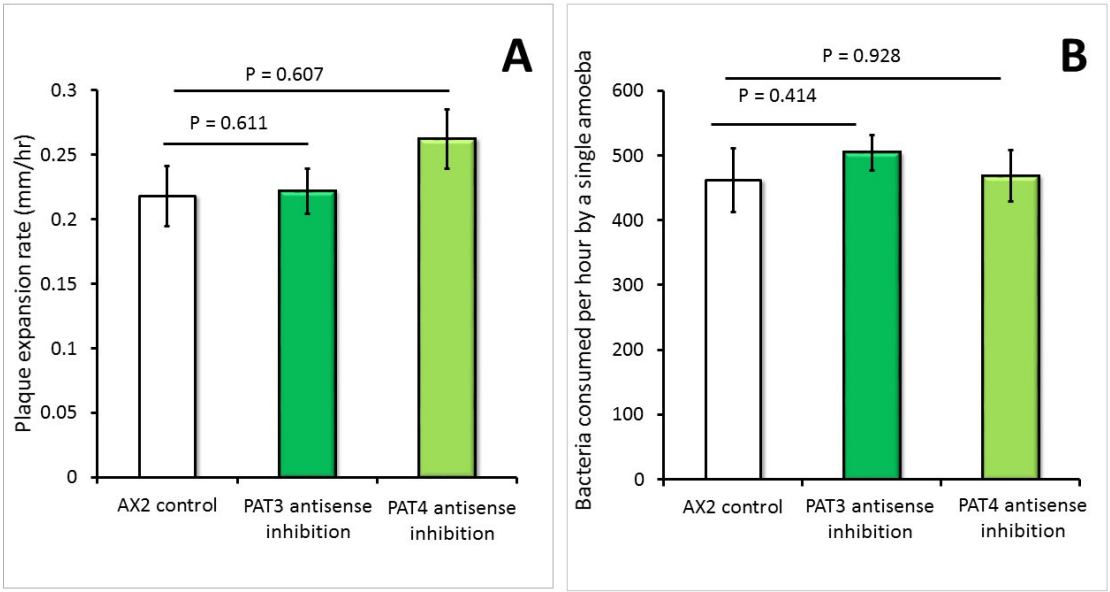

Figure 5.9 KD of PAT3 and PAT4 does not affect plaque expansion rates or the rate of bacterial consumption by phagocytosis.

(A) Plaque expansion rates (growth velocity) were measured from linear regressions of plaque diameters *vs* time during growth at 21°C on an *E. coli* B lawn. Growth velocity was not significantly altered in KD transformants ($p > 0.05$, One-Way ANOVA, with pairwise comparisons made by the Least Squares Difference method). Error bars are standard errors of the mean. Plaque expansion rates for each antisense inhibition strain was measured in two to four separate experiments and data from all groups of transformants was pooled to determine the mean across groups. PAT3 11 strains (n= 34), PAT4 12 strains (n= 38) control AX2 one strain (n= 6). **(B)** Uptake of *E. coli* cells expressing the fluorescent protein Ds-Red via phagocytosis was not affected in PAT3 or PAT4 KD transformants (significance probabilities as indicated, $p > 0.05$, One-Way ANOVA with pairwise comparisons made by the Least Squares Difference method). Error bars are standard errors of the mean. Each strain antisense inhibition strain was measured in two to three separate experiments and data from all groups of transformants pooled to determine the mean across groups. PAT3: nine strains (n=18); PAT4: nine strains (n= 25); control AX2: one strain (n=8).

5.2.3.3 Knockdown of PAT3 and PAT4 had no effect on fruiting body morphologies

Multicellular developmental in *Dictyostelium* is initiated by starvation, cells undergo a developmental program which involves various stages leading to multicellular

morphogenesis and culmination into mature fruiting bodies consisting of a spore head, stalk and basal disc. In the fruiting body, the spore head (sorus) contains around 80 % of the cells, and the stalk and basal disc around 20 %. The spores can then be dispersed when conditions are favorable and germinate to give rise to amoebae. The stalk cells are formed by a process of autophagic cell death and are therefore non-viable. The developmental timing of expression of *pat3* and *pat4* mRNA (Figures 5.5 and 5.6) suggests they are involved at the early stages leading up to chemotactic aggregation which occurs from around 8 hours into the program. The dramatic drop in mRNA expression of both proteins at 8 hours suggests their roles are less important during the progression through multicellular morphogenesis. Calcium signaling also plays an important role during development, from chemotactic aggregation to cell type differentiation. To investigate how expression levels of PAT3 and PAT4 affects multicellular morphogenesis in *Dictyostelium*, knockdown strains were observed at fruiting body stage. The fruiting bodies formed by the transformants were indistinguishable from those formed by the control strain AX2 (Fig. 5.10). Similar to these results, PAT1 knockdown strains also develop normally on non-nutrient agar (Moniakis *et al*., 1999).

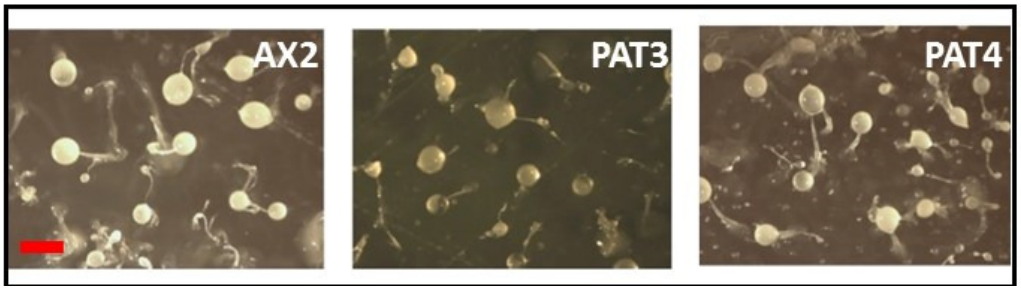

Figure 5.10 PAT3 and PAT4 KD strains are morphologically similar to parental AX2.
Effects of KD of PAT3 and PAT4 on multicellular morphogenesis in *Dictyostelium*. Cells were grown on lawns of *K. aerogenes* at 21°C for ~ 24 h until mature fruiting bodies had formed. Photographs were captured for each strain at the same magnification using an Olympus SZ61 Moticam 2300 camera attached to a dissection microscope from above. AX2, PAT3 KD strain HPF865 and PAT4 KD strain HPF852. Fruiting bodies formed by the transformants were indistinguishable from those formed by AX2. Scale bar = 1mm.

5.2.3.4 PAT3 expression is upregulated in PAT4 knockdown strains

Since the knockdown of either PAT3 or PAT4 did not alter any of the phenotypes analysed, it was possible that the cells deployed a compensatory mechanism in order to cope with loss of PAT3 or PAT4. I hypothesized that the cells upregulate one or more other Ca^{2+}-ATPases to compensate for the loss of a homologue. To investigate this, the level of *pat3* mRNA transcripts was measured in vegetative AX2 and five PAT4 knockdown strains using semiquantitative RT-PCR. Indeed, in four out of the five PAT4 knockdown strains, *pat3* mRNA expression was significantly increased when compared to AX2 (Fig. 5.11). The strain which showed no detectable upregulation of *pat3* mRNA expression (HPF850) also had the smallest level of antisense inhibition of *pat4* expression (Table 5.1). These results support the idea that there is functional redundancy between PAT3 and PAT4, and that reduction in expression of one pump can lead to compensatory overexpression of another homologue. Due to time restraints *pat4* expression was not measured in the PAT3 knockdown strains.

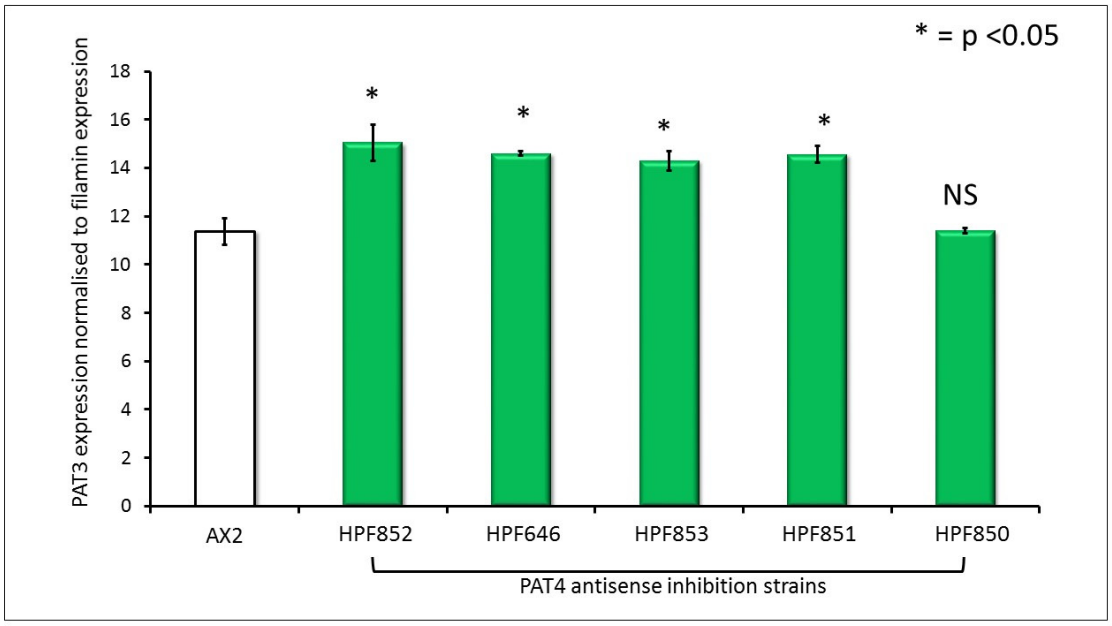

Figure 5.11 *pat3* mRNA expression in *pat4* antisense inhibition strains is increased.

Semiquantitative RT-PCR was used to determine the *pat3* mRNA expression in vegetative AX2 and *pat4* KD strains. *pat3* expression is normalized to filamin expression, error bars are standard errors of the mean. RNA was extracted from vegetative cells in two biological replicates. mRNA expression was significantly increased in four out of 5 transformants compared to AX2. (Significance of differences from AX2 in independent t-tests: (HPF852, p = 0.028; HPF646, p = 0.057; HPF853, p = 0.039; HPF851, p = 0.049; HPF850, p = 0.936).

5.2.3.5 Knockdown of PAT3 and PAT4 has no effect on folic acid calcium response magnitude but cAMP calcium response magnitudes are increased.

To investigate the roles of PAT3 and PAT4 in Ca^{2+} signalling in *Dictyostelium* the $[Ca^{2+}]_{cyt}$ responses to the chemoattractants cAMP and folic acid, were measured in the knockdown strains. These strains also express the Ca^{2+}-sensitive luminescent protein aequorin, to allow real time recordings of cytosolic Ca^{2+} responses. The characteristics of the Ca^{2+} responses in the strains were analysed and compared with responses of the control strain HPF401. Surprisingly, the magnitudes of the Ca^{2+} responses to folic acid were not altered in the PAT3 and PAT4 knockdown strains compared the control HPF401 (Fig. 5.12A). However, the magnitudes of the responses to cAMP were significantly increased in both PAT3 and PAT4 knockdown strains compared to the control, by an average of 22.8% and 25.1% respectively (Fig. 5.12B). Therefore, knocking down a single Ca^{2+} pump affects only the response magnitudes in aggregation competent cells and not vegetative cells.

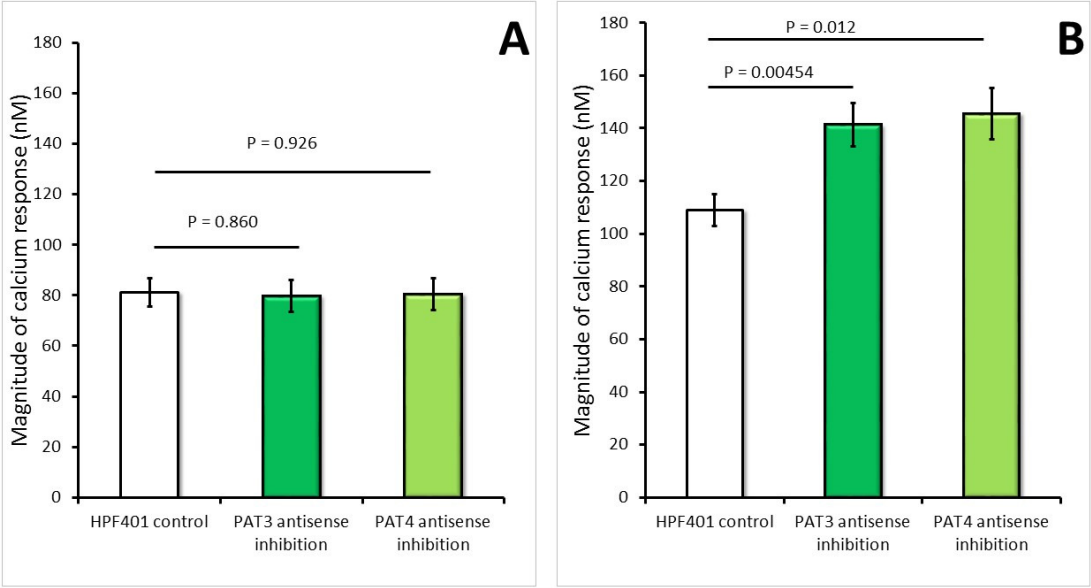

Figure 5.12 Mean calcium response magnitudes in vegetative cells stimulation with folic acid and developed cells stimulated with cAMP.

(A) Folic acid response magnitudes. Ca^{2+} response magnitudes were measured in PAT3 and PAT4 knockdown strains and the control strain HPF401. Vegetative cells were stimulated with 1µM folic acid. knockdown of PAT3 and PAT4 did not significantly alter the magnitude of the response compared to the control strain ($p > 0.05$, One-Way ANOVA, with pairwise comparisons made by the Least Squares Difference method). Errors are standard errors of the mean. Individual antisense inhibition strains were tested in 2-5 independent experiments and all experiments were pooled

to determine the mean. PAT3 five strains (n=19), PAT4 seven strains (n= 27) control HPF401 one strain (n=13). **(B)** cAMP response magnitudes. Ca^{2+} response magnitudes (Ca^{2+} nM) were measured in in PAT3 and PAT4 antisense inhibition strains and control strain HPF401 after stimulation with 1μM cAMP. Cells were developed to 7 hours in MED-DB. Knockdown of both PAT3 and PAT4 increases the response magnitude significantly compared to both control HPF401 and antisense strains. ($p < 0.01$, One-Way ANOVA, with pairwise comparisons made by the Least Squares Difference method). Errors are standard errors of the mean. Individual antisense inhibition strains were tested in 2-4 independent experiments and all experiments were pooled to determine the mean. PAT3 four strains (n= 15), PAT4 seven strains (n=21), control HPF401 one strain (n= 12).

These intriguing results prompted further analysis of the calcium responses. Measurements of basal $[Ca^{2+}]_{cyt}$ can indicate the ability of the cells to regulate cytosolic Ca^{2+} homeostasis and can highlight proteins that are crucial for regulation. Decreasing expression of a Ca^{2+}-ATPase might be expected to impact on the resting cytosolic Ca^{2+} homeostasis. However, the basal $[Ca^{2+}]_{cyt}$ was not significantly altered in PAT3 and PAT4 knockdown strains, either in vegetative or differentiated cells (Fig 5.13A, B). These results suggest that there are compensatory mechanisms, possibly by way of upregulation of alternative Ca^{2+} pumps, as has been indicated by the mRNA expression analysis (Fig 5.11), which are enough to maintain resting Ca^{2+} levels even when PAT3 or PAT4 are knocked down.

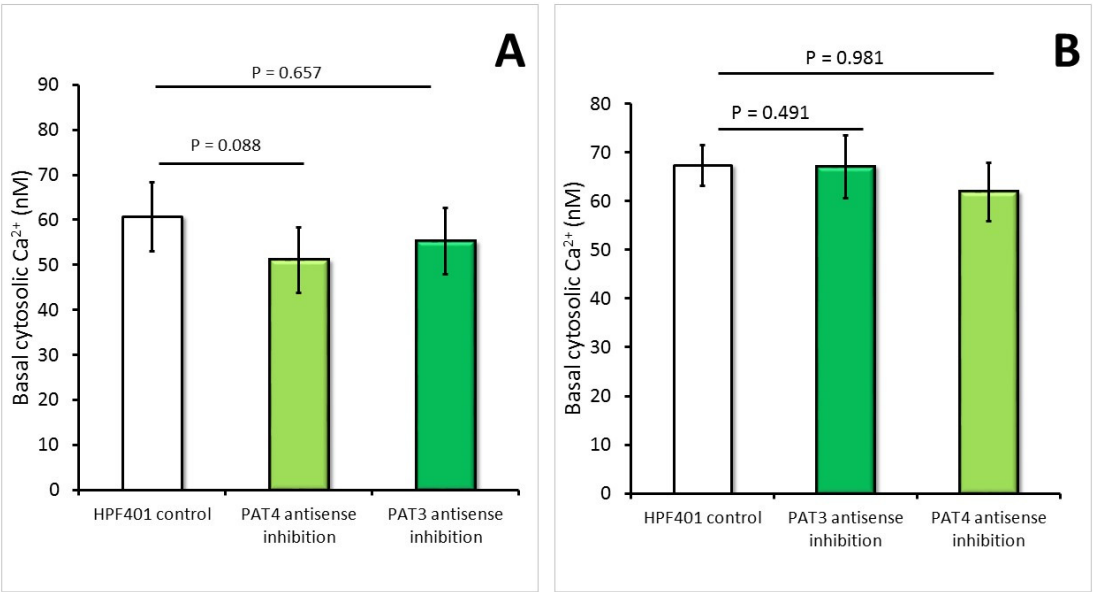

Figure 5.13 Basal cytosolic calcium concentration was not altered significantly in PAT3 and PAT4 knockdown transformants.

(A) Basal $[Ca^{2+}]_{cyt}$ of vegetative cells growing in HL5 medium. There was no significant difference in the basal cytosolic Ca^{2+} levels between the wild type and PAT3 of PAT4 antisense inhibition strains ($p > 0.05$, One-Way ANOVA, with pairwise comparisons made by the Least Squares Difference method). Error bars are standard errors of the mean. PAT3 five strains (n=19), PAT4 seven strains (n= 27) control HPF401 one strain (n=13). **(B)** Basal $[Ca^{2+}]_{cyt}$ of differentiated cells at 7 hours in MES-DB. There was no significant difference in the basal cytosolic Ca^{2+} levels between the wild type and PAT3 of PAT4 antisense inhibition strains ($p > 0.05$, One-Way ANOVA, with pairwise comparisons made by the Least Squares Difference method). Error bars are standard errors of the mean. Sample sizes were: PAT3, four strains x 3 to 4 experiments (n= 15); PAT4, seven strains x 3 experiments (n=21); control HPF401 one strain x 12 experiments (n= 12).

5.2.3.6 Kinetics of the calcium responses

The kinetics of the chemotactic Ca^{2+} responses to cAMP and folic acid in wild type cells have previously been analysed to reveal that rate of Ca^{2+} increase into the cytoplasm is tightly coupled to the rate of Ca^{2+} extrusion from the cytoplasm, ie. a more rapid Ca^{2+} increases in the rising phase of the response are tightly coupled with more rapid decreases in the falling phase of the response (Wilczynska *et al*., 2005). Therefore, the response kinetics for PAT3 and PAT4 knockdown strains were analysed. The rates of Ca^{2+} influx and efflux from the cytoplasm at all stages in the responses were calculated from the Ca^{2+}

concentrations at successive time points and the maximum rates of Ca^{2+} increase and decrease then determined graphically using features of the R statistics and graphics package and the maximum rise and fall rates for the PAT3 and PAT4 knockdown and control responses were plotted.

Analysis of the kinetics of the folic acid responses revealed a statistically significant regression coefficient between the maximum rise and fall rates for all three sets of strains, however the slopes of both PAT3 and PAT4 lines are steeper than the controls, and PAT3 is steeper than PAT4 (Fig 5.14A). This means that for a given rate of increase in the rising phase, the rate of calcium decrease in the falling phase is greater in the PAT4 knockdown strains than control and greater again in the PAT3 knockdown strains. For the cAMP responses the maximum rise and fall rates for control and PAT3 knockdown strains were significantly correlated. Knocking down PAT3 did not change the relationship between rate of increase and decrease. On the other hand, in the PAT4 knockdown strains the slope and intercept significantly differed from that of the control and PAT3 knockdown strains, which flattened the line significantly, so the rate of decrease was less sensitively controlled by the rate of increase (Fig 5.14B). This implies that PAT4 contributes more to the coupling between the rates of increase and decrease in aggregation-competent cells.

So why would knocking down a Ca^{2+} pump increase the rate of Ca^{2+} clearance? The answer may lie in the fact that all the pumps may not respond equally well to calcium levels. For example, if PAT4 is more sensitively activated by calcium than PAT3 (or one or more other pumps), then calcium pumping by the other pumps that take over its function when it is knocked down, would be less responsive to the calcium increases which occur in the rising phase. Thus, the slope of the line is a measure of the collective sensitivity of the pumps to cytosolic calcium and removing or reducing the contribution of less sensitive pumps would increase the overall calcium-responsiveness of the remaining pumps.

This would not necessarily affect the total pumping capacity if the remaining pumps are sufficient to remove the accumulated Ca^{2+} in the cytosol efficiently. To test this, I used the area under the curve of the falling phase of the response as a measure of the net pumping capacity in each of the strain sets and indeed this was not significantly different between strain sets for both folic acid and cAMP responses. Although the knockdown strains

exhibited a slight decrease in the net pumping capacity during the falling phase of the folate responses and a slight increase during the cAMP responses, these did not reach statistical significance (Fig 5.15A,B). This is consistent with homeostatic regulation of the total cellular Ca^{2+} pumping capacity, direct evidence for which was found in the mRNA expression analysis (section 5.2.3.4).

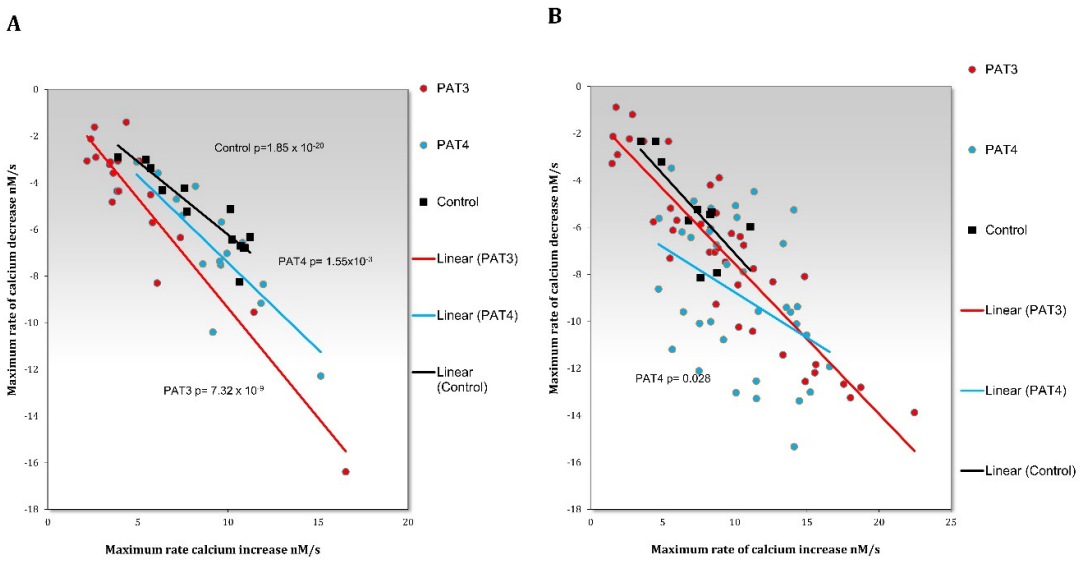

Figure 5.14 Kinetics of chemotactic Ca^{2+} responses.

(A) Folic acid responses, relationship between maximum rise and fall rates in control (black squares), PAT3 knockdown (red dots) and PAT4 knockdown (blue dots). Each point represents an individual experiment. Rise and fall rates at all stages in the responses were calculated from the Ca^{2+} concentrations at successive time points and the maximum rates of Ca^{2+} increase and decrease then determined graphically using features of the R statistics and graphics package. Consistent with previously published work, the slope for the control was significantly less than 0, indicating a coupling between the rates of Ca^{2+} increase in the rising phase and decrease in the falling phase of the response. The slopes of both PAT3 and PAT4 lines are steeper than the controls, and the slope for PAT3 knockdowns is steeper than for PAT4. This means that after knocking down expression of either PAT3 or PAT4, the overall Ca^{2+} responsiveness of the remaining pumps was increased and suggests the presence of other pumps that are more Ca^{2+}-responsive than PAT3 or PAT4. It also suggests that the contribution of PAT4 to the overall Ca^{2+}-responsiveness of the pumps is greater than that of PAT3, because the Ca^{2+}-responsiveness of remaining pumps was greater in PAT3 knockdown strains than in PAT4 knockdown strains. Multiple regression analysis details are provided in Appendix 6 (p values as indicated). (**B)** cAMP responses. Negative relationship between maximum rise and fall rates in control HPF401 (black

squares) and PAT3 antisense strains (red dots) and PAT4 antisense strains (blue dots). The overall regression was significant, p= 2.79 x 10^{-20} and multiple regression analysis showed that the slope and intercept for the PAT4 knockdown line was significantly different from the lines of the control and PAT3 (intercept p= 0.00192, slope p= 0.0279) (Appendix 6). This means that knocking down PAT4 (but not PAT3) significantly reduced the overall Ca^{2+} responsiveness of the pumps and, as was the case for the folate responses, PAT4 makes a greater contribution than PAT3 to the overall Ca^{2+} responsiveness.

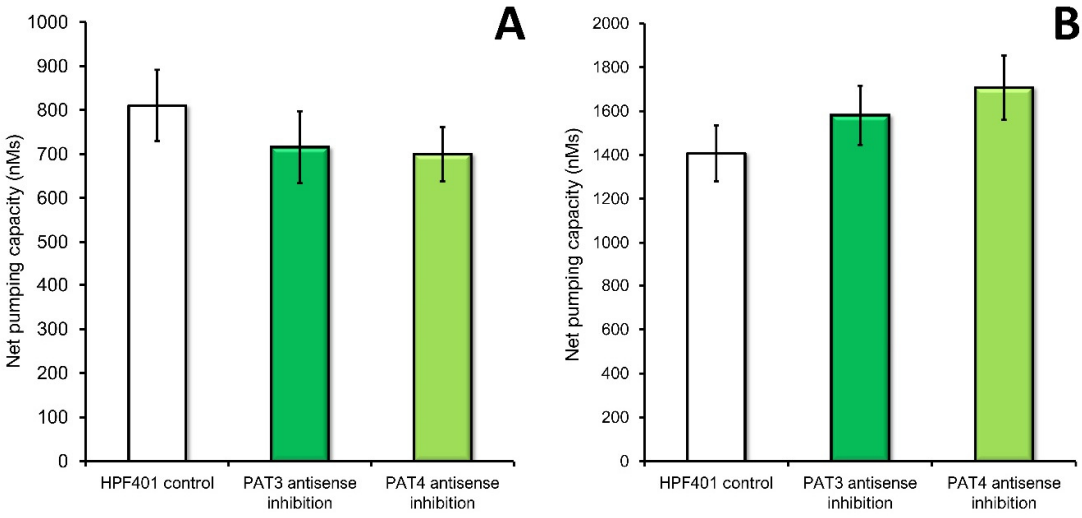

Figure 5.15 Estimated net calcium pumping capacity in control, PAT3 and PAT4 strains.
(A) The pumping capacity was not significantly different for folic acid responses. (ANOVA, p>0.05, error bars are standard errors of the means, control n=12, PAT3 n=19, PAT4 n=27). **(B)** The pumping capacity was slightly increased however not significantly different for cAMP responses (ANOVA, p>0.05, error bars are standard errors of the means, control n=12, PAT3 n=15, PAT4 n=21). Net calcium pumping capacity was estimated using the area under the falling phase of the Ca^{2+} response curve, approximated as net pumping capacity = (peak amplitude) x (time from peak to finish) / 2.

The timing of chemotactic Ca^{2+} responses is known to depend (partly) on the response magnitude itself. This has been attributed to Ca^{2+}-dependent autoregulation of Ca^{2+}

responses – larger responses imply more channels opening for longer times, thereby producing an earlier, more rapid influx, and the local Ca^{2+} concentrations more rapidly reach levels sufficient to inhibit and close the channels, as well as activate the pumps. In this way the response onset time is coupled to the magnitude of the calcium response (Wilczynska *et al*., 2005).

In the case of the folate responses, the mean response onset times, peak times and response duration were not different in the knockdown strains compared to the controls (Fig 5.16A and Fig 5.17A and Fig 5.18A), and the relationship between the onset time and response magnitude is maintained in all strain sets (Fig 5.19A). This is consistent with the response magnitudes not being altered as shown in Fig 5.12A. This means that for the folic acid responses the functional relationship between $[Ca^{2+}]_{cyt}$ and the time of onset is the same in all strains. Thus, the mechanism of the folic acid response is unchanged, and the only thing that is affected in the folic acid responses is a change in the kinetics of the response influx and efflux in the PAT4 knockdown cells.

Initial analysis of the cAMP responses in my strains revealed that the mean response onset times were later in both PAT3 and PAT4 knockdown strains compared to controls (Fig 5.16B). This was surprising considering that the response magnitudes were increased in the PAT3 and PAT4 knockdown strains compared to the control (Fig 5.12B). Thus, for the cAMP responses, knocking down the pumps caused larger responses that started later, but also trended toward having an overall shorter duration, although this did not reach statistical significance (Fig 5.17B) and the time of the peak of the response was also not different in the mutants compared to the controls (Figure 5.18B). Analysis of the relationship between the response magnitude and onset time for these cAMP responses revealed that the coupling is retained in the responses from the control cells as expected, but it is lost in the PAT3 and PAT4 knockdown strains (Fig 5.19B). Thus, multiple regression analysis showed that the slope for the control was negative and significantly different from 0 ($p = 9.60 \times 10^{-4}$), but this was not the case for both PAT3 and PAT4 knockdown responses (Appendix 6), indicating that the coupling between the two parameters was lost. When both pumps are present at normal levels (wild type situation), the onset time for cAMP responses is shorter and the magnitude of the response for any given onset time is smaller than in the pump knockdown mutants. However, this coupling between the

onset time and the response magnitude in the cAMP responses is dependent on the presence of both the PAT3 and PAT4 pumps at normal levels in the wild type. I conclude that both pumps contribute to coupling the cAMP response onset time with its magnitude and that decreased expression of either pump is sufficient to reduce this coupling, so that it became statistically undetectable in my experiments. It is not immediately clear why PAT3 and PAT4 should be needed for the coupling between response onset time and magnitude in the case of Ca^{2+} responses to cAMP but not folate. However, my results indicate that PAT3 and PAT4 contribute to the control of calcium responses in subtly different ways in vegetative and differentiated cells.

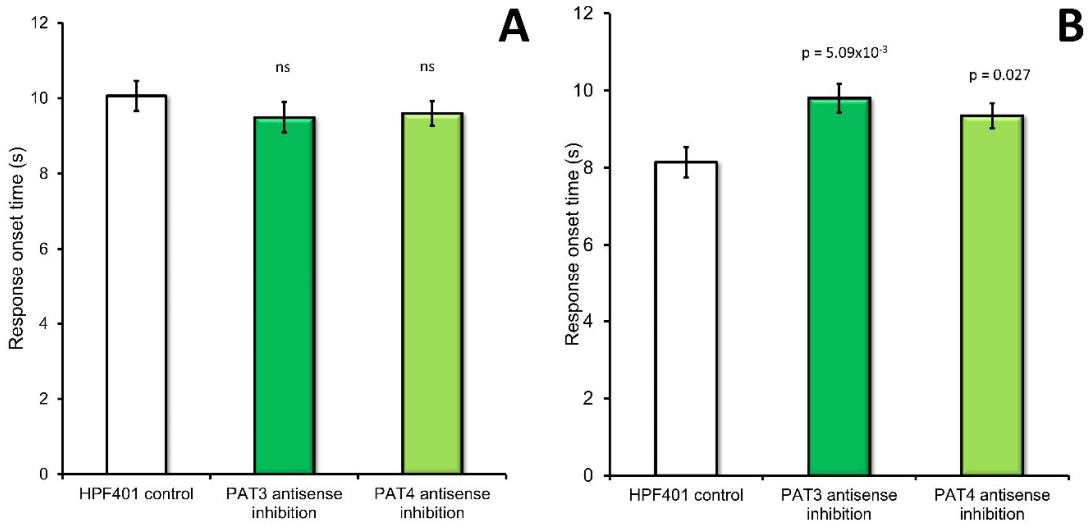

Figure 5.16 Onset times of PAT3 and PAT4 knockdown strains calcium responses.
(A) Response onset times for folic acid responses. The onset time was measured as the time taken for the response to begin after injection of the stimulus. The means were calculated for each strain set and plotted. The onset times for PAT3 and PAT4 were not significantly different from those of the control, ($p > 0.05$, One-Way ANOVA, with pairwise comparisons made by the Least Squares Difference method) (HPF401 control n=12, PAT3 knockdown n=18, PAT4 knockdown n=27), errors are standard errors. **(B)** Response onset times for cAMP responses. The means were calculated for each strain set and plotted. The onset times for PAT3 and PAT4 were significantly longer than those of the control, p values indicated (pairwise comparison between HPF401 and mutant, independent t-test) (HPF401 control n=12, PAT3 knockdown n=15, PAT4 knockdown n=21) errors are standard errors.

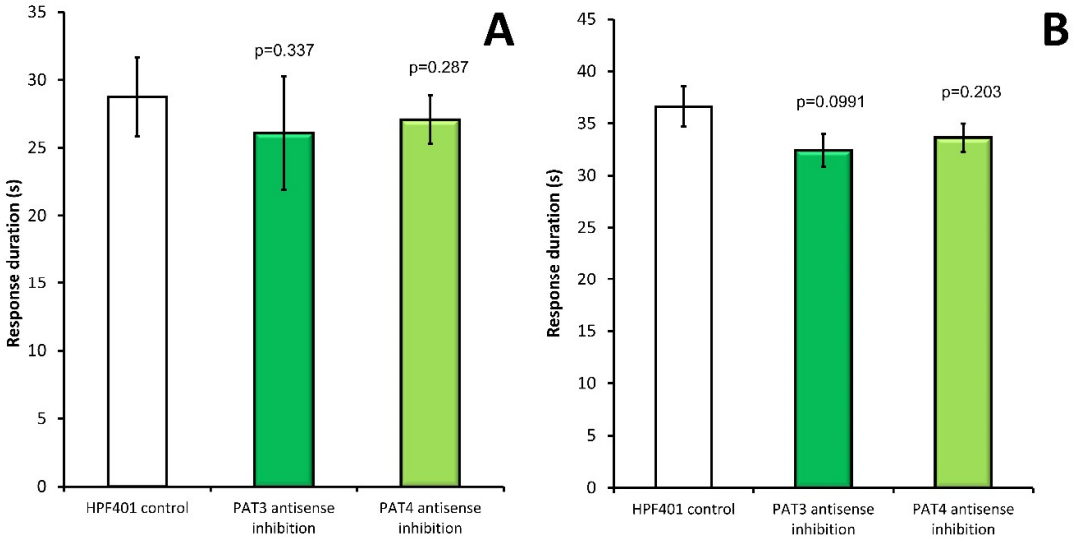

Figure 5.17 Calcium response durations for PAT3 and PAT4 knockdown strains.

(A) Response duration for folic acid responses. The duration was measured from the time of injection of the stimulus until the time the calcium levels returned to basal. The means were calculated for each strain set and plotted. The means were calculated for each strain set and plotted. The response durations for PAT3 and PAT4 were not significantly different from those of the control (Independent t-test between mutant and control) (HPF401 control n=12, PAT3 knockdown n=19, PAT4 knockdown n=27), errors are standard errors. **(B)** Durations of cAMP responses. The response durations for PAT3 and PAT4 knockdown strains were slightly shorter than those of the control, although did not reach statistical significance, p values indicated (Independent t-test between mutant and control) (HPF401 control n=12, PAT3 knockdown n=14, PAT4 knockdown n=21) errors are standard errors.

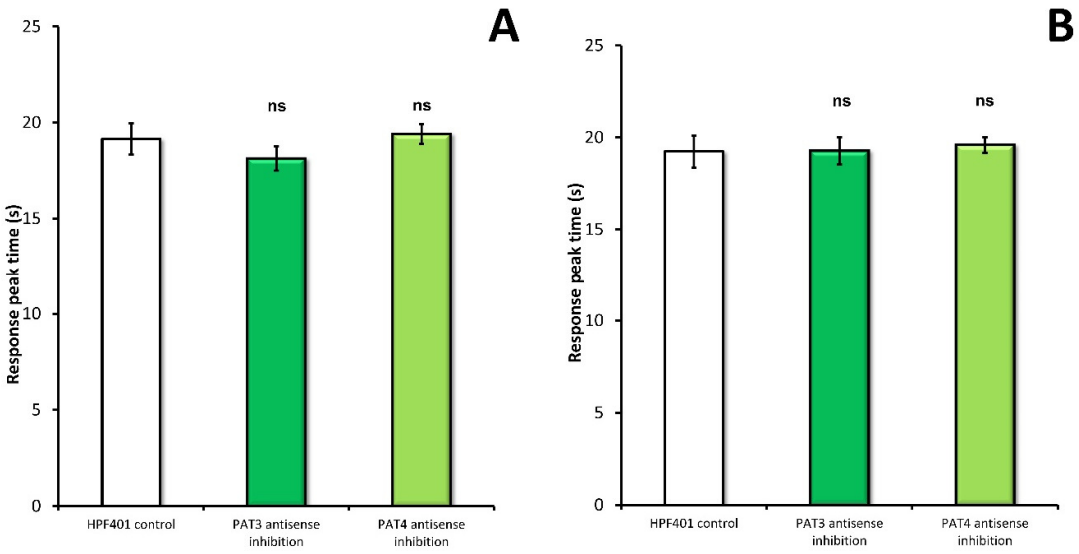

Figure 5.18 Calcium response peak times for PAT3 and PAT4 knockdown strains.

(A) Time of the peak for folic acid responses. The peak time was measured from the time of injection of the stimulus until the time the calcium levels reached a maximum The means were calculated for each strain set and plotted. The response peaks for PAT3 and PAT4 were not significantly different from those of the control ($p > 0.05$, One-Way ANOVA, with pairwise comparisons made by the Least Squares Difference method) (HPF401 control n=12, PAT3 knockdown n=18, PAT4 knockdown n=27), errors are standard errors. **(B)** Time of peak for cAMP responses. The means were calculated for each strain set and plotted. The response peaks for PAT3 and PAT4 were not significantly different from those of the control ($p > 0.05$, One-Way ANOVA, with pairwise comparisons made by the Least Squares Difference method) (HPF401 control n=12, PAT3 knockdown n=15, PAT4 knockdown n=21) errors are standard errors.

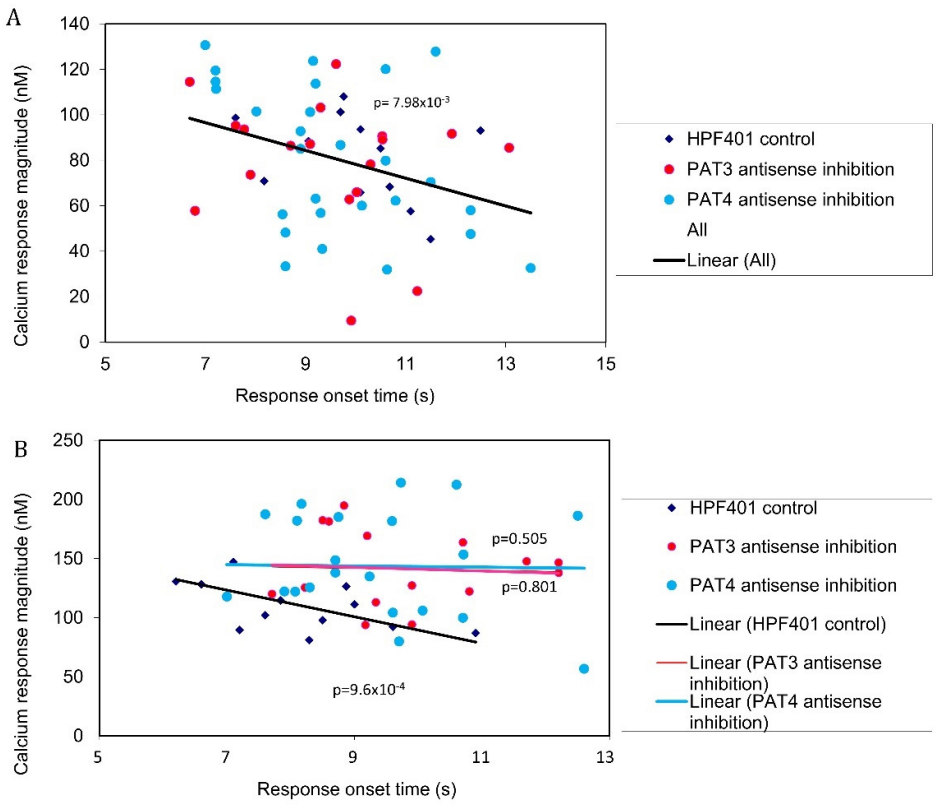

Figure 5.19 Relationship between response magnitude onset time in PAT3 and PAT4 knockdown strains.

(A) Folic acid responses, relationship between the magnitude of the calcium response and the response onset time, each point represents a single experiment. The regression is negative and significant ($p= 7.98x10^{-3}$, F test) and multiple regression analysis showed that the intercepts and slopes were the same for the 3 strain sets (Appendix 6) therefore the line was fitted to all points (HPF401, n=10, PAT3 knockdown, n=18, PAT4 knockdown n=27). **(B)** Relationship between the magnitude of the cAMP calcium response and the response onset time, each point represents a single experiment. Multiple regression analysis (Appendix 6) showed that the slope for the control strain HPF401 was negative and significantly different from 0 ($p=9.6x10^{-4}$). The intercepts for PAT3 and PAT4 knockdown strains did not significantly differ from the control ($p>0.05$), therefore PAT3 and PAT4 slopes were not significant, p values indicated, F test (HPF401 n = 12; PAT3 n= 16; PAT4 n=20).

5.3 Discussion

Tight spatiotemporal control of Ca^{2+} signals and resting Ca^{2+} levels is crucial to proper cell biological function. Sequestration of Ca^{2+} from the cytosol after release via PM and intracellular Ca^{2+} channels is essential to restrict and terminate Ca^{2+} signals, restore low resting cytosolic levels and refill intracellular stores. The proteins responsible must transport Ca^{2+} across cellular membranes against the electrochemical gradient. These include: a) the cation/Ca^{2+} exchangers (including H^+/Ca^{2+} (CAX) exchangers and Na^+/Ca^{2+} (NCX) exchangers) which utilize the downhill gradients of other cations (H^+, Na^+ or K^+) to energize transport of cytosolic Ca^{2+} across membranes (Cai & Lytton, 2004; Giladi *et al*., 2016) b) the mitochondrial uniporter which is a high capacity Ca^{2+}-uptake transporter of the inner mitochondrial membrane (Gunter & Gunter 1994; Bernardi 1999; De Stefani *et al*., 2011) and c) the Ca^{2+}-ATPases PMCA, SERCA and SPCA.

Ca^{2+}-ATPases are cation translocases which maintain basal Ca^{2+} levels and terminate Ca^{2+} signals by sequestering Ca^{2+} out of the cytosol after influx events. These enzymatic pumps couple the energy provided by ATP hydrolysis to power uphill transport of cations across the membrane. PMCAs expressed in low levels at the PM, reported to comprise <0.1% of the total proteins in the PM (Vanagas, 2007), are generally associated with maintenance of the low resting cytosolic Ca^{2+} levels and fine tuning of Ca^{2+} signals. SERCA pumps are integral SR/ER membrane enzymes and are solely responsible for transfer of Ca^{2+} into the ER/SR lumen to refill stores and shape Ca^{2+} signals (Stammers *et al*., 2015). During a global Ca^{2+} wave, SERCAs are integral to shaping the response by tempering ~70% of the cytosolic Ca^{2+}, while PMCAs deal with only ~1%, the remainder being sequestered by the PM NCX (~28%) and mitochondrial uniporter (~1%) (Bers, 2000). In *Dictyostelium*, as with all cells, Ca^{2+} signalling is involved in many biological processes, however little is known about the Ca^{2+}-ATPases that function to maintain resting Ca^{2+} levels and regulate Ca^{2+} signals. The *Dictyostelium* genome encodes three P-type Ca^{2+}-ATPases–- PAT1, which localises to the membrane of the contractile vacuole (Moniakis *et al*., 1995; Moniakis *et al*., 1999) and two predicted homologues of PMCA/SERCA, PAT3 (DDB_G0284605) and PAT4 (DDB_G0289473). The role for PAT1 in the CV is likely to both maintain cytosolic Ca^{2+} concentrations and also facilitate Ca^{2+} signalling events related to CV functioning such as osmoregulation. Evidence also suggests that PAT1 also helps to maintain cellular Ca^{2+}

levels during Ca^{2+} stress, particularly in vegetative cells (Moniakis *et al*., 1995; Moniakis *et al*., 1999). PAT3 and PAT4 however have not previously been experimentally investigated, so this chapter has explored how PAT3 and PAT4 are involved in Ca^{2+} homeostasis, chemotactic Ca^{2+} signaling, growth and development in *Dictyostelium*.

To analyze the function of PAT3 and PAT4 experimental models were created by knockdown of expression of both pumps using asRNA expression. A collection of strains expressing decreased levels of the proteins were then phenotypically characterized. Of interest was to study the function of PAT3 and PAT4 in Ca^{2+} homeostasis and chemotactic signalling. This was achieved by expressing the Ca^{2+} sensitive luminescent protein, apoaequorin, in the PAT3 and PAT4 knockdown transformants. Analysis of resting Ca^{2+} levels and chemotactic Ca^{2+} signals was accomplished by recording real-time cytosolic Ca^{2+} transients in these transformants during their chemotactic response to the cAMP and folic acid. It was hypothesized that reducing the expression of a Ca^{2+}-ATPase might affect resting Ca^{2+} levels and signaling by inhibiting sequestration. This would potentially increase basal cytosolic concentrations and the magnitude and duration of Ca^{2+} responses by reducing the cellular capacity to terminate the responses. Biochemical studies have shown that treating cells with inhibitors that block intracellular Ca^{2+} accumulation, such as the SERCA pump blocker thapsigargin, can result passive release of Ca^{2+} from the ER which enhances Ca^{2+}-activated cytosolic Ca^{2+} entry (Putney, 2003). Accordingly, the particular subcellular localization of the pumps might have different consequences, as loss of an ER pump might impact the cell differently than loss of a plasma membrane pump.

5.3.1 Folic acid calcium responses in vegetative cells

Because *Dictyostelium* exhibits different life stages, I analysed the calcium signals in cells that were in the vegetative state and also at the state of aggregation competence–- 6-7 hours post starvation. In vegetative cells, surprisingly, knockdown of either PAT3 or PAT4 did not affect the resting Ca^{2+} levels in the cytosol, and also did not affect the magnitude of the Ca^{2+} responses to folic acid. The known relationship between the response onset time and response magnitude (Wilczynska *et al*., 2005) was maintained in vegetative PAT3 and PAT4 knockdown strains, consistent with the response magnitudes not being altered. Therefore, the mechanism of the response was unchanged in the mutants, however the kinetics of the calcium influx and efflux during the responses were altered. The

relationship between the maximum rise and fall rates for the PAT3 and PAT4 knockdown strains were steeper than the controls, and PAT3 was steeper than PAT4. This means that for a given rate of increase in the rising phase, the rate of calcium decrease in the falling phase was greater in the PAT4 knockdown strains than in control cells and greater again in the PAT3 knockdown strains. These results could reflect different calcium sensitivities of the various pumps potentially due to differing calcium binding affinities. In mammals, different calcium affinities of the various PMCA splice variants have been reported (Corradi *et al*., 2021). This could mean that in *Dictyostelium* the pumps do not respond equally well to calcium levels, thus it is possible that PAT3 is less sensitively activated by calcium than PAT4, or the other pumps. My results suggest that if PAT3 is knocked down, and because of compensatory upregulation of the other pumps, the net calcium pumping would be achieved by pumps that are more responsive to the calcium increases. This would enhance the rate of calcium efflux in the falling phase because removing or reducing the contribution of less Ca^{2+}-sensitive pumps, and possibly upregulating pumps that are more Ca^{2+}-sensitive, makes the overall calcium-responsiveness of the pumps greater. Indeed, the net pumping capacity in each of the strain sets was similar to controls which means that despite the knockdown, the total net calcium pumping capacity remains unchanged. This provides further evidence that the knockdown of one pump is compensated for by upregulation of others and my results suggest the other pumps eg. PAT1 are more calcium-responsive than PAT3 or PAT4, but especially PAT3.

5.3.2 cAMP responses in aggregation competent cells

It was intriguing to find that the magnitudes of the cAMP-elicited calcium responses in aggregation-competent cells of PAT3 and PAT4 knockdown strains were larger than the controls. The cAMP responses in the PAT3 and PAT4 knockdown strains were on average increased by 22.8% and 25.1% respectively compared to the control. The cAMP responses were also delayed compared to the control, thus the coupling between the response onset time and response magnitude in PAT3 and PAT4 knockdown strains was lost. Normally larger responses would have an earlier onset time (Wilczynska *et al*., 2005). The overall duration of the cAMP responses were trending toward being slightly shorter, although this did not reach statistical significance. It is possible that the total calcium entering and leaving the cytoplasm is unchanged, because although the peak concentration reached is higher (larger response magnitude), the overall response is

shorter as it starts later. The most obvious explanation of larger responses when specific Ca^{2+} pumps are knocked down is that those pumps contribute to Ca^{2+} efflux from the cytoplasm during the response. However, this should also cause the responses to peak and to terminate more slowly. This was not the case. In fact, the responses in the knockdown strains peaked at the same time as controls and were, if anything, slightly shorter (although this did not reach statistical significance). Alternatively, although net pumping capacity the PAT3 and PAT4 knockdown differentiated cells was not significantly different from the wild type, there was a trend toward a slight increase in net pumping. If this slight increase is enough to disrupt the overall pumping ability of the cells this may lead to over filling of the calcium stores such as the ER or contractile vacuole. Therefore, there would be a greater store of calcium to release upon cAMP stimulation which could result in larger response magnitudes. This was not seen in the folic acid responses because the net pumping capacity in vegetative cells was slightly lower than wild type, although also not significantly so. My hypothesis is outlined in Figure 5.20 A,B.

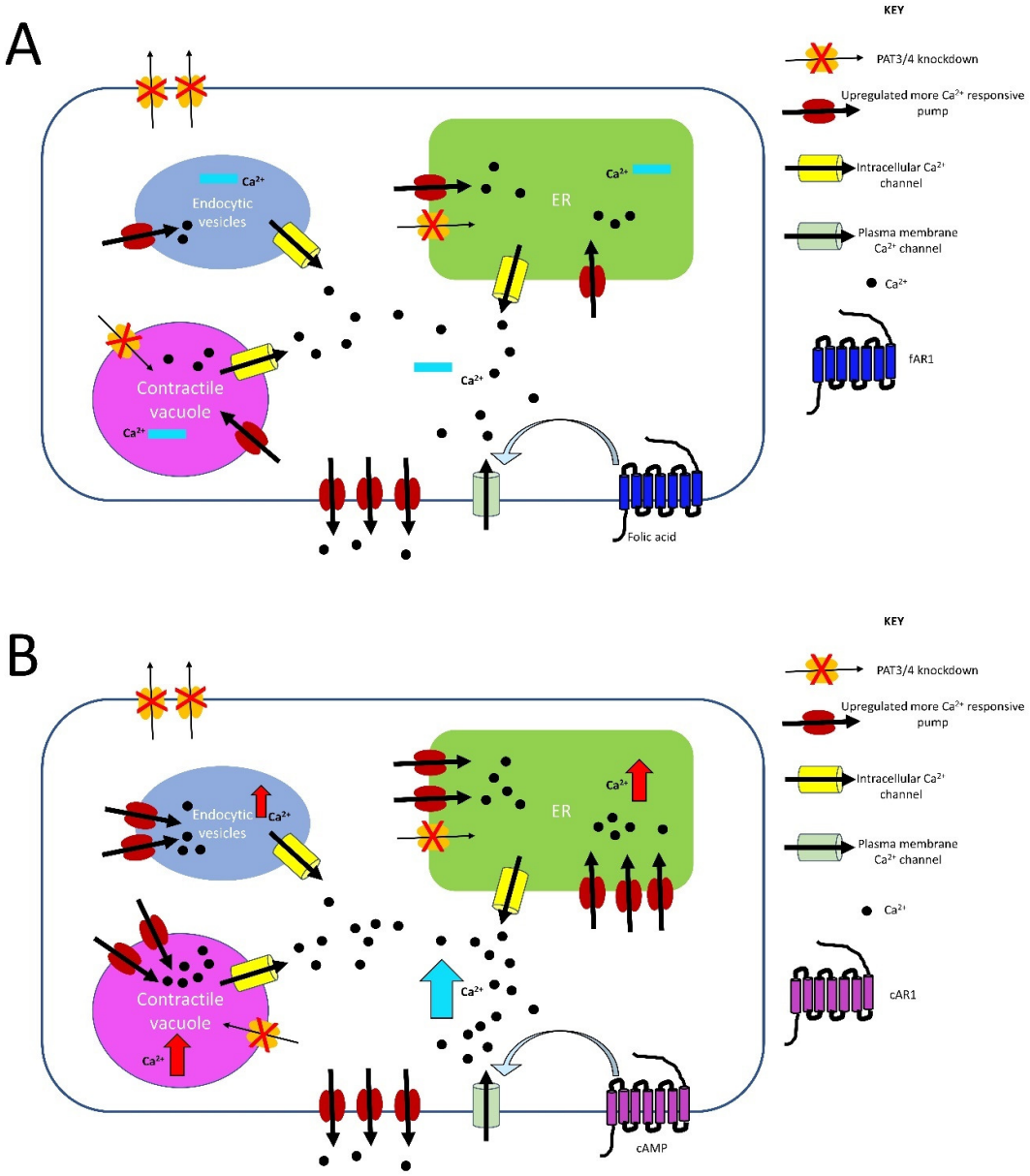

Figure 5.20 Hypothetical model of calcium signals in PAT4 and PAT4 knockdown cells.

(A) Vegetative cells. When PAT3 or PAT4 is knocked down (orange pump with red cross) other more calcium responsive pumps (red pump with thicker arrow) are up regulated by compensatory mechanisms, however the total cellular pumping capacity is balanced so that there is no disruption in basal Ca^{2+} levels (blue bar). When the cell is stimulated with folic acid, fAR1 is activated and signals to plasma membrane Ca^{2+} channels (light green) and Ca^{2+} enters the cell across the plasma membrane, Ca^{2+} is then is released from the internal Ca^{2+} stores through calcium channels (yellow). Because the calcium levels are balanced, the folic acid responses are at the same level as wild type cells (blue bar). Consequently, there were no altered phenotypes in vegetative cells.

(B) Developed cells (7hrs). When PAT3 or PAT4 is knocked down (orange pump with red cross) other more calcium responsive pumps (red pump with thicker arrow) are up regulated by

compensatory mechanisms. In this case the compensation overshoots and the total pumping capacity of the cell is greater than the wild type cell, and could result in increased calcium in the internal stores (red arrows). When the cell is stimulated with cAMP, cAR1 is activated and signals to plasma membrane Ca^{2+} channels (light green) and Ca^{2+} enters the cell across the plasma membrane, Ca^{2+} is then is released from the internal Ca^{2+} stores through calcium channels (yellow). Because there is more Ca^{2+} in the internal stores, the cytosolic calcium response to cAMP is enhanced (Blue arrow). Note that PAT3/4 pumps are pictured in each of the potential subcellular locations, as their actual location is unknown.

My data shows that the coupling between the onset time and the response magnitude in the cAMP responses is dependent on the presence of the pumps in the wild type and thus PAT3 and PAT4 contribute to shaping the cAMP-elicited calcium responses. The mechanism must be different in vegetative cells, because this functional relationship between the onset time and response magnitude was retained unchanged in folate-elicited responses in PAT3 and PAT4 knockdown cells.

In the cAMP response kinetics, knocking down PAT3 did not change the relationship between the Ca^{2+} rise and fall rates. On the other hand, in the PAT4 knockdown strains the rate of decrease in the falling phase of the response was less sensitively coupled to the rate of increase in the rising phase. This implies that PAT4 contributes more than PAT3 to the coupling between the rates of increase and decrease, possibly by being more responsive to cytosolic Ca^{2+} as has been previously discussed. This difference between PAT3 and PAT4 knockdowns was also present in the folic acid responses in which the PAT4 knockdowns exhibited a shallower relationship between the rates of Ca^{2+} increase and decrease than did the PAT3 knockdowns. The fact that knockdown of PAT3 and PAT4 affected the kinetics of the cAMP responses differently to the folic acid responses, may reflect different activities and/or subcellular locations of the calcium pumps at the different *Dictyostelium* life stages, as well the differences in the signalling pathways in vegetative and differentiated cells that connect the chemotactic receptors to the pumps and channels that influence the responses (Nebl *et al*., 2002) (Discussed in section 1.2.3.1).

Furthermore, since PAT3 and PAT4 display different sensitivities to calcium, this may reflect that the pumps are of different types. I do not know if these pumps are located in the plasma membrane (PMCA) or in internal calcium stores such as the ER (SERCA) or others. In other cell types PMCAs and SERCAs are activated by different mechanisms and display different kinetic properties. For example, PMCAs are the only calcium pumps directly activated by Ca^{2+}-calmodulin (amongst other activators) and the different isoforms have different affinities for calmodulin. Calmodulin itself displays different sensitivities to calcium due to subtle differences in the structures of the C- and N-lobes which contain the EF-hand calcium binding motifs (Boczek *et al*., 2021), which adds an extra level of calcium-sensitivity to PMCA activation. SERCAs on the other hand are regulated by a collection of regulatory subunits (Xu and Van Remmen, 2021) and binding of two Ca^{2+} ions at specific calcium binding sites are necessary for pump activation (Espinoza-Fonseca and Thomas, 2011). The various SERCA isoforms have different calcium sensitivities in relation to both calcium binding and calcium transport velocity. This means that the pumps can perform appropriately to address different calcium transport needs when expressed in different tissues and cell types (Boczek *et al*., 2021). In *Dictyostelium*, PAT3 and PAT4 may or may not be located at different subcellular locations, but they do possess obvious differences in calcium responsiveness compared to each other and whether expressed in either vegetative or developed cells, likely related to the reasons mentioned above. It is interesting to note that both PAT3 and PAT4 are predicted to encode calmodulin-binding helical peptide IQ motifs, as does PAT1 (Wilczynska *et al*., 2005) so may be calmodulin regulated like PMCAs. Localisation studies to determine the subcellular location of the pumps would be of interest in future studies.

5.3.3 Phenotypic characterization

I have shown that in vegetative cells the chemotactic calcium signalling in PAT3 and PAT4 knockdown cells is mechanistically the same as wild type cells, differing only in the response kinetics probably because of different calcium sensitivities of the pumps. Accordingly, the ability of the cells to maintain appropriate calcium levels means that I observed no phenotypic defects in the growth rates of transformants, both axenically and on *E. coli* lawns or in nutrient uptake via macropinocytosis and phagocytosis. Similar findings have been reported in *patA* antisense-inhibition transformants. Moniakis *et al*.

(1999) reported that PAT1 knockdown transformants grew the same as wild type in MES/HL5 medium, and on lawns of *E. coli*, however endocytosis rates were not measured. A simple and probable explanation is that the cells compensate for the loss of one pump by upregulation of other Ca^{2+}- ATPases. Such compensatory responses have been reported in mouse models. Mice with deletion of the *Atp2a2* gene, which encodes a cardiac specific SERCA2a isoform, retained normal cardiac function and exhibited a 45 % increase in PMCA1 expression (Andersson *et al*., 2009). Similarly, the heterozygous knock-out of *Atp2a2* in mice did not induce cardiac disease, and only had a mild impact on cardiac contractility and relaxation, again presumably due to compensation by an alternative SERCA (Periasamy *et al*., 1999; Ji *et al*., 2000). I also found that in four out of the five PAT4 knockdown strains, PAT3 mRNA expression was significantly increased when compared to AX2, further supporting the idea that there is functional redundancy between PAT3 and PAT4 that is combined with homeostatic regulation of total pump expression levels.

As knockdown of PAT3 and PAT4 did not affect any of the phenotypes tested in vegetative cells, it was important to assess the roles of the pumps during development. PAT1 antisense inhibition strains reportedly developed normally when plated on water agar (Moniakis *et al*., 1999). Similarly, I saw no obvious morphological defects in the PAT3 and PAT4 knockdown transformants as the fruiting bodies were indistinguishable from wild type. PAT1 knockdown strains also develop normally in 60 mM $CaCl_2$, whereas vegetative growth is inhibited under these conditions, suggesting that the sensitivity of PAT1-deficient cells to high $CaCl_2$ is greater during vegetative growth than during differentiation. This implies a more prominent role for PAT1 in regulating Ca^{2+} homeostasis in vegetative cells than in differentiating cells (Moniakis *et al*., 1999), a notion supported by the RNA-Seq data which shows *patA* mRNA expression decreased over the first 4 hours of development. This might suggest that the roles of PAT3 and PAT4 differ in vegetative and differentiated cells. Increases in expression of PAT3 and PAT4 after starvation suggests that they are important for Ca^{2+} signalling over the developmental cycle, *pat3* mRNA expression increased for the first 8 hours during differentiation to aggregation competence. My qRT-PCR experiments suggested similar conclusions for PAT4 while the published RNASeq results suggested that this increase in expression continued potentially up to the later stages of streaming and early stages in formation of

tipped aggregates. The subsequent drop in expression of all three pumps implies that the proteins become less important during the later multicellular stages and culmination. The lower expression at these later stages could be partly a result of cell type-specific expression, since Schaap *et al.* (1996) showed that prolonged elevation of resting cytosolic Ca^{2+} levels mediates stalk cell differentiation and Cubitt *et al*. (1995) showed that cytosolic Ca^{2+} levels are higher in anterior (prestalk) cells in the multicellular migratory (slug) stage of development.

5.3.4 Concluding remarks

The results here have shown that reducing expression of a single calcium pump does not greatly impact the phenotypes assessed. In vegetative cells mechanistically the folic acid calcium responses are the same in the knockdown cells as wild type, only differing in the kinetics of the PAT4 knockdown responses possibly due to the calcium responsiveness of the pump. On the other hand, the kinetics and mechanism of the cAMP responses were altered in the pump knockdown cells, which suggests that PAT3 and PAT4 contribute more to shaping cAMP cytosolic Ca^{2+} responses, than folic acid responses, thus have a more prominent role during development. This is also reflected in the expression pattern of the pumps which increase over development. I have provided evidence that PAT3 and PAT4 may be less calcium responsive than other calcium pumps- ie. PAT1. The results presented here support the hypothesis that the Ca^{2+} signalling system is homeostatically regulated at the transcriptional level to control the resting Ca^{2+} levels and Ca^{2+} response magnitudes. The cells are able to compensate for loss of expression of a single pump by upregulation of alternative calcium pumps so that the basal cytosolic calcium levels and total pumping capacity during the calcium response is maintained at wild type levels. While knocking down expression of PAT3 and PAT4 in *Dictyostelium* had no effect on growth and endocytosis rates or development, my results cannot exclude the involvement of the pumps in these processes. To more thoroughly investigate the biological function of these pumps, strains with all three homologues knocked down would be beneficial. The work in this chapter has highlighted the dynamic nature of the Ca^{2+} signaling machinery in *Dictyostelium* and the extraordinary capability of the cells to regulate protein expression in such a manner as to maintain normal cell biological function.

Chapter six

Overall conclusions

Calcium regulates many processes in the *Dictyostelium* lifecycle, and intracellular calcium levels must be tightly controlled to ensure proper biological function. *Dictyostelium* encodes a collection of calcium channels, pumps and binding proteins that tightly control cellular calcium levels. In this thesis I have studied four of these proteins: the *Dictyostelium* homologues of the calcium channels polycystin-2 (Ddpolycystin) and mucolipin (Ddmucolipin) which are associated with the diseases polycystic kidney disease and mucolipidosis type IV respectively, and two putative Ca^{2+}-ATPases PAT3 and PAT4. My work has demonstrated that changing the level of expression of the channels can have dire cellular consequences through disruption of cellular calcium handling, which in turn impacts the many calcium-regulated processes. However, functional redundancy and compensatory changes in expression amongst the calcium pumps means that loss of expression of a single pump does not greatly impact the cellular phenotypes.

One feature of the *Dictyostelium* lifecycle is that they display chemotactic behaviour both during the vegetative state and after starvation during multicellular development. In both instances stimulation with chemoattractant substances (including folic acid and cAMP) induces a temporary rise in cytosolic calcium due to influx of calcium across the plasma membrane, and release from intracellular stores which is facilitated by calcium channels. The channels responsible for the calcium influx are still to be conclusively identified. Evidence has shown that IplA may be involved, but it is only expressed at low levels in the plasma membrane (Lusche *et al*., 2012) so is likely not the only plasma membrane channel involved. Another study has shown that knockout of Ddpolycystin does not ablate the calcium response (Traynor and Kay, 2017) so this channel also may not be the main channel responsible. Even so, this does not mean that Ddpolycystin does not contribute to these responses. In my current work, I have shown that Ddpolycystin can in fact contribute to cytosolic calcium responses, both to folate in vegetate cells and cAMP in aggregation competent cells. Thus, I found that overexpressing and knocking down Ddpolycystin expression respectively enhanced and reduce the calcium responses to

these attractants. As Ddpolycystin is expressed at the plasma membrane, it is partially responsible for calcium influx from the extracellular milieu. It is likely that both Ddpolycystin and IplA facilitate calcium influx and may even be interaction partners. I have also shown that Ddpolycystin plays a role in resting calcium homeostasis because knockdown strains had lower basal cytosolic calcium levels. However, in overexpression strains basal calcium levels were unaffected. I found that expression of PAT4 mRNA in these cells was increased, which demonstrates that the cells were able to upregulate calcium sequestering capacity to homeostatically control resting calcium levels.

Intracellular calcium stores include the ER, mitochondria, contractile vacuole and vesicles of the endocytic pathway. While calcium channels are predicted to be expressed at these organelles, the channels that are responsible for release from these stores have not been confirmed. The ER does contribute to chemotactic calcium signalling (Wilczynska *et al*., 2005; Fisher and Wilczynska, 2006), however the channel responsible is not known, although IplA is predicted to reside there. Calcium release from the mitochondria may also contribute to the response, however this has not yet been demonstrated. Fatty acids induce calcium release from the acidic stores (Schaloske *et al*., 1998) which include the contractile vacuole and acidic vesicles of the endocytic pathway. At the contractile vacuole P2X receptors release calcium when activated by ATP (Parkinson *et al*., 2014), but it is not known if they contribute to chemotactic calcium responses. The two pore channel may also be expressed in the vacuolar membrane but a knockout mutant retains cAMP calcium responses (Chang *et al*., 2020), so it is not the only calcium release channel. Ddmucolipin localises predominantly to post-lysosomes but also to other vesicles of the endocytic pathway (Lima *et al*., 2012). In this thesis I have shown that Ddmucolipin can measurably contribute to the global calcium responses to chemoattractants when it is overexpressed, suggesting that it can in fact function as a calcium release channel, and that these vesicles can contribute to chemotactic calcium signals. However, when knocked down, folic acid responses were enhanced, possibly due to lack of calcium buffering in the diseased cells, and cAMP responses were not affected. This suggests that rather than contributing to global calcium signalling, Ddmucolipin's normal role may be more related to regulating local calcium signalling associated with processes along the endocytic pathways.

Termination of the calcium responses occurs when calcium is sequestered from cytosol back into the intracellular stores or across the plasma membrane by calcium-ATPases or exchangers. *Dictyostelium* encodes three P-type Ca^{2+}-ATPases: PAT1 of the contractile vacuole, and two putative pumps PAT3 and PAT4. The subcellular localisation of PAT3/4 is unknown, and my work in this thesis is the first to characterise their role in chemotactic calcium signalling. I have shown that the Ca^{2+}-sensitive Ca^{2+} pumps PAT3 and PAT4, are functionally redundant. The pumps appear to contribute more to chemotactic calcium signalling in aggregating cells than in vegetative cells, with PAT4 exerting a larger influence than PAT3 on the Ca^{2+} responsiveness of the response kinetics. Their more prominent role in aggregation was also reflected in their developmental expression patterns that increase at the onset of starvation through to aggregation competence. Because of the redundancy between the calcium pumps, and homeostatic transcriptional regulation of the Ca^{2+} signalling system, calcium regulation remains similar to wild type in the single pump knockdown strains. Therefore, single pump knockdown strains appear phenotypically similar to wildtype. A similar lack of obvious phenotypes has been reported for PAT1 knockdown strains (Moniakis *et al*., 1999).

The same was not so when assessing the phenotypes associated with Ddpolycystin and Ddmucolipin strains. I found that the aberrant calcium signalling in my Ddpolycystin and Ddmucolipin strains impacted on all the phenotypes assayed. This demonstrates the sensitivity of these cellular processes to calcium regulation. This was particularly obvious in the Ddpolycystin strains as the phenotypes were all in the same direction as the altered calcium signalling. Ddpolycysin positively regulated axenic growth, plaque expansion on lawns of bacteria, macropinocytosis and phagocytosis. Ddpolycystin-dependent Ca^{2+} signalling was also involved in controlling cell type specific differentiation, spore germination and autophagic cell death. This makes sense because there is evidence that calcium is involved in the regulation of all these phenotypes. Ddmucolipin likely regulates local calcium signalling, and disruptions in this caused abnormalities in the vesicles of the endocytic pathway. The processes of the endocytic pathway were sensitive to loss of Ddmucolipin dependent calcium signalling possibly due to defects in membrane fusion and fission if the vesicles. Consequently, the cells appeared unable to catabolize efficiently, so were in a state of partial starvation and upregulated endocytic processes of macropinocytosis and phagocytosis as a compensatory mechanism. This phenotype is

common amongst *Dictyostelium* lysosomally diseased cells, as is defective stalk morphogenesis (autophagic cell death), which was also present in my mucolipin mutants.

In combination with other published work, my results demonstrate that all the elements of the *Dictyostelium* calcium signalling machinery play roles in mediating cytosolic calcium responses. While each element is an important contributor, the cytopathological outcomes are constrained by a combination of homeostatic transcriptional regulation and overlapping or redundant functions. Where these safeguards are insufficient (eg. because of different subcellular locations and roles of channels), cytopathological phenotypes ensue and produce disease outcomes for the organism. These disease outcomes can be used to study the function of proteins associated with human diseases, in this case mucolipidosis type IV and polycystic kidney disease.

References

Allan, C. Y. and Fisher, P. R. (2009). *In vivo* measurements of cytosolic calcium in *Dictyostelium discoideum*. *Methods Mol Biol* **571**, 291–308.

Allan, C. Y. and Fisher P. F. (2022). The *Dictyostelium* model for Mucolipidosis Type IV. *Front. Cell Dev. Biol* **10,** *doi:* 10.3389/fcell.2022.741967

Abe, F. and Maeda, Y. (1995). Specific expression of a gene encoding a novel calcium-binding protein, *CAF-1*, during transition of *Dictyostelium* cells from growth to differentiation. *Growth Differ* **37**, 39-48.

AbouAlaiwi, W. A., Takahashi, M., Mell, B. R., Jones, T. J., Ratnam, S., Kolb, R. J. *et al*. (2009). Ciliary polycystin-2 is a mechanosensitive calcium channel involved in nitric oxide signaling cascades. *Circ Res* **104**(7), 860–9.

Aguilar, A. (2017). Polycystic kidney disease: Autophagy boost to treat ADPKD? *Nat Rev Nephrol* **13**(3), 134.

Andersson, K. B., Birkeland, J. A., Finsen, A. V., Louch, W. E., Sjaastad, I., Wang, Y. *et al*. (2009). Moderate heart dysfunction in mice with inducible cardiomyocyte-specific excision of the Serca2 gene. *J Mol Cell Cardiol* **47**(2), 180-7.

Andre, B., Noegel, A. A. and Schleicher, M. (1996). *Dictyostelium discoideum* contains a family of calmodulin-related EF-hand proteins that are developmentally regulated. *FEBS Lett* **382**, 198-202.

Annesley, S. J., and Fisher, P. R. (2009). *Dictyostelium discoideum*-a model for many reasons. *Mol Cell Biochem* **329**, 73–91.

Annesley, S. J., Bago, R., Bosnar, M. H., Filic, V., Marinović, M., Weber, I., Mehta, A. and Fisher, P. R. (2011). *Dictyostelium discoideum* nucleoside diphosphate kinase C plays a negative regulatory role in phagocytosis, macropinocytosis and exocytosis. *PloS one* **6**, e26024.

Annesley, S. J., Carilla-Latorre, S., Escalante, R. and Fisher, P. R. (2013). Mitochondrial respiratory complex function and the phenotypic consequences of dysfunction. In *Dictyostelium discoideum Protocols* pp. 345-366: Springer.

Annesley, S. J., Chen, S., Francione, L. M, Sanislav, O., Chavan, A. J., Farah, C. *et al*. (2014). *Dictyostelium*, a microbial model for brain disease. *Biochimica et Biophysica Acta (BBA)-General Subjects* **1840**, 1413-1432.

Anyatonwu, G. I., Estrada, M., Tian, X., Somlo, S. and Ehrlich, B. E. (2007). Regulation of ryanodine receptor-dependent calcium signalling by polycystin-2. *PNAS USA* **104**, 6454–6459.

Arnadóttir, J. and Chalfie, M. (2010). Eukaryotic mechanosensitive channels. *Annu Rev Biophys* **39**, 111-37.

Artemenko, Y., Axiotakis, L., Jr., Borleis, J., Iglesias, P. A. and Devreotes, P. N. (2016). Chemical and mechanical stimuli act on common signal transduction and cytoskeletal networks. *PNAS USA* **113**, E7500-E7509.

Ausubel, F. M., Brent, R., Kingston, R. E., Moore, D. O., Seidman, J. G., Smith, J. A. and Struhl, K. (1994). Current protocols in molecular biology. *Greene publishing associates and Wiley-Interscience*.

Azhar, M., Saran, S. and Nanjundiah, V. (1995). Spatial gradients of calcium in the slug of *Dictyostelium discoideum*. *Current Science* **68**, 337-342.

Azhar, M., Manogaran, P. S., Kennady, P. K., Pande, G., and Nanjundiah, V. (1996). A Ca^{2+}-dependent early functional heterogeneity in amoebae of *Dictyostelium discoideum* revealed by flow cytometry. *Exp Cell Res,* **227**(2), 344–351.

Azhar, M., Kennady, P. K., Pande, G. and Nanjundiah, V. (1997). Stimulation by DIF causes an increase of intracellular Ca^{2+} in *Dictyostelium discoideum*. *Exp Cell Res* **230**(2), 403-406.

Azhar, M., Kennady, P. K., Pande, G., Espiritu, M., Holloman, W., Brazill, D. *et al*. (2001). Cell cycle phase, cellular Ca^{2+} and development in *Dictyostelium discoideum*. *Int J Dev Biol* **45**(2), 405-14.

Bähler, M. and Rhoads, A. (2002). Calmodulin signalling via the IQ motif. *FEBS Lett* **513**, 107–113.

Bai, C. X., Giamarchi, A., Rodat-Despoix, L., Padilla, F., Downs, T., Tsiokas, L. *et al*. (2008). Formation of a new receptor operated channel by heteromeric assembly of TRPP2 and TRPC1 subunits. *EMBO Rep* **9**(5), 472–479.

Baines, A., Parkinson, K., Sim, J. A., Bragg, L., Thompson, C. R. L. and North, R. A. (2013). Functional properties of five *Dictyostelium discoideum* P2X receptors. *J Biol Chem* **288**, 20992-21000.

Baker, H. L., Errington, R. J., Davies, S. C. and Campbell, A. K. (2002). A mathematical model predicts that calreticulin interacts with the endoplasmic reticulum Ca^{2+}-ATPase. *Biophys J* **82**(2), 582-90.

Baksh, S. and Michalak, M. (1991). Expression of calreticulin in *Escherichia coli* and identification of its Ca^{2+} binding domains. *J Biol Chem* **266**, 21458–21465.

Bargal, R. and Bach, G. (1997). Mucolipidosis type IV: abnormal transport of lipids to lysosomes. *J Inherit Metab Dis* **20**, 625–632.

Barr, M. M., DeModena, J., Braun, D., Nguyen, C. Q., Hall, D. H., Sternberg, P. W. (2001). The *Caenorhabditis elegans* autosomal dominant polycystic kidney disease gene homologs lov-1 and pkd-2 act in the same pathway. *Curr Biol* **11**(17), 1341-6.

Barth, C., Fraser, D. J. and Fisher, P. R. (1998). Co-insertional replication is responsible for tandem multimer formation during plasmid integration into the *Dictyostelium* genome. *Science Direct* **39**, 141-153.

Baskar, R., Chhabra, P., Mascarenhas, P. and Nanjundiah, V. (2000). A cell type-specific effect of calcium on pattern formation and differentiation in *Dictyostelium discoideum*. *Int J Dev Biol* **44**(5), 491-8.

Bazari, W. L. and Clarke, M. J. (1981). Characterization of a novel calmodulin from *Dictyostelium discoideum. Biol Chem* **256**(7), 3598-603.

Benini, A., Bozzato, A., Mantovanelli, S., Calvarini, L., Giacopuzzi, E., Bresciani, R., Moleri, S., Zizioli, D., Beltrame, M. and Borsani, G. (2013). Characterization and expression analysis of mcoln1.1 and mcoln1.2, the putative zebrafish co-orthologs of the gene responsible for human mucolipidosis type IV. *Int J Dev Biol* 57(1), 85-93.

Berman, E. R., Livni, N., Shapira, E., Merin, S. and Levij, I. S. (1974). Congenital corneal clouding with abnormal systemic storage bodies: a new variant of Mucolipidosis. *J Pediatrics* **84**(4), 519-526.

Bernardi, P. (1999). *Mitochondrial transport of cations: channels, exchangers, and permeability transition. Physiol Rev* **79**, 1127–1155.

Berridge, M. J., Lipp, P., and Bootman, M. D. (2000). The versatility and universality of calcium signalling. *Nat Rev Mol Cell Biol* **1**(1), 11–21.

Berridge, M. J., Bootman, M. D. and Roderick, H. L. (2003). Calcium signalling: dynamics, homeostasis and remodelling. *Nat Rev Mol Cell Biol* **4**(7), 517-29.

Bers, D. M. (2000). Calcium fluxes involved in control of cardiac myocyte contraction. *Circ Res* **87**, 275–281.

Bharat T. A., Malsam J., Hagen W. J., Scheutzow A., Söllner T. H., Briggs J. A. G. (2014). SNARE and regulatory proteins induce local membrane protrusions to prime docked vesicles for fast calcium-triggered fusion. *EMBO Rep* **15**, 308–314.

Birnboim, H. C. and Doly, J. (1979). A rapid alkaline extraction procedure for screening recombinant plasmid DNA. *Nucleic Acids Res* **7**(6), 1513-23.

Boczek, T., Sobolczyk, M., Mackiewicz, J., Lisek, M., Ferenc, B., Guo, F., and Zylinska, L. (2021). Crosstalk among Calcium ATPases: PMCA, SERCA and SPCA in Mental Diseases. Int *J Mol Sci*, **22**(6), 2785.

Boeckeler, K., Tischendorf, G., Mutzel, R., Weissenmayer, B. (2006). Aberrant stalk development and breakdown of tip dominance in *Dictyostelium* cell lines with RNAi-silenced expression of calcineurin B. *BMC Dev Biol* **6**, 12.

Böhme, R., Bumann, J., Aeckerle, S. and Malchow, D. (1987). A highaffinity plasma membrane Ca^{2+}-ATPase in *Dictyostelim discoideum*: its relation to cAMP induced Ca^{2+} fluxes. *Biochim Biophys Acta* **904**, 125-130.

Bokko, P. B., Francioni, L., Ahmed, A. U., Bandala-Sanchez, E., Annesley, S. J., Huang, X., Khurana, T., Kimmel, A. R. and Fisher, P. R. (2007). Diverse mitochondrial cytopathologies are caused by AMPK signalling. *Mol Biol Cell* **18**, 1874–1886.

Bootman, M. D., Berridge, M. J. and Roderick, H. L. (2002). Calcium signalling: more messengers, more channels, more complexity. *Curr Biol* **12**, R563–R565.

Bootman, M. D., Chehab, T., Bultynck, G., Parys, J. B. and Rietdorf, K. (2018). The regulation of autophagy by calcium signals: Do we have a consensus? *Cell Calcium* **70**, 32-46.

Boudewyn, L. C. and Walkley, S. U. (2109). Current concepts in the neuropathogenesis of mucolipidosis type IV. *J Neurochem* **148**, 669–689.

Brailoiu, E., Churamani, D., Cai, X., Schrlau, M. G., Brailoiu, G. C., Gao, X. *et al.* (2009). Essential requirement for two-pore channel 1 in NAADP-mediated calcium signaling. *J Cell Biol* **186**(2), 201–209.

Brailoiu, G. C., Brailoiu, E. (2016). Modulation of calcium entry by the endo-lysosomal system. *Adv Exp Med Biol* **898**, 423-47.

Bravo-Sagua R., Parra V., López-Crisosto C., Díaz P., Quest A. F., Lavandero S. (2017). Calcium transport and signaling in mitochondria. *Compr Physiol* **7**(2):623-634.

Brill, A. L. and Ehrlich, B. E. (2020). Polycystin 2: A calcium channel, channel partner, and regulator of calcium homeostasis in ADPKD. *Cell Signal* **66**, 109490.

Brini, M. and Carafoli, E. (2011). The plasma membrane Ca^{2+} ATPase and the plasma membrane sodium calcium exchanger cooperate in the regulation of cell calcium. *Cold Spring Harb Perspect Biol* **3**(2), a004168.

Brini, M., Calì, T., Ottolini, D. and Carafoli, E. (2012). Calcium pumps: why so many? *Compr Physiol* **2**(2), 1045-60.

Brini, M., Carafoli, E. and Calì, T. (2017). The plasma membrane calcium pumps: focus on the role in (neuro)pathology. Biochem *Biophys Res Commun* **483**(4), 1116-1124.

Bumann, J., Wurster, B. and Malchow, D. (1984). Attractant-induced changes and oscillations of the extracellular Ca^{2+} concentration in suspensions of differentiating *Dictyostelium* cells. *J Cell Biol* **98**, 173-178.

Burgoyne, R. D. and Clague, M. J. (2003). Calcium and calmodulin in membrane fusion *Biochim Biophys Acta* **1641***,* 137–143*.*

Cai, Y., Maeda, Y., Cedzich, A., Torres, V. E., Wu, G., Hayashi, T. *et al*. (1999). Identification and characterization of polycystin-2, the PKD2 gene product. *J Biol Chem* **274**(40), 28557–28565.

Cai, X. and Lytton, J. (2004). The cation/Ca^{2+} exchanger superfamily: phylogenetic analysis and structural implications. *Mol Biol Evol* **21**(9), 1692-703.

Cai, Y., Anyatonwu, G., Okuhara, D., Lee, K. B., Yu, Z., Onoe, T *et al*. (2004). Calcium dependence of polycystin-2 channel activity is modulated by phosphorylation at Ser^{812}. *J Biol Chem* **279**, 19987–19995.

Cai, H., Devreotes, P. N. (2011). Moving in the right direction: how eukaryotic cells migrate along chemical gradients. *Semin Cell Dev Biol* **22**(8):834-41.

Cai, H., Huang, C.-H., Devreotes, P. N., and Iijima, M. (2012). Analysis of chemotaxis in *Dictyostelium*. *Methods in Molecular Biology (Clifton, N.j.)* **757**, 451–468.

Calcraft, P. J., Ruas, M., Pan, Z., Cheng, X., Arredouani, A., Hao, X. *et al.* (2009). NAADP mobilizes calcium from acidic organelles through two- pore channels. *Nature* **459**, 596 –600.

Calvo-Garrido, J., Carilla-Latorre, S., Kubohara, Y., Santos-Rodrigo, N., Mesquita, A., Soldati, T., *et al*. (2010). Autophagy in *Dictyostelium*: Genes and pathways, cell death and infection. *Autophagy* **6**(6), 686-701.

Camacho, P. and Lechleiter, J. D. (1995). Calreticulin inhibits repetitive intracellular Ca^{2+} waves. *Cell* **82**, 765-771.

Cang, C., Aranda, K. and Ren, D. (2014). A non-inactivating high-voltage-activated two-pore Na^{+} channel that supports ultra-long action potentials and membrane bistability. *Nat Commun* **5**, 5015.

Cantero Mdel, R. and Cantiello, H. F (2015). Polycystin-2 (TRPP2) regulation by Ca^{2+} is effected and diversified by actin-binding proteins. *Biophys J* **108**, 2191–2200.

Cantiello, H. F., Montalbetti, N., Goldmann, W. H., Raychowdhury, M. K., Gonzalez-Perrett, S., Timpanaro, G. A. *et al*. (2005). Cation channel activity of mucolipin-1: the effect of calcium. *Pflügers Arch* **451**, 304–312.

Cao, Q., Zhong, X. Z., Zou, Y., Zhang, Z., Toro, L. and Dong, X. P. (2015). BK channels alleviate lysosomal storage diseases by providing positive feedback regulation of lysosomal Ca^{2+} release. *Dev Cell* **33**(4), 427-41.

Cao, Q., Yang, Y., Zhong, X. Z., and Dong, X. P. (2017). The lysosomal Ca^{2+} release channel TRPML1 regulates lysosome size by activating calmodulin. *J Biol Chem* **292**(20), 8424–8435.

Carafoli, E., Tiozzo, R., Lugli, G., Crovetti, F. and Kratzing, C. (1974). The release of calcium from heart mitochondria by sodium. *J Mol Cell Cardiol* **6**(4), 361-71.

Cardelli, J. (2001). Phagocytosis and macropinocytosis in *Dictyostelium*: phosphoinositide-based processes, biochemically distinct. *Traffic* **2**, 311–320.

Carreras-Sureda, A., Pihán, P. and Hetz, C. (2018). Calcium signaling at the endoplasmic reticulum: fine-tuning stress responses. *Cell Calcium*. **70**, 24-31.

Catalano, A. and O'Day, D. H. (2008). Calmodulin-binding proteins in the model organism *Dictyostelium*: a complete and critical review. *Cell Signal* **20**(2), 277-91.

Celic, A. S., Petri, E. T., Benbow, J., Hodsdon, M. E., Ehrlich, B. E. and Boggon, T. J. (2012). Calcium-induced conformational changes in C-terminal tail of polycystin-2 are necessary for channel gating. *J Biol Chem* **287**, 17232–17240.

Chang, F. S., Wang, Y., Dmitriev, P., Gross, J., Galione, A., and Pears, C. (2020). A two-pore channel protein required for regulating mTORC1 activity on starvation. *BMC biology* **18**(1), 8.

Charette, S. J. and Cosson, P. (2008). Altered composition and secretion of lysosome-derived compartments in *Dictyostelium* AP-3 mutant cells. *Traffic* **9**, 588-596.

Chazin, W. J. (2011). Relating form and function of EF-hand calcium binding proteins. *Accounts of Chemical Research* **44**(3), 171–179.

Chen, C. S., Bach, G. and Pagano, R. E. (1998). Abnormal transport along the lysosomal pathway in Mucolipidosis, type IV disease. *PNAS USA* **95**, 6373-6378.

Chen, C. C., Butz, E. S., Chao, Y. K., Grishchuk, Y., Becker, L., Heller, S. *et al*. (2017). Small molecules for early endosome-specific patch clamping. *Cell Chem Biol* **24**(7):907-916.e4.

Chen, J., Sitsel, A., Benoy, V., Sepúlveda, M. R., and Vangheluwe, P. (2020). Primary active Ca^{2+} transport systems in health and disease. *Cold Spring Harb Perspect Biol* **12**, a035113.

Cheng, X., Shen, D., Samie, M. and Xu, H. (2010). Mucolipins: Intracellular TRPML1-3 channels. *FEBS Letters* **584**, 2013–2021.

Chisholm, R. L., Gaudet, P., Just, E. M., Pilcher, K. E., Fey, P., Merchant, S. N., and Kibbe, W. A. (2006). dictyBase, the model organism database for *Dictyostelium discoideum*. *Nucleic Acids Research* **34***,* (Database issue), D423–D427.

Chitayat, D., Meunier, C. M., Hodgkinson, K. A., Silver, K., Flanders, M., Anderson, I.J. *et al*. (1991). Mucolipidosis type IV: clinical manifestations and natural history. *Am J Med Genet* **41**, 313-318.

Christensen, K. A., Myers, J. T. and Swanson, J. A. (2002). pH-dependent regulation of lysosomal calcium in macrophages. *J Cell Sci* **115**, 599–607.

Christoforidis, S., McBride, H. M., Burgoyne, R. D. and Zerial, M. (1999). The Rab5 effector EEA1 is a core component of endosome docking. *Nature* **397**, 621-625.

Churchill, G. C., Okada, Y., Thomas, J. M., Genazzani, A. A., Patel, S. and Galione, A. (2002). NAADP mobilizes Ca^{2+} from reserve granules, lysosome-related organelles, in sea urchin eggs. *Cell* **111**, 703–708.

Clapham, D. E. (1995). Calcium signalling. *Cell* **80**, 259–268.

Clapham, D. (2003). TRP channels as cellular sensors. *Nature* **426**, 517–524.

Clapham, D. (2007). Calcium signaling. *Cell* **131**, 1047–1058.

Clarke, M., Köhler, J., Arana, Q., Liu, T., Heuser, J. and Gerisch, G. (2002). Dynamics of the vacuolar H^+ATPase in the contractile vacuole complex and the endosomal pathway of *Dictyostelium* cells. *J Cell Sci* **115**(14), 2893-905.

Clarke, M., Köhler, J., Heuser, J. and Gerisch, G. (2002b). Endosome fusion and microtubule-based dynamics in the early endocytic pathway of *Dictyostelium*. *Traffic* **3**(11), 791-800.

Coe, H. and Michalak, M. (2009). Calcium binding chaperones of the endoplasmic reticulum. *Gen Physiol Biophys* **28**, F96-F103.

Conte, I. L., Keith, N., Gutiérrez-Gonzalez, C., Parodi, A. J. and Caramelo, J. (2007). The Interplay between calcium and the in vitro lectin and chaperone activities of calreticulin. *Biochemistry* **46**, 4671–4680.

Corradi, G. R., Mazzitelli, L. R., Petrovich, G. D., de Tezanos Pinto, F., Rochi, L., & Adamo, H. P. (2021). Plasma membrane Ca^{2+} pump PMCA4z is more active than splicing variant PMCA4x. *Frontiers in cellular neuroscience* **15**, 668371.

Cosson, P. (2006). Selective membrane exclusion in phagocytic and macropinocytic cups. *Journal of cell science* **119**(19), 4079-87.

Cosson, P. and Soldati, T. (2008). Eat, kill or die: when amoeba meets bacteria. *Current opinion in microbiology* **11**(3), 271–6.

Coste, B., Mathur, J., Schmidt, M., Earley, T. J., Ranade, S., Petrus, M. J. *et al*. (2010). Piezo1 and Piezo2 are essential components of distinct mechanically activated cation channels. *Science* **330**(6000), 55–60.

Cotter, D. A. and Raper, K. B. (1966). Spore germination in *Dictyostelium discoideum. PNAS USA* **56**, 880-887.

Cotter, D. A., Sands, T. W., Virdy, K. J., North, M. J., Klein, G. and Satre, M. (1992). Patterning of development in *Dictyostelium discoideum* factors regulating growth, differentiation, spore dormancy and germination. *Biochem Cell Biol* **70**, 892-919.

Coukell, B., Li, Y., Moniakis, J. and Cameron, A. (2004). The Ca^{2+}/calcineurin-regulated cup gene family in *Dictyostelium discoideum* and its possible involvement in development. *Eukaryot Cell* **3**, 61-71.

Criollo, A., Altamirano, F., Pedrozo, Z., Schiattarella, G. G., Li, D. L., Rivera-Mejías, P. *et al*. (2018). Polycystin-2-dependent control of cardiomyocyte autophagy. *J Mol Cell Cardiol* **118**, 110-121.

Csordás, G., Golenár, T., Seifert, E. L., Kamer, K. J., Sancak, Y., Perocchi, F. *et al*. (2013). MICU1 controls both the threshold and cooperative activation of the mitochondrial Ca^{2+} uniporter. *Cell Metab* **17**(6), 976–987.

Cubitt, A. B., Firtel, R. A., Fischer, G., Jaffe, L. F. and Miller, A. L. (1995). Patterns of free calcium in multicellular stages of *Dictyostelium* expressing jellyfish apoaequorin. *Development* **121**, 291-2301.

Curcio-Morelli, C., Charles, F. A., Micsenyi, M. C., Cao, Y., Venugopal, B., Browning, M. F. *et al*. (2010). Macroautophagy is defective in mucolipin-1-deficient mouse neurons. *Neurobiol Dis* **40**, 370-377.

Dammann, H., Hellstern, S., Husain, Q., Mutzel, R. (1996). Primary structure, expression and developmental regulation of a *Dictyostelium* calcineurin A homologue. *Eur J Biochem* **238**(2), 391-9.

Dayam, R. M., Saric, A., Shilliday, R. E., Botelho, R. J. (2015). The phosphoinositide-gated lysosomal Ca^{2+} channel, TRPML1, is required for phagosome maturation. *Traffic* **16**(9), 1010-26.

De Chastellier, C., and Ryter, A. (1977). Changes of the cell surface and of the digestive apparatus of *Dictyostelium discoideum* during the starvation period triggering aggregation. *J Cell Biol* **75**, 218–236.

De Marchi, U., Santo-Domingo, J., Castelbou, C., Sekler, I., Wiederkehr, A. and Demaurex, N. J. (2014). NCLX protein, but not LETM1, mediates mitochondrial Ca^{2+} extrusion, thereby limiting Ca^{2+}-induced NAD(P)H production and modulating matrix redox state. *Biol Chem* **289**(29), 20377-85.

De Stefani, D., Raffaello, A., Teardo, E., Szabò, I. and Rizzuto, R. (2011). A forty-kilodalton protein of the inner membrane is the mitochondrial calcium uniporter. *Nature* **476**(7360), 336-40.

Decuypere, J. P., Bultynck, G. and Parys, J. B. (2011). A dual role for Ca^{2+} in autophagy regulation. *Cell Calcium* **50**, 242–50.

Deery, W. J., Gao, T., Ammann, R., Gomer, R. H. (2002). A single cell density-sensing factor stimulates distinct signal transduction pathways through two different receptors. *J Biol Chem* **277**(35), 31972-9.

Denessiouk, K., Permyakov, S., Denesyuk, A., Permyakov, E., and Johnson, M. S. (2014). Two structural motifs within canonical EF-hand calcium-binding domains identify five different classes of calcium buffers and sensors. *PloS one* **9**(10), e109287.

Denis, V. and Cyert, M. S. (2002). Internal Ca^{2+} release in yeast is triggered by hypertonic shock and mediated by a TRP channel homologue. *J Cell Biol* **156**(1), 29-34.

Di Leva, F., Domi, T., Fedrizzi, L., Lim, D. and Carafoli, E. (2008). The plasma membrane Ca^{2+} ATPase of animal cells: structure, function and regulation. *Arch Biochem Biophys* **476**, 65–74.

Di Palma, F., Belyantseva, I. A., Kim, H. J., Vogt, T. F., Kachar, B. and Noben-Trauth, K. (2002). Mutations in Mcoln3 associated with deafness and pigmentation defects in varitint-waddler (Va) mice. *PNAS USA* **99**, 14994–14999.

Dilão, R. and Hauser, M. J. (2013). Chemotaxis with directional sensing during *Dictyostelium* aggregation. *C R Biol* **336**(11-12), 565-71.

Dobrovolny, R., Liskova, P., Ledvinova, J., Poupetova, H., Asfaw, B., Filipec, M. *et al*. (2007). Mucolipidosis IV: report of a case with ocular restricted phenotype caused by leaky splice mutation. *Am J Ophthalmol* **143**, 663– 671.

Dong, X. P., Cheng, X., Mills, E., Delling, M., Wang, F., Kurz, T. and Xu, H. (2008). The type IV mucolipidosis-associated protein TRPML1 is an endolysosomal iron release channel. *Nature* **455**, 992–996.

Dong, X. P., Wang, X. and Xu, H. (2010). TRP channels of intracellular membranes. *J Neurochem* **113**, 313–328.

Dong, X., Shen, D., Wang, X., Dawson, T., Li, X., Zhang, Q. *et al*. (2010a). PI(3,5)P2 controls membrane traffic by direct activation of mucolipin Ca^{2+} Release channels in the endolysosome. *Nature communications* **1**(4), 38.

Dowson, J. H., Armstrong, D., Koppang, N., Lake, B. D. and Jolly R. D. (1982). Autofluorescence emission spectra of neuronal lipopigment in animal and human ceroidoses (ceroid-lipofuscinoses). *Acta Neuropathol* **58**, 152–156.

Drayer, A. L., Van der Kaay, J., Mayr, G. W. and Van Haastert, P. J. (1994). Role of phospholipase C in *Dictyostelium*: formation of inositol 1,4,5-trisphosphate and normal development in cells lacking phospholipase C activity. *EMBO J* **13**, 1601–1609.

Du, F., Edwards, K., Shen, Z., Sun, B., De Lozanne, A., Briggs, S. and Firtel, RA. (2008). Regulation of contractile vacuole formation and activity in *Dictyostelium*. *EMBO J* **27**(15), 2064-76.

Egger, M. and Niggli, E. J. (1999). Regulatory function of Na-Ca exchange in the heart: milestones and outlook. *Membr Biol* **168**, 107–130.

Eichelsdoerfer, J. L., Evans, J. A., Slaugenhaupt, S. A. and Cuajungco, M. P. (2010). Zinc dyshomeostasis is linked with the loss of mucolipidosis IV-associated TRPML1 ion channel. *J Biol Chem* **285**, 34304-34308.

Espinoza-Fonseca, L. M., and Thomas, D. D. (2011). Atomic-level characterization of the activation mechanism of SERCA by calcium. PloS one, **6**(10), e26936.

Europe-Finner, G. N., McClue, S. J. and Newell, P. C. (1984). Inhibition of aggregation in *Dictyostelium* by EGTA-induced depletion of calcium. *FEMS Microbiol Lett* **21**(1), 21-25.

Europe-Finner, G. N. and Newell, P. C. (1986). Inositol 1,4,5-triphosphate induces calcium release from a non-mitochondrial pool in amoebae of *Dictyostelium*. *Biochim Biophys Acta* **887**(3), 335–340.

Europe-Finner, G. N. and Newell, P. C. (1986a). Inositol 1,4,5-trisphosphate and calcium stimulate actin polymerization in *Dictyostelium discoideum*. *J Cell Sci* **82**, 41–51.

Europe-Finner, G. N. and Newell, P. C. (1987). Cyclic AMP stimulates accumulation of inositol trisphosphate in *Dictyostelium. J Cell Sci* **87**(2), 221–229.

Fache, S., Dalous, J., Engelund, M., Hansen, C., Chamaraux, F, Fourcade, B. *et al*. (2005). Calcium mobilization stimulates *Dictyostelium discoideum* shear-flow-induced cell motility. *J Cell Sci* **118**(15), 3445-3457.

Fajardo, M., Schleicher, M., Noegel, A., Bozzaro, S., Killinger, S., Heuner, K. *et al*. (2004). Calnexin, calreticulin and cytoskeleton-associated proteins modulate uptake and growth of *Legionella pneumophila* in *Dictyostelium discoideum*. *Microbiology* **150**, 2825–2835.

Falchetto, R., Vorherr, T., Brunner, J. and Carafoli, E. (1991). The plasma membrane Ca^{2+} pump contains a site that interacts with its calmodulin-binding domain. *J Biol Chem* **266**, 2930–2936.

Falchetto, R., Vorherr, T. and Carafoli, E. (1992). The calmodulin-binding site of the plasma membrane Ca^{2+} pump interacts with the transduction domain of the enzyme. *Protein Sci* **1**, 1613–1621.

Fares, H. and Greenwald, I. (2001). Regulation of endocytosis by CUP-5, the *Caenorhabditis elegans* mucolipin-1 homolog. *Nat Genet* **28**, 64-68.

Feijóo-Bandín, S., García-Vence, M., García-Rúa, V., Roselló-Lletí, E., Portolés, M., Rivera, M. *et al*. (2017). Two-pore channels (TPCs): Novel voltage-gated ion channels with pleiotropic functions. *Channels **11**,* 20-33.

Feng, X., Huang, Y., Lu, Y., Xiong, J., Wong, C.O., Yang, P. *et al*. (2014). Drosophila TRPML forms PI(3,5)P2-activated cation channels in both endolysosomes and plasma membrane. *J Biol Chem* **289**(7), 4262-72.

Fernando, S., Allan, C. Y., Mroczek, K., Pearce, X., Sanislav, O., Fisher, P. R. *et al*. (2020). Cytotoxicity and mitochondrial dysregulation caused by α-Synuclein in *Dictyostelium discoideum. Cells* **9**(10), 2289.

Fey, P., Compton, K. and Cox, E. C. (1995). Green fluorescent protein production in the cellular slime molds Polysphondylium pallidum and *Dictyostelium* discoideum. *Gene* **165**, 127-130.

Fey, P., Gaudet, P., Curk, T., Zupan, B., Just, E. M., Basu, S., *et al*. (2009). dictyBase--a *Dictyostelium* bioinformatics resource update. *Nucleic Acids Res* (Database issue):D515-9.

Fisher, P. R., Merkl, G. and Gerisch, G. (1989). Quantitative analysis of cell motility and chemotaxis in *Dictyostelium* discoideum using an image processing system and a novel chemotaxis chamber providing stationary chemical gradients. *J Cell Biol* **108**, 973-984.

Fisher, P. R. (1990). Pseudopodium activation and inhibition signals in chemotaxis by *Dictyostelium* discoideum amoebae. *Seminars in Cell Biology* **1**, 87-97.

Fisher, P. R. and Wilczynska, Z. (2006). Contribution of endoplasmic reticulum to Ca^{2+} signals in *Dictyostelium* depends on extracellular Ca^{2+}. *FEMS Microbiol Lett* **257**(2), 268–77.

Flaadt, H., Jaworski, E., Schlatterer, C. and Malchow, D. (1993). Cyclic AMP- and Ins(1,4,5)P3-induced Ca^{2+} fluxes in permeabilised cells of *Dictyostelium discoideum*: cGMP regulates Ca^{2+} entry across the plasma membrane. *J Cell Sci* **105**, 255–261.

Flayiih, R. (2018). The role of calcium signalling in neurodegenerative and mitochondrial diseases using *Dictyostelium discoideum* as a simple model. [Dissertation thesis]. [Melbourne (Vic)]: La Trobe University.

Foskett, J. K., White, C., Cheung, K. H. and Mak, D-O. D. (2007). Inositol trisphosphate receptor Ca^{2+} release channels*. Physiol Rev* **87**(2), 593–658.

Fountain, S. J., Parkinson, K., Young, M. T., Cao, L., Thompson, C. R. L, and North, R. A. (2007). An intracellular P2X receptor required for osmoregulation in *Dictyostelium discoideum*. *Nature* **448**(7150), 200–203.

Galione, A. (2006). NAADP, a new intracellular messenger that mobilizes Ca^{2+} from acidic stores. *Biochem Soc Trans* **34**, 922-926.

Galione, A. (2015). A primer of NAADP-mediated Ca^{2+} signalling: from sea urchin eggs to mammalian cells. *Cell Calcium* **58**, 27–47.

Gao, Z., Joseph, E., Ruden, D. M. and Lu, X. (2004). Drosophila Pkd2 is haploid-insufficient for mediating optimal smooth muscle contractility. *J Biol Chem* **279**(14), 14225-31.

Garrity, A. G., Wang, W., Collier, C. M., Levey, S. A., Gao, Q. and Xu, H. (2016). The endoplasmic reticulum, not the pH gradient, drives calcium refilling of lysosomes. *Elife* **5**, e15887.

Gees, M., Colsoul, B. and Nilius, B. (2010). The role of transient receptor potential cation channels in Ca^{2+} Signaling. *Cold Spring Harb Perspect Biol* **2**(10), a003962.

Gerasimenko, J. V., Tepikin, A. V., Petersen, O. H. and Gerasimenko, O. V. (1998). Calcium uptake via endocytosis with rapid release from acidifying endosomes. *Curr Biol* **8**, 1335–1338.

Gerasimenko, J. V., Petersen, O. H., and Gerasimenko, O. V. (2014). Monitoring of intra- ER free Ca^{2+}. *WIREs Membr Transp Signal* **3**, 63-71.

Gilabert, J. A. (2012). Cytoplasmic calcium buffering. *Adv Exp Med Biol* **740**, 483-98.

Giladi, M., Shor, R., Lisnyansky, M. and Khananshvili, D. (2016). Structure-functional basis of ion transport in sodium-calcium exchanger (NCX) proteins. *Int J Mol Sci* **17**(11), e1949.

Ginsburg, T., Gollop, R., Yu, Y., Louis, M., Saxe, L., Kimmel, R., (1995). The regulation of *Dictyostelium* development by transmembrane signalling. *J Eukaryot Microbiol* **42**, 200-205.

Giusti, C., Tresse, E., Luciani, M -F. and Golstein, P. (2009). Autophagic cell death: Analysis in *Dictyostelium*. *Biochimica et Biophysica Acta* **1793**(9), 1422–1431.

Giusti, C., Luciani, M -F., Ravens, S., Gillet, A. and Golstein, P. (2010). Autophagic cell death in *Dictyostelium* requires the receptor histidine kinase DhkM. *Mol Biol Cell* **21**, 1825–1835.

Glancy B. and Balaban R. S. (2012). Role of mitochondrial Ca^{2+} in the regulation of cellular energetics. *Biochemistry* **51**(14), 2959-73.

Glaves, J. P., Primeau, J. O., Gorski, P. A., Espinoza-Fonseca, L. M., Lemieux, M. J., Young, H. S. (2020). Interaction of a sarcolipin pentamer and monomer with the sarcoplasmic reticulum calcium pump, SERCA. *Biophys J* **118**(2), 518-531.

Goldin, E., Blanchette-Mackie, E. J., Dwyer, N. K., Pentchev, P. G. and Brady, R. O. (1995). Cultured skin fibroblasts derived from patients with mucolipidosis 4 are auto-fluorescent. *Pediatr Res* **37**, 687–92.

Goldin, E., Blanchette-Mackie, E. J., Dwyer, N. K., Pentchev, P. G., and Brady, R. O. (1995). Cultured skin fibroblasts derived from patients with mucolipidosis 4 are auto-fluorescent. *Pediatr Res* **37**, 687–92.

Goldin, E., Caruso, R. C., Benko, W., Kaneski, C. R., Stahl, S., and Schiffmann, R. (2008). Isolated ocular disease is associated with decreased Mucolipin-1 channel conductance. *IOVS* **49**, 3134-3142.

Gomer, R. H., Yuen, I. S., Firtel, R. A. (1991). A secreted 80 x 10(3) Mr protein mediates sensing of cell density and the onset of development in *Dictyostelium*. *Development* **112**(1), 269-78.

Gómez, N. M., Lu, W., Lim, J. C., Kiselyov, K., Campagno, K. E., Grishchuk, Y., *et al*. (2018). Robust lysosomal calcium signaling through channel TRPML1 is impaired by lysosomal lipid accumulation. *FASEB J* **32**(2), 782-794.

Gong, D., Chi, X., Ren, K., Huang, G., Zhou, G., Yan, N. *et al*. (2018). Structure of the human plasma membrane Ca^{2+}-ATPase 1 in complex with its obligatory subunit neuroplastin. *Nat comm* **9**(1), 3623.

Gonzalez, C., Klein, G. and Satre, M. (1990). Caffeine, an inhibitor of endocytosis in *Dictyostelium discoideum* amoebae. *J Cell Physiol* **144**, 408–415.

González-Perrett, S., Kim, K., Ibarra, C., Damiano, A. E., Zotta, E., Batelli, M. *et al*. (2001). Polycystin-2, the protein mutated in autosomal dominant polycystic kidney disease (ADPKD), is a Ca^{2+}-permeable nonselective cation channel. *PNAS USA* **98**(3), 1182-1187.

Goury-Sistla, P., Nanjundiah, V. and Pande, G. (2012). Bimodal distribution of motility and cell fate in *Dictyostelium discoideum*. *Int J Dev Biol* **56**(4), 263-72.

Grimes, D. T., Keynton, J. L., Buenavista, M. T., Jin, X., Patel, S. H., Kyosuke, S. *et al.* (2016). Genetic analysis reveals a hierarchy of interactions between polycystin-encoding genes and genes controlling cilia function during left-right determination. *PLoS Genet* **12**(6), e1006070.

Grimm, C., Cuajungco, M. P., van Aken, A. F., Schnee, M., Jörs, S., Kros, C. J. *et al*. (2007). A helix-breaking mutation in TRPML3 leads to constitutive activity underlying deafness in the varitint-waddler mouse. *PNAS U S A* **104**(49), 19583-8.

Grimm, C., Jörs, S., Guo, Z., Obukhov, A. G. and Heller, S. (2012). Constitutive activity of TRPML2 and TRPML3 channels versus activation by low extracellular sodium and small molecules. *J Biol Chem* **287**(27), 22701-8.

Grimm, C., Hassan, S., Wahl-Schott, C. and Biel, M. (2012b). Role of TRPML and two-pore channels in endo-lysosomal cation homeostasis. *J Pharmacol Exp Ther* **342**, 236-244.

Groner, M. and Malchow, D. (1996). Calmodulin-antagonists inhibit vesicular Ca^{2+} uptake in *Dictyostelium*. Cell Calcium **19**, 105-111.

Gross, J. D. (2009). Acidic Ca^{2+} stores, excitability, and cell patterning in *Dictyostelium* discoideum. *Eukaryot Cell* **8**(5), 696-702.

Tirlapur, U. K., Gross, J. and Nanjundiah, V. (1991). Spatial variation of sequestered calcium in multicellular stage of *Dictyostelium discoideum* as assayed by chlortetracycline fluorescence. *Differentiation* **48**, 137-146.

Guerini, D., Zecca-Mazza, A. and Carafoli, E. (2000). Single amino acid mutations in transmembrane domain 5 confer to the plasma membrane Ca^{2+} pump properties typical of the Ca^{2+} pump of endo(sarco)plasmic reticulum. *J Biol Chem* **275**, 31361–31368.

Gunter, K. K. and Gunter, T. E. (1994). *Transport of calcium by mitochondria*. *J Bioenerg Biomembr* **26**, 471–485.

Habermacher, C., Dunning, K., Chataigneau, T., and Grutter T. (2016). Molecular structure and function of P2X receptors. *Neuropharmacology* **104**, 18-30.

Hammes, A., Oberdorf, S., Strehler, E. E., Stauffer, T., Carafoli, E., Vetter, H. *et al*. (1994). Differentiation-specific isoform mRNA expression of the calmodulin-dependent plasma membrane Ca^{2+}-ATPase. *FASEB J* **8**, 428–435.

Han, J., Pluhackova, K., and Böckmann, R. A. (2017). The multifaceted role of SNARE proteins in membrane fusion. *Front Physiol* **8**, 5.

Hanahan, D. (1983). Studies on transformation of Escherichia coli with plasmids. *J Mol Biol* **166**, 557-580.

Hanaoka, K., Qian, F., Boletta, A., Bhunia, A. K., Piontek, K., Tsiokas, L. *et al*. (2000). Co-assembly of polycystin-1 and -2 produces unique cation-permeable currents. *Nature* **408**(6815), 990-994.

Hay, J. C. (2007). Calcium, a fundamental regulator of membrane fusion? *EMBO rep* **8**(3), 236-40.

Hegedus, L., Zámb,ó, B., Pászty, K., Padányi, R., Varga, K., Penniston, J. T., and Enyedi, Á. (2020). Molecular diversity of plasma membrane Ca^{2+} transporting ATPases: their function under normal and pathological conditions. *Adv Exp Med Biol* **1131**, 93–129.

Hereld, D. and Devreotes, P. N. (1992). The cAMP receptor family of *Dictyostelium. Int Rev Cytol* **137B**, 35-47.

Hilge, M., Aelen, J. and Vuister, G. W. (2006). Ca^{2+} regulation in the Na^{+}/Ca^{2+} exchanger involves two markedly different Ca^{2+} sensors. *Mol Cell* **22**(1),15-25.

Horn, F. *and* Gross, J. (1996). A role for calcineurin in *Dictyostelium discoideum* development. *Differentiation* **60**, 269–275.

Huber, R. J. (2020). Molecular networking in the neuronal ceroid lipofuscinoses: insights from mammalian models and the social amoeba *Dictyostelium discoideum*. *J Biomed Sci* **27**(1), 64.

Huber, R. J., Myre, M. A. and Cotman, S. L. (2014). Loss of Cln3 Function in the social amoeba *Dictyostelium discoideum* causes pleiotropic effects that are rescued by human CLN3. *PLoS ONE* **9**(10): e110544.

Huber, R. J., Myre, M. A. and Cotman, S. L. (2017). Aberrant adhesion impacts early development in a *Dictyostelium* model for juvenile neuronal ceroid lipofuscinosis. *Cell Adh Migr* **11**(4), 399-418.

Huber, R. J. and Mathavarajah, S. (2019). Comparative transcriptomics reveals mechanisms underlying cln3-deficiency phenotypes in *Dictyostelium*. *Cell Signal* **58**, 79-90.

Hughes, J., Ward, C. J., Peral, B., Aspinwall, R., Clark, K., San Millan, J. L., Gamble, V. and Harris, P. C. (1995). The Polycystic kidney disease 1 (PKD1) gene encodes a novel protein with multiple cell recognition domains. *Nat Genet* **10**, 151–160.

Jain, R., Yuen, I. S., Taphouse, C. R. and Gomer, R. H. (1992). A density-sensing factor controls development in *Dictyostelium*. *Genes Dev* **6**(3), 390-400.

Ilacqua, A. N., Price, J. E., Graham, B. N., Buccilli, M. J., McKellar, D. R. and Damer, C. K. (2018). Cyclic AMP signaling in *Dictyostelium* promotes the translocation of the copine family of calcium-binding proteins to the plasma membrane. *BMC Cell Biol* **19**(1), 13.

Jaiswal, J. K. and Nanjundiah, V. (2003). Calcium regulates the expression of a *Dictyostelium discoideum* asparaginyl tRNA synthetase gene. *J Biosci* **28**, 697–707.

James, P., Inui, M., Tada, M., Chiesi, M. and Carafoli, E. (1989). Nature and site of phospholamban regulation of the Ca^{2+} pump of sarcoplasmic reticulum. *Nature* **342**(6245), 90-2.

Jenne, N., Rauchenberger, R., Hacker, U., Kast, T. and Maniak, M. (1998). Targeted gene disruption reveals a role for vacuolin B in the late endocytic pathway and exocytosis. *J Cell Sci* **111**, 61–70.

Jennings, J. J. Jr., Zhu, J., Rbaibi, Y., Luo, X., Chu, C. T. and Kiselyov, K. (2006). Mitochondrial aberrations in mucolipidosis Type IV *J Biol Chem* **281**, 39041-39050.

Ji, Y., Lalli, M. J., Babu, G. J., Xu, Y., Kirkpatrick, D. L., Liu, L. H. *et al.* (2000). Disruption of a single copy of the SERCA2 gene results in altered Ca^{2+} homeostasis and cardiomyocyte function. *J Biol Chem* **275**(48), 38073-80.

John, L. M., Lechleiter, J. D. and Camacho, P. (1998). Differential modulation of SERCA2 isoforms by calreticulin. *J Cell Biol* **142**(4), 963–73.

Jurado, L. A., Chockalingam, P. S. and Jarrett, H. W. (1999). Apocalmodulin. *Physiol Rev* **79**(3), 661-82.

Karczewski, P., Kuschel, M., Baltas, L. G., Bartel, S., Krause, E. G. (1997). Site-specific phosphorylation of a phospholamban peptide by cyclic nucleotide- and Ca^{2+}/calmodulin-dependent protein kinases of cardiac sarcoplasmic reticulum. *Basic Res Cardiol* **92 Suppl 1**, 37-43.

Kay, R. R. (1987). Cell differentiation in monolayers and the investigation of slime mold morphogens. *Methods Cell Biol* **28**, 433–448.

Kessin R. H. (2001). *Dictyostelium*—evolution, cell biology, and the development of multicellularity. Cambridge University Press, New York, NY.

Kilpatrick, B. S., Eden, E. R., Schapira, A. H., Futter, C. E. and Patel, S. (2013). Direct mobilisation of lysosomal Ca^{2+} triggers complex Ca^{2+} signals. *J Cell Sci* **126**, 60-66.

Kilpatrick, B. S., Yates, E., Grimm, C., Schapira, A. H. and Patel, S. (2016). Endo-lysosomal TRP mucolipin-1 channels trigger global ER Ca^{2+} release and Ca^{2+} influx. *J Cell Sci* **129**(20), 3859-3867.

Kim, H. J., Li, Q., Tjon-Kon-Sang, S., So, I., Kiselyov, K. and Muallem, S. (2007). Gain-of-function mutation in TRPML3 causes the mouse varitint-waddler phenotype. *J Biol Chem* **282**, 36138 –36142.

Kim, H. J., Yamaguchi, S., Li, Q., So, I. and Muallem, S. (2010). Properties of the TRPML3 channel pore and its stable expansion by the Varitint-Waddler-causing mutation. *J Biol Chem* **285**(22), 16513-20.

Kim, B., Takeuch, I. A., Koga, O., Hikida, M. and Matsuoka S. (2013). Mitochondria Na^{+}-Ca^{2+} exchange in cardiomyocytes and lymphocytes. *Adv Exp Med Biol **961**, 193-201.*

Kim, B., Takeuchi, A., Hikida, M. and Matsuoka, S. (2016). Roles of the mitochondrial Na^{+}-Ca^{2+} exchanger, NCLX, in B lymphocyte chemotaxis. *Sci Rep* **22**(6), 28378.

Kintzer, A. F and Stroud, R. M. (2018). On the structure and mechanism of two-pore channels. *FEBS J* **285**(2), 233-243.

Kirichok, Y., Krapivinsky, G. and Clapham, D. E. (2004). The mitochondrial calcium uniporter is a highly selective ion channel. *Nature* **427**, 360-364.

Kiselyov, K., Chen, J., Rbaibi, Y., Oberdick, D., Tjon-Kon-Sang, S., Shcheynikov, N. *et al.* (2005). TRP-ML1 is a lysosomal monovalent cation channel that undergoes proteolytic cleavage. *J Biol Chem* **280***,* 43218–43223*.*

Kiselyov, K., Yamaguchi, S., Lyons, C. W., and Muallem, S. (2010). Aberrant Ca^{2+} handling in lysosomal storage disorders. *Cell Calcium* **47**, 103–111.

Klein, G. and Satre, M. (1986). Kinetics of fluid-phase pinocytosis in *Dictyostelium discoideum* amoebae. *Biochem Biophys Res Commun* **138**, 1146–1152.

Kollmar, M. (2006). Thirteen is enough: the myosins of *Dictyostelium discoideum* and their light chains. *BMC Genomics* **7**, 183.

Kopachik, W., Oohata, A., Dhokia, B., Brookman, J. J. and Kay, R. R. (1983). *Dictyostelium* mutants lacking DIF, a putative morphogen. *Cell* **33**, 397-403.

Kotsifas, M., Barth, C., Lay, S. T., de Lozanne, A. and Fisher, P. R. (2002). Chaperonin 60 and mitochondrial disease in *Dictyostelium. J Muscle Res Cell Motil* **23**, 839–852.

Köttgen, M., Buchholz, B., Garcia-Gonzalez, M. A., Kotsis, F., Fu, X., Doerken, M. *et al*. (2008). TRPP2 and TRPV4 form a polymodal sensory channel complex. *J Cell Biol* **182**(3), 437–447.

Koulen, P., Cai, Y., Geng, L., Maeda, Y., Nishimura, S., Witzgall, R. *et al*. (2002). Polycystin-2 is an intracellular calcium release channel. *Nat Cell Biol* **4**, 191–197.

Koulen, P., Duncan, R. S., Liu, J., Cohen, N. E., Yannazzo, J. A., McClung, N. *et al*. (2005). Polycystin-2 accelerates Ca^{2+} release from intracellular stores in *Caenorhabditis elegans*. *Cell Calcium* **37**(6), 593-601.

Kovács-Bogdán, E., Sancak, Y., Kamer, K. J., Plovanich, M., Jambhekar, A., Huber, R. J., Myre, M. A., Blower, M. D., and Mootha, V. K. (2014). Reconstitution of the mitochondrial calcium uniporter in yeast. *PNAS* **111**(24), 8985-8990.

Kreppel, L., Fey, P., Gaudet, P., Just, E., Kibbe, W. A., Chisholm, R. L., and Kimmel, A. R. (2004). dictyBase: a new *Dictyostelium discoideum* genome database. *Nucleic Acids Research*, **32**, (Database issue), D332–D333.

Kuhlmann, M., Popova, B. and Nellen, W. (2006). RNA interference and antisense-mediated gene silencing in *Dictyostelium*. *Methods Mol Biol* **346**, 211-26.

Kuo, I. Y., Keeler, C., Corbin, R., Ćelić, A., Petri, E. T., Hodsdon, M. E., and Ehrlich, B. E. (2014). The number and location of EF hand motifs dictates the calcium dependence of polycystin-2 function. *FASEB J* **28**(5), 2332–2346.

Kushner, S. R., Nagaishi, H., Templin, A. and Clark, A. J. (1971). Genetic Recombination in *Escherichia coli*: The Role of Exonuclease I. *PNAS* **68**, 824-827.

Kuwayama, H. and Van Haastert, P. J. (1998). cGMP potentiates receptor stimulated Ca^{2+} influx in *Dictyostelium discoideum*. *Biochim Biophys Acta* **1402**, 102–108.

Lagostena, L., Festa, M., Pusch, M. and Carpaneto, A. (2017). The human two-pore channel 1 is modulated by cytosolic and luminal calcium. *Sci Rep* **7**, 43900.

Lam, D., Kosta, A., Luciani, M.F. and Golstein, P. (2008). The Inositol 1,4,5-Trisphosphate receptor is required to signal autophagic cell death. *Mol Biol Cell* **19**, 691–700.

Lam, A. K. and Galione, A. (2013). The endoplasmic reticulum and junctional membrane communication during calcium signaling. *Biochim Biophys Acta.* **1833**(11), 2542-59.

Lange, I., Penner, R., Fleig, A., Beck, A. (2008). Synergistic regulation of endogenous TRPM2 channels by adenine dinucleotides in primary human neutrophils. *Cell Calcium.* **44**(6), 604-15.

Lange, I., Yamamoto, S., Partida-Sanchez, S., Mori, Y., Fleig, A. and Penner, R. (2009). TRPM2 functions as a lysosomal Ca^{2+}-release channel in beta cells. *Sci Signal* **2**(71), ra23.

LaPlante, J. M., Falardeau, J., Sun, M., Kanazirska, M., Brown, E. M., Slaugenhaupt, S. A. *et al*. (2002). Identification and characterization of the single channel function of human mucolipin-1 implicated in mucolipidosis type IV, a disorder affecting the lysosomal pathway. *FEBS Lett* **532**, 183-187.

LaPlante, J. M., Ye, C. P., Quinn, S. J., Goldin, E., Brown, E. M., Slaugenhaupt, S. A. *et al*. (2004). Functional links between mucolipin-1 and Ca^{2+}-dependent membrane trafficking in mucolipidosis IV. *Biochem Biophys Res Commun* **322**, 1384–1391.

LaPlante, J. M., Sun, M., Falardeau, J., Dai, D., Brown. E,M., Slaugenhaupt, S.A. *et al*. (2006). Lysosomal exocytosis is impaired in mucolipidosis type IV. *Mol Genet Metab* **89**(4), 339-48.

Lawe, D. C., Sitouah, N., Hayes, S., Chawla, A., Virbasius, J. V., Tuft, R. *et al*. (2003). Essential role of Ca^{2+}/Calmodulin in early endosome antigen-1 localization. *Mol Biol Cell* **14**(7), 2935–2945.

Lee, K., Jo, Y. Y., Chung, G., Jung, J. H., Kim, Y. H., and Park, C. K. (2021). Functional importance of transient receptor potential (TRP) channels in neurological disorders. *Front Cell Dev Biol* **9**:611773.

Lelouvier, B. and Puertollano, R. (2011). Mucolipin-3 regulates luminal calcium, acidification, and membrane fusion in the endosomal pathway. *J Biol Chem* **286**, 9826–9832.

Lemasters, J. J., Theruvath, T. P., Zhong, Z. and Nieminen, A. L. (2009). Mitochondrial calcium and the permeability transition in cell death. *Biochim Biophys Acta* **1787**, 1395–1401.

Li, Y., Wright, J. M., Qian, F., Germino, G. G. and Guggino, W. B. (2005). Polycystin 2 interacts with type I inositol 1,4,5-trisphosphate receptor to modulate intracellular Ca^{2+} signaling. *J Biol Chem* **280**, 41298–41306.

Li, M., Zhang, W. K., Benvin, N. M., Zhou, X., Su, D., Li, H. *et al*. (2017). Structural basis of Ca^{2+}/pH dual regulation of the endolysosomal TRPML1 channel. *Nature Structural and Molecular Biology*, **24**(3), 205–213.

Li, W., Liang, J., Outeda, P., Turner, S., Wakimoto, B. T. and Watnick, T. (2020). A genetic screen in *Drosophila* reveals an unexpected role for the KIP1 ubiquitination-promoting complex in male fertility. *PLoS Genet* **16**(12), e1009217.

Liang, G., Yang, J., Wang, Z., Li, Q., Tang, Y., Chen, X. Z. (2008). Polycystin-2 down-regulates cell proliferation via promoting PERK-dependent phosphorylation of eIF2alpha. *Hum Mol Genet* **17**, 3254–3262.

Lièvremont JP, Rizzuto R, Hendershot L, Meldolesi J. (1997). BiP, a major chaperone protein of the endoplasmic reticulum lumen, plays a direct and important role in the storage of the rapidly exchanging pool of Ca^{2+}. *J Biol Chem* **272**(49), 30873-9.

Lima, W. C., Leuba, F., Soldati, T., and Cosson, P. (2012). Mucolipin controls lysosome exocytosis in *Dictyostelium*. *J Cell Sci* **125**, 2315–2322.

Lima, W. C., Vinet, A., Pieters, J. and Cosson, P. (2014). Role of PKD2 in Rheotaxis in *Dictyostelium*. *PLoS One* **9**(2): e88682.

Liu, T., Williams, G. and Clarke, M. (1992). Inducible expression of calmodulin antisense RNA in *Dictyostelium* cells inhibits the completion of cytokinesis. *Mol Biol Cell* **3**, 1403-1413.

Liu, W., Xu, S., Woda, C., Kim, P., Weinbaum, S., and Satlin, L. M. (2003). Effect of flow and stretch on the $[Ca^{2+}]_i$ response of principal and intercalated cells in cortical collecting duct. *Am J Physiol Renal Physiol* **285**(5), F998–F1012.

Liu, X., Vien, T., Duan, J., Sheu, S. H., DeCaen, P. G. and Clapham, D. E. (2018). Polycystin-2 is an essential ion channel subunit in the primary cilium of the renal collecting duct epithelium. *eLife* **7**, e33183.

Lloyd-Evans, E., Peterneva, K., Lewis, A., Churchill, G. and Platt, F. (2008). Abnormal lysosomal calcium homeostasis in mucolipidosis type IV. *Mol Genet Metab* **93**, S29–S30.

Lombardi, M. L., Knecht, D. A. and Lee, J. (2008). Mechano-chemical signaling maintains the rapid movement of *Dictyostelium* cells. *Exp Cell Res* **314**, 1850-1859.

López, J., Dionisio, N., Berna-Erro, A., Galán, C., Salido, G. M., and Rosado, J. A. (2012). Two-pore channel 2 (TPC2) modulates store-operated Ca^{2+} entry. *Biochim Biophys Acta* **1823**(10), 1976-83.

López-Sanjurjo, C. I., Tovey, S. C., Prole, D. L., and Taylor, C. W. (2013). Lysosomes shape Ins(1,4,5)P3-evoked Ca^{2+} signals by selectively sequestering Ca^{2+} released from the endoplasmic reticulum. *J. Cell Sci* **126**(1), 289-300.

López Sanjurjo, C. I., Tovey, S. C. and Taylor, C. W. (2014). Rapid recycling of Ca^{2+} between IP3-sensitive stores and lysosomes. *PLoS One* **9**(10), e111275.

Lu, J., Boheler, K. R., Jiang, L., Chan, C. W., Tse, W. W., Keung, W. *et al*. (2018). Polycystin-2 plays an essential role in glucose starvation-induced autophagy in human embryonic stem cell-derived cardiomyocytes. *Stem Cells* **36**(4), 501-513.

Lubensky, I. A., Schiffmann, R., Goldin, E. and Tsokos, M. (1999). Lysosomal inclusions in gastric parietal cells in Mucolipidosis type IV: a novel cause of achlorhydria and hypergastrinemia. *Am J Surg Pathol* **23**, 1527-1531.

Luciani, M. F., Kubohara, Y., Kikuchi, H., Oshima, Y. and Golstein, P. (2009). Autophagic or necrotic cell death triggered by distinct motifs of the differentiation factor DIF-1. *Cell Death Differ* **16**, 564-70.

Luciani, M. F., Giusti, C., Marms, B., Oshima, Y., Kikuchi, H., Kubohara, Y. *et al*. (2011). Atg1 allows second-signaled autophagic cell death in *Dictyostelium*. *Autophagy* **7**, 501-508.

Ludlow, J., Traynor, D., Fisher, R., Ennion, J. (2008). Purinergic-mediated Ca^{2+} influx in *Dictyostelium discoideum*. *Cell Calcium* **44**, 567-79.

Ludlow, J., Durai, L., Ennion, J. (2009). Functional characterization of intracellular *Dictyostelium discoideum* P2X receptors. *J Biol Chem* **284**, 35227-39.

Luo, Y., Vassilev, P. M., Li, X., Kawanabe, Y. and Zhou, J. (2003). Native polycystin-2 functions as a plasma membrane Ca^{2+}-permeable cation channel in renal epithelia. *Mol Cell Biol* **23**(7), 2600–2607.

Lusche, D. F. and Malchow, D. (2005). Developmental control of cAMP-induced Ca^{2+}-influx by cGMP: influx is delayed and reduced in a cGMP-phosphodiesterase D deficient mutant of *Dictyostelium discoideum*. *Cell Calcium* **37**(1), 57-67.

Lusche, D. F., Bezares-Roder, K., Happle, K., Schlatterer, C. (2005). cAMP controls cytosolic Ca^{2+} levels in *Dictyostelium discoideum*. *BMC Cell Biology* **6(1)**, 12.

Lusche, D. F., Wessels, D. and Soll, D. R. (2009). The effects of extracellular calcium on motility, pseudopod and uropod formation, chemotaxis, and the cortical localization of myosin II in *Dictyostelium discoideum*. *Cell Motil Cytoskeleton* **66**, 567-587.

Lusche, D. F., Wessels, D., Ryerson, D. E. and Soll, D. R. (2011). Nhe1 is essential for potassium but not calcium facilitation of cell motility and the monovalent cation requirement for chemotactic orientation in *Dictyostelium discoideum*. *Eukaryot Cell* **10**, 320-331.

Lusche, D. F., Wessels, D., Scherer, A., Daniels, K., Kuhl, S. and Sol,l D. R. (2012). The IplA Ca^{2+} channel of *Dictyostelium discoideum* is necessary for Ca^{2+}, but not cAMP

chemotaxis, and plays a fundamental role in natural aggregation. *J Cell Sci* **125**(7), 1770-83.

Luz JM, Lennarz WJ. (1996). Protein disulfide isomerase: a multifunctional protein of the endoplasmic reticulum. *EXS* **77**, 97-117.

Luzio, J. P., Bright, N. A. and Pryor, P. R. (2007). The role of calcium and other ions in sorting and delivery in the late endocytic pathway. *Biochem Soc Trans* **35**(5), 1088-1091.

Luzio, J. P., Pryor, P. R. and Bright, N. A. (2007a). Lysosomes: fusion and function. *Nat Rev Mol Cell Biol* **8**(8), 622-32.

Lydan, M. A. and Cotter, D. A. (1995). The role of Ca^{2+} during spore germination in *Dictyostelium*: autoactivation is mediated by the mobilization of Ca^{2+} while amoebal emergence requires entry of external Ca^{2+}. *J Cell Sci* **108**(5), 1921-30.

Lytton, J., Westlin, M. and Hanley, M.R. (1991). Thapsigargin inhibits the sarcoplasmic or endoplasmic reticulum Ca^{2+}-ATPase family of calcium pumps. *J Biol Chem* 266, 17067–17071.

Ma, R., Li, W. P., Rundle, D., Kong, J., Akbarali, H.I . and Tsiokas, L. (2005). PKD2 functions as an epidermal growth factor-activated plasma membrane channel. *Mol Cell Biol* **25**(18), 8285–8298.

Maeda, Y. (1970). Influence of ionic conditions on cell differentiation and morphogenesis of the cellular slime molds. *Dev Growth Differ* **12**(3), 217-27.

Maeda, Y., and Maeda, M. (1973). The calcium content of the cellular slime mold, *Dictyostelium discoideum*, during development and differentiation. *Exp Cell Res* **82**(1), 125-30.

Maeda, Y. and Kawamoto, T. (1986). Pinocytosis in *Dictyostelium discoideum* cells: A possible implication of cytoskeletal actin for pinocytotic activity. *Exp Cell Res* **164**(2), 516-526.

Malchow, D., Schaloske, R., and Schlatterer, C. (1996). An increase in cytosolic Ca^{2+} delays cAMP oscillations in *Dictyostelium* cells. *Biochem J* **319**(1), 323-7.

Malchow, D., Mutzel, R., and Schlatterer, C. (1996a). On the role of calcium during chemotactic signalling and differentiation of the cellular slime mould *Dictyostelium discoideum. J Dev Biol* **40**(1), 135-9.

Malchow, D., Lusche, D. F. and Schlatterer, C. (2004). A link of Ca^{2+} to cAMP oscillations in *Dictyostelium*: the calmodulin antagonist W-7 potentiates cAMP relay and transiently inhibits the acidic Ca^{2+}-store. *BMC Dev Biol* **17**, 4-7.

Malchow, D., Lusche, D. F., Schlatterer, C., De Lozanne, A., and Müller-Taubenberger, A. (2006). The contractile vacuole in Ca^{2+}-regulation in *Dictyostelium*: its essential function for cAMP-induced Ca^{2+}-influx. *BMC Developmental Biology* **6**, 31.

Malchow, D., Lusche, D. F., De Lozanne, A. and Schlatterer, C. (2008). A fast Ca^{2+}-induced Ca^{2+}-release mechanism in *Dictyostelium discoideum*. *Cell Calcium* **43**(6), 521-30.

Mallilankaraman, K., Doonan, P., Cárdenas, C., Chandramoorthy, H. C., Müller, M., Miller, R. *et al.* (2012). MICU1 is an essential gatekeeper for MCU-mediated mitochondrial Ca^{2+} uptake that regulates cell survival. *Cell* **151**, 630-644.

Mandal, A., Liyanage, M. R., Zaidi, A., and Johnson, C. K. (2008). Interchange of autoinhibitory domain conformations in plasma-membrane Ca^{2+}-ATPase–calmodulin complexes. *Protein Sci* **17**(3), 555–562.

Maniak, M. (2001). Fluid-phase uptake and transit in axenic *Dictyostelium* cells. *Biochim Biophys Acta* **1525**, 197–204.

Maniak, M. (2003). Fusion and fission events in the endocytic pathway of *Dictyostelium. Traffic* **4**, 1-5.

Maniak, M. (2011). *Dictyostelium* as a model for human lysosomal and trafficking diseases. *Semin Cell Dev Biol* **22**(1), 114-119.

Manzoni, M., Monti, E., Bresciani, R., Bozzato, A., Barlati, S., Bassi, M. T. *et al*. (2004). Overexpression of wild-type and mutant mucolipin proteins in mammalian cells: effects on the late endocytic compartment organization. *FEBS Letters* **567**, 219-224.

Marcassa, E., Raimondi, M., Anwar, T., Eskelinen, E. L., Myers, M. P., Triolo, G., *et al*. (2017). Calpain mobilizes Atg9/Bif-1 vesicles from Golgi stacks upon autophagy induction by thapsigargin. *Biology Open* **6**, 551–562.

Marchesini, N., Ruiz, F. A., Vieira, M. and Docampo, R. (2002). Acidocalcisomes are functionally linked to the contractile vacuole of *Dictyostelium* discoideum, *J Biol Chem* **277**, 8146–8153.

Marchi, S. and Pinton, P. (2014). The mitochondrial calcium uniporter complex: Molecular components, structure and physiopathological implications. *J Physiol* **592**, 829–839.

Marchi, S., Patergnani, S. and Pinton, P. (2014). The Endoplasmic reticulum-mitochondria connection: one touch, multiple functions. *Biochim Biophys Acta* **1837**(4), 461–469.

Marchi, S., Bittremieux, M., Missiroli, S., Morganti, C., Patergnani, S., Sbano, L. *et al*. (2017). Endoplasmic reticulum-mitochondria communication through Ca^{2+} Signalling: The importance of mitochondria-associated membranes (MAMs). *Adv Exp Med Biol* **997**, 49-67.

Marshak, D. R., Clarke, M., Roberts, D. M. and Watterson, D. M. (1984). Structural and functional properties of calmodulin from the eukaryotic microorganism *Dictyostelium discoideum*. *Biochemistry* **23**, 2891–2899.

Martina, J. A., Lelouvier, B. and Puertollano, R. (2009). The calcium channel mucolipin-3 is a novel regulator of trafficking along the endosomal pathway. *Traffic* **10**, 1143–1156.

Martín-González, J., Montero-Bullón, J. F., and Lacal, J. (2021). *Dictyostelium discoideum* as a non-mammalian biomedical model. *Microb. Biotechnol* **14**(1), 111-125.

Maselli, A., Laevsky, G. and Knecht, D. A. (2002). Kinetics of binding, uptake and degradation of live fluorescent (DsRed) bacteria by *Dictyostelium discoideum*. *Microbiology* **148**(2), 413-20.

McLaren, M. D., Mathavarajah, S., Kim, W. D., Yap, S. Q., and Huber, R. J. (2021). Aberrant autophagy impacts growth and multicellular development in a *Dictyostelium* KO model of CLN5 disease. *Front cell dev biol*, **9**, 657406.

Medina D. L., Di Paola, S., Peluso, I., Armani, A., De Stefani, D., Venditti, R. *et al*. (2015). Lysosomal calcium signalling regulates autophagy through calcineurin and TFEB. *Nat Cell Biol* **17**, 288–299.

Melchionda, M., Pittman, J. K., Mayor, R. and Patel, S. (2016). Ca^{2+}/H^{+} exchange by acidic organelles regulates cell migration in vivo. *J Cell Biol* **212**(7), 803-13.

Meldolesi, J. and Pozzan,T. (1998). The endoplasmic reticulum Ca^{2+} store: a view from the lumen. *Trends Biochem*. *Sci.* 23, 10–14.

Menz, S., Bumann, J., Jaworski, E. and Malchow, D. (1991). Mutant analysis suggests that cyclic GMP mediates the cyclic AMP induced Ca^{2+} uptake in *Dictyostelium*. J Cell Sci **99** (1), 187–191.

Mesaeli, N., Nakamura, K., Zvaritch, E., Dickie, P., Dziak, E., Krause, K. H., *et al*. (1999). Calreticulin is essential for cardiac development. *J Cell Biol* **144**(5), 857-68.

Mesquita, A., Cardenal-Muñoz, E., Dominguez, E., Muñoz-Braceras, S., Nuñez-Corcuera, B., Phillips, B. A. *et al*. (2017). Autophagy in *Dictyostelium*: Mechanisms, regulation and disease in a simple biomedical model. *Autophagy* **13**(1), 24–40.

Micsenyi, M. C., Dobrenis, K., Stephney, G., Pickel, J., Vanier, M. T., Slaugenhaupt, S. A. *et al*. (2009). Neuropathology of the Mcoln1(-/-) knockout mouse model of mucolipidosistypeIV. *J Neuropathol Exp Neurol* **68**, 125–135.

Miedel, M.T., Weixel, K. M., Bruns, J. R., Traub, L. M. and Weisz O. A. (2006). Posttranslational cleavage and adaptor protein complex-dependent trafficking of mucolipin-1. *J Biol Chem* **281**(18), 12751-12759.

Miedel, M. T., Rbaibi, Y., Guerriero, C. J. Colletti, G., Weixel, K. M., Weisz, O.A. *et al*. (2008). Membrane traffic and turnover in TRP-ML1-deficient cells: a revised model for mucolipidosis type IV pathogenesis. *J Exp Med* **205**, 1477-1490.

Miller, R. J. (1992). Voltage-sensitive Ca^{2+} channels. *J Biol Chem* **267**, 1403–1406.

Mills, I. G., Jones, A. T. and Clague, M. J. (1998). Involvement of the endosomal autoantigen EEA1 in homotypic fusion of early endosomes. *Curr Biol* **8**, 881-884.

Milne, L. and Coukell, B. (1988). Isolation and characterization of a plasma membrane calcium pump from *Dictyostelium discoideum*. *Biochem J* **249**, 223-30.

Milne, J. L. and Coukell, M. B. (1989). Identification of a high-affinity Ca^{2+} pump associated
with endocytotic vesicles in *Dictyostelium discoideum*. *Exp Cell Res* **185**(1), 21–32.

Milne, J. L. and Coukell, M. B. (1991). A Ca^{2+} transport system associated with the plasma membrane of *Dictyostelium discoideum* is activated by different chemoattractant receptors. *J Cell Biol* **112**, 103-110.

Milne, J. L. and Devreotes, P. N. (1993). The surface cyclic AMP receptors, cAR1, cAR2, and cAR3, promote Ca^{2+} influx in *Dictyostelium discoideum* by a G alpha 2- independent mechanism. *Mol Biol Cell* **4**, 283-292.

Milne, J. L., Wu, L., Caterina, M. J. and Devreotes, P. N. (1995). Seven helix cAMP receptors stimulate Ca^{2+} entry in the absence of functional G proteins in *Dictyostelium.* J Biol Chem **270**, 5926–5931.

Missiroli, S., Danese, A., Iannitti, T., Patergnani, S., Perrone, M., Previati, M. *et al.* (2017). Endoplasmic reticulum-mitochondria Ca^{2+} crosstalk in the control of the tumor cell fate. *Biochim Biophys Acta* **1864**(6), 858–864.

Mochizuki, T., Wu, G., Hayashi, T., Xenophontos, S. L., Veldhuisen, B., Saris, J. J. *et al*. (1996). PKD2, a gene for polycystic kidney disease that encodes an integral membrane protein. *Science* **272**, 1339–1342.

Moniakis, J., Coukell, M. B. and Forer, A. (1995). Molecular cloning of an intracellular P-type ATPase from *Dictyostelium* that is up-regulated in calcium-adapted cells. *J Biol Chem* **270**(47), 28276–28281.

Moniakis, J., Coukell, M. B. and Janiec, A. (1999). Involvement of the Ca^{2+}-ATPase PAT1 and the contractile vacuole in calcium regulation in *Dictyostelium discoideum*. *J Cell Sci.* 112, 405–414.

Montell, C., Birnbaumer, L. and Flockerzi, V. (2002). The TRP channels, a remarkably functional family. *Cell.* **108**(5), 595-8.

Mony, V. K., Benjamin, S., and O'Rourke, E. J. (2016). A lysosome-centered view of nutrient homeostasis. *Autophagy* **12**(4), 619–631.

Morel, N., Vandenberg, G., Ahrabi, A. K., Caron, N., Desjardins, F., Balligand, J. L. *et al*. (2009). PKD1 haploinsufficiency is associated with altered vascular reactivity and abnormal calcium signaling in the mouse aorta. *Pflugers Arch* **457**(4), 845–856.

Morgan, A. J., Platt, F. M., Lloyd-Evans, E., Galione, A. (2011). Molecular mechanisms of endolysosomal Ca^{2+} signalling in health and disease. *Biochem J* **439**(3), 349-74.

Morris, H. R., Taylor, G. W., Masento, M. S., Jermyn, K. A. and Kay, R. R. (1987). Chemical structure of the morphogen differentiation inducing factor from *Dictyostelium discoideum Nature 328*(6133), 811-4.

Muller-Taubenberger, A., Lupas, A. N., Li, H., Ecke, M., Simmeth, E., and Gerisch, G. (2001). Calreticulin and calnexin in the endoplasmic reticulum are important for phagocytosis. *EMBO J* **20**(23), 6772–6782.

Müller, I., Šubert, N., Otto, H., Herbst, R., Rühling, H., Maniak, M. and Leippe M. (2005). A *Dictyostelium* mutant with reduced lysozyme levels compensates by increased phagocytic activity. *J Biol Chem* **280**, 10435–10443.

Myre, M. A. and O'Day, D. H. (2002). Nucleomorphin: A novel, acidic, nuclear calmodulin-binding protein from *Dictyostelium* that regulates nuclear number *J Biol Chem* **277**, 19735.

Nagai, T., Sawano, A., Park, E. S. and Miyawaki, A. (2001). Circularly permuted green fluorescent proteins engineered to sense Ca^{2+}. *PNAS USA* **98**, 3197–3202.

Nakamura, K., Zuppini, A., Arnaudeau, S., Lynch, J., Ahsan, I., Krause, R. *et al*. (2001). Functional specialization of calreticulin domains. *J Cell Biol* **154**(5), 961-72.

Naraynan, N. and Xu, A. (1997). Phosphorylation and regulation of the Ca^{2+}-pumping ATPase in cardiac sarcoplasmic reticulum by calcium/calmodulin-dependent protein kinase *Basic Res Cardiol* **92**(Suppl 1), 25.

Nauli, S. M., Alenghat, F. J., Luo, Y., Williams, E., Vassilev, P., Li, X. *et al*. (2003). Polycystins 1 and 2 mediate mechanosensation in the primary cilium of kidney cells. *Nat Genet* **33**, 129–137.

Nebl, T. and Fisher, P. R. (1997). Intracellular Ca^{2+} responses by *Dictyostelium* amoebae to nanomolar chemoattractant stimuli are mediated exclusively by Ca^{2+} influx. *J Cell Sci* **110**, 2845-2853.

Nebl, T., Kotsifas, M., Schaap, P. and Fisher, P. R. (2002). Multiple pathways connect chemoattractant receptors and Ca^{2+} channels in *Dictyostelium*. *J Muscle Res Cell Motil* **23**, 853–865.

Neher E. (1998). Vesicle pools and Ca^{2+} microdomains: new tools for understanding their roles in neurotransmitter release. *Neuron* **20**, 389–399.

Nellen, W., Silan, C., Firtel, R. A. (1984). DNA-Mediated transformation in *Dictyostelium discoideum*: regulated expression of an actin gene fusion. *Mol Cell Biol* **4**, 2890–2898.

Neuhaus, E. M. and Soldati, T. (1999). Molecular mechanisms of membrane trafficking. What do Ilearn from *D. discoideum*? *Protist* **150**, 235–243.

Neuhaus, E. M., Almers, W. and Soldati, T. (2002). Morphology and dynamics of the endocytic pathway in *Dictyostelium discoideum*. *Mol Biol Cell* **13**, 1390-1407.

Newell, P. C., Malchow, D. and Gross, J. D. (1995). The role of calcium in aggregation and development of *Dictyostelium*. *Experientia* **51**(12), 1155-1165.

North, R. A. (2016). P2X receptors. *Philos Trans R Soc Lond B Biol Sci* **371**(1700), 20150427.

Nunomura, W., Takakuwa, Y., Parra, M., Conboy, J. G. and Mohandas, N. (2000). Ca^{2+}-dependent and Ca^{2+}-independent calmodulin binding sites in erythrocyte protein 4.1. Implications for regulation of protein 4.1 interactions with transmembrane proteins. *J Biol Chem.* **275**(9), 6360-7.

Oatley, P., Stewart, A. P., Sandford, R. and Edwardson, J. M. (2012). Atomic force microscopy imaging reveals the domain structure of polycystin-1. *Biochemistry* **51**, 2879–2888.

O'Day, D. H. (2003). CaMBOT: profiling and characterizing calmodulin-binding proteins. *Cell Signal* **5**(4), 347-54.

O'Day, D. H., Huber, R. J. and Suarez, A. (2012). Extracellular calmodulin regulates growth and cAMP-mediated chemotaxis in *Dictyostelium discoideum*. *Biochem Biophys Res Commun.* **425**(4), 750-4.

O'Hagan, R., Wang, J., Barr, M. M. (2014). Mating behavior, male sensory cilia, and polycystins in *Caenorhabditis elegans*. *Semin Cell Dev Biol* **33**, 25-33.

Omasits, U., Ahrens, C. H., Müller, S. and Wollscheid, B. (2014). Protter: interactive protein feature visualization and integration with experimental proteomic data. *Bioinformatics* **30**(6), 884-6.

Onyenwoke R. U., Sexton J. Z., Yan F., Díaz M. C. H., Forsberg L. J., Major M. B. *et al*. (2015). The mucolipidosis IV Ca^{2+} channel TRPML1 (MCOLN1) is regulated by the TOR kinase. *Biochem J* **470**, 331–342.

Paillard, M., Csordás, G., Szanda, G., Golenár, T., Debattisti, V., Bartok, A. *et al*. (2017). Tissue-specific mitochondrial decoding of cytoplasmic Ca^{2+} signals is controlled by the stoichiometry of MICU1/2 and MCU. *Cell Reports*, **18**(10), 2291–2300.

Palty, R., Silverman, W. F., Hershfinkel, M., Caporale, T., Sensi, S.L., Parnis, J. *et al*. (2010). NCLX is an essential component of mitochondrial Na^{+}/Ca^{2+} exchange. *PNAS USA* **107**(1), 436-41.

Palty, R. and Sekler, I. (2012). The mitochondrial Na^+/Ca^{2+} exchanger. *Cell Calcium.* **52**(1), 9-15.

Pan, P., Hall, E. M.and Bonner, J. T. (1972). Folic acid as a second chemotic substance in the cellular slime molds. *Nature (London) New Biol* **237**, 181-182.

Pan, P., Hall, E. M.and Bonner, J. T. (1975). Determination of the active portion of the folic acid molecule in cellular slime mold chemotaxis. *J Bacteriol* **122**, 185-191.

Pan, M., Xu, X., Chen, Y. and Jin, T. (2016). Identification of a chemoattractant G-Protein-Coupled Receptor for folic acid that controls both chemotaxis and phagocytosis. *Dev Cell* **36**(4), 428-39.

Pani, B., Cornatzer, E., Cornatzer, W., Shin, D.-M., Pittelkow, M. R., Hovnanian, A. *et al*. (2006). Up-Regulation of Transient Receptor Potential Canonical 1 (TRPC1) following Sarco(endo)plasmic Reticulum Ca^{2+} ATPase 2 gene silencing promotes cell survival: A potential role for TRPC1 in Darier's disease. *Mol Biol Cell* **17**(10), 4446–4458.

Parikh, A., Miranda, E. R., Katoh-Kurasawa, M., Fuller, D., Rot, G., Zagar, L. *et al*. (2010). Conserved developmental transcriptomes in evolutionarily divergent species. *Genome Biol* **11**(3), R35.

Park, B., Shin, D. Y., Jeon, T. J. (2018). CBP7 Interferes with the multicellular development of *Dictyostelium* cells by inhibiting chemoattractant-mediated cell aggregation. *Mol Cells* **41**(2), 103-109.

Parkash J. and Asotra K. (2012). Calcium oscillations and waves in cells. In: *Islam M. (eds) Calcium Signaling. Advances in Experimental Medicine and Biology*, **740**. Springer, Dordrecht.

Parkinson, K., Baines, A. E., Keller, T., Gruenheit, N., Bragg, L., North, R. A. *et al*. (2014). Calcium-dependent regulation of Rab activation and vesicle fusion by an intracellular P2X ion channel. *Nat Cell Biol* **16**, 87–98.

Parnis, J., Montana, V., Delgado-Martinez, I., Matyash, V., Parpura, V., Kettenmann, H., *et al*. (2013). Mitochondrial exchanger NCLX plays a major role in the intracellular Ca^{2+} signaling, gliotransmission, and proliferation of astrocytes. *J Neurosci* **33**(17), 7206-19.

Patel, S. and Docampo, R. (2010). Acidic calcium stores open for business: expanding the potential for intracellular Ca^{2+} signaling. *Trends Cell Biol* **20**(5), 277-86.

Patel, S. and Cai, X. (2015). Evolution of acidic Ca^{2+} stores and their resident Ca^{2+}-permeable channels. *Cell Calcium* **57**(3), 222–230.

Payne, R., Hoff, H., Roskowski, A. and Foskett, J. K. (2017). MICU2 restricts spatial crosstalk between $InsP_3R$ and MCU channels by regulating threshold and gain of MICU1-mediated inhibition and activation of MCU. *Cell reports* **21**(11), 3141-3154.

Pazour, G. J., San Agustin, J. T., Follit, J. A., Rosenbaum, J. L. and Witman, G. B. (2002). Polycystin-2 localizes to kidney cilia and the ciliary level is elevated in orpk mice with polycystic kidney disease. *Curr Biol* **12**(11), R378–80.

Pedersen, P. L. and Carafoli, E. (1987). Ion motive ATPases. I. Ubiquity, properties, and significance to cell function. *Trends Biochem Sci* **12**, 146–150.

Peña-Oyarzun, D., Troncoso, R., Kretschmar, C., Hernando, C., Budini, M., Morselli, E. *et al*. (2017). Hyperosmotic stress stimulates autophagy via polycystin-2. *Oncotarget* **8**(34), 55984–55997.

Pennekamp, P., Karcher, C., Fischer, A., Schweickert, A., Skryabin, B., Horst, J. *et al*. (2002). The ion channel polycystin-2 is required for left-right axis determination in mice. *Curr Biol* **12**(11), 938-43.

Periasamy, M., Reed, T. D., Liu, L. H., Ji, Y., Loukianov, E., Paul, R. J. *et al*. (1999). Impaired cardiac performance in heterozygous mice with a null mutation in the sarco(endo)plasmic reticulum Ca^{2+}-ATPase isoform 2 (SERCA2) gene. *J Biol Chem* **274**(4), 2556-62.

Periasamy, M. and Kalyanasundaram, A. (2007). SERCA pump isoforms: their role in calcium transport and disease. *Muscle Nerve* **35**(4), 430-42.

Perocchi, F., Gohil, V. M., Girgis, H. S., Bao, X. R., McCombs, J. E., Palmer, A. E. *et al*. (2010). MICU1 encodes a mitochondrial EF hand protein required for Ca^{2+} uptake. *Nature* **467**(7313), 291-6.

Petri E. T., Celic A., Kennedy S. D., Ehrlich B. E., Boggon T. J. and Hodsdon M. E. (2010). Structure of the EF-hand domain of polycystin-2 suggests a mechanism for Ca^{2+}-dependent regulation of polycystin-2 channel activity. *PNAS USA* **107**, 9176–9181.

Phillips, J. E. and Gomer, R. H. (2015). Partial genetic suppression of a loss-of-function mutant of the neuronal ceroid lipofuscinosis-associated protease TPP1 in *Dictyostelium discoideum*. *Dis Model Mech* **8**, 147–156.

Pikzack, C., Prassler, J., Furukawa, R., Fechheimer, M. and Rivero, F. (2005). Role of calcium-dependent actin-bundling proteins: characterization of *Dictyostelium* mutants lacking fimbrin and the 34-kilodalton protein. *Cell Motil Cytoskeleton* **62**, 210–231.

Pinter, K. and Gross, J. (1995). Calcium and cell-type-specific gene expression in *Dictyostelium*. *Differentiation* **59**(4), 201-206.

Pizzo, P., Lissandron, V., Capitanio, P. and Pozzan, T. (2011). Ca^{2+} signalling in the Golgi apparatus. *Cell Calcium* **50**(2), 184-192.

Plesch, E., Chen, C. C., Butz, E., Scotto Rosato, A., Krogsaeter, E. K., Yinan, H. *et al.* (2018). Selective agonist of TRPML2 reveals direct role in chemokine release from innate immune cells. *Elife* **7**, e39720.

Poloz, Y. and O'Day, D. (2012). Colchicine affects cell motility, pattern formation and stalk cell differentiation in *Dictyostelium* by altering calcium signaling. *Differentiation* **83**(4), 185-199.

Poloz, Y. and O'Day, D. H. (2012a). Ca^{2+} signaling regulates ecmB expression, cell differentiation and slug regeneration in *Dictyostelium*. *Differentiation* **84**(2), 163-175.

Pryor, P. R., Mullock, B. M., Bright, N. A., Gray, S. R, and Luzio, J. P. (2000). The role of intraorganellar Ca^{2+} in late endosome-lysosome heterotypic fusion and in the reformation of lysosomes from hybrid organelles. *J Cell Biol* **149**(5), 1053-62.

Pryor, P. R., Reimann, F., Gribble, F. M. and Luzio, J. P. (2006). Mucolipin-1 is a lysosomal membrane protein required for intracellular lactosylceramide traffic. *Traffic* **7**(10), 1388–1398.

Puertollano, R. and Kiselyov, K. (2009). TRPMLs: in sickness and in health. *Am J Physiol Renal Physiol* **296**, F1245–F1254.

Putney, J. W. Jr. (1986). A model for receptor-regulated calcium entry. *Cell Calcium* **7**(1), 1-12.

Putney, J.W. Jr. (1997). Type 3 inositol 1,4,5-trisphosphate receptor and capacitative calcium entry. *Cell Calcium* **21**, 257–261.

Putney, J. W. Jr (2003). Capacitative calcium entry in the nervous system. *Cell Calcium* **34**(4-5), 339-44.

Putney, J. W. (2009). Capacitative calcium entry: from concept to molecules. *Immunol Rev* **231**(1), 10-22.

Qian, F. Germino, F. J. Cai, Y. Zhang, X. Somlo, S. Germino, G. G. (1997). PKD1 Interacts with PKD2 through a probable coiled-coil domain. *Nat Genet* **16**, 179–183.

Qian, Q., Hunter, L. W., Li, M., Marin-Padilla, M., Prakash, Y. S., Somlo, S. *et al*. (2003). Ddpolycystin haploinsufficiency alters intracellular calcium regulation in vascular smooth muscle cells. *Hum Mol Genet* **12**(15), 1875–1880.

R Core Team (2020). R: A language and environment for statistical computing. R Foundation for Statistical Computing, Vienna, Austria. URL https://www.R-project.org/.

Raffaello, A., Mammucari, C., Gherardi, G. and Rizzuto, R. (2016). Calcium at the center of cell signaling: Interplay between endoplasmic reticulum, mitochondria, and lysosomes. *Trends Biochem Sci* **41**(12), 1035-1049.

Rhoads, A. R. and Friedberg, F. (1997). Sequence motifs for calmodulin recognition. *FASEB J* **11**(5), 331-40.

Rizzuto, R., Simpson, A. W., Brini, M. and Pozzan, T. (1992). Rapid changes of mitochondrial Ca^{2+} revealed by specifically targeted recombinant aequorin. *Nature* **358**, 325–327.

Rizzuto R., Brini M., Murgia M., and Pozzan T. (1993). Microdomains with high Ca^{2+} close to IP3-sensitive channels that are sensed by neighboring mitochondria. *Science* **262**(5134), 744-7.

Rizzuto, R., Pinton, P., Carrington, W., Fay, F. S., Fogarty, K. E., Lifshitz, L. M. *et al.* (1998). Close contacts with the endoplasmic reticulum as determinants of mitochondrial Ca^{2+} responses. *Science* **280**, 1763–1766.

Rizzuto, R., Bernardi, P. and Pozzan, T. (2000). *Mitochondria as all-round players of the calcium game. J Physiol (Lond.)* **529**, 37–47.

Rizzuto, R. and Pozzan, T. (2006). Microdomains of intracellular Ca^{2+}: molecular determinants and functional consequences. *Physiol Rev* **86**(1), 369-408.

Rizzuto, R., De Stefani, D., Raffaello, A. and Mammucari, C. (2012). Mitochondria as sensors and regulators of calcium signalling. *Nat Rev Mol Cell Biol* **13**, 566–578.

Roderick, H. L. Lechleiter, J. D. and Camacho, P. (2000). Cytosolic phosphorylation of calnexin controls intracellular Ca^{2+} oscillations via an interaction with SERCA2b. *J Cell Biol* **149**(6), 1235.

Roitbak, T., Ward, C. J., Harris, P. C., Bacallao, R., Ness, S. A. and Wandinger-Ness, A. (2004). A Polycystin-1 multiprotein complex is disrupted in polycystic kidney disease cells. *Mol Biol Cell* **15**(3), 1334–1346.

Romero-Lorca, A., Gaibar, M., Armesilla, A. L., Fernandez-Santander, A., and Novillo, A. (2018). Differential expression of PMCA2 mRNA isoforms in a cohort of Spanish patients with breast tumor types. *Oncology letters* **16**(6), 6950–6959.

Ronco, V., Potenza, D. M., Denti, F., Vullo, S., Gagliano, G., Tognolina, M., *et al*. (2015). A novel Ca^{2+}-mediated cross-talk between endoplasmic reticulum and acidic organelles: implications for NAADP-dependent Ca^{2+} signalling. *Cell Calcium*. 57(2), 89-100.

Rooney, E. K. and Gross, J. D. (1992). ATP-driven, Ca^{2+}/H^{+} antiport in acid vesicles from *Dictyostelium*. *PNAS USA* **89**, 8025–8029.

Rooney, E. K., Gross, J. D. and Satre, M. (1994). Characterisation of an intracellular Ca^{2+} pump in *Dictyostelium*. *Cell Calcium* **16**, 509-522.

Rosenbaum, E. E., Hardie, R.C., Colley, N. J. (2006). Calnexin is essential for rhodopsin maturation, Ca^{2+} regulation, and photoreceptor cell survival. *Neuron* **49**(2), 229-41.

Ross F. M. and Newell P. C. (1981). Streamers: Chemotactic mutants of *Dictyostelium discoideum* with altered cGMP metabolism. *J Gen Microbiol* **127**, 339–350.

Rossi, A. E. and Dirksen, R. T. (2006). Sarcoplasmic reticulum: the dynamic calcium governor of muscle. *Muscle Nerve* **33**(6), 715-31.

Rossi, A., Pizzo, P. and Filadi, R. (2019). Calcium, mitochondria and cell metabolism: A functional triangle in bioenergetics. *Biochim Biophys Acta Mol Cell Res* **1866**(7), 1068-1078.

Ruas, M., Rietdorf, K., Arredouani, A., Davis, L. C., Lloyd-Evans, E., Koegel, H. *et al*. (2010). Purified TPC isoforms form NAADP receptors with distinct roles for Ca^{2+} signaling and endolysosomal trafficking. *Curr Biol* **20**(8-6), 703–70.

Ruas, M., Davis, L. C., Chen, C- C., Morgan, A. J., Chuang, K- T., Walseth, T. F. *et al*. (2105). Expression of Ca^{2+}-permeable two-pore channels rescues NAADP signalling in TPC-deficient cells. *EMBO J* **34**, 1743–1758.

Salehi-Najafabadi, Z., Li, B., Valentino, V., Ng, C., Martin, H., Yu, Y. *et al*. (2017). Extracellular loops are essential for the assembly and function of polycystin receptor-ion channel complexes. *J Biol Chem* **292**(10), 4210-4221.

Samanta, K. and Parekh A. B. (2017). Spatial Ca^{2+} profiling: decrypting the universal cytosolic Ca^{2+} oscillation. *J Physiol* **595**(10), 3053-3062.

Samie, M. A., Grimm, C., Evans, J. A., Curcio-Morelli, C., Heller, S., Slaugenhaupt, S. A. and Cuajungco, M. P. (2009). The tissue-specific expression of TRPML2 (MCOLN-2) gene is influenced by the presence of TRPML1. *Pflugers Arch* **459**, 79–91.

Sammels, E., Devogelaere, B., Mekahli, D., Bultynck, G., Missiaen, L., Parys, J. B. *et al*. (2010). Polycystin-2 activation by inositol 1,4,5-trisphosphate-induced Ca^{2+} Release requires its direct association with the inositol 1,4,5-trisphosphate receptor in a signaling microdomain. *J Biol Chem* **285**(24), 18794–18805.

Sancak, Y., Markhard, A. L., Kitami, T., Kovács-Bogdán, E., Kamer, K. J., Udeshi, N. D. *et al*. (2013). EMRE is an essential component of the mitochondrial calcium uniporter complex. *Science* **342**(6164), 1379–1382.

Sang, D., Bai, S., Yin, S., Jiang, S., Ye, L., Hou, W. *et al*. (2019). Role of TRPP2 in mouse airway smooth muscle tension and respiration. *Am J Physiol Lung Cell Mol Physiol* **317**(4), L466-L474.

Santo-Domingo, J., Wiederkehr, A. and De Marchi, U. (2015). Modulation of the matrix redox signaling by mitochondrial Ca^{2+}. *World J Biol Chem* **6**(4), 310-23.

Santoni, G., Maggi, F., Amantini, C., Marinelli, O., Nabissi, M. and Morelli, M. B. (2020). Pathophysiological role of transient receptor potential mucolipin channel 1 in calcium-mediated stress-induced neurodegenerative diseases. *Frontiers in physiology* **11**, 251.

Saran, S., Azhar, M., Manogaran, P. S., Pande, G. and Nanjundiah, V. (1994). The level of sequestered calcium in vegetative amoebae of *Dictyostelium discoideum* can predict post-aggregative cell fate. *Differentiation* **57**, 163–169.

Saran, S., Nakao, H., Tasaka, M., Iida, H., Tsuji, F. I., Nanjundiah, V. and Takeuchi, I. (1994a). Intracellular free calcium level and its response to cAMP stimulation in developing *Dictyostelium* cells transformed with jellyfish apoaequorin. *FEBS Lett* **337**, 43–47.

Saxe, L., Johnson, R., Devreotes, N. and Kimmel, R. (1991). Multiple genes for cell surface cAMP receptors in *Dictyostelium discoideum*. *Dev Genet* **12**, 6-13.

Saxton, R. A., and Sabatini, D. M. (2017). mTOR signaling in growth, metabolism, and disease. *Cell* **168**(6), 960–976.

Schaap, P., Nebl, T. And Fisher, P. R. (1996). A slow sustained increase in cytosolic Ca^{2+} levels mediates stalk gene induction by differentiation inducing factor in *Dictyostelium*. *EMBO J* **15**(19), 5177–5183.

Schaloske, R., and Malchow. D. (1997). Mechanism of cAMP-induced Ca^{2+} influx in *Dictyostelium*: role of phospholipase A2. *Biochem J* **327**, 233–238.

Schaloske, R., Sonnemann, J. Malchow, D. and Schlatterer. C. (1998). Fatty acids induce release of Ca^{2+} from acidosomal stores and activate capacitative Ca^{2+} entry in *Dictyostelium discoideum. Biochem J* **332**, 541–548.

Schaloske, H., Lusche, F., Bezares-Roder, K., Happle, K., Malchow, D. and Schlatterer, C. (2005). Ca^{2+} regulation in the absence of the iplA gene product in *Dictyostelium discoideum*. *BMC Cell Biol* **6**(1), 13.

Schatzmann, H. J. (1966). ATP-dependent Ca^{2+}-extrusion from human red cells. *Experientia* **22**, 364–365.

Scherer, A., Kuhl, S., Wessels, D., Lusche, D. F., Raisley, B. and Soll, D. R. (2010). Ca^{2+} chemotaxis in *Dictyostelium discoideum*. *J Cell Sci* **123**(21), 3756-67.

Schiffmann, R., Dwyer, N. K., Lubensky, I. A., Tsokos, M., Sutliff, V. E., Latimer, J. S. *et al*. (1998). Constitutive achlorhydria in mucolipidosis type IV. *PNAS USA* **95**, 1207–1212.

Schlatterer, C., Gollnick, F., Schmidt, E., Meyer, R. and Knoll, G. (1994). Challenge with high concentrations of cyclic AMP induces transient changes in the cytosolic free calcium concentration in *Dictyostelium discoideum*. *J Cell Sci* **107**, 2107-2115.

Schlatterer, C. and Schaloske, R. (1996). Calmidazolium leads to an increase in the cytosolic Ca^{2+} concentration in *Dictyostelium discoideum* by induction of Ca^{2+} release from intracellular stores and influx of extracellular Ca^{2+}. *Biochem J* **313**, 661-7.

Schlatterer, C., Walther, P., Möuller, M., Mendgen, K., Zierold, K. and Knoll, G. (2001). Calcium stores in differentiated *Dictyostelium discoideum:* prespore cells sequester calcium more efficiently than prestalk cells. *Cell Calcium* **29**, 171–182.

Schlatterer, C., Happle, K., Lusche, D. F. and Sonnemann, J. (2004). Cytosolic Ca^{2+}-transients in *Dictyostelium discoideum* depend on the filling state of internal stores and on an active SERCA Ca^{2+}-pump. *J Biol Chem* **279**, 18407-18414.

Schmidt, N., Kollewe, A., Constantin, C. E., Henrich, S., Ritzau-Jost, A., Bildl, W. *et al*. (2017). Neuroplastin and basigin are essential auxiliary subunits of plasma membrane Ca^{2+}-ATPases and rey regulators of Ca^{2+} Clearance. *Neuron* **96**(4), 827-838.e9.

Schrag, J. D., Bergeron, J. J., Li, Y., Borisova, S., Hahn, M., Thomas, D. Y. and Cygler, M.(2001). The Structure of calnexin, an ER chaperone involved in quality control of protein folding. *Mol Cell* **8**(3), 633-44.

Schulze, C., Sticht, H., Meyerhoff, P. and Dietrich, P. (2011). Differential contribution of EF-hands to the Ca^{2+}-dependent activation in the plant two-pore channel TPC1. *Plant J* **68**(3), 424-32.

Schumann, F., Hoffmeister, H., Bader, R., Schmidt, M., Witzgall, R. and Kalbitzer, H. R. (2009). Ca^{2+}-dependent conformational changes in a C-terminal cytosolic domain of polycystin-2. *J Biol Chem* **284**, 24372–24383.

Scotto-Rosato, A., Montefusco, S., Soldati, C., Di Paola, S., Capuozzo, A., Monfregola, J. *et al*. (2019). TRPML1 links lysosomal calcium to autophagosome biogenesis through the activation of the CaMKKβ/VPS34 pathway. *Nat Commun*. **10**(1), 5630.

Seth, M., Sumbilla, C., Mullen, S. P., Lewis, D., Klein, M. G., Hussain, A. *et al.* (2004). Sarco(endo)plasmic reticulum Ca^{2+} ATPase (SERCA) gene silencing and remodelling of the Ca^{2+} signaling mechanism in cardiac myocytes. *PNAS USA* **101**(47), 16683-8.

Shanley, L. J., Walczysko, P., Bain, M., MacEwan, D. J. and Zhao, M. (2006). Influx of extracellular Ca^{2+} is necessary for electrotaxis in *Dictyostelium*. *J Cell Sci* 119, 4741–4748.

Shao, J., Fu, Z., Ji, Y., Guan, X., Guo, S., Ding, Z. *et al*. (2016). Leucine zipper-EF-hand containing transmembrane protein 1 (LETM1) forms a Ca^{2+}/H^{+} antiporter. *Sci Rep* **27**, 34174.

Shen, D., Wang, X., Li, X., Zhang, X., Yao, Z., Dibble, S. *et al.* (2012). Lipid storage disorders block lysosomal trafficking by inhibiting a TRP channel and lysosomal calcium release. *Nat Commun* **3**, 731.

Shigaki, T., Rees, I., Nakhleh, L. and Hirschi, K. D. (2006). Identification of three distinct phylogenetic groups of CAX cation/proton antiporters. *J Mol Evol* **63**, 815-25.

Shoshan-Barmatz, V. and Ben-Hail, D. (2012). VDAC, a multi-functional mitochondrial protein as a pharmacological target. *Mitochondrion.* **12**(1), 24-34.

Shoshan-Barmatz, V., De Pinto, V., Zweckstetter, M., Raviv, Z., Keinan, N. and Arbel, N. (2010). VDAC, a multi-functional mitochondrial protein regulating cell life and death. *Mol Aspects Med* **31**(3), 227-85.

Shuk-Kwan Lee, C., Chun-Kit Tong, B., Wing-Hei Cheng, C., Chun-Hin Hung, H. and Cheung, K. (2016). Characterization of Two-Pore Channel 2 by nuclear membrane electrophysiology. *Scientific Reports* **6**(6), 20282.

Sivaramakrishnan, V. and Fountain, S. J. (2012). A mechanism of intracellular P2X receptor activation. *J Biol Chem* **287**(34), 28315–28326.

Sivaramakrishnan, V. and Fountain, S. J. (2013). Intracellular P2X receptors as novel calcium release channels and modulators of osmoregulation in *Dictyostelium*: A comparison of two common laboratory strains. *Channels Austin* **7**(1), 43-6.

Smeazzetto, S., Armanious, G. P., Moncelli, M. R., Bak, J. J., Lemieux, M. J., Young, H. S., and Tadini-Buoninsegni, F. (2017). Conformational memory in the association of the transmembrane protein phospholamban with the sarcoplasmic reticulum calcium pump SERCA. *J Biol Chem* **292**(52), 21330–21339.

Smith, D. E. and Fisher, P. A. (1984). Identification, developmental regulation, and response to heat shock of two antigenically related forms of a major nuclear envelope protein in *Drosophila* embryos: application of an improved method for affinity purification of antibodies using polypeptides immobilized on nitrocellulose blots. *J Cell Biol* **99**, 20-28.

Smith, M. J.and Koch G. L. (1989). Multiple zones in the sequence of calreticulin (CRP55, calregulin, HACBP), a major calcium binding ER/SR protein. *EMBO J* **8**, 3581–3586.

Smith, J. A., Chan, C. C., Goldin, E. and Schiffmann, R. (2002). Noninvasive diagnosis and ophthalmic features of mucolipidosis type IV. *Ophthalmology* **109**, 588 –594.

Smith, E. W., Lima, W. C., Charette, S. J. and Cosson, P. (2010). Effect of starvation on the endocytic pathway in *Dictyostelium* Cells. *Eukaryotic Cell* **9**(3), 387-392.

Smith, P. K., Sen, M. G., Fisher, P. R. and Annesley, S. J. (2019). Modelling of neuronal ceroid lipofuscinosis Type 2 in *Dictyostelium discoideum* suggests that cytopathological outcomes result from altered TOR signalling. C*ells* **8**(5), 469.

Soll, D. R., Wessels, D., Kuhl, S. and Lusche, D. F. (2009). How a cell crawls and the role of cortical myosin II. *Eukaryotic Cell* **8**, 1381-1396.

Soll, D., Wessels, D., Lusche, D. F., Kuhl, S., Scherer, A and, Grimm, S. (2011). Role of extracellular cations in cell motility, polarity, and chemotaxis. *Res Rep Biol* **2011**(2), 89–99.

Soyombo, A. A., Tjon-Kon-Sang, S., Rbaibi, Y., Bashllari, E., Bisceglia, J., Muallem, S. and Kiselyov, K. (2006). TRP-ML1 regulates lysosomal pH and acidic lysosomal lipid hydrolytic activity. *J Biol Chem* **281**, 7294–7301.

Spirli, C., Locatelli, L., Fiorotto, R., Morell, C. M., Fabris, L., Pozzan, T. *et al*. (2012). Altered store operated calcium entry increases cyclic 3',5'-adenosine monophosphate production and extracellular signal-regulated kinases 1 and 2 phosphorylation in polycystin-2–defective cholangiocytes. *Hepatology* **55**, 856–868.

Sriskanthadevan, S., Brar, S. K., Manoharan, K. and Siu, C. H. (2013). Ca^{2+} -calmodulin interacts with DdCAD-1 and promotes DdCAD-1 transport by contractile vacuoles in *Dictyostelium* cells. *FEBS J* **280**, 1795-1806.

Srivastava, N., Traynor, D., Piel, M., Kabla, A. J. and Kay, R. R. (2020). Pressure sensing through Piezo channels controls whether cells migrate with blebs or pseudopods. PNAS USA **117**, 2506-2512.

Stajdohar, M., Jeran, L., Kokosar, J., Blenkus, D., Janez, T., Kuspa, A. *et al*. (2015). dictyExpress: visual analytics of NGS gene expression in *Dictyostelium*. [https://www.dictyexpress.org]

Stajdohar, M., Rosengarten, R. D., Kokosar, J., Jeran, L., Blenkus, D., Shaulsky, G. *et al*. (2017). dictyExpress: a web-based platform for sequence data management and analytics in *Dictyostelium* and beyond. *BMC Bioinformatics* **18**(1), 291.

Stammers, A. N., Susser, S. E., Hamm, N. C., Hlynsky, M. W., Kimber, D. E., Kehler, D. S. and Duhamel, T. A. (2015). The regulation of sarco(endo)plasmic reticulum calcium-ATPases (SERCA). *Can J Physiol Pharmacol* **93**(10), 843-54.

Stauffer, T. P., Hilfiker, H., Carafoli, E. and Strehler, E. E. (1993). Quantitative analysis of alternative splicing options of human plasma membrane calcium pump genes. *J Biol Chem* **268**, 25993–26003.

Stendahl, O., Krause, K- H., Krischer, J., Jerström, P., Theler, J- M., Clark, R. A. *et al*. (1994). Redistribution of intracellular Ca^{2+} stores during phagocytosis in human neutrophils. *Science* **265**, 1439–1441.

Stojilkovic, S. S., Leiva-Salcedo, E., Rokic, M. B., & Coddou, C. (2014). Regulation of ATP-gated P2X channels: from redox signaling to interactions with other proteins. *Antioxidants & redox signaling* **21**(6), 953–970.

Strehler, E. E. and Zacharias, D. A. (2001). Role of alternative splicing in generating isoform diversity among plasma membrane calcium pumps. *Physiol Rev* **81**(1), 21-50.

Strehler, E. E. (2015). Plasma membrane calcium ATPases: From generic calcium sump pumps to versatile systems for fine-tuning cellular Ca^{2+}. *Biochem Biophys Res Commun* **460**, 26-33.

Sugden, C., Urbaniak, M. D., Araki, T., and Williams, J. G. (2015). The *Dictyostelium* prestalk inducer differentiation-inducing factor-1 (DIF-1) triggers unexpectedly complex global phosphorylation changes. *Molecular biology of the cell* **26**(4), 805-20.

Sun, M., Goldin, E., Stahl, S., Falardeau, J. L., Kennedy, J. C., Acierno Jr., J. S. *et al.* (2000). Mucolipidosis type IV is caused by mutations in a gene encoding a novel transient receptor potential channel. *Hum Mol Genet* **9**, 2471–2478.

Sun X., Yang Y., Zhong X. Z., Cao Q., Zhu X.-H., Zhu X. and Dong X.-P. (2018). A negative feedback regulation of MTORC1 activity by the lysosomal Ca^{2+} channel MCOLN1 (mucolipin 1) using a CALM (calmodulin)-dependent mechanism. *Autophagy* **14**, 1–15.
Sussman, R. and Sussman, M. (1967). Cultivation of *Dictyostelium discoideum* in axenic medium. *Biochem Biophys Res Commun* **29**(1), 53-5.

Swer, P. B., Lohia, R. and Saran, S. (2014). Analysis of rapamycin induced autophagy in *Dictyostelium discoideum*. *Indian J Exp Biol* **52**(4), 295-304.

Swer, P. B., Mishra, H., Lohia, R. and Saran S. (2016). Overexpression of TOR (target of rapamycin) inhibits cell proliferation in *Dictyostelium discoideum*. *J Basic Microbiol* **56**(5), 510-9.

Tada, M. and Toyofuku, T. (1996). SR Ca^{2+}-ATPase/phospholamban in cardiomyocyte function. *J Card Fail* **2**(4 Suppl), S77-85.

Tan, W. and Colombini M. (2007). VDAC closure increases calcium ion flux. *Biochim Biophys Acta* **1768** (10), 2510-5.

Tanaka, Y., Itakura, R., Amagai A. and Maeda Y. (1998). The signals for starvation response are transduced through elevated $[Ca^{2+}]_i$ in *Dictyostelium* cells. *Exp Cell Res* , 340-348.

Taylor C. W., Genazzani A. A. and Morris, S. A. (1999). Expression of inositol trisphosphate receptors*. Cell Calcium* **26***,* 237–251.

Temesvari, L. A., Rodriguez-Paris, J. M., Bush, J. M., Zhang, L., and Cardelli, J. A. (1996). Involvement of the vacuolar proton-translocating ATPase in multiple steps of the endolysosomal system and in the contractile vacuole system of *Dictyostelium discoideum*. *J Cell Sci*, 1479–1495.

Thewes, S., Schubert, S. K., Park, K. and Mutzel, R. (2014). Stress and development in *Dictyostelium discoideum*: the involvement of the catalytic calcineurin A subunit. *J Basic Microbiol* **54**(6), 607-13.

Thompson, C. R. L. and Kay R. R. (2000). The role of DIF-1 signaling in *Dictyostelium* development. *Mol Cell* **6**, 1509-14.

Thul, R., Rietdorf, K., Bootman, M. D., Coombes, S. (2015). Unifying principles of calcium wave propagation - Insights from a three-dimensional model for atrial myocytes. *Biochim Biophys Acta* **1853**(9), 2131-43.

Thul, P. J., Åkesson, L., Wiking, M., Mahdessian, D., Geladaki, A., Ait Blal, H. *et al*. (2017). A subcellular map of the human proteome. *Science* **356**(6340).

Tidow, H., Poulsen, L. R., Andreeva, A., Knudsen, M., Hein, K. L., Wiuf, C., Palmgren, M.G. and Nissen, P. (2012). A bimodular mechanism of calcium control in eukaryotes. *Nature* **491**(7424), 468-72.

Tidow, H. and Nissen, P. (2013). Structural diversity of calmodulin binding to its target sites. *FEBS J* **280**(21), 5551-65.

Tjoelker, L. W., Seyfried, C. E., Eddy, R. L., Byers, M. G., Shows, T. B., Calderon, J., Schreiber, R. B., and Gray, P. W. (1994). Human, mouse, and rat calnexin cDNA cloning: identification of potential calcium binding motifs and gene localization to human chromosome 5. *Biochemistry* **33**, 3229–3236.

Todkar, K., Ilamathi H. S. and Germain, M. (2017). Mitochondria and Lysosomes: Discovering Bonds. *Frontiers in Cell and Developmental Biology* **5**, 106.

Tomchik, K. J. and Devreotes, P. N. (1981). Adenosine 3',5'-monophosphate waves in *Dictyostelium discoideum*: a demonstration by isotope dilution--fluorography. *Science* **212**(4493), 443-6.

Toyoshima, C., Nakasako, M., Nomura, H. and Ogawa, H. (2000). Crystal structure of the calcium pump of sarcoplasmic reticulum at 2.6 A resolution. *Nature* **405**(6787), 647-55.

Traynor D., Milne J. L., Insall R. H., Kay R. R. (2000). Ca^{2+} signalling is not required for chemotaxis in *Dictyostelium. EMBO J* **19**(17), 4846–4854.

Traynor, D. and Kay, R. R. (2017). A polycystin-type transient receptor potential (Trp) channel that is activated by ATP. *Biology Open* **6**, 200-209.

Tresse, E., Giusti, C., Kosta, A., Luciani, M. F. and Golstein, P. (2008). Autophagy and autophagic cell death in *Dictyostelium*. *Methods Enzymol* **451**, 343-58.

Treusch, S., Knuth, S., Slaugenhaupt, S. A., Goldin, E., Grant, B. D. and Fares, H. (2004). *Caenorhabditis elegans* functional orthologue of human protein h-mucolipin-1 is required for lysosome biogenesis. *PNAS USA* **101**, 4483–4488.

Troll, H., Malchow, D., Muller-Taubenberger, A., Humbel, B., Lottspeich, F., Ecke, M. *et al*. (1992). Purification, functional characterization, and cDNA sequencing of mitochondrial porin from *Dictyostelium discoideum*. *J Biol Chem* **267**, 21072-9.

Tsiokas, L., Arnould, T., Zhu, C., Kim, E., Walz, G. and Sukhatme, V. P. (1999). Specific association of the gene product of polycystin 2 with the TRPC1 channel. *PNAS USA* **96**(7), 3934–3939.

Turk, V., Stoka, V., Vasiljeva, O., Renko, M., Sun, T., Turk, B. *et al*. (2012). Cysteine

cathepsins: From structure, function and regulation to new frontiers. *Biochimica et Biophysica Acta* **1824**, 68–88.

Unterweger, N. and Schlatterer, C. (1995). Introduction of calcium buffers into the cytosol of *Dictyostelium discoideum* amoebae alters cell morphology and inhibits chemotaxis. *Cell Calc* **17**, 97-110.

Van Driessche, N., Shaw, C., Katoh, M., Morio, T., Sucgang, R. *et al*. (2002). A transcriptional profile of multicellular development in *Dictyostelium discoideum*. *Development* **129**, 1543–1552.

Van Duijn, B. and Haastert, P. J. M. (1992). Independent control of locomotion and orientation during *Dictyostelium discoideum* chemotaxis. *J Cell Sci* **102**, 763-768.

Van Haastert, P. J., De Vries, M. J., Penning, L. C., Roovers, E., Van der Kaay, J., Erneux, C. *et al.* (1989). Chemoattractant and guanosine 5'-[gamma-thio] triphosphate induce the accumulation of inositol 1,4,5-trisphosphate in *Dictyostelium* cells that are labelled with [3H]inositol by electroporation. *Biochem J* **258**, 577–586.

Vanagas, L., Rossi, R. C., Caride, A. J., Filoteo, A. G., Strehler, E. E. and Rossi, J. P. (2007). Plasma membrane calcium pump activity is affected by the membrane protein concentration: evidence for the involvement of the actin cytoskeleton. *Biochim Biophys Acta* **1768**(6), 1641–1649.

Veltman, D. M., De Boer, J. S. and van Haastert, P. J. M. (2003). Chemoattractant stimulated calcium influx in *Dictyostelium discoideum* does not depend on cGMP. *Biochim Biophys Acta Gen Subj* **1623**, 129–134.

Venkatachalam, K., Long, A. A., Elsaesser, R., Nikolaeva, D., Broadie, K. and Montell, C. (2008). Motor deficit in a *Drosophila* model of mucolipidosis type IV due to defective clearance of apoptotic cells. *Cell* **135**, 838–851.

Vergarajauregui, S., Connelly, P. S., Daniels, M. P., and Puertollano, R. (2008). Autophagic dysfunction in mucolipidosis type IV patients. *Hum Mol Genet* **17**, 2723–2737.

Vergarajauregui, S., Martina, J. A. and Puertollano, R. (2009). Identification of the Penta-EF-hand Protein ALG-2 as a Ca^{2+}-dependent Interactor of Mucolipin-1. *J Biol Chem* **284**, 36357–36366.

Verkhratsky, A., Trebak, M., Perocchi, F., Khananshvili, D. and Sekler, I. (2018). Crosslink between calcium and sodium signalling. *Exp Physiol* **103**(2), 157-169.

Vernary, A. and Cosson, P. (2013). Immunofluorescence labeling of cell surface antigens in *Dictyostelium. BMC Research Notes*, 317.

Villamil Giraldo, A.M., Lopez Medus, M., Gonzalez Lebrero, M., Pagano, R. S., Labriola, C.A., Landolfo, L. *et al*. (2010). The structure of calreticulin C-terminal domain is

modulated by physiological variations of calcium concentration. *J Biol Chem* **285**(7), 4544-53.

Wada, I., Rindress, D., Cameron, P. H., Ou, W. J., Doherty, J. J. 2nd, Louvard, D. *et al*. (1991). SSR alpha and associated calnexin are major calcium binding proteins of the endoplasmic reticulum membrane. *J Biol Chem* **266**(29), 19599-610.

Waheed, A., Ludtmann, M. H., Pakes, N., Robery, S., Kuspa, A., Dinh, C. *et al*. (2014). Naringenin inhibits the growth of *Dictyostelium* and MDCK-derived cysts in a polycystin-2 (TRPP2)-dependent manner. *Br J Pharmacol* **171**(10), 2659-2670.

Wang, X., Zhang, X., Dong, X. -P., Samie, M., Li, X., Cheng, X. *et al*. (2012). TPC proteins are phosphoinositide- activated sodium-selective ion channels in endosomes and lysosomes. *Cell* **151**, 372–383.

Watnick, T. J., Jin, Y., Matunis, E., Kernan, M. J. and Montell, C. (2003). A flagellar polycystin-2 homolog required for male fertility in *Drosophila*. *Curr Biol* **13**(24), 2179-84.

Watts, D. J. and Ashworth, J. M. (1970). Growth of myxamoebae of the cellular slime mould *Dictyostelium discoideum* in axenic culture. *Biochemical Journal* **119**(2), 171-4.

Weissenmayer, B., Boeckeler, K., Lahrz, A. *and* Mutzel, R. (2005). The calcineurin inhibitor gossypol impairs growth, cell signalling and development in *Dictyostelium discoideum.* FEMS Microbiol **242**(1), 19-25.

Wessels, D., Lusche, D. F., Steimle, P.A., Scherer, A., Kuhl, S., Wood, K. *et al*. (2012). Myosin heavy chain kinases play essential roles in Ca^{2+}, but not cAMP, chemotaxis and the natural aggregation of *Dictyostelium discoideum*. *J Cell Sci* **125**(20), 4934-44.

Whittingham, W. F. and Raper, K. B. (1960). Non-viability of stalk cells in *Dictyostelium*. *PNAS USA* **46**(5), 642-9.

Wick, U., Malchow, D. and Gerisch, G. (1978). Cyclic-AMP stimulated calcium influx into aggregating cells of *Dictyostelium discoideum*. *Cell Biol Int Rep* **2**(1), 71-79.

Wilczynska, Z. and Fisher, P.R. (1994). Analysis of a complex plasmid insertion in a phototaxis-deficient transformant of *Dictyostelium discoideum* selected on a *Micrococcus luteus* lawn. *Plasmid* **32**,182-194.

Wilczynska, Z., Barth, C. and Fisher, P.R. (1997). Mitochondrial mutations impair signal transduction in *Dictyostelium discoideum* slugs. *Biochem Biophys Res Comm* **234**, 39-43.

Wilczynska, Z., Schlatterer, C., Müller-Taubenberger, A., Malchow, D. and Fisher, P. R. (2005). Release of Ca^{2+} from the endoplasmic reticulum contributes to Ca^{2+} signalling in *Dictyostelium*. *Eukaryotic Cell* **4**(9), 1513-1525.

Willard, S. S. and Devreotes, P. N. (2006). Signaling pathways mediating chemotaxis in the social amoeba, *Dictyostelium discoideum*. *Eur J Cell Biol* **85**(9-10), 897-904.

Williams, D. B. (2006). *Beyond lectins: the calnexin/calreticulin chaperone system of the endoplasmic reticulum. J Cell Sci* **119**, 615–623.

Williams, T. D., and Kay, R. R. (2018). The physiological regulation of macropinocytosis during *Dictyostelium* growth and development. *J Cell Sci* **131**, jcs-213736.

Witke, W., Nellen, W. and Noegel, A. (1987). Homologous recombination in the *Dictyostelium* alpha-actinin gene leads to an altered mRNA and lack of the protein. *EMBO J* **6**, 4143-4148.

Witke, W., Hofmann, A., Koppel, B., Schleicher, M. and Noegel, A. A. *(*1993*). The Ca^{2+}-binding domains in non-muscle type alpha-actinin: Biochemical and genetic analysis. J Cell Biol* **121***,* 599 *-606.*

Wong, C. O., Montell, R. Li, C. and Venkatachalam, K. (2012). *Drosophila* TRPML is required for TORC1 activation. *Curr Biol* **22**, 1616-1621.

Wong, C- O., Palmieri, M., Li, J., Akhmedov, D., Chao, Y., Broadhead, G. T. *et al*. (2015). Diminished mTORC1-Dependent JNK activation underlies the neurodevelopmental defects associated with lysosomal dysfunction. *Cell Reports* **12**(12), 2009-2020.

Wu, G., D'Agati, V., Cai, Y., Markowitz, G., Park, J. H., Reynolds, D. M. *et al*. (1998). *Somatic inactivation of polycystin 2 results in polycystic kidney disease. Cell* **93**(2), 177–188.

Wu, G., Markowitz, G. S., Li, L., D'Agati, V. D., Factor, S. M., Geng, L. *et al*. (2000). Cardiac defects and renal failure in mice with targeted mutations in Pkd2. *Nat Genet* **24**(1), 75-8.

Wu, X, Weng, L, Zhang, J, Liu, X and Huang, J. (2018). The plasma membrane calcium ATPases in calcium signaling network. *Curr Protein Pept Sci* **19**(8), 813-822.

Wu, G., Yang, X., Shen, Y.(2018a). Identification of a single aspartate residue critical for both fast and slow calcium-dependent inactivation of the human TRPML1 channel. *J Biol Chem* **293**(30), 11736-11745.

Xu, H., Delling, M., Li, L., Dong, X., and Clapham, D. E. (2007). Activating mutation in a mucolipin transient receptor potential channel leads to melanocyte loss in varitint–waddler mice. *PNAS USA* **104**, 18321–18326.

Xu, H. and Van Remmen, H. (2012). The SarcoEndoplasmic Reticulum Calcium ATPase (SERCA) pump: a potential target for intervention in aging and skeletal muscle pathologies. *Skeletal Muscle* **11,** 25.

Yamaguchi, T., Wallace, D. P., Magenheimer, B. S., Hempson, S. J., Grantham, J. J. and Calvet, J. P. (2004). Calcium restriction allows cAMP activation of the B-Raf/ERK

pathway, switching cells to a cAMP-dependent growth-stimulated phenotype. *J Biol Chem* **279**, 40419-40430.

Yamaguchi, T., Hempson, S. J., Reif, G. A., Hedge, A. M. and Wallace, D. P. (2006). Calcium restores a normal proliferation phenotype in human polycystic kidney disease epithelial cells. *J Am Soc Nephrol* **17**(1), 178–187.

Yamaguchi, S., Jha, A., Li, Q., Soyombo, A. A., Dickinson, G. D., Churamani, D., Brailoiu, E. *et al*. (2011). Transient receptor potential mucolipin 1 (TRPML1) and two-pore channels are functionally independent organellar ion channels. *J Biol Chem* **286**, 22934–22942.

Yamamoto, A. and Takeuchi, I. (1983). Vital staining of autophagic vacuoles in differentiating cells of *Dictyostelium discoideum. Differentiation* **24**(1-3) 83–87.
Yáñez, M., Gil-Longo, J. and Campos-Toimil, M. (2012). Calcium Binding proteins. *Adv Exp Med Biol* **740**, 461-82.

Yang, Y., Hodsdon, M. E., Lolis, E. J. and Ehrlich, B. E. (2016). Conformational dynamics of Ca^{2+}-dependent responses in the polycystin-2 C-terminal tail. *Biochem J* **473**(3), 285-96.

Yap, K. L., Kim, J., Truong, K., Sherman, M., Yuan, T. and Ikura, M. (2000). Calmodulin target database. *J Struct Funct Genomics* **1**(1), 8-14.

Ye, M. and Grantham, J. J. (1993). The secretion of fluid by renal cysts from patients with autosomal dominant polycystic kidney disease. *N Engl J Med* **329**(5), 310–313.

Yoshiba, S. and Hamada, H. (2014). Roles of cilia, fluid flow, and Ca^{2+} signaling in breaking of left-right symmetry. *Trends Genet* **30**(1), 10-7.

Yu, R. and Hinkle, P. M. (2000). Rapid turnover of calcium in the endoplasmic reticulum during signaling: studies with cameleon calcium indicators. *J Biol Chem* **275**, 23648–23653.

Yu Y., Ulbrich M. H., Li M. H., Buraei Z., Chen X. Z., Ong A. C. *et al*. (2009). Structural and molecular basis of the assembly of the TRPP2/PKD1 complex. *PNAS USA* **106**, 11558–11563.

Yuan, A., Siu, C. H. and Chia, C. P. (2001). Calcium requirement for efficient phagocytosis by *Dictyostelium discoideum*. *Cell Calcium* **29**(4), 229-238.

Yuan, Y., Chan, C., Maorong, W., Min, L., Ying, D., Lijie, Wu. *et al*. (2020). Structural characterization of the N-terminal domain of the *Dictyostelium discoideum* mitochondrial calcium uniporter. *ACS Omega* **5**(12), 6452-6460.

Yuen, I. S., Jain, R., Bishop, J. D., Lindsey, D. F., Deery, W. J., Van Haastert, P. J. *et al*. (1995). A density-sensing factor regulates signal transduction in *Dictyostelium*. *J Cell Biol* **129**(5), 1251-62.

Yumura, S. and Kitanishi-Yumura, T. (1993). A mechanism for the intracellular localization of myosin II filaments in the *Dictyostelium* amoeba. *J Cell Sci* **105**, 233-242.

Yumura, S. (1996). Rapid redistribution of myosin II in living *Dictyostelium* amoebae, as revealed by fluorescent probes introduced by electroporation. *Protoplasma* **192**, 217–227.

Yumura, S., Furuya, K. and Takeuchi, I. (1996). Intracellular free calcium responses during chemotaxis of *Dictyostelium* cells. *J Cell Sci* **109**, 2673–2678.

Zacharias, D. A. and Kappen, C. (1999). Developmental expression of the four plasma membrane calcium ATPase (PMCA) genes in the mouse. *Biochim Biophys Acta* **1428**(2-3), 397-405.

Zaika, O., Mamenko, M., Berrout, J., Boukelmoune, N., O'Neil, R. G. and Pochynyuk, O. (2013). TRPV4 dysfunction promotes renal cystogenesis in autosomal recessive polycystic kidney disease. *J Am Soc Nephrol* **24**, 604–616.

Zhang, F., Jin, S., Yi, F. and Li, P. L. (2009). TRP-ML1 functions as a lysosomal NAADP-sensitive Ca^{2+} release channel in coronary arterial myocytes. *J Cell Mol Med* **13**, 3174–3185.

Zhang, M., Tanaka, T. and Ikura, M. (1995). Calcium-induced conformational transition revealed by the solution structure of apo calmodulin. *Nat Struct Biol* **2**, 758–767.

Zhang, F., Xu, M., Han, W. Q. and Li, P. L. (2011). Reconstitution of lysosomal NAADP-TRP-ML1 signaling pathway and its function in TRP- ML1-/- cells. *Am J Physiol Cell Physiol* **301**, C421–C430.

Zheng, W., Yang, X., Hu, R., Cai, R., Hofmann, L., Wang, Z. *et al.* (2018). Hydrophobic pore gates regulate ion permeation in polycystic kidney disease 2 and 2L1 channels. *Nature Communications* **9**, 2302.

Zhu, Q. and Clarke, M. (1992). Association of calmodulin and an unconventional myosin with the contractile vacuole complex of *Dictyostelium discoideum*. *J. Cell Biol* **118**(2), 347.

Zhu, X., Bouffanais, R., and Yue, D. K. (2015). Interplay between motility and cell-substratum adhesion in amoeboid cells. *Biomicrofluidics* **9**(5), 054112.

Zong, X., Schieder, M., Cuny, H., Fenske, S., Gruner, C., Rötzer, K. *et al.* (2009). The two-pore channel TPCN2 mediates NAADP-dependent Ca^{2+}-release from lysosomal stores. *Pflugers Arch* **458**(5), 891–899.

APPENDICES

Appendix 1: List of chemicals and their suppliers

Chemicals	Supplier
Acetic acid (glacial)	AJAX Finechem
Acrylamide (30%) BIS solution (37:5:1)	Bio-Rad
Activated Charcoal	Sigma-Aldrich
Agar (Technical no.3)	Oxoid
Agarose	Promega
L- Alanine	Sigma
Ampicillin	Roche
Ammonium persulphate (APS)	Sigma-Aldrich
L- Arginine	Sigma
Bacteriological peptone	Oxoid
Bacto™ proteose peptone	Difco
Bacto™ tryptone	Difco
Bacto™ yeast extract	Difco
Blocking reagent	Roche
Boric acid	Sigma-Aldrich
Bovine serum albumin (type V)	Sigma-Aldrich
Bromophenol blue	Sigma-Aldrich
Calcium acetate	Sigma-Aldrich
Calcium chloride	Ajax
cAMP	Sigma-Aldrich
CCCP (Carbonyl cyanide m-chlorophenyl hydrazone)	Sigma-Aldrich
Caesium chloride	Roche
Chloroform	AJAX Finechem
Coomassie brilliant blue	Sigma
D- Glucose	BDH
Diethlypyrocarbonate (DEPC)	Sigma-Aldrich

DIF-1	Sigma
Dimethlysulphoxide (DMSO)	AJAX Finechem
Dipotassium hydrogen orthophosphate	Ajax
DL-Phenylalanine	Sigma
DNAzol	MRC
Ethanol (absolute)	AJAX Finechem
Ethidium bromide	Sigma
Ethylenediamine-tetraacetic acid (EDTA)	Sigma-Aldrich
Fluorescein isothiocyanate (FITC)-dextran	Sigma
Folic Acid	Sigma-Aldrich
Formaldehyde	Sigma
Gene Ruler^{TM}1 kb DNA ladder	Thermo Fisher Scientific
Geneticin	Promega
L-Glutamine	Sigma
Glycerol	Ajax
Glycine	APS
HEPES	Sigma-Aldrich
Horse Blood Serum	Sigma-Aldrich
Horse Serum	JRH Biosciences
Hydrochloric acid	Ajax
Hydrochloric acid	May and Baker
Isoamyl alcohol	Ajax
Isoproponal	Ajax
Isopropyl-1-thio-ß-D-galactoside (IPTG)	Roche
Lysosensor^{TM} DND-167	Invitrogen
Magnesium chloride	Ajax
Magnesium sulphate	APS
Maleic acid	BDH
ß-mercaptoethanol	Sigma
Methanol	Ajax
Mineral oil	Sigma
Neutral Red	Sigma

Nigericin	Sigma
N-Lauroyl sarcosine	Sigma
Phenol	Sigma
Potassium acetate	Ajax
Potassium chloride	Ajax
Potassium dihydrogen orthophosphate	Ajax
Potassium hydroxide	APS
Potassium phosphate	Ajax
SDS (Sodium dodecyl sulphate)	Ajax
L- Serine	Sigma
Sodium acetate	Ajax
Sodium chloride	Ajax
Trisodium citrate	Ajax
Disodium hydrogen orthophosphate	Ajax
Sodium hydroxide	Ajax
Sodium phosphate	APS
Sucrose	Ajax
TEMED	Sigma
Tris	ICN
Triton X-100	Sigma
Trizol	Ambion, Life technologies
L-Tryptophan	Sigma
Tween 20 (polyoxyethylene-sorbitan Monolaurate)	Pharmacia
Yeast extract	Oxoid

Appendix 2: Composition of media and buffers

All the media and buffers were sterilized by autoclaving or filter sterilization as stated.

2.1 Composition of media

Growth of bacterial cultures

Medium	Composition	
Luria Broth (LB)	1.0 % (w/v)	DifcoBacto tryptone
	0.5 % (w/v)	Difco yeast extract
	86 mM	NaCl
	10 mM	NaOH
LB agar		Luria Broth
	1 % (w/v)	Oxoid agar

SOC for electroporation

Solution 1	0.25 % (w/v)	DifcoBacto™Tryptone
	2 % (w/v)	Difco Bacto™Yeast Extract
	10 mM	NaCl
	2.5 mM	KCl
	10 mM	$MgCl_2$
	10 mM	$MgSO_4$
Solution 2		
	20 mM	Glucose

Solutions 1 and 2 were autoclaved separately and then mixed aseptically.

Growth of *D. discoideum* cultures

HL5 medium, pH 6.4

Solution 1

1 % (w/v)	Bacto™ Proteose peptone
0.5 % (w/v)	Bacto™ Yeast Extract
2.8 mM	$Na_2HPO_4.2H_2O$
2.6 mM	KH_2PO_4

Solution 2	1 % (w/v)	Glucose

Solutions 1 and 2 were autoclaved separately and then mixed aseptically.

MES-HL5	6.7 mM	MES, pH 7.1
	1.0 % (w/v)	Proteose peptone
	0.5 % (w/v)	Yeast Extract
	1.0 % (w/v)	Glucose
***D. discoideum* Storage Buffer**	45 % (v/v)	Horse Blood Serum
	45 % (v/v)	SS
	10 % (v/v)	DMSO
SM agar	1.0 % (w/v)	Oxoid Agar
	1.0 % (w/v)	Oxoid Bacteriological peptone
	1.0 % (w/v)	Glucose
	0.1 % (w/v)	Oxoid Yeast extract
	4.1 mM	$MgSO_4.7H_2O$
	16.2 mM	KH_2PO_4
	5.8 mM	K_2HPO_4
Water agar	1.0 % (w/v)	Oxoid Agar
Normal Agar, pH6	2.0 % (w/v)	Difco Agar
	0.1% (w/v)	Oxoid peptone
	0.11 % (w/v)	Anhydrous glucose
	0.19972 % (w/v)	KH_2PO_4

	0.0356 % (w/v)	$Na_2HPO_4.2H_2O$

20 g L–1 agar (Difco, Detroit, MI, United States); 1 g L–1 peptone (Oxoid, Basingstoke, United Kingdom), 1.1 g L–1 anhydrous glucose, 1.9972 g L–1 KH2PO4, and 0.356 g L–1 Na2HPO4_2H2O, pH 6.0]

Buffers

10 X PBS (Phosphate Buffered Saline) pH 7.5	1.37 M	NaCl
	27 mM	KCl
	43 mM	$Na_2HPO_4.17H_20$
	14.7 mM	KH_2PO_4

1 X PBS was used by diluting 10 X stock with distilled water.

10 X TBS (Tris Buffered Saline) pH 7.6	0.2 M	Tris Base
	1.5 M	NaCl

1 X TBS was used by diluting 10 X stock with distilled water.

TE, pH 8.0	10 mM	Tris-HCl
EDTA stock, pH 8	0.5 M	EDTA
Ethidium bromide (stock)	1 mg mL^{-1}	Ethidium bromide
NaOH solution	2 M	NaOH
Phosphate buffer, pH 6.5	12 mM	Na_2HPO_4
	12 mM	$NaH_2PO_4.2H_20$

Alkaline lysis Minipreps		
Resuspension Buffer	50 mM	Tris-HCl pH 8.0
	10 mM	EDTA
	100 g mL^{-1}	RNase A
Lysis buffer	0.2 M	Sodium hydroxide
	1.0 % (w/v)	SDS
Neutralisation buffer	5 M	Potassium acetate, pH 4.8

Sterile saline (SS)	10 mM	NaCl
	10 mM	KCl
	2.7 mM	$CaCl_2$
Gel Electrophoresis		
Molecular Weight Markers	0.5 µg mL^{-1}	1 kb Gene Ruler DNA ladder
Agarose Gel	1-2 % (w/v)	Agarose
	10 % (v/v)	TBE (10 X)
	90 % (v/v)	Distilled water
	0.5 µg mL^{-1}	Ethidium bromide
DNA loading dye (SBE)	50 % (w/v)	Sucrose
	0.15 % (w/v)	Bromophenol blue
	0.2 M	EDTA
10 x TBE (Electrophoresis Running Buffer)	0.089 M	Tris-HCl
	0.089 M	Boric acid
	0.02 M	EDTA
Restriction enzyme digestion buffer One-Phor-All buffer (10 x)	100 mM	Tris-acetate (pH 7.5)
	100 mM	Magnesium acetate
	500 mM	Potassium acetate
	500 mM	Sodium chloride
10 x DNA ligation buffer, pH 7.5	660 mM	Tris-HCl
	50 mM	Magnesium chloride
	10 mM	Dithioerythritol (DTE)

	10 mM	ATP
Dephosphorylation of DNA	500 mM	Tris-acetate, pH 7.5
10 X CIAP Buffer		
	100 mM	Mg-acetate
	500 mM	K-acetate
	500 mM	NaCl
Polymerase Chain Reaction		
	5 UmL^{-1}	Taq polymerase enzyme
PCR Buffer (10X), pH 4.8	500 mM	Potassium chloride
	200 mM	Tris-HCl
	50 mM	$MgCl_2$
	20 mM	dNTPs (Pharmica)
		5 mM dATP
		5 mM dCTP
		5 mM dGTP
		5 mM dTTP
***D. discoideum* transformation**		
2 X HBS (Hepes Buffered Saline) pH 7.05, filter sterile	42 mM	HEPES
	274 mM	NaCl
	9.4 mM	KCl
	1.3 mM	$NaH_2PO_4.2H_2O$
	0.2 % (w/v)	Glucose
$CaCl_2$ Stock Solution	2 M	$CaCl_2.2H_2O$
Phagocytosis assay		
20 mM Phosphate buffer	2.35 mM	NaH_2PO_4
	17.65 mM	KH_2PO_4

	40 mM	Sodium azide
Na_2Pi-Triton X-100	0.25 % (v/v)	Triton X-100
	100 mM	Na_2PO_4

Pinocytosis assay

FITC-dextran	20 mg mL^{-1}	FITC-dextran in HL5
Sorensen's phosphate buffer, pH 6.0	2 mM	$Na_2HPO_4.2H_20$
	14.67 mM	KH_2PO_4
Na2Pi-Triton X-100	0.25 % (v/v)	Triton X-100
	100 mM	Na_2PO_4

Measurement of lysosomal mass	1 mM in DMSO	Lysosensor DND-167

Calcium Experiments

	20% (w/v) in methanol	Pluronic F-127
MES development buffer	10 mM	MES, pH 6.2
	10 mM	KCl
	0.25 mM	$CaCl_2$
Lysis solution	10 mM	MOPS
	10 mM	Ca-acetate
	1%	Triton X-100

Immunofluorescence

Lo-flo-HL5 medium	0.385 % (w/v)	D-glucose
	0.178 % (w/v)	Proteose peptone
	0.045 % (w/v)	Yeast extract
	0.0485 % (w/v)	KH_2PO_4
	0.12 % (w/v)	$Na_2HPO_4.12H_20$
Fixing solution	4 %	Paraformaldehyde
Blocking buffer in 1 x PBS	1 % (w/v)	BSA

	1 % (v/v)	cold water fish gelatin
	0.05 %	Na-Azide
	0.05 %	Tween 20

Antibiotic Stock Solutions, filter sterilized

Ampicillin	Ampicillin (sodium salt)	100 mg mL^{-1}
Streptomycin	Streptomycin (sulfate)	100 mg mL^{-1}
Kanamycin	Kanamycin (monosulfate)	25 mg mL^{-1}
Tetracycline	Tetracycline (hydrochloride)	10 mg mL^{-1}
Geneticin	Geneticin (sulphate	20 mg mL^{-1}

Appendix 3: List of enzymes

Restriction endonucleases	Promega
CIAP (Calf intestinal alkaline phosphatise)	Roche
RNase A	Roche
Taq DNA polymerase	Invitrogen
T4 DNA ligase	Promega
dNase I	Ambion
Pfu DNA polymerase	Promega
I Script Reverse Transcriptase	Bio-Rad

Appendix 4: Kits used

Name	Supplier
iScript™ One-Step RT-PCR Kit with SYBR® Green	Bio-Rad
Jetstar™ 2.0 Maxi Prep Kit 120	Gentaur
Eppendorf Perfectprep Gel Cleanup	Progen Biosciences

Appendix 5: Full names of suppliers

Invitrogen Corp., Mount Waverley, VIC, AUS

Millipore Corp., Billerica, MA, USA

Promega Corp., Madison, WI, USA

Roche Pty. Ltd., Basel, Switzerland

Sigma-Aldrich Chemical Company Pty. Ltd., Castle Hill, NSW, AUS

Bio-Rad Laboratories Pty. Ltd., Gladesville, NSW, AUS

Difco Laboratories Pty. Ltd., Detroit, MI, USA

Eppendorf South Pacific Pty. Ltd., North Ryde, NSW, AUS

Bioline Pty. Ltd., Alexandria, NSW, AUS

Astral Scientific, Gymea, NSW, AUS

Millipore Australia Pty. Ltd., North Ryde, NSW, AUS

Oxoid Australia Pty. Ltd., Adelaide, South Australia, AUS

Terumo Corporation, North Ryde, NSW, AUS

Turner Biosystems, Sunnyvale, CA, USA

ThermoFisher Scientific, Scoresby, VIC, AUS

Merck Pty. Ltd., Kilsyth, VIC, AUS

NuncTM. Part of Thermo Fisher Scientific, Rochester, NY, USA

Olympus Pty. Ltd., North Ryde, NSW, AUS

Sarstedt Australia Pty. Ltd., South Australia, AUS

Savant Instruments Inc., Minnesota, USA

Ajax Chemicals Pty. Ltd., Auburn, NSW, AUS

GenScript Biotech Corporation, New Jersey, USA

Appendix 6: Multiple regression analysis for section 5.2.3.6

Multiple Regression

X-Variables: Max rate increase nM/s
PAT3
intercept
PAT4
intercept
PAT3 slope
PAT4 slope

Y-Variable: Rate max decrease nM/s

Method: Stepwise

Steps	**P**	**R-Square**	**Corrected**
Max rate increase nM/s (+)	2.95425E-18	0.726525639	0.72189048
PAT3 slope (+)	6.33577E-07	0.82233003	0.816203479
PAT4 slope (+)	0.001553308	0.851183522	0.843351076

Summary

	N	**R**	**R-Square**	**Std.Error**
normal	61	0.922596078	0.851183522	1.053549503
corrected		0.918341481	0.843351076	

Equation

	Coefficient	**95% Conf. (±)**	**Std.Error**	**T**	**P**
Constant (intercepts all)	0.031491296	0.69197888	0.345563434	0.091130291	0.927708568
Control slope	-0.625736053	0.087846375	0.043869106	-14.26370641	1.85277E-20
PAT3 slope	-0.314807398	0.092942327	0.046413945	-6.782603729	7.32073E-09
PAT4 slope	-0.121355222	0.073099165	0.03650458	-3.324383472	0.001553308

Analysis of variance

	Sum of Squares	Degrees of Freedom	Mean Square	F	P
Regression	361.873629	3	120.624543	108.6740339	1.48721E-23
Residue	63.26809362	57	1.109966555		
Total	425.1417226	60	7.085695377		

Figure 8.1. Multiple regression analysis for Figure 5.14A. Folic acid responses, relationship between maximum rise and fall rates in control, PAT3 knockdown. and PAT4 knockdown. The slopes for the control HPF401, PAT3 and PAT4 responses are significantly different (p= 1.85277E-20; p=7.32073E-09 and p=0.001553308 respectively highlighted in green). The intercepts for all three strain sets are not significantly different, highlighted in blue (p=0. 927708568), therefore all strains share the same intercept.

Multiple Regression

X-Variables: Max rate increase nM/s
PAT3
intercept
PAT4
intercept
PAT3 slope
PAT4 slope

Y-Variable: Rate max decrease nM/s

Method: Stepwise

Steps	**P**	**R-Square**	**Corrected**
Max rate increase nM/s (+)	1.89126E-19	0.584841924	0.580377858
PAT4 intercept (+)	0.002881832	0.623240508	0.615050085
PAT4 slope (+)	0.027905169	0.642835765	0.63106112

Summary

	N	**R**	**R-Square**	**Std.Error**
normal	95	0.801770394	0.642835765	2.068526582
corrected		0.794393555	0.63106112	

Equation

	Coefficient	**95% Conf. (±)**	**Std.Error**	**T**	**P**
Control and PAT3 intercept	-0.835958409	1.149600493	0.57874228	-1.444439845	0.152049705
Control and PAT3 slope	-0.655428437	0.119013209	0.059914706	-10.93935826	2.83828E-18
PAT4 intercept	-4.062636474	2.525625647	1.271473312	-3.195219621	0.001920822
PAT4 slope	0.269105252	0.239233343	0.120437014	2.234406551	0.027905169

Analysis of variance

	Sum of Squares	**Degrees of Freedom**	**Mean Square**	**F**	**P**

Regression	700.8025488	3	233.6008496	54.59491644	2.79981E-20
Residue	389.3710019	91	4.278802219		
Total	1090.173551	94	11.59759097		

Figure 8.2. Multiple regression analysis for Figure 5.14B. cAMP responses, relationship between maximum rise and fall rates in control, PAT3 knockdown. and PAT4 knockdown. The overall regression was significant, p= 2.79981 x 10^{-20}, however the slope and intercept for the PAT4 knockdown line was significantly different from the lines of the control and PAT3, highlighted in green (intercept p= 0.001920822, slope p= 0.027905169).

Multiple Regression

X-Variables: Time onset (-5)
PAT3 onset time intercept
PAT4 onset time intercept
PAT3 onset time slope
PAT4 onset time slope

Y-Variable: Delta Ca rise

Method: Stepwise

Steps	**P**	**R-Square**	**Corrected**
Time onset (-5) (+)	0.029994904	0.081348576	0.064944087

Summary

	N	**R**	**R-Square**	**Std.Error**
normal	58	0.285216718	0.081348576	27.25376768
corrected		0.254841297	0.064944087	

Equation

	Coefficient	**95% Conf. (±)**	**Std.Error**	**T**	**P**
Intercept all strains	97.98988425	17.42238522	8.697100115	11.26696059	5.08563E-16
Slope all strains	-3.92691369	3.532570866	1.763428032	-2.226863597	0.029994904

Analysis of variance

	Sum of Squares	**Degrees of Freedom**	**Mean Square**	**F**	**P**
Regression	3683.32746	1	3683.32746	4.958921479	0.029994904
Residue	41594.99976	56	742.7678529		
Total	45278.32722	57	794.3566179		

Figure 8.3. Multiple regression analysis for Figure 5.19A. Folic acid responses onset time vs. response magnitude. Strain type made no difference to the intercept, they were not significantly different from each other. The slopes for all three lines were not significantly different from each other. Since all of the responses began after 5 seconds, the regression analysis was done using onset time – 5 seconds to facilitate more accurate regression analysis of the responses from a time just before they started.

Multiple Regression

X-Variables: Time onset (-5)
PAT3 onset time intercept
PAT4 onset time intercept
PAT3 onset time slope
PAT4 onset time slope
Control onset time slope

Y-Variable: Delta Ca rise

Method: Stepwise

Steps	**P**	**R-Square**	**Corrected**
Control onset time slope (+)	0.000960455	0.217235725	0.199840964

Summary

	N	**R**	**R-Square**	**Std.Error**
normal	47	0.466085534	0.217235725	33.11164354
corrected		0.447035752	0.199840964	

Equation

95%

	Coefficient	**95% Conf. (±)**	**Std.Error**	**T**	**P**
Intercept all strains	145.7460292	11.00733354	5.465128371	26.66836336	3.26285E-29
Control slope	-11.26715286	6.421545474	3.188289901	-3.533917306	0.000960455

Analysis of variance

	Sum of Squares	**Degrees of Freedom**	**Mean Square**	**F**	**P**
Regression	13692.23176	1	13692.23176	12.48857152	0.000960455
Residue	49337.14219	45	1096.380938		
Total	63029.37395	46	1370.203781		

Figure 8.4. Multiple regression analysis for Figure 5.19B. cAMP responses onset time vs. response magnitude. The slope for the control is negative and significantly different from 0, highlighted in green (p=0.000960455). The intercepts for each strain set were not significantly different from each other so all passed through 145.746. Since all of the responses began after 5 seconds, the regression analysis was done using onset time – 5 seconds to facilitate more accurate regression analysis of the responses from a time just before they started.

Appendix 7: Mass spectrometry protocol for identification of Ddmucolipin in gel bands

Excised SDS-PAGE gel bands were destained in 50% acetonitrile, 50 mM ammonium bicarbonate (ABC) until clear of Coomassie dye before dehydration in 100 % acetonitrile. Protein in the gel band was reduced with 2 mM tris-2-carboxyethyl-phosphine (TCEP) in 20 mM ABC (60 min incubation), followed by exchange to iodoacetamide (40 mM in ABC for 45 min, in darkness). The gel band was then washed in 50% acetonitrile, 20 mM ABC for 30 min, dehydrated with 100 % acetonitrile, before rehydration with sequencing grade trypsin (125 ng, Promega) in 100 uL of 20 mM ABC. Trypsin digestion was completed overnight at 37 °C. Tryptic peptides were recovered as the supernatant and the gel band was then subjected to repeated dehydration in 85% acetonitrile, 0.5% Trifluoracetic acid (TFA) to extract the remaining peptides in the gel band. Recovered peptides were concentrated on a speedvac and resuspended in 15 uL of 5 % acetonitrile, 0.5% TFA. Samples were briefly centrifuged to pellet any debris before transfer to mass-spec vials for LC-MS analysis of the peptides.

Tryptic peptides were separated on a Thermo Ultimate 3000 RSLCnano UHPLC system and Thermo Q-Exactive HF Orbitrap mass-spectrometer (Thermo-Fisher Scientific, Waltham, MA, USA). Peptides (5 µL) were loaded onto a PepMap C18 5 µm 0.5 cm trapping cartridge (Thermo-Fisher Scientific, Waltham, MA, USA) and washed at 10 µL/min for 6 min (Buffer C: 0.1% (v/v) trifluoracetic acid, 2% (v/v) ACN) before switching the pre-column in line with the analytical column held at 55 °C (nanoEase M/Z Peptide BEH C18 Column, 1.7 µm, 130 Å and 75 µm ID × 25 cm, Waters). The separation of peptides was performed at 250 nL/min using a linear ACN gradient of buffer A (0.1% (v/v) formic acid, 2% (v/v) ACN) and buffer B (0.1% (v/v) formic acid, 80% (v/v) ACN), starting at 12% buffer B to 30% over 54 min, then rising to 50% B over 10 min followed by 95% B in 6 min. The column was then cleaned for 5 min at 95% B and then afterward a 13 min short equilibration step completed at 1% B. Blanks were run between sample injections.

Data were collected with Orbitrap HCD parameters including Data Dependent Acquisition (DDA) using as MS scan range and CID MS/MS spectra collected. Dynamic exclusion parameters were set as follows: exclude isotope on, exclude after n = 1 times, duration 60 s, charge state 2-7, cycle time was set to 3 seconds, and used the peptide monoisotopic peak determination mode. Other instrument parameters were: MS1 scan at 60,000 resolution, m/z 350–1500, AGC target 3e6, injection time max 30 ms. MS2 scans were at

60,000 resolution, m/z 200–2000, AGC target 1e5, injection time max 110 ms. The top seven ions were fragmented per cycle. The isolation window of the quadrupole for the precursor was 1.4 m/z. Lock mass was set using m/s 445.12003 for internal mass calibration.

Raw files were searched using PEAKS studio XPRO (v 10.6). Search was performed against the dictyBase reference proteome. The protein database was supplemented with sequences from the Common Repository of Adventitious Proteins to account for typical lab contaminants (https://www.thegpm.org/crap). Fixed modification of carbamidomethyl cysteine, and variable modifications of oxidation of methionine, acetylation of protein n-terminus, carbamylation of lysine and protein n-terminus were used in the search. The parent ion mass error tolerance was 10.0ppm and the fragment mass error tolerance was 0.05 Da. Up to three missed trypsin cleavages were permitted and the search false discovery rate was set to a maximum of 1%.

Appendix 8: Published work

The following statements refer to the published manuscript:

Allan, C. Y. and Fisher P. F. (2022). The *Dictyostelium* model for Mucolipidosis Type IV. *Front. Cell Dev. Biol* **10,** *doi:* 10.3389/fcell.2022.741967

Statement of contributions of joint authorship:

Allan, C.Y. (Candidate)

Experimental design, conducted all experiments, analysis of data, wrote manuscript.

Fisher, P.R. (Principal supervisor)

Experimental design, contributed to analysis of data and contribution to the drafting of the manuscript.

frontiers | Frontiers in Cell and Developmental Biology

ORIGINAL RESEARCH
published: 13 April 2022
doi: 10.3389/fcell.2022.741967

The *Dictyostelium* Model for Mucolipidosis Type IV

*Claire Y. Allan and Paul R. Fisher**

Department of Physiology, Anatomy and Microbiology, La Trobe University, Melbourne, VIC, Australia

Mucolipidosis type IV, a devastating neurological lysosomal disease linked to mutations in the transient receptor potential channel mucolipin 1, TRPML1, a calcium permeable channel in the membranes of vesicles in endolysosomal system. TRPML1 function is still being elucidated and a better understanding of the molecular pathogenesis of Mucolipidosis type IV, may facilitate development of potential treatments. We have created a model to study mucolipin function in the eukaryotic slime mould *Dictyostelium discoideum* by altering expression of its single mucolipin homologue, *mcln*. We show that in *Dictyostelium* mucolipin overexpression contributes significantly to global chemotactic calcium responses in vegetative and differentiated cells. Knockdown of mucolipin also enhances calcium responses in vegetative cells but does not affect responses in 6–7 h developed cells, suggesting that in developed cells mucolipin may help regulate local calcium signals rather than global calcium waves. We found that both knocking down and overexpressing mucolipin often, but not always, presented the same phenotypes. Altering mucolipin expression levels caused an accumulation or increased acidification of Lysosensor Blue stained vesicles in vegetative cells. Nutrient uptake by phagocytosis and macropinocytosis were increased but growth rates were not, suggesting defects in catabolism. Both increasing and decreasing mucolipin expression caused the formation of smaller slugs and larger numbers of fruiting bodies during multicellular development, suggesting that mucolipin is involved in initiation of aggregation centers. The fruiting bodies that formed from these smaller aggregates had proportionately larger basal discs and thickened stalks, consistent with a regulatory role for mucolipin-dependent Ca^{2+} signalling in the autophagic cell death pathways involved in stalk and basal disk differentiation in *Dictyostelium*. Thus, we have provided evidence that mucolipin contributes to chemotactic calcium signalling and that *Dictyostelium* is a useful model to study the molecular mechanisms involved in the cytopathogenesis of Mucolipidosis type IV.

Keywords: mucolipidosis IV, calcium signalling, acidic vesicles, lysosomes, endocytosis, plasma membrane, aggregation, growth

OPEN ACCESS

Edited by:
Robert J. Huber,
Trent University, Canada

Reviewed by:
Stephane Lefrancois,
Université du Québec, Canada
Sabateeshan Mathavarajah,
Dalhousie University, Canada
Pierre Cosson,
Université de Genève, Switzerland

****Correspondence:***
Paul R. Fisher
p.fisher@latrobe.edu.au

Specialty section:
This article was submitted to Molecular and Cellular Pathology, a section of the journal Frontiers in Cell and Developmental Biology

Received: *15 July 2021*
Accepted: *21 March 2022*
Published: *13 April 2022*

Citation:
Allan CY and Fisher PR (2022) The Dictyostelium Model for Mucolipidosis Type IV. Front. Cell Dev. Biol. 10:741967. doi: 10.3389/fcell.2022.741967

1 INTRODUCTION

Transient receptor potential mucolipins (TRPML) belong to a conserved family of ion channels (Dong et al., 2010), which localize to the membranes of components of the endocytic pathway. The three mammalian mucolipin homologues, TRPML1, TRPML2 and TRPML3, are encoded by the genes *MCOLN 1–3* (Cheng et al., 2010; Grimm et al., 2012). TRPML channels are non-selective

cation channels permeable to a range of cations. Alongside two pore channels (TPC), TRPML channels are believed to facilitate endolysosomal Ca^{2+} signalling which regulates trafficking and sorting of the membranes of endocytic vesicles (Cheng et al., 2010), organelle homeostasis, compartmental acidification (Gerasimenko et al., 1998; Dong et al., 2010; Morgan et al., 2011) and homotypic and heterotypic vesicle fusion and reformation (Pryor et al., 2000; Hay, 2007; Luzio et al., 2007; Brailoiu and Brailoiu, 2016; Cao et al., 2017). Additionally, TRPML1 is implicated in regulation of autophagy, mechanistic target of rapamycin (mTOR) and transcription factor EB (TFEB) signalling (Sun et al., 2018; Boudewyn and Walkley, 2019). Loss of function mutations in TRPML1, causes the neurological disease Mucolipidosis Type IV (MLIV) (Sun et al., 2000), and TRPML-associated dysfunction in the endolysosomal system is implicated in other neurodegenerative diseases (Santoni et al., 2020; Lee et al., 2021). Therefore, TRPMLs may underpin the pathophysiology of neurodegenerative disease more generally and are suggested to be a therapeutic target.

It is not well understood how loss TRPML1 function causes lysosomal storage and neuronal dysfunction, but it is believed that Ca^{2+} signalling plays a central role. The vesicles of the endolysosomal system are essential to maintenance of cellular homeostasis through macromolecule recycling and are important Ca^{2+} storage organelles which are integral to cellular Ca^{2+} signalling (Patel and Docampo, 2010; Patel and Cai, 2015) and can help regulate ER calcium signals by sequestering calcium (López-Sanjurjo et al., 2013; López-Sanjurjo et al., 2014). Ca^{2+}-dependent signalling is thought to regulate the soluble N-ethylmaleimide-sensitive-factor attachment protein receptors (SNARE) complex proteins, which are proteins involved in the fusion of vesicle membranes (Bharat et al., 2014; Han et al., 2017). Alongside SNAREs, the protein early endosome antigen-1 (EEA1) is necessary for vesicle tethering prior to fusion, and is regulated by Ca^{2+}/calmodulin dependent signalling through its IQ domain (Mills et al., 1998; Christoforidis et al., 1999; Lawe et al., 2003). TRPML specific perilysosomal calcium signals have been notoriously difficult to measure due to the localised nature of the signals which are often clouded by larger global calcium signals. In an attempt to resolve the local calcium signals genetically encoded calcium sensors directly tagged to TRPML1 have been used to measure local calcium transients (Shen et al., 2012; Cao et al., 2015; Medina et al., 2015). The TRPML agonist ML-SA1 stimulates calcium release into the cytoplasm (Shen et al., 2012), which in some cell types is independent of extracellular and ER calcium pools (Gómez et al., 2018). However, some evidence shows that TRPML channels can affect ER calcium release and activate influx of calcium across the plasma membrane to contribute to global calcium signals (Kilpatrick et al., 2016), and small calcium release from the acidic stores can prime and amplify calcium release from the ER (Ronco et al., 2015).

A variety of model organisms have been used to study TRPML proteins including the mouse (Kim et al., 2007; Micsenyi et al., 2009; Curcio-Morelli et al., 2010), zebrafish (Benini et al., 2013), *Drosophila* (Venkatachalam et al., 2008; Wong et al., 2012; Feng et al., 2014), *C. elegans* (Fares and Greenwald, 2001; Treusch et al., 2004) and yeast (Denis and Cyert, 2002). One important cellular model, the eukaryotic social amoeba, *Dictyostelium*, encodes a single mucolipin homologue, *mcln* (Wilczynska et al., 2005; Lima et al., 2012) which has been the subject of only a limited number of studies. *Dictyostelium* is a well-established model to study neurodegenerative and lysosomal disease (Annesley and Fisher 2009; Maniak, 2011; Annesley et al., 2014; Martín-González et al., 2021). This model organism has been extensively employed to study neuronal ceroid lipofuscinosis (NCL) (Huber, 2020), a group of lysosomal diseases linked to mutations in the genes, *CLN1–CLN8* and *CLN10–CLN14* (Yap et al., 2021). Therefore, *Dictyostelium* is an ideal model to study lysosomal disorders and mucolipin function. In other work, expression of FLAG-tagged mucolipin was used to show that the protein localizes predominately to post-lysosomes, but may also be present in other endocytic compartments (Lima et al., 2012), and accordingly controls lysosome exocytosis. Evidence suggests that mucolipin is involved in Ca^{2+} homeostasis and signalling because knockout cells had reduced Ca^{2+} concentrations in secretory lysosomes (Lima et al., 2012) and are also defective in rheotaxis, a calcium-regulated mechanosensing mechanism (Lima et al., 2014). The role of this putative channel in Ca^{2+} signalling has not been studied, so it was of particular interest to investigate the role of mucolipin in chemotactic calcium signalling in *Dictyostelium*.

Dictyostelium is a well-established model to study calcium signalling, and cells experience cytosolic calcium transients when stimulated with various extracellular stimuli including the chemoattractants cAMP and folic acid (Nebl and Fisher, 1997; Traynor et al., 2000; Nebl et al., 2002; Schaloske et al., 2005; Fisher and Wilczynska, 2006; Malchow et al., 2008). These Ca^{2+} signals originate from the extracellular environment, the endoplasmic reticulum (ER) (Wilczynska et al., 2005) and the contractile vacuole (CV) (Malchow et al., 2006; Gross, 2009). Other intracellular Ca^{2+} stores including mitochondria, acidocalcisomes and vesicles of the endocytic pathway are likely to also contribute to the calcium responses. Given the localisation of mucolipin at the post-lysosomes and potentially other vesicles of the endocytic pathway, we decided to determine if mucolipin and these endocytic vesicles are involved in cytosolic Ca^{2+} responses to chemoattractants.

To achieve this, we created mucolipin overexpression and knockdown strains which coexpress the calcium-sensitive luminescent protein apoaequorin which allowed us to analyze real-time chemotactic induced cytoplasmic Ca^{2+} responses (Nebl and Fisher, 1997). Our experiments revealed that when overexpressed, mucolipin is involved in chemoattractant-elicited Ca^{2+} responses because overexpression strains had enhanced responses to both cAMP and folic acid. Surprisingly, chemoattractant Ca^{2+} responses in knockdown strains were also enhanced, but only in vegetative cells. Responses in aggregation-competent cells were not affected in the knockdown strains, suggesting that, unless overexpressed, mucolipin is not a major contributor to cAMP-mediated calcium responses. However, it may be involved in local Ca^{2+} signalling associated with changes in the vesicle trafficking pathways throughout the developmental cycle, in particular aggregation center formation and autophagic

cell death. In other work, the cellular phenotypes of growth, endocytosis and multicellular development were found to be unaffected in mucolipin knockout cells created from the parental strain DH1-10 (Lima et al., 2012). Therefore, we decided to analyze these phenotypes in our strains which were created from the parental strain AX2. We discovered that mucolipin expression did affect growth rates and nutrient uptake via macropinocytosis and phagocytosis in AX2. Surprisingly however, the phenotypes were not linear in that both increasing and decreasing expression of mucolipin often, but not always, resulted in the same phenotypic outcome. Both overexpression and knockdown strains had increased fluorescence in cells stained with Lysosensor blue, indicating either increased acidification of the vesicles or increased abundance of the vesicles. Phagocytosis and pinocytosis rates were upregulated, but this did not correlate with an increase in growth rates, which suggests defects in catabolism, in endocytic vesicle trafficking or in endolysosomal breakdown of macromolecular contents. Mucolipin is involved in the regulation of aggregation as both overexpression and knockdown strains formed smaller, more numerous slugs and fruiting bodies than AX2, a phenotype that is also present in other *Dictyostelium* lysosomal disease models of NCL (Huber et al., 2014; Huber et al., 2017; Smith et al., 2019; McLaren et al., 2021). Increased numbers of cells entering the autophagic cell death pathway were also evident in mucolipin mutants because they had thickened stalks compared to AX2. Our results suggest that normal growth and development of *Dictyostelium* is sensitive to mucolipin expression, and our strains show similar phenotypes to other *Dictyostelium* lysosomal disease models further affirming that *Dictyostelium* is an ideal model to study lysosomal disease.

2 MATERIALS AND METHODS

2.1 Gene Cloning and Sequence Analysis

To create a mucolipin overexpression construct, the 2,599 bp *mcln* genomic DNA (DictyBase gene no. DDB_G0291275) was amplified in two sections from parental strain AX2 genomic DNA using the primers MUF (CGCGGATCCATCGATATGACATCT TTTAAAGGTGACAG) and MuMR (AACTAACGGT ACCAGGTACTTC) for the 5′ fragment, and MuMF (GAA GTACCTGGTACCGTTAGTTC) and MUR2 (CGCGGA TCCCTCGAGCATCATATC TCAATACCTGAATC) for the 3′ fragment. A three fragment ligation allowed the full length genomic DNA to be cloned into the bacterial vector pZErO™-2(Invitrogen, Carlsbad, CA, United States) with the restriction enzyme *Bam*HI (underlined). To join the 5′ and 3′ fragments of the gene together, the primers used in amplification of the two fragments spanned a region of the gene that encodes the restriction site *Kpn*I (bold) this allowed seamless ligation of the two gene fragments. The full-length gene was then subcloned for overexpression into the *Dictyostelium* vector pA15GFP using the restriction cut sites *Cla*I and *Xho*I, this plasmid was named pPROF638. To create the *mcln* antisense RNA inhibition plasmid (pPROF650) a fragment encoding 1411bp of the gene from position 1365bp to position 3776bp in the gDNA sequence was amplified via PCR with the primers MuMF (GAAGTACCTGGTACCGTTAGTTC) and MUR2 (CGCGGATCCCTCGAGCATCATATC TCAATACCTGAATC) from genomic DNA extracted from vegetative AX2 cells using DNAzol® (Invitrogen). The products were then cloned into pZErO™-2 using *Bam*H1 and *Kpn*1 and subcloned into the *Dictyostelium* expression vector pDNeo2 (Witke et al., 1987) with *Bam*H1 and *Kpn*1. Clones were verified by restriction digestion as well as sequencing at the Australian Genome Research Facility, Brisbane, Australia. Sequence analyses, alignments, and database searches were conducted using Web-based software through DictyBase.org (Fey et al., 2009), ExPASy and the Australian Genome Research Facility.

2.2 Strains and Culture Conditions

All experiments were conducted with *Dictyostelium* parental strain AX2, and transformants derived from it (names beginning with HPF). Each transformant strain carried multiple copies of the constructs: 1) pPROF120 (apoaequorin expression plasmid) and pPROF650 (antisense strains: HPF812-818, HPF640); 2) pPROF120 and pPROF652 (sense strains: HFP819 and HPF861) and 3) pPROF120 and pPROF638 (overexpression strains: HPF820-829, HFP654-656). The $Ca(PO_4)_2$/DNA coprecipitation method was used to isolate all transformants, by cotransformation with both plasmids (Nellen et al., 1984). Transformants were selected as isolated colonies on lawns of *Micrococcus luteus* (Wilczynska and Fisher, 1994) on standard medium agar [(SM) 1.0% (w/v) Oxoid agar; 1.0% (w/v) Oxoid bacteriological peptone; 1.0% (w/v) glucose; 0.1% (w/v) Oxoid yeast extract; 4.1 mM $MgSO_4{\cdot}7H_2O$; 16.2 mM KH_2PO_4; 5.8 mM K_2HPO_4 supplemented with 20 μg ml^{-1} Geneticin (G-418) (Promega Corporation, Madison, WI, United States)]. *D. discoideum* cells were grown on lawns of *Enterobacter aerogenes* as a food source on SM (Standard Medium) nutrient agar and incubated at 21°C for 3–4 days and subcultured as required from a single colony. To prepare liquid cultures, 5–10 spores were inoculated into a well of a 24-well Costar plate containing 1.5 ml HL5 axenic medium (1% (w/v) Bacto™ proteose peptone; 0.5% (w/v) Bacto™ yeast extract; 2.8 mM $Na_2HPO_4{\cdot}2H_2O$; 2.6 mM KH_2PO_4; 1% (w/v) glucose pH 6.4) supplemented with geneticin (20 μg ml^{-1}), ampicillin (100 μg ml^{-1}), streptomycin (500 μg ml^{-1}) and tetracycline (100 μg ml^{-1}), and incubated at 21°C to allow spores to germinate and form amoebae. Once confluence was reached 1 ml of culture was inoculated into 10 ml HL5 in T25 flask (Falcon) and cells were grown to the density of 1–2 × 10^6 cells ml^{-1} shaking at 150 rpm and 21°C. Strains were then subcultured at least once into HL5 without antibiotics and grown for 24–48 h prior to use in phenotypic assays to remove possible effects of the antibiotics on phenotypic readouts. Unless otherwise stated, cells were harvested by centrifugation at 500 ×*g* for 5 min.

2.3 Estimation of Plasmid Copy Number

Genomic DNA was extracted from transformants using DNAzol® (Invitrogen). Quantitative Southern blot was used to estimate

plasmid copy number of *mcln* overexpression strains (Fernando et al., 2020). DNA loaded gels were stained with SYBR® Green I nucleic acid gel stain (Sigma-Aldrich®) and DNA was quantified using the Storm 860 Fluroimager (GE Healthcare, United Kingdom) in fluorescence mode. Southern blots of the same DNA samples were quantitated using fluorescein-labelled DNA probes, in conjunction with anti-fluorescein alkaline peroxidase conjugate antibody, and enhanced with the chemi-fluorescein substrate (GE Healthcare, United Kingdom). The Storm 860 Fluroimager fluorescence mode was used to quantitate Southern blots.

Quantitative real time PCR was used to estimate plasmid copy number in *mcln* antisense RNA strains (Fernando et al., 2020). SYBR® Green (BioRad, Hercules, CA, United States) was used for amplicon detection of a 135 bp fragment of *mcln* with the primers (500 nM final concentration) MF1.1 (5-GATTGGTCTTGGTAC TTTGTTA-3) and MR1.2 (5-GGGAGACTTCCAGCCGAG-3), within the genomic DNA extracts, and to construct a standard curve, over a range of DNA concentrations using purified pPROF650 as a template. To quantify genomic DNA extracts a 100 bp filamin amplicon was amplified with the primers FIL1588F (5-CCCTCAATGATGAAGCC-3) and FIL1688R (5-CCATCTAAACCTGGACC-3) in genomic DNA from all strains, and the concentrations calculated from a standard curve. The PCR amplification used 35 cycles of denaturation at 95°C for 30 s, annealing at 58°C for 30 s and extension and data collection at 72°C for 1 min.

2.4 Expression Analysis

Quantitative real time RT-PCR was used to quantitate expression levels of *mcln* messenger RNA. RNA was collected from 10^7 vegetative cells or developing cells harvested from water agar at the time points indicated over the course of development, and extracted using TRIzol® (Invitrogen). The iScript™ One-Step RT-PCR Kit with SYBR® Green (BioRad, Hercules, CA, United States) was used for amplicon detection of a 135 bp fragment of *mcln* with the primers MF1.1 and MR1.2, and a 100 bp amplicon of the constitutively expressed protein filamin, with the primers FIL1588F and FIL1688R. A total RNA template of 50–100 ng was added to the total reaction mixture of 50 µl; cDNA synthesis was performed at 50°C for 10 min, and the PCR amplification used 35 cycles of denaturation at 95°C for 30 s, annealing at 58°C for 30 s and extension and data collection at 72°C for 1 min. Expression levels were normalised against the filamin levels to adjust for loading and then measured relative to AX2 controls.

2.5 Protein Techniques

2.5.1 Antibody Production

A polyclonal antibody called anti-MUECD directed against the *Dictyostelium* mucolipin was used in the study. A 200aa His-tagged portion of mucolipin (aa101–aa301) was expressed in *E. coli* and purified by Genscript®. Polyclonal antibodies directed against MUECD were raised in a rabbit by the Institute of Medical and Veterinary Science (Adelaide, SA, Australia), and affinity purified as described previously (Smith and Fisher, 1984).

2.5.2 Western Blot

Cells were grown in HL5 medium and 1×10^6 cells harvested and lysed in 100 µl 1 × Bolt LDS sample buffer (Thermo Fisher Scientific) with a protease inhibitor 1 cocktail (Complete-EDTA free, Roche) on ice from 30 min then centrifuged at 1,200 rpm for 2 min. 10 µl of lysate was mixed with 1% Bolt sample reducing agent (Thermo Fisher Scientific) was incubated at 70°C for 10 min then loaded onto a Bolt™ 4–12%, Bis-Tris-Plus, 1.0 mm, Protein Gel, 12-well (Invitrogen) with the Broad Multi Color Pre-Stained Protein Standard (Genscript) and subject to electrophoresis. To visualise the protein bands, protein was transferred to PVDF membrane (Amersham Hybond™-P, GE Healthcare) for 1 h at 100 V at 4°C. Protein was visualised on the membrane by staining with No Stain Protein Labelling Reagent (Invitrogen) as per the manufactures instructions, and visualised on a Bio Rad Chemidoc MP imaging system. Membraned we then blocked with 1% casein in 1 × TBS for 3 h RT and probed with polyclonal rabbit anti-MUECD 1:500 in 1% casein in 1 × TBS with 0.1% Tween-20 for 2 h RT. The SNAP i.d.® 2.0 Protein Detection System was used for application of anti-rabbit HRP conjugate (Life technologies) 1: 10,000 in TBS-T as per manufacturer's instructions. Bands were detected with Clarity Western ECL substrate (Bio Rad), with chemiluminescence imaged on Amersham Imager 600 (GE Healthcare Life Sciences). The intensities of the total loaded protein in each lane and specific antigen bands were quantified digitally using the Image Quant TL 1D v 8.1 software 19 (GE Healthcare Life Sciences).

2.6 Determination of Growth Rates

2.6.1 Growth on Bacterial Lawns

Growth rates of *Dictyostelium* on lawns of bacteria were measured as previously described (Bokko et al., 2007). Lawns of *E. coli* B2 were prepared on normal agar [20 g L^{-1} agar (Difco, Detroit, MI, United States); 1 g L^{-1} peptone (Oxoid, Basingstoke, United Kingdom), 1.1 g L^{-1} anhydrous glucose, 1.9972 g L^{-1} KH_2PO_4, and 0.356 g L^{-1} $Na_2HPO_4{\cdot}2H_2O$, pH 6.0]. An aliquot of 20 µl of *Dictyostelium* culture at a density of 1×10^6 cells ml^{-1}, was inoculated onto the center of each lawn and incubated at 21°C for 100 h, during which time the plaque diameter (mm) was measured at intervals of 8–12 h. The recorded values were analyzed by linear regression using the "R" environment for statistical computing and graphics (http://www.R-project.org) to determine the plaque expansion rate (mm/h).

2.6.2 Growth Rates of Axenically Growing Cultures

Generation times of axenically growing *Dictyostelium* cultures was measured as previously described (Bokko et al., 2007). Cultures of *Dictyostelium* were grown to exponential phase in HL5 medium to a density of ~1–2 × 10^6 cells ml^{-1} and were used to inoculate 50 ml of fresh HL5 medium (no antibiotics) to an initial density of 1×10^4 cells ml^{-1}. Cultures were incubated at 21°C on an orbital shaker at 150 rpm for 100 h, during which time cell densities were determined at 8–12 h intervals, by counting 10 µl aliquots using a hemocytometer. The cell densities were then analyzed by log-linear regression using the "R"

programming environment computer software to determine the generation time from the exponential growth curve.

2.7 Measurements of Macropinocytosis Rates

Measurements of macropinocytosis rates as previously described (Bokko et al., 2007), were performed using fluorescein isothiocyanate (FITC)-dextran (Sigma-Aldrich; average mol. mass, 70 kDa; working concentration, 2 mg ml^{-1} in HL5 growth medium). Cultures of axenically growing *Dictyostelium* cells were harvested, and resuspended in fresh HL5 medium and shaken at 150 rpm for 30 min at 21°C, and after the addition of FITC-dextran, duplicate aliquots at time points 0 and 70 min were lysed in 0.25% (vol/vol) Triton X-100 in 100 mM Na_2HPO_4, pH 9.2 and the fluorescence of the lysate was measured in a Modulus fluorometer (Turner BioSystems) using the (Green Module 525 nm excitation and 580–640 nm emission). The cell density, increase in fluorescence over 70 min, and a separate calibration curve relating fluorescence signal to the volume of fluorescent medium, were used to calculate the hourly rate of uptake of medium.

2.8 Measurements of Phagocytosis Rates

The rate of uptake of *E. coli* expressing the fluorescent protein DsRed (Maselli et al., 2002) was used to measure phagocytosis rates in *Dictyostelium* strains. DsRed-expressing *E. coli* (DsRed-Ec) cells were harvested from NB cultures (containing 75 μg ml^{-1} ampicillin and 1 mM IPTG), grown at 37°C shaking for 24 h and resuspended to a density of 2–4 × 10^{10} bacteria ml^{-1} in 20 mM Sorenson's buffer (2.353 mM $Na_2HPO_4 2H_2O$ and 17.65 mM KH_2PO_4, pH 6.3). The density and fluorescence of the bacterial culture in a given experiment, were used to determine the fluorescence signal per million bacteria. A separate calibration curve was used to determine the relationship between OD600 and the density of the bacterial suspension.

Cultures of *Dictyostelium* were harvested, washed, and resuspended in Sorenson's buffer at 1 × 10^6 cells ml^{-1} and starved for 30 min at 21°C shaking. Following the 30 min incubation 1 ml of the prepared DsRed-Ec suspension was added to the *Dictyostelium* cultures and immediately duplicate ^{0}T aliquots were removed and added to preprepared ice cold 20 mM Sorenson's buffer containing 5 mM sodium azide. The remaining amoebae were allowed to uptake DsRed-Ec for 30 min with shaking. During this time amoebae in the ^{0}T samples were collected by centrifugation at 1, 000 × g for 30 s and cells washed with 20 mM Sorenson's buffer containing 5 mM sodium azide, resuspended in 3 ml of 20 mM Sorenson's buffer and counted using a hemocytometer. After 30 min of uptake duplicate T30 aliquots of the amoebae/DsRed-Ec suspension we removed and added to preprepared ice cold 20 mM Sorenson's buffer containing 5 mM sodium azide and the amoebae washed free of bacteria. A Modulus fluorometer 9200-003 (Turner Bio-Systems, Sunnyvale, CA, United States) fitted with a specially constructed module designed for DsRed-Ec (530-nm excitation and 580-nm emission) was used to measure fluorescence in samples that had been lysed by the addition of 0.25% (v/v) Triton X-100 in Na_2HPO_4. Increase in fluorescence over 30 min was used to calculate ingestion of DsRed-Ec cells per hour by a single amoeba.

ΔF (bacteria ml^{-1}) = difference in fluorescence over the course of the assay (fluorescence at T30–T0).

Uptake (bacteria $amoeba^{-1}$ h^{-1}) = ΔF × 10^6/total cell count (amoebae ml^{-1})/time (h).

2.9 Quantification of Aggregate Size

Quantification of aggregate size was achieved by determining the number of cells in individual slugs. Strains were grown to exponential phase in HL5 medium and 1 × 10^7 cells were harvested, washed 2 × in PBS and resuspended in 1 ml 1 × PBS. The suspension was then inoculated onto a water agar plate (10 g agar/1 L dH_2O) in a 1 cm × 5 cm line, to give a density of 2 × 10^6 cells/cm^2 and allowed to dry. The plate was placed in a dark container with a single point of light source and incubated at 21°C until slugs had formed and migrated away from the point of inoculation (typically ~12–16 h). Individual slugs were then isolated using a sterile needle and resuspended in 100 μl of saline and dissociated by repeat pipetting. The number of cells per slug was then calculated after counting the number of cells in duplicate 10 μl suspensions using a hemocytometer in 30 individual slugs for each strain.

2.10 Morphology, Quantification of Number of Fruiting Bodies and Quantification of Sorus Area

Mature fruiting body morphology was observed, after multicellular development on lawns of *Enterobacter* as described previously (Kotsifas et al., 2002). Images were taken after 24 h of development. Photographs were taken using from above or from the side on an excised piece of agar using a Moticam 2300 camera attached to an Olympus SZ61 stereomicroscope. To quantify the number of fruiting bodies images were taken from above at the same magnification for all strains. The number of fruiting bodies in the same area of photograph were counted and the means calculated. Sorus area was quantified from the same photographs of fruiting bodies from above using the ImageJ measurement tool. The area was then converted to volume on the assumption that the sorus is approximately spherical using equation [V = 4/3 * A/sqrt (A/pi)] (A = area) and presented as mm^3.

2.11 Quantification of LysoSensor™ Blue DND-167 Staining in Cells

Dictyostelium cells were grown in HL5 medium to a density of 1–3 × 10^6 cells ml^{-1}1 × 10^7 cells were harvested (1,500 ×*g* for 2 min) and diluted 1:10 in Lo-Flo HL5 either with or without 500 nM LysoSensor™ Blue DND-167 (Invitrogen) and incubated covered in foil at 21°C shaking for 30 min. Cells were washed twice with 1 × PBS and resuspended to a density of 0.5 × 10^6 cells ml^{-1} in PBS and the fluorescence of a 2 ml sample measured in a Modulus™ 9200-003 fluorometer (Turner

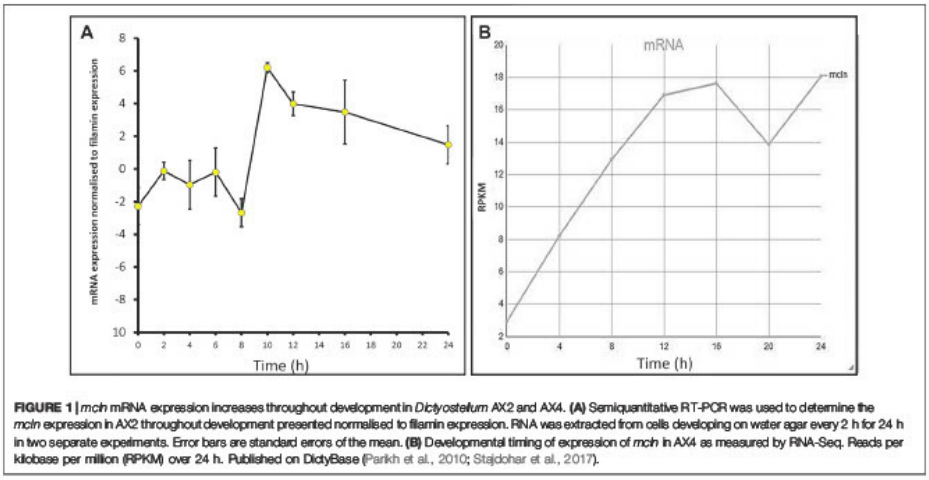

FIGURE 1 | *mcln* mRNA expression increases throughout development in *Dictyostelium* AX2 and AX4. **(A)** Semiquantitative RT-PCR was used to determine the *mcln* expression in AX2 throughout development presented normalised to filamin expression. RNA was extracted from cells developing on water agar every 2 h for 24 h in two separate expeiments. Error bars are standard errors of the mean. **(B)** Developmental timing of expression of *mcln* in AX4 as measured by RNA-Seq. Reads per kilobase per million (RPKM) over 24 h. Published on DictyBase (Parikh et al., 2010; Stajdohar et al., 2017).

BioSystems, Sunnyvale, CA, United States) using the UV module kit 9200-041 (Ex. 365 nm, Em. 410–460 nm). The background fluorescence of the cells that had not been dyed was subtracted from the fluorescence recorded from the Lysosensor Blue stained cells.

2.12 LysoSensor Blue DND-167 Imaging of Live Cells

Cells were grown in HL5 medium to a density of 1–3 × 10^6 cells ml^{-1}. An aliquot containing 10^6 cells were harvested (1,500 ×*g* for 2 min) and resuspended in Lo-Flo HL5 containing 500 nM LysoSensor Blue DND-167 (Invitrogen) and incubated at 21°C shaking for 30 min. Cells were washed 2 times in 1 × PBS, resuspended to a density of 1 × 10^6 cells ml^{-1} and 10 µl of suspension mounted onto microscope slides. Live cells were viewed through the DAPI filter with an Olympus BX61 fluorescent microscope.

2.13 Measurement of Cellular Autofluorescence

Cells were harvested and processed in the same manner as **Section 2.11**, however omitting the treatment with LysoSensor ™ Blue DND-167. Fluorescent readings of 1 × 10^6 cells were recorded immediately after two washes in 1 × PBS with the UV module kit 9200-041 (Ex. 365 nm, Em. 410–460 nm).

2.14 Calcium Experiments

2.14.1 *Dictyostelium* Culture and Development

Expression of the Ca^{2+} sensitive luminescent protein aequorin, in each *Dictyostelium*, strain was used to measure cytosolic Ca^{2+} concentration. *Dictyostelium* cultures were grown and allowed to develop as described previously (Nebl and Fisher, 1997). Axenic cultures in HL5 medium were grown to a density of 1–2 × 10^6 cells ml^{-1}, and 1 × 10^8 cells were harvested, washed twice in 20 ml of MES-DB [(MES development buffer) (10 mM MES/NaOH, pH 6.2, 10 mM KCl, 0.25 mM $CaCl_2$)], resuspended in MES-DB or HL5 to a final density of 2 × 10^7 cells ml^{-1} and loaded with 5 µM Coelenterazine-h (Invitrogen). Cultures were incubated at 21°C shaking at 150 rpm for 4 h (vegetative cells) or 7 h (aggregation competent cells).

2.14.2 Aequorin Consumption and *In Vivo* Ca^{2+} Measurements

Aequorin consumption was carried out as previously described (Nebl and Fisher 1997). All measurements were taken inside a Lumitran® model L-3000 photometer (New Brunswick Scientific). During measurements, the cells were stirred at 100 rpm in 20 ml sample vessels and placed in front of a photomultiplier. Luminescence signals were recorded from 5 ml cell suspensions stimulated with 1 µm chemoattractant, either cAMP or folic acid. The signal was captured by a model PCI-20428 multifunction I/O data acquisition board (Intelligent Instruments Pty. Ltd.). The signal was then converted into values of cytosolic calcium concentration on a PC using in-house purpose-designed software (Prof. P. R. Fisher).

2.15 Statistical Analysis

Data was analysed in Excel. Means were compared using independent t-tests or One-Way ANOVA, with pairwise comparisons made by the Least Squares Difference method. Significant correlations were determined by Pearson product-

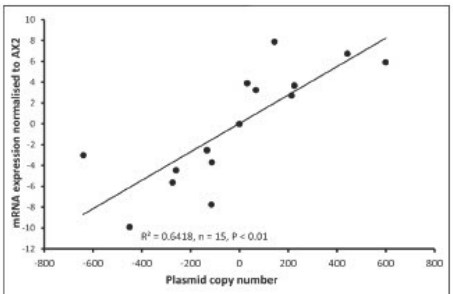

FIGURE 2 | Plasmid copy number of mucolipin strains was correlated with mRNA expression levels in the transformants. Semiquantitative RT-PCR was performed to determine mRNA expression levels in each strain. Copy numbers of overexpressing strains were determined by quantitative Southern blotting, and copy numbers of antisense strains were determined by quantitative real time PCR. Expression levels were normalised against the filamin mRNA to adjust for loading and then measured relative to AX2 expression. Expression correlates with plasmid copy number showing that the antisense RNA construct decreases *mcln* expression and the overexpression increases it. The correlation was highly significant, $p = 2.36 \times 10^{-5}$ (Pearson product-moment correlation coefficient, ρ) and similar results were also obtained using non-parametric methods (Spearman's rank $p = 1.195 \times 10^{-5}$ and Kendall's rank $p = 9.995 \times 10^{-6}$). Each point represents mean data for a single strain for three experiments. Negative values refer to copy numbers of antisense constructs and positive values to copy numbers of overexpression constructs, AX2 has a copy number of 0 as contains neither construct.

moment, Spearman's rank and Kendall's rank correlation coefficients.

3 RESULTS

3.1 Developmental Expression of *mcln* Over 24 h

The expression profiles of many *Dictyostelium* genes change throughout development. To determine the *mcln* mRNA expression levels throughout development, AX2 cells were developed on water agar plates for 24 h, and RNA extracts were taken at 2-h intervals. Semiquantitative RT-PCR was used to assess the relative expression of *mcln* in cells at these time points. Expression changed throughout development, rising slightly during early differentiation in response to the onset of starvation, falling to a trough at 8 h, but then increasing rapidly to a maximum at 10 h during aggregation. Expression remained at high levels during subsequent multicellular development (**Figure 1A**). The measured developmental expression profile is similar to the RNA-Seq expression profile of *D. discoideum* AX4 published on DictyBase (Parikh et al., 2010; Stajdohar et al., 2017), which shows increased *mcln* expression over the course of development (**Figure 1B**). Subtle differences in the patterns of expression in our experiments compared to those published on DictyBase (Parikh et al., 2010) could arise from differences in the parental strain used (AX2 in our experiments and AX4 for DictyBase) and also from the fact that in our experiments the cells were developed on water agar, as opposed to filters. This expression pattern suggests important roles for mucolipin-dependent calcium signalling in early starvation-induced differentiation, in chemotactic aggregation and subsequently during the multicellular stages of the life cycle.

3.2 Genetic Alteration of *Dictyostelium* Changes *mcln* mRNA Expression

Dictyostelium strains were created by transformation with expression constructs to either knockdown expression via antisense mRNA inhibition or overexpress the protein. Integration of the plasmid construct occurs randomly in the genome by recombination and rolling circle replication, therefore each strain contains different numbers of the plasmid constructs thus different levels of expression (Barth et al., 1998). For this reason, the copy number of the plasmid in each strain was determined, as was the mRNA expression level. As expected, antisense inhibition caused a measurable decrease in mRNA transcripts and overexpression caused an increase in mRNA transcripts. The relative mRNA expression was correlated with the copy number of the plasmid construct in the strains (**Figure 2**).

3.3 Overexpressed Mucolipin Can Be Detected in Western Blot

We created a polyclonal antibody directed against a 200aa portion of *Dictyostelium* mucolipin, anti-MUECD. In a western blot this antibody detected multiple bands so was not suitable to be used for localisation studies. To determine if any of these bands did represent mucolipin, we tested the antibody the against mucolipin knockout cell lysate (Lima et al., 2012) and ran these proteins alongside protein extracted from DH1-10 (the parental strain for the knockout cell line), AX2 and our mucolipin overexpression and knockdown strains. Indeed, there were two bands absent in the mucolipin knockout lysate but present in the mucolipin overexpression strains which ran at approximately 95 and 120 kDa. The 120 kDa band was also detected in DH1-10 (**Figures 3A,B**). It was not observed in the knockout strain derived from DH1-10, despite a similar protein loading in the gel. These bands were not detected in AX2 or our mucolipin antisense strains, presumably because the wild type and knockdown expression levels for mucolipin were insufficient for detection by our antibody. Mass spectrometry analysis of bands excised from a Coomassie Blue-stained Bis-Tris-Plus gel (**Supplementary Figure S1** and **Supplementary Method 1**) confirmed the presence of mucolipin in these two bands (indicated by the red stars in **Figure 3B**), but not the smaller molecular weight bands. We thus confirmed that there are two genuine mucolipin bands—one at the predicted MW position ~95 kDa and one running at ~120 kDa. There are two possible explanations for the presence of two bands. Firstly, the upper band could be a posttranslationally modified (glycosylated) form of the protein as is reported for

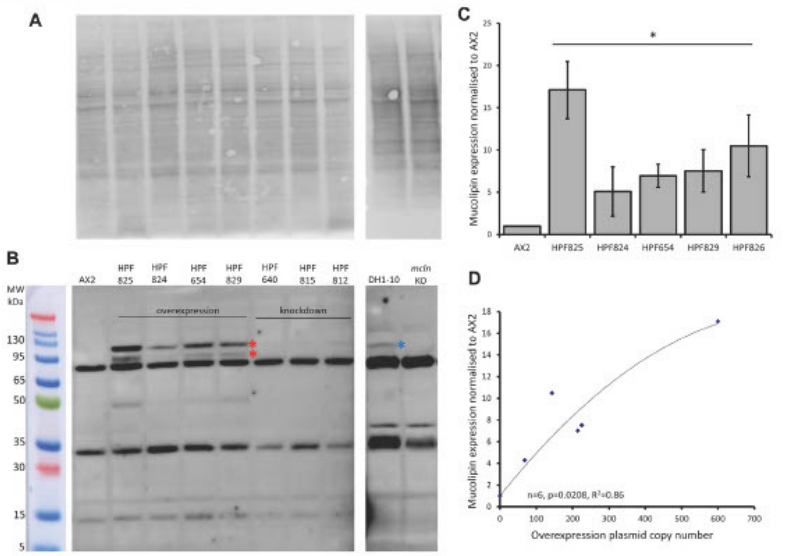

FIGURE 3 | Mucolipin can be detected in protein extracted from overexpression strains. **(A)** Total protein extracted from AX2, four representative mucolipin overexpression strains, three representative mucolipin knockdown strains, DH1-10 and mucolipin knockout, were separated by on a Bis-Tris-Plus gel by electrophoresis, transferred to PVDF membrane and stained with No Stain Protein Labelling Reagent (Invitrogen). Protein lysate for DH1-10 and *mcln* KO were kindly provided by Professor Pierre Cosson (Lima et al., 2012). **(B)** Western blot of the same membrane, the anti-MUECD antibody detects multiple bands. Markers were the Broad Multi Color Pre-Stained Protein Standard (Genscript). Two bands of ~95 and ~120 kDa were absent in the mucolipin knockout cells but present in the mucolipin overexpression strains (Red stars) and the higher MW band also detected in DH1-10 (blue star). **(C)** Quantification of mucolipin expression in overexpression strains. To quantify mucolipin expression the combined intensity of the 120 and 95 kDa bands was measured in Image Lab™ and normalised to the intensity of the total protein loaded in each lane **(A)**. Expression in each strain was then and normalised to AX2 expression. As no bands were visualised for AX2 at these sizes, AX2 expression was determined by measuring the intensity of a similar sized area on the blot where the bands would be located. Each strain was tested 2–4 times and data was pooled from each experiment and the means calculated (error bars are standard errors of the mean). Expression is relative to AX2 and is increased in overexpression strains (* = <0.05, One-Way ANOVA, with pairwise comparisons made by the Least Squares Difference method, AX2 vs. strain). **(D)** Protein expression in overexpression strains correlates with overexpression construct copy number. AX2 had a construct copy number of 0 as does not contain an overexpression construct. The correlation was highly significant (Spearman's rank p = 0.0208 and Kendall's rank p = 0.0194).

human TRPML1 (Miedel et al., 2006), and the lower band could be the native nonglycosylated protein. Secondly, the upper band could be the native, full-length protein running a little more slowly than expected, and the lower band could be a cleavage product. The human TRPML1 has a proteolytic cleavage site in the intralumenal loop between transmembrane domains 1 and 2, and this cleavage is believed to be involved in regulation of channel activity (Kiselyov et al., 2005). Since we confirmed that these bands represented mucolipin, we were able to confirm by quantification that mucolipin expression is increased in our overexpression strains (**Figure 3C**), and the protein expression was significantly correlated with copy number of the overexpression plasmid construct (**Figure 3D**).

3.4 Mucolipin Contributes to Chemotactic Calcium Signals in *Dictyostelium*

TRPMLs are thought to be important for Ca^{2+} signalling events associated with Ca^{2+}-dependent fusion/fission events of membranes along the late endocytic pathway (LaPlante et al., 2004; Luzio et al., 2007; Brailoiu and Brailoiu 2016). In *Dictyostelium* DH1-10 cells, knockout of mucolipin reduces Ca^{2+} concentrations in secretory post-lysosomes, measured using dextran-coupled fluorophores (Lima et al., 2012) suggesting a role in regulation of calcium homeostasis/signalling. To further investigate the role of mucolipin in Ca^{2+} signalling, and the possible contribution of the acidic stores to chemotactic Ca^{2+} responses, we measured the cytosolic Ca^{2+} transients in

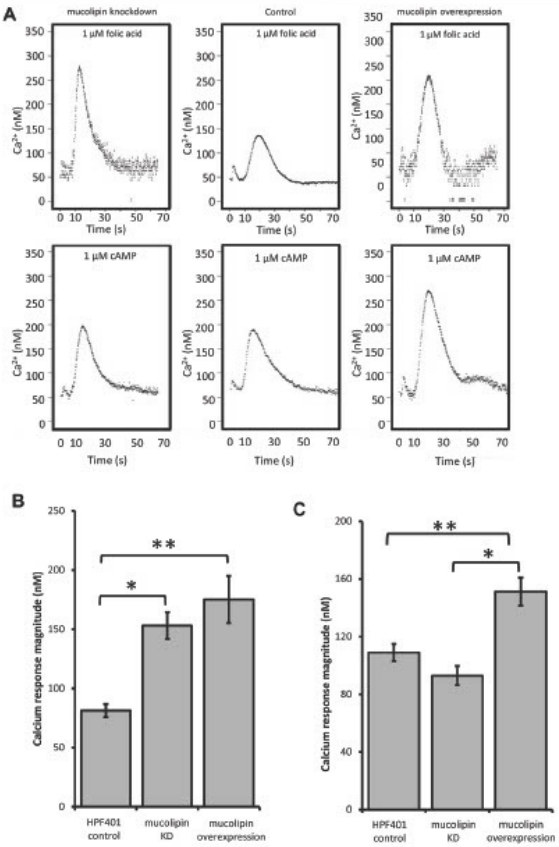

FIGURE 4 | Cytosolic calcium responses to cAMP and folic acid stimulation. **(A)** Representative real time recordings of cytoplasmic Ca^{2+} responses to chemoattractants. Upper panel: Real time recordings of Ca^{2+} responses to 1 µM folate in vegetative cells. Left to right: mucolipin KD (knockdown), HPF401 control strain and mucolipin overexpression. Lower panel: Real time recordings of Ca^{2+} responses to 1 µM cAMP in cells at 7 h development. Left to right: as above. Recordings began at 0 s and the stimulus was injected immediately after. The small peak preceding the Ca^{2+} response is due to a Ca^{2+} response to the mechanical stimulus of chemoattractant injection, which has no effect on the chemoattractant responses (Nebl and Fisher, 1997). **(B)** Mean calcium response magnitudes in vegetative cells stimulation with 1 µM folic acid. Ca^{2+} response magnitudes (Ca^{2+} nM) were measured in mucolipin KD, mucolipin overexpression and control strain HPF401. There was no correlation with copy number so data from strain groups was pooled and the means compared. Both knockdown and overexpression of mucolipin significantly enhances the magnitude of the response compared to the control strain HPF401 (*$p = 3.15 \times 10^{-6}$, **$p = 4.7 \times 10^{-4}$). Means were compared using an independent one-tailed *t*-test. Errors are standard errors of the mean. Individual strains were tested in 3–9 independent experiments in five mucolipin overexpression ($n = 13$), six mucolipin knockdown strains ($n = 30$) and control strain HPF401 ($n = 12$), and all experiments from each strain group were pooled to determine the mean. **(C)** Mean calcium response magnitudes (Ca^{2+} nM) in developed cells stimulated with 1 µM cAMP. Ca^{2+} response magnitudes were measured in overexpression, knockdown and control strain HPF401. Cells were developed to 7 h in MED-DB. Overexpression of mucolipin increases the response magnitude significantly compared to both control HPF401 and knockdown strains (*$p = 1.33 \times 10^{-6}$, **$p = 5{,}928 \times 10^{-4}$). knockdown of mucolipin has no effect on response magnitude in developed cells when compared to wildtype ($p = 0.083$). Means were compared using an independent one-tailed *t*-test. Errors are standard errors of the mean. Individual strains were tested in 2–9 independent experiments and all experiments were pooled to determine the mean. Mucolipin overexpression eight strains ($n = 37$), mucolipin knockdown seven strains ($n = 33$), control HPF401 ($n = 12$).

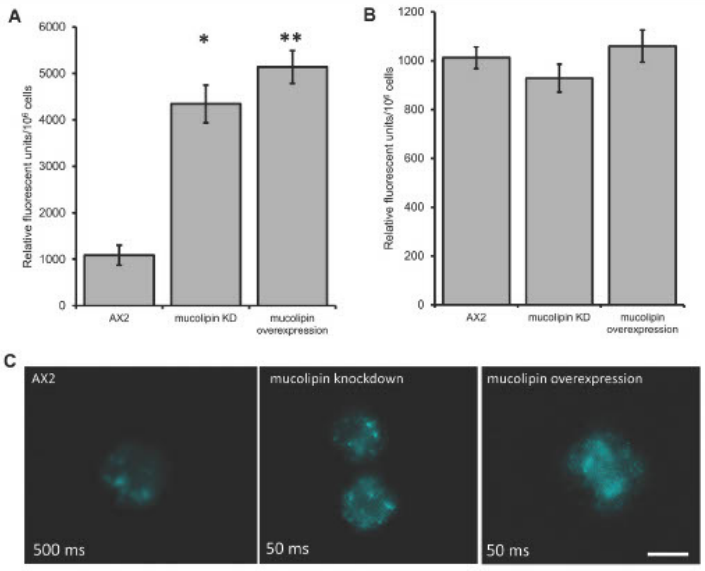

FIGURE 5 | Altering mucolipin expression causes accumulation or increased acidification of vesicles stained with LysoSensor™ Blue DND-167 but does not cause autofluorescence. **(A)** Quantification of LysoSensor™ Blue DND-167 was performed by measuring the increase in fluorescence in 1 × 10^6 vegetative cells after incubation with 500 nM LysoSensor™ Blue DND-167. Data was collected from seven knockdown strains and six overexpression strains in three individual experiments and the mean calculated, error bars are standard errors of the mean. There was no correlation with copy number of the plasmid constructs, therefore data for strain groups was pooled. The mean fluorescence of AX2 (n = 3) was significantly different to the means of either knockdown (n = 21) or overexpression strains (n = 18) (Pairwise comparisons, Independent t-test, *p = 0.00067, **p = 0.01107312). **(B)** Fluorescence measured in *Dictyostelium* strains harvested from low fluorescence medium. The level of fluorescence in knockdown and overexpression strains was measured in 1 × 10^6 cells. Autofluorescence was measured in a fluorometer (Modulus 9200-003 Turner Bio systems) using the UV module (excitation 365 nm, emission 410–460 nm). Fluorescence displayed in relative fluorescent units, was measured in two independent experiments for AX2 (n = 2), six knockdown strains (n = 12) and six overexpression strains (n = 12) and the mean within each group calculated. Error bars are standard errors of the mean. There was no significant difference (p > 0.05, One-Way ANOVA, multiple comparisons made by the Least Squares Difference method). **(C)** Representative live cells stained with LysoSensor™ Blue DND-167. *Dictyostelium* AX2, mucolipin knockdown (copy number 274) and overexpression (copy number 443) were incubated in the presence of 500 nM LysoSensor™ Blue DND-167 for 1 h and observed under fluorescence microscopy (Excitation- 373 nm, Emission- 425 nm). The AX2 image was taken at 500 ms exposure, the knockdown and overexpression cells were overexposed at this exposure so were taken at 50 ms. Scale bar = 5 μm.

vegetative cells (folic acid responses), and in aggregation competent cells (cAMP responses) in mucolipin knockdown and overexpressing strains. All strains also ectopically expressed a recombinant Ca^{2+}-sensitive luminescent protein, apoaequorin, to allow real time recordings of cytosolic Ca^{2+} responses. These chemotactic Ca^{2+} responses have been well characterized in wild type cells expressing apoaequorin (HPF401) (Nebl and Fisher, 1997). In this work we compared the mutants' Ca^{2+} responses with wild type responses to gain insight into the molecular mechanisms involved. Representative real-time recordings of cytosolic calcium concentration in wild type aequorin-expressing strain (HPF401), mucolipin knockdown strain (HPF812) and mucolipin overexpression strain (HPF825) when stimulated with 1 μM chemoattractant are shown in **Figure 4A**.

3.4.1 Overexpression of Mucolipin Enhances the Ca^{2+} Responses to cAMP and Folic Acid

Real time recordings of the Ca^{2+} responses for control, knockdown and overexpression strains to both cAMP and folic acid were recorded over multiple experiments and analysed. As there was no correlation between the various parameters and plasmid copy number, data was pooled for all transformants within each group for combined analysis. Overexpression of mucolipin significantly enhanced Ca^{2+} response magnitudes to both folic acid (vegetative cells) and cAMP (aggregation competent cells) compared to the control (**Figures 4B,C**). The response magnitudes were increased

compared to the control by an average of 46.4% and 28.0% for the folic acid responses and cAMP responses respectively. This result suggests, mucolipin is involved in Ca^{2+} chemotactic calcium responses and because the channel localises to post-lysosomes and possibly other endocytic compartments (Lima et al., 2012), the results suggest that these vesicles are also involved in the calcium response.

3.4.2 Knockdown of Mucolipin Increases Ca^{2+} Response Magnitudes in Vegetative Cells, but Not in Aggregation Competent Cells

Given that overexpression of mucolipin enhances the responses to folic acid and cAMP, it was expected that knockdown of mucolipin would reduce the magnitude of calcium responses. Surprisingly, the magnitude of the Ca^{2+} responses to 1 μM folic acid was significantly increased in knockdown strains compared to the control (**Figure 4B**). Contrary to the folate responses, the magnitude of the cAMP Ca^{2+} responses in aggregation competent cells were slightly reduced in mucolipin knockdown strains compared to the control (**Figure 4C**), but the difference did not reach statistical significance ($p = 0.083$).

3.5 The Role of Mucolipin in the Endocytic Pathway

Dictyostelium mucolipin overexpression and knockdown strains both exhibit increased Ca^{2+} signalling in vegetative cells. As Ca^{2+} plays an important role in the endocytic pathways it was of interest to assess the role of mucolipin in these processes.

3.5.1 Overexpression and Knockdown of Mucolipin Increases Fluorescence of Cells Stained With LysoSensor™ Blue DND-167

One of the hallmarks of MLIV cells is an accumulation of hybrid late endosome-lysosome compartments (LELs) with defective exit of lipids from LELs to the trans-Golgi network (Chen et al., 1998; LaPlante et al., 2004). The connection between Ca^{2+} release via TRPMLs and build-up of hybrid LELs is somewhat undecided. To assess this phenotype in AX2 *Dictyostelium* cells, we stained vegetative mucolipin knockdown and overexpressing cells with LysoSensor™ Blue DND-167 which has a pK_a of is ~5.1 and accumulates in acidic vesicles. There was a significant increase in fluorescence in the mutants compared to AX2 (**Figure 5A**) representative images of live stained cells are presented in **Figure 5C**. This could reflect an increase in lysosomal mass, or because the fluorescence of LysoSensor™ Blue DND-167 increases as the pH decreases, our results could reflect increased acidification of the lysosomes.

3.5.2 Altering Mucolipin Expression Does Not Cause Autofluorescence

Accumulation of autofluorescent material has been observed in MLIV cell lines and is thought to be related to specific compounds stored in the lysosomes (Goldin et al., 1995). Autofluorescence is also a hallmark of NCL (Dowson et al., 1982), and has been detected in some *Dictyostelium* NCL models. In the cln3 model, *cln3*$^-$ cells do not accumulate autofluorescent material during the growth stage (Huber et al., 2014), however in starved *cln3*$^-$ cells autofluorescent material was detected (Huber and Mathavarajah, 2019). In the cln2 lysosomal disease model, mutants with knockdown and knockout of the *tpp1/cln2* gene, which encodes the lysosomal protein tripeptidyl peptidase I (TPP-I), a soluble lysosomal aminopeptidase, accumulate cellular autofluorescent material (Phillips and Gomer, 2015; Smith et al., 2019). Therefore, we

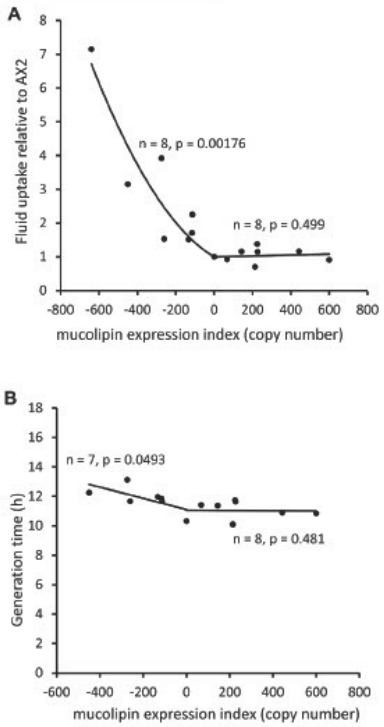

FIGURE 6 | Mucolipin knockdown affects macropinocytic uptake and growth rates of cells in HL5 medium. **(A)** Consumption of HL-5 medium containing FITC dextran via macropinocytosis in knockdown strains (negative copy numbers), overexpression strains (positive copy numbers) and wild type normalised to AX2. In the antisense strains fluid uptake normalized to AX2 was increased and correlates with mucolipin expression index (Pearson correlation coefficient, $p = 0.00176$), however there was no correlation in the overexpression strains (Pearson correlation coefficient, $p = 0.499$). Each point represents the mean uptake from a single strain. Duplicate samples were assayed for each strain in two to six separate experiments and data was normalised within each experiment to AX2. **(B)** Generation times (h) of mucolipin strains and AX2 grown in HL5 medium. In the antisense strains generation time was increased and correlates with mucolipin expression index (Pearson correlation coefficient, $p = 0.0493$), however there was no correlation in the overexpression strains (Pearson correlation coefficient, $p = 0.481$). AX2 has a copy number of 0.

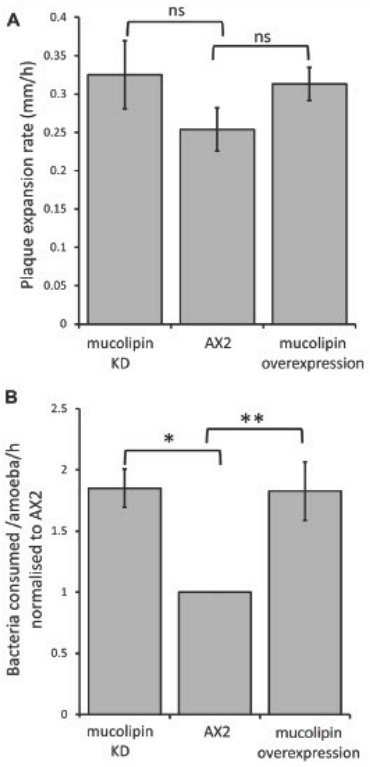

FIGURE 7 | Mucolipin expression did not affect plaque expansion rates but increased phagocytosis rates. **(A)** Plaque expansion rates (growth velocity) were measured from linear regressions of plaque diameters vs. time during growth at 21°C on an *E. coli* B lawn. Growth velocity was not significantly altered in mucolipin knockdown compared to AX2 ($p = 0.278$) or overexpression compared to AX2 ($p = 0.133$) (One-Way ANOVA, with pairwise comparisons made by the Least Squares Difference method). Analysis revealed that all there was no correlation between construct copy number and growth velocity of the mucolipin overexpressing strains therefore, the growth velocities for different strains in each of the two sets of transformants were pooled to calculate the means for comparison with AX2. Individual strains were each tested in 2–4 independent experiments and the data pooled to calculate the mean. Eight overexpression strains ($n = 33$), seven knockdown strains ($n = 20$) and the control strain ($n = 4$) were tested (n = total number of experiments in each strain group). Errors are standard errors of the mean. **(B)** Uptake of *E. coli* cells expressing the fluorescent red protein Ds-Red via phagocytosis was significantly increased in both knockdown and overexpression mucolipin transformants when compared to AX2 (*$p = 3.35 \times 10^{-6}$, **$p = 0.002$, One-Way ANOVA, with pairwise comparisons made by the Least Squares Difference method). All of the mucolipin overexpressing strains exhibited similarly elevated phagocytosis rates so that there was no correlation amongst them between construct copy number and phagocytosis rates (Pearson product-moment correlation coefficient, ρ, overexpression $p = 0.15$). The same was true of the mucolipin knockdown strains (Pearson product-moment correlation coefficient, ρ, $p = 0.48$). Accordingly, the uptake rates obtained from different strains within each group were pooled and the means calculated. Individual strains were tested in 2–4 independent experiments. Seven overexpression ($n = 24$), seven knockdown strains ($n = 19$) and the control strain ($n = 4$) were tested (n = total number of experiments). Errors are standard errors of the mean.

(*Continued*)

measured autofluorescence in *Dictyostelium* mucolipin knockdown and overexpression strains under UV light. No increase of autofluorescence was detected in any of our mucolipin mutants (**Figure 5B**). This phenotype in *Dictyostelium* lysosomal disease models seems to be specific to the particular disease gene in question.

3.5.3 Knockdown of Mucolipin Increases Macropinocytic Uptake, but Decreases Growth Rates of Cells in Liquid Medium, While Overexpression Does Not Affect Growth or Macropinocytosis

An analysis of uptake of medium as compared to growth rates can indicate whether ingested nutrients are efficiently catabolised. The rate of fluid uptake by macropinocytosis was increased in mucolipin knockdown strains and correlated with plasmid copy number, however overexpression had no affect (**Figure 6A**). Surprisingly the growth rates of mucolipin knockdown strains were slower than AX2 (longer generation times) and similarly correlated with plasmid copy number, while overexpression had no affect (**Figure 6B**).

3.5.4 Mucolipin Knockdown and Overexpression Increase Phagocytosis, but Do Not Affect Growth Rates on Lawns of Bacteria

Dictyostelium consume bacteria by phagocytosis in their natural environment and can be cultured on lawns of bacteria where they grow as plaques which gradually expand as the amoebae consume bacteria. The plaque expansion rates (growth velocity) of mucolipin transformants were slightly but not significantly elevated compared to AX2 (**Figure 7A**). The rates of phagocytosis in mucolipin transformants and AX2 control were assayed by measuring the uptake of fluorescently labelled live *E. coli* cells. Surprisingly, unlike the plaque expansion rates on bacterial lawns, both overexpression and knockdown of mucolipin significantly increased the rates of phagocytosis of *E.coli* (**Figure 7B**). These results indicate although these transformants are engulfing bacteria at a faster rate than AX2, this does not significantly increase the growth rates.

3.6 Mucolipin Expression Affects *Dictyostelium* Multicellular Development

Multicellular development in *Dictyostelium* is initiated by starvation upon which the cells undergo a developmental program leading to multicellular morphogenesis and culmination into mature fruiting bodies consisting of a spore

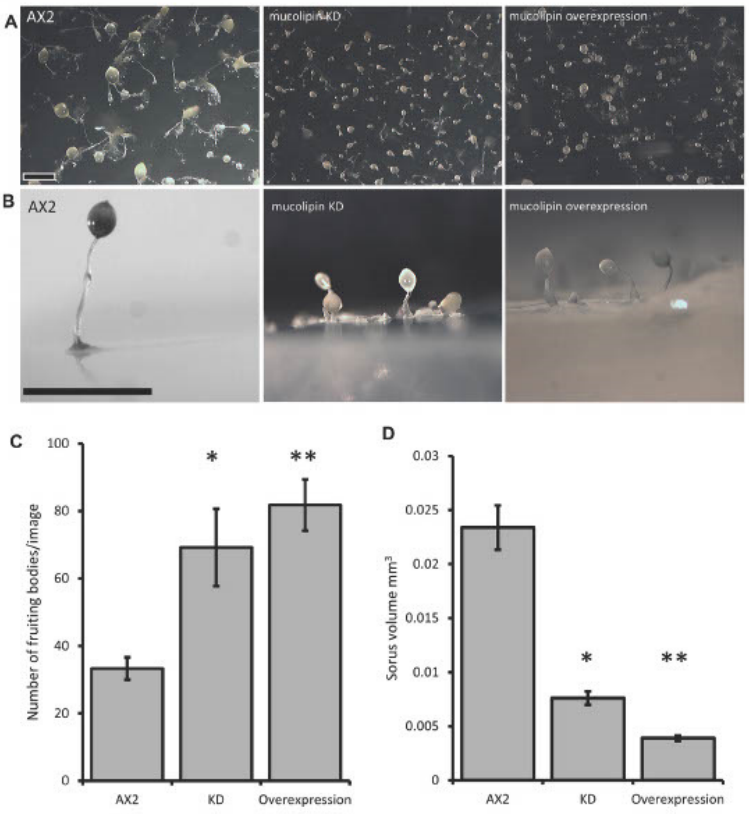

FIGURE 8 | Mucolipin knockdown and overexpression strains form smaller more numerous fruiting bodies. **(A)** AX2 wild type, mucolipin KD (knockdown) strain HPF817 (copy number 450) and mucolipin overexpression strain HPF825 (copy number 600). Cells grown on lawns of *E. aerogenes* at 21°C for ~24 h until fruiting bodies had formed which were photographed from above. **(B)** The same strains photographed from the side. Both increasing and decreasing mucolipin expression results in very small fruiting bodies compared to that of AX2. In high copy number strains the stalks and basal disks are thickened and enlarged. Scale bar = 1 mm. **(C)** The number of fruiting bodies were significantly increased in mucolipin knockdown and overexpression strains. Images were taken from above at the same magnification for all strains and the number of fruiting bodies in the same area of photograph were counted and the means calculated. (AX2: $n = 3$; KD: $n = 5$, overexpression: $n = 5$) (independent *t*-test *$p = 0.0470$ vs. AX2, **$p = 0.00303$ vs. AX2). **(D)** Sorus volume was smaller in the knockdown and overexpression strains than AX2. Sorus area was quantified from photographs of fruiting bodies from above using the ImageJ measurement tool and then converted to volume on the assumption that the sorus is approximately spherical using equation (V = 4/3*A/sqrt (A/pi) (A = area) and presented as mm^3. For each strain 30–111 sori were measured. The sorus size was significantly reduced in knockdown ($p = 2.402 \times 10^{-30}$ vs. AX2) and overexpression strains (**$p = 1.8998 \times 10^{-56}$ vs. AX2). Sample sizes: AX2—N = 3 images, $n = 97$ sori; KD—N = 5 strains, $n = 349$ sori; overexpression—N = 5 strains, $n = 298$ sori) (independent *t*-test).

droplet (sorus), stalk and basal disc. The stalk cells undergo autophagic cell death and so are nonviable. The developmental timing of expression of mucolipin suggests it is involved in chemotactic aggregation and progression through multicellular morphogenesis, likely through mucolipin-dependent calcium signalling, and its effects on the endocytic system. Calcium signalling plays an important role during development, from chemotactic aggregation to cell type differentiation. To investigate how expression levels of mucolipin affect multicellular morphogenesis in *Dictyostelium*, knockdown and overexpression strains were observed at the slug and fruiting body stage. Both knockdown and overexpression strains formed

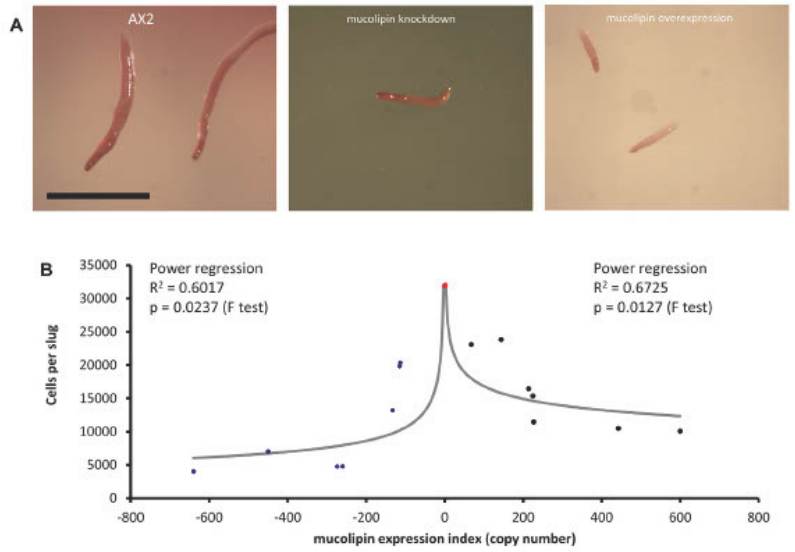

FIGURE 9 | Slug sizes are smaller in mucolipin knockdown and overexpression strains and is copy number dependent. **(A)** Slugs formed after ~16 h of development on water agar. Mutants formed smaller slugs than AX2 Scale bars = 1 mm. **(B)** Both increasing and decreasing mucolipin expression reduces aggregate size. The aggregate size of overexpression and knockdown strains was quantified by determining the number of cells per slug. The mean aggregate size for each transformant was determined by isolating single slugs and counting the number of cells in each slug using a haemocytometer ($n = 30$). The mean aggregate size was reduced in a copy number dependent manner, the regressions were significant indicated by the p values. Positive copy numbers represent overexpression strains and negative numbers knockdown strains, AX2 had a copy number of 0 as it contains neither plasmid (indicated as red circle).

smaller fruiting bodies than AX2. In high copy number strains, the stalks and basal disks of the fruiting bodies appear thickened indicating increased stalk cell differentiation (**Figures 8A,B**), fruiting bodies were more numerous (**Figures 8C**) and formed smaller sori (**Figures 8D**). We then determined if the smaller fruiting bodies were the result of small aggregate and slug formation in the mutants. Indeed, both knockdown and overexpression strains developed into smaller slugs containing fewer cells compared to AX2 (**Figure 9A**). The aggregate size was quantified by determining the number of cells per slug, revealing a dramatic copy number-dependent reduction in slug size in both overexpression and knockdown strains (**Figure 9B**). This phenotype is also present in *dn2* knockdown mutants (Smith et al., 2019), and similarly *dn3*$^{-}$ and *dn5*$^{-}$ mutants have increased numbers of tipped mounds, fingers, slugs and fruiting bodies for the same density of cells (Huber et al., 2014; Huber et al., 2017; McLaren et al., 2021).

4 DISCUSSION

In this study we have used the model organism *Dictyostelium* to investigate if mucolipin expression can affect global calcium signals during chemotactic calcium responses. Gross (2009) suggested that the *Dictyostelium* acidic stores, which includes the endolysosomal vesicles, the contractile vacuole system and the acidocalcisomes, can release Ca^{2+} and increase cytosolic Ca^{2+} during chemotaxis. A selection of calcium channels have been identified to be associated with the acidic stores including the P2X receptors of the contractile vacuole (Fountain et al., 2007), the two pore channel (TPC) (Wilczynska et al., 2005; Chang et al., 2020), and mucolipin. Given that mucolipin resides in late endosomes and other endocytic vesicles (Lima et al., 2012), we hypothesized that mucolipin could contribute to calcium release from these stores. We measured cytosolic Ca^{2+} responses to chemoattractants in mucolipin knockdown and overexpression transformants using the luminescence of the Ca^{2+}-sensitive luminescent protein, apoaequorin, which we ectopically expressed in the same cells (Nebl and Fisher 1997). We found that overexpression of mucolipin significantly increased the magnitudes of the cytosolic Ca^{2+} responses to folic acid and cAMP. While we cannot determine if the increased calcium influx into the cytosol is the result of direct release of calcium from the endocytic compartments through mucolipin itself, our results do implicate mucolipin in cytosolic calcium signalling. Lima et al.

(2012) provided evidence of mucolipin involvement in calcium homeostasis because knockout cells grew faster in calcium-depleted medium and had reduced lumenal calcium concentrations in the post-lysosomes, below 0.2 μM, much lower than the 1–3 μM of the wild type control. In other cell types TRPML1 has been shown to affect lysosomal pH (Soyombo et al., 2006; Miedel et al., 2008), therefore, knocking out mucolipin in *Dictyostelium* could affect the proton/Ca^{2+} exchange between the vesicle lumen and cytoplasm, thereby reducing steady state Ca^{2+} levels in the lumen as has been reported (Lima et al., 2012). This could in turn mean that overexpressing mucolipin may result in elevated resting lumenal Ca^{2+}, again because of the disturbed pH gradient across the vesicle membrane. This, and the greater number of available channels could then facilitate the larger responses in our overexpressing strains. Lima et al. (2012) hypothesized that mucolipin may be responsible for transfer of calcium from the cytosol to the lumen where the vesicles meet high local cytosolic calcium concentrations. Our results suggest that, at least when overexpressed, mucolipin significantly contributes to cytosolic signals, thus could function as a calcium release channel. It is possible that the channel could work both ways depending on the particular cellular requirements.

As stated previously, in other cell types TRPML channels are known to regulate localised calcium signals, as well as global calcium waves via activation of ER and plasma membrane calcium flux (Kilpatrick et al., 2016). The same may be true in *Dictyostelium*—if mucolipin is capable of activating calcium release from ER and across the plasma membrane, then overexpressing the channel would enhance the cytosolic calcium responses as we observed in our experiments. It is also possible that overexpression of mucolipin results in expression at the plasma membrane, as this has been reported for TRPML1 expression in HEK293 cells (Kiselyov et al., 2005), or it may be translocated there during exocytosis as TRPML1 is in *Xenopus* oocytes (LaPlante et al., 2002). The *Dictyostelium* channels responsible for plasma membrane and ER calcium release are still not confirmed. Contenders are IplA, a channel related to the mammalian ER IP_3 receptors (Taylor et al., 1999; Lusche et al., 2012) and pkd2 the *Dictyostelium* polycystin-2, another member of the TRP superfamily (Lima et al., 2014; Traynor and Kay, 2017). Both IplA and pkd2 have been localised to the plasma membrane (Lusche et al., 2012; Lima et al., 2014). However, IplA localises primarily to unidentified cytoplasmic inclusions, and it has not been determined whether this includes the ER (Lusche et al., 2012). Some studies have found that knockout of IplA abolishes calcium responses to chemoattractants (Traynor et al., 2000; Traynor and Kay, 2017), however another reported that the Ca^{2+}response to high concentrations of cAMP is maintained but smaller (Schaloske et al., 2005). Calcium responses to cAMP and folic acid are retained in pkd2 knockout cells (Traynor and Kay, 2017). Therefore, clarification of which channels involved in ER and plasma membrane calcium signalling is still necessary. Future work to investigate if mucolipin contributes to calcium influx across the plasma membrane and release from the ER calcium could include measurement of the uptake of $^{45}Ca^{2+}$ from the extracellular milieu, treatment of overexpression cells with thapsigargin to reduce ER calcium content (Lytton et al., 1991), and with EGTA to chelate extracellular calcium.

We also analysed cytosolic calcium signals in mucolipin knockdown strains, and were surprised to find that reducing mucolipin expression resulted in larger, rather than smaller Ca^{2+} responses. However, this occurred only in vegetative cells, the magnitudes of the calcium responses in differentiated cells stimulated with cAMP were not significantly different from controls (**Figure 4**). The enhanced Ca^{2+} responses observed in our vegetative mucolipin knockdown strains might be caused by a decrease in Ca^{2+} buffering capacity by the acidic stores. Lysosomes can shape calcium signals by tempering cytosolic calcium released from the ER (López-Sanjurjo et al., 2013). It has been reported that the ability of lysosomes to buffer Ca^{2+} in lysosomally diseased cells is greatly reduced, possibly because of the accumulation of undigested lysosomal cargo (Lloyd-Evans et al., 2008). Furthermore, buffering of cytosolic calcium by the mitochondria is defective in MLIV cells (Jennings et al., 2006). As calcium buffering is a mechanism involved in tempering calcium responses, loss of buffering capacity could actually result in enhanced global calcium signals. A similar mechanism has been demonstrated in *Dictyostelium* cells lacking the ER calcium binding proteins calnexin and calreticulin, as these strains had much larger calcium responses to chemoattractants than control cells (Wilczynska et al., 2005).

Since our mucolipin knockdown strains exhibited increased, as opposed to decreased, cytosolic Ca^{2+} signals during the vegetative phase of the lifecycle, it was surprising to find that when these strains were allowed to differentiate to aggregation-competence, their Ca^{2+} responses to cAMP were unaffected. Similarly, Chang et al. (2020) reported that in *Dictyostelium* TPC-null cells the magnitude of cAMP-mediated Ca^{2+} responses was comparable to that in wild type AX2 cells. Together these results suggest that mucolipin-dependent calcium signalling is not a major contributor to cytosolic calcium responses at this stage of development. Instead the role of mucolipin in the differentiated cells may be restricted to regulating local calcium signalling. Accordingly, the cAMP responses in the TPC null cells were slightly delayed in the time of onset, and this may be related to local calcium release from the acidic stores in "priming" ER calcium release (Chang et al., 2020), but this will require further investigation.

In previous work, the cellular phenotypes of growth, endocytosis and multicellular development were unaffected in mucolipin knockout cells created from the parental strain DH1-10 (Lima et al., 2012). Since our strains were made in the parental strain AX2, we wanted to also characterise these phenotypes in our strains. We found that surprisingly our strains did have abnormal phenotypes and many, but not all of these, presented similarly in the knockdown cells as overexpression cells. Furthermore, some of the phenotypes in our strains were similar to those reported in *Dictyostelium* NCL models.

Phagocytosis rates were increased in both mucolipin knockdown and overexpression cells. This may be directly related to the increased calcium signalling in these strains as evidence suggests that calcium is involved in phagocytosis (Muller-Taubenberger et al., 2001; Yuan et al., 2001; Fajardo et al., 2004; Pikzack et al., 2005). Pinocytosis rates were increased in knockdown strains, but

unaffected in overexpression strains which suggests the defect is not directly caused by the abnormal calcium signalling. The involvement of Ca^{2+} in macropinocytosis is unclear. Extracellular Ca^{2+} is not essential (Williams and Kay, 2018), but both liberation of intracellular Ca^{2+} by caffeine treatment and inhibition of Ca^{2+} transport by La^{3+} treatment reduces macropinocytosis (Gonzalez et al., 1990). However, both caffeine and La^{2+} can affect other processes. Our results suggest different roles for mucolipin function in macropinocytosis and phagocytosis.

When measuring growth rates, we expected that the increase in phagocytosis rates would correlate with an increase in growth rates on bacterial lawns, however both knockdown and overexpression strains grew normally on *E. coli*. Furthermore, axenic growth rates were slightly reduced in knockdown strains, so again did not correlate with the increase in pinocytic uptake. This phenotype was also present in *dn2* knockdown mutants (Smith et al., 2019) and together these results may represent the presence of compensatory feedback pathways that upregulate rates of endocytosis as a response to nutrient deprivation caused by defective endolysosomal trafficking. This kind of reverse coupling of growth and endocytosis rates has also been observed in relation to other *Dictyostelium* lysosomal proteins. A *Dictyostelium* knockout of *alyA* (encoding the major lysozyme isoform) has 40% reduction in total lysozyme activity, exhibits slow growth on bacterial lawns but increased phagocytosis of fluorescently labelled yeast cells due to a compensatory pathway (Müller et al., 2005). Knocking down expression of lysosomal Tpp1 (tripeptidyl peptidase I encoded by *cln2/tpp1*) caused reductions in the growth rate in liquid medium, slower plaque expansion rates on bacterial lawns, but elevated rates of phagocytosis (Smith et al., 2019). These effects were mediated by reduced activity of the *Dictyostelium* TORC1 (homologue of the human mechanistic Target of Rapamycin Complex I) signalling pathway, being mimicked by rapamycin treatment (inhibitor of TORC1) and Rheb knockdown (upstream activator of TORC1), and rescued by Rheb overexpression (Smith et al., 2019). Other *Dictyostelium* NCL models have shown varying phenotypes in their growth and nutrient uptake phenotypes. Mutants lacking *cln3* and *cln5* displayed enhanced proliferation in HL5 medium, however pinocytic uptake was not significantly different from AX3, and the *cln3*$^-$ phenotype was rescued by overexpression of GFP-cln3 (Huber et al., 2014; McLaren et al., 2021). Combined these results indicate abnormalities in nutrient uptake and growth and the pathways that connect them in the different lysosomal disease models.

The defects in catabolism that we observed in our strains could also be caused by disruptions in mucolipin-mediated Ca^{2+}-dependent vesicle fragmentation/fusion which is characteristic of MLIV and other MLIV models (Berman et al., 1974; Bargal and Bach, 1997; Lubensky et al., 1999). We observed that mucolipin knockdown and overexpression strains had increased fluorescence when stained with Lysosensor Blue. This may be linked to accumulation of Lysosensor Blue-stained vesicles as a result of Ca^{2+}-dependent increases in homotypic or heterotypic vesicle fusion during the endosomal mixing stage and subsequent failure to progress through to exocytosis. Studies in other models reported that the defective membrane trafficking can be caused by both knockout and overexpression of TRPMLs causing accumulation of large hybrid late endosome-lysosomal compartments (Berman et al., 1974; Lubensky et al., 1999) as well as enlargement and clustering of endosomes (Fares and Greenwald, 2001; Kim et al., 2007; Martina et al., 2009; Vergarajauregui et al., 2009). In *Dictyostelium* DH1-10 mucolipin knockout cells, a significant increase in generation of post-lysosomes was reported, however as this was coupled with enhanced rate of post-lysosome fusion with the plasma membrane, and subsequent exocytosis, so that there was no measurable build-up of vesicles (Lima et al., 2012). We did not measure exocytosis rates in our strains, so further experiments could determine if exocytosis is blocked in our strains and account for the accumulation.

Alternatively, because Lysosensor Blue fluorescence increases as the pH becomes more acidic, the increased fluorescence in our knockdown and overexpression strains could also be caused by a decrease in the pH of the vesicles. Dysregulated lysosomal pH is common to lysosomal storage disease cells, however this is generally linked to increased pH as reported in MLIV fibroblasts type (Bach et al., 1999) and most NCLs (Holopainen et al., 2001). However, decreased lysosomal pH has been described in some MLIV fibroblasts (Soyombo et al., 2006). It is important to note that *Dictyostelium* cells lacking mucolipin exhibited no change in the pH of endosomal compartments (Lima et al., 2012).

A further consequence of dysfunctional catabolism, retention of unprocessed nutrients and decreased release of amino acids from the vesicles, could be that the cells are in a state of partial starvation and this would favour the initiation of aggregation. In support of this, both mucolipin knockdown and overexpression strains exhibited increased numbers of aggregation centers and accordingly formed slugs and fruiting bodies significantly smaller than those of AX2. This implicates mucolipin in activation of aggregation center formation and could be linked to calcium-dependent regulation of developmental processes (Sakamoto et al., 2003; Poloz and O'Day, 2012). The same phenotype is present in *IplA*$^-$ cells which form smaller mounds and fruiting bodies due to fragmented aggregation streams (Traynor et al., 2000; Schaloske et al., 2005). Similar phenotypes are also present in other *Dictyostelium* lysosomal disease models. Mutants with knocked down *cln2/tpp1* form smaller aggregates and fruiting bodies (also mediated by reduced TORC1 signalling, Smith et al., 2019), and *cln2/tpp1*$^-$ mutants progress faster through development (Phillips and Gomer, 2015). Cells lacking *cln3* and *cln5* exhibit precocious development, increased numbers of tipped mounds, fingers and slugs, similar to our mucolipin strains (Huber et al., 2014; Huber et al., 2017; McLaren et al., 2021). Interestingly, the precocious development in *cln3*$^-$ cells was rescued by chelation of calcium with EGTA. This implicates Cln3 in calcium regulation, likely due to its localisation at the contractile vacuole, a major calcium regulatory organelle (Malchow et al., 2006; Huber et al., 2014), and suggests calcium dysregulation may be common to lysosomal disease cells.

In addition to the increased numbers of aggregates formed in our knockdown and overexpression mutants, an increased proportion of the cells in the aggregates appear to be entering the autophagic cell death pathway. This was suggested by the proportionately thicker stalks and enlarged basal disks, a phenotype associated with increased autophagic cell death (Bokko et al., 2007). This is another phenotype common among *Dictyostelium* lysosomal disease mutants. It is also present in *tpp1* knockdown cells where it is mediated by reduced

TORC1 signalling (Smith et al., 2019). Furthermore, enhanced autophagy has been reported in *tpp1* knockout cells (Phillips and Gomer, 2015) and *chi5*$^{-}$ cells display aberrant autophagy (McLaren et al., 2021). TPC knockout cells also accumulate autophagosomes (Chang et al., 2020) which further implicates calcium signalling through the acidic stores in autophagic processes. As autophagic cell death occurs late in the developmental cycle during stalk formation, it is possible that during autophagy, mucolipin together with other calcium channels in that location (TPC in particular) could play similar roles in generating a local Ca^{2+} cloud to facilitate fusion of the autophagosome and lysosome during formation of the stalk cell vacuole. Schaap et al. (1996) showed that a sustained elevation of resting cytoplasmic Ca^{2+} levels mediates late stalk gene (*ecmB*) induction by the morphogen DIF (Differentiation Inducing Factor) in *Dictyostelium*. Mucolipin could play a role in this process. In that case, as we have seen in the endolysosomal pathway, mucolipin overexpression and knockdown would both cause increased Ca^{2+} signals and subsequent disturbances in autophagolysosome formation, possibly explaining the stalk phenotype. An increase in cellular autophagic vacuoles is a characteristic associated with MLIV (Vergarajauregui et al., 2008) is observed both in mouse models (Curcio-Morelli et al., 2010), and *Drosophila* mucolipin knockout flies (Wong et al., 2012). The underlying nature of the autophagic defect may be related to disruption in signalling by the nutrient stress sensor mTORC1, a key regulator of autophagy. One study has shown that mTORC1 can directly phosphorylate TRPML1 to negatively regulate channel activity and decrease autophagy (Onyenwoke et al., 2015). To add further complexity, recent evidence has revealed that TRPML1 Ca^{2+} release can regulate mTORC1 autophagic pathways through a nutrient-sensitive negative feedback loop (Sun et al., 2018). Furthermore, TRPML1 is directly involved in the Ca^{2+}/calmodulin dependent protein kinase β (CaMKKβ) activation of AMP-activated protein kinase (AMPK) (Scotto-Rosato et al., 2019). AMPK in turn inhibits TORC1 and thereby activates autophagy.

The nature of these complex signalling pathways still needs to be unravelled, therefore our study supports the view that *Dictyostelium* offers a tractable, simple model for MLIV cytopathology. The results suggest it would be valuable in future experiments to investigate further the signalling pathways involved in mucolipin Ca^{2+} signalling-dependent regulation of cellular growth and autophagy through *Dictyostelium* TORC1. This is of particular interest because the role of Ca^{2+} signalling in regulation of mTORC1 autophagy pathways is evident, but details are still unclear (Decuypere et al., 2011), as are mTORC1-TRPML signalling pathways. Therefore, it would be relevant to explore whether the growth and developmental defects can be rescued by genetically altering *Dictyostelium* TORC1 and *Dictyostelium* AMPK expression in mucolipin knockdown and overexpression backgrounds.

The results we have presented here highlight common phenotypes amongst *Dictyostelium* lysosomal disease models suggesting they may share common pathologies. We have also shown that both increasing and decreasing mucolipin expression levels can cause the same phenotypic outcome. Our results are similar to other studies where reports of both increased and decreased expression of mucolipin proteins can cause problems along the endocytic pathways. For example, when TRPML3 is knocked down there are defects in endosomal acidification and also increased homotypic endosomal fusion (Lelouvier and Puertollano, 2011), while when TRPML3 is overexpressed, endosomes become enlarged (Martina et al., 2009; Lelouvier and Puertollano, 2011). In *C. elegans*, both mucolipin knockout and some overexpression coelomocytes, exhibited the formation of large vacuoles (Fares and Geenwald, 2001). Similarly, overexpression of TRPML1 results in accumulation of enlarged endosomes containing both early (Hrs) and late (CD63) endocytic markers (Vergarajauregui et al., 2009) and induces an aberrant distribution of these compartments within the cell (Manzoni et al., 2004). These combined reports show that the endocytic pathway is clearly impacted by disturbances in both directions in the expression levels or activities of mucolipin proteins and the resultant alterations in Ca^{2+} signalling.

DATA AVAILABILITY STATEMENT

Raw data will be made available by contacting the corresponding authors, without reservation.

AUTHOR CONTRIBUTIONS

CA performed the experiments, curated the data and wrote the manuscript. PF conceptualized the project, supervised. CA, helped analyse data, reviewed and helped write the manuscript.

FUNDING

This work was funded by Australian Research Council Discovery Project Grant DP140104276.

ACKNOWLEDGMENTS

We are grateful to Professor Pierre Cosson for kindly providing us with nitrocellulose membranes and cell lysate from DH1-10 and mucolipin knockout cells and Anna Dardel for carefully preparing and sending the materials to us. We are grateful to Dr. Sarah Annesley who provided advice on some of the techniques and critiqued the manuscript for us.

SUPPLEMENTARY MATERIAL

The Supplementary Material for this article can be found online at: https://www.frontiersin.org/articles/10.3389/fcell.2022.741967/full#supplementary-material

REFERENCES

Annesley, S. J., Chen, S., Francione, L. M., Sanislav, O., Chavan, A. J., and Farah, C. (2014). *Dictyostelium*, a Microbial Model for Brain Disease. *Biochim. Biophys. Acta* 1840, 1413–1432. doi:10.1016/j.bbagen.2013.10.019

Annesley, S. J., and Fisher, P. R. (2009). *Dictyostelium discoideum*-a Model for many Reasons. *Mol. Cel Biochem.* 329, 73–91. doi:10.1007/s11010-009-0111-8

Bach, G., Chen, C. S., and Pagano, R. E. (1999). Elevated Lysosomal pH in Mucolipidosis Type IV Cells. *Clin. Chim. Acta* 280 (1-2), 173–179. doi:10.1016/s0009-8981(98)00183-1

Bargal, R., and Bach, G. (1997). Mucolipidosis Type IV: Abnormal Transport of Lipids to Lysosomes. *J. Inherit. Metab. Dis.* 20, 625–632. doi:10.1023/a:1005362123443

Barth, C., Fraser, D. J., and Fisher, P. R. (1998). Co-insertional Replication Is Responsible for Tandem Multimer Formation during Plasmid Integration into the *Dictyostelium* Genome. *Plasmid* 39, 141–153. doi:10.1006/plas.1997.1326

Benini, A., Bozzato, A., Mantovanelli, S., Calvarini, L., Giacopuzzi, E., Bresciani, R., et al. (2013). Characterization and Expression Analysis of mcoln1.1 and mcoln1.2, the Putative Zebrafish Co-orthologs of the Gene Responsible for Human Mucolipidosis Type IV. *Int. J. Dev. Biol.* 57 (1), 85–93. doi:10.1387/ijdb.120033gb

Berman, E. R., Livni, N., Shapira, E., Merin, S., and Levij, I. S. (1974). Congenital Corneal Clouding with Abnormal Systemic Storage Bodies: a New Variant of Mucolipidosis. *J. Pediatr.* 84 (4), 519–526. doi:10.1016/s0022-3476(74)80671-2

Bharat, T. A., Malsam, J., Hagen, W. J., Scheutzow, A., Söllner, T. H., and Briggs, J. A. G. (2014). SNARE and Regulatory Proteins Induce Local Membrane Protrusions to Prime Docked Vesicles for Fast Calcium-Triggered Fusion. *EMBO Rep.* 15, 308–314. doi:10.1002/embr.201337807

Bokda, P. B., Francione, L., Bandala-Sanchez, E., Ahmed, A. U., Annesley, S. J., Huang, X., et al. (2007). Diverse Cytopathologies in Mitochondrial Disease Are Caused by AMP-Activated Protein Kinase Signalling. *Mol. Biol. Cel.* 18, 1874–1886. doi:10.1091/mbc.E06-09-0881

Boudewyn, L. C., and Walkley, S. U. (2019). Current Concepts in the Neuropathogenesis of Mucolipidosis Type IV. *J. Neurochem.* 148, 669–689. doi:10.1111/jnc.14462

Brailoiu, G. C., and Brailoiu, E. (2016). Modulation of Calcium Entry by the Endo-Lysosomal System. *Adv. Exp. Med. Biol.* 898, 423–447. doi:10.1007/978-3-319-26974-0_18

Cao, Q., Yang, Y., Zhong, X. Z., and Dong, X. P. (2017). The Lysosomal Ca^{2+} Release Channel TRPML1 Regulates Lysosome Size by Activating Calmodulin. *J. Biol. Chem.* 292, 8424–8435. doi:10.1074/jbc.M116.772160

Cao, Q., Zhong, X. Z., Zou, Y., Zhang, Z., Toro, L., and Dong, X. P. (2015). BK Channels Alleviate Lysosomal Storage Diseases by Providing Positive Feedback Regulation of Lysosomal Ca^{2+} Release. *Dev. Cel* 33 (4), 427–441. doi:10.1016/j.devcel.2015.04.010

Chang, F. S., Wang, Y., Dmitriev, P., Gross, J., Galione, A., and Pears, C. (2020). A Two-Pore Channel Protein Required for Regulating mTORC1 Activity on Starvation. *BMC Biol.* 18 (1), 8. doi:10.1186/s12915-019-0735-4

Chen, C. S., Bach, G., and Pagano, R. E. (1998). Abnormal Transport along the Lysosomal Pathway in Mucolipidosis, Type IV Disease. *PNAS USA* 95, 6373–6378. doi:10.1073/pnas.95.11.6373

Cheng, X., Shen, D., Samie, M., and Xu, H. (2010). Mucolipins: Intracellular TRPML1-3 Channels. *FEBS Lett.* 584, 2013–2021. doi:10.1016/j.febslet.2009.12.056

Christoforidis, S., McBride, H. M., Burgoyne, R. D., and Zerial, M. (1999). The Rab5 Effector EEA1 Is a Core Component of Endosome Docking. *Nature* 397, 621–625. doi:10.1038/17618

Curcio-Morelli, C., Charles, F. A., Micsenyi, M. C., Cao, Y., Venugopal, B., Browning, M. F., et al. (2010). Macroautophagy Is Defective in Mucolipin-1-Deficient Mouse Neurons. *Neurobiol. Dis.* 40, 370–377. doi:10.1016/j.nbd.2010.06.010

Decuypere, J. P., Bultynck, G., and Parys, J. B. (2011). A Dual Role for Ca^{2+} in Autophagy Regulation. *Cell Calcium* 50, 242–250. doi:10.1016/j.ceca.2011.04.001

Denis, V., and Cyert, M. S. (2002). Internal Ca^{2+} Release in Yeast Is Triggered by Hypertonic Shock and Mediated by a TRP Channel Homologue. *J. Cel. Biol.* 156, 29–34. doi:10.1083/jcb.200111004

Dong, X. P., Wang, X., and Xu, H. (2010). TRP Channels of Intracellular Membranes. *J. Neurochem.* 113, 313–328. doi:10.1111/j.1471-4159.2010.06626.x

Dowson, J. H., Armstrong, D., Koppang, N., Lake, B. D., and Jolly, R. D. (1982). Autofluorescence Emission Spectra of Neuronal Lipopigment in Animal and Human Ceroidoses (Ceroid-lipofuscinoses). *Acta Neuropathol.* 58, 152–156. doi:10.1007/BF00691656

Fajardo, M., Schleicher, M., Noegel, A., Bozzaro, S., Killinger, S., Heuner, K., et al. (2004). Calnexin, Calreticulin and Cytoskeleton-Associated Proteins Modulate Uptake and Growth of *Legionella pneumophila* in *Dictyostelium discoideum*. *Microbiology* 150, 2825–2835. doi:10.1099/mic.0.27111-0

Fares, H., and Greenwald, I. (2001). Regulation of Endocytosis by CUP-5, the *Caenorhabditis elegans* Mucolipin-1 Homolog. *Nat. Genet.* 28, 64–68. doi:10.1038/88281

Feng, X., Huang, Y., Lu, Y., Xiong, J., Wong, C. O., Yang, P., et al. (2014). *Drosophila* TRPML Forms PI(3,5)P2-activated Cation Channels in Both Endolysosomes and Plasma Membrane. *J. Biol. Chem.* 289, 4262–4272. doi:10.1074/jbc.M113.506501

Fernando, S., Allan, C. Y., Mroczek, K., Pearce, X., Sanislav, O., Fisher, P. R., et al. (2020). Cytotoxicity and Mitochondrial Dysregulation Caused by α-Synuclein in. *Dictyostelium discoideum*. *Cell* 9 (10), 2289. doi:10.3390/cells9102289

Fey, P., Gaudet, P., Curk, T., Zupan, B., Just, E. M., Basu, S., et al. (2009). dictyBase-a *Dictyostelium* Bioinformatics Resource Update. *Nucleic Acids Res. (Database Issue)*, D515–D519. doi:10.1093/nar/gkn844

Fisher, R., and Wilczynska, Z. (2006). Contribution of Endoplasmic Reticulum to Ca^{2+} Signals in *Dictyostelium* Depends on Extracellular Ca^{2+}. *FEMS Microbiol. Lett.* 257, 268–277. doi:10.1111/j.1574-6968.2006.00180.x

Fountain, S. J., Parkinson, K., Young, M. T., Cao, L., Thompson, C. R. L., and North, R. A. (2007). An Intracellular P2X Receptor Required for Osmoregulation in *Dictyostelium discoideum*. *Nature* 448 (7150), 200–203. doi:10.1038/nature05926

Gerasimenko, J. V., Tepikin, A. V., Petersen, O. H., and Gerasimenko, O. V. (1998). Calcium Uptake via Endocytosis with Rapid Release from Acidifying Endosomes. *Curr. Biol.* 8, 1335–1338. doi:10.1016/S0960-9822(07)00565-9

Goldin, E., Blanchette-Mackie, E. J., Dwyer, N. K., Pentchev, P. G., and Brady, R. O. (1995). Cultured Skin Fibroblasts Derived from Patients with Mucolipidosis 4 Are Auto-Fluorescent. *Pediatr. Res.* 37, 687–692. doi:10.1203/00006450-199506000-00003

Gómez, N. M., Lu, W., Lim, J. C., Kiselyov, K., Campagno, K. E., Grishchuk, Y., et al. (2018). Robust Lysosomal Calcium Signaling through Channel TRPML1 Is Impaired by Lysosomal Lipid Accumulation. *FASEB J.* 32 (2), 782–794. doi:10.1096/fj.201700220RR

Gonzalez, C., Klein, G., and Satre, M. (1990). Caffeine, an Inhibitor of Endocytosis in *Dictyostelium discoideum* Amoebae. *J. Cel Physiol.* 144, 408–415. doi:10.1002/jcp.1041440307

Grimm, C., Jörs, S., Guo, Z., Obukhov, A. G., and Heller, S. (2012). Constitutive Activity of TRPML2 and TRPML3 Channels versus Activation by Low Extracellular Sodium and Small Molecules. *J. Biol. Chem.* 287 (27), 22701–22708. doi:10.1074/jbc.M112.369876

Gross, J. D. (2009). Acidic Ca^{2+} Stores, Excitability, and Cell Patterning in *Dictyostelium discoideum*. *Eukaryot. Cel* 8 (5), 696–702. doi:10.1128/ec.00360-08

Han, J., Pluhackova, K., and Böckmann, R. A. (2017). The Multifaceted Role of SNARE Proteins in Membrane Fusion. *Front. Physiol.* 8, 5. doi:10.3389/fphys.2017.00005

Hay, J. C. (2007). Calcium, a Fundamental Regulator of Membrane Fusion? *EMBO Rep.* 8 (3), 236–240. doi:10.1038/sj.embor.7400921

Holopainen, J. M., Saarikoski, J., Kinnunen, P. K. J., and Järvelä, I. (2001). Elevated Lysosomal pH in Neuronal Ceroid Lipofuscinoses (NCLs). *Eur. J. Biochem.* 268, 5851–5856. doi:10.1046/j.0014-2956.2001.02530.x

Huber, R. J., and Mathavarajah, S. (2019). Comparative Transcriptomics Reveals Mechanisms Underlying Cln3-Deficiency Phenotypes in *Dictyostelium*. *Cell Signal* 58, 79–90. doi:10.1016/j.cellsig.2019.02.004

Huber, R. J. (2020). Molecular Networking in the Neuronal Ceroid Lipofuscinoses: Insights from Mammalian Models and the Social Amoeba *Dictyostelium discoideum*. *J. Biomed. Sci.* 27 (1), 64. doi:10.1186/s12929-020-00653-y

Huber, R. J., Myre, M. A., and Cotman, S. L. (2017). Aberrant Adhesion Impacts Early Development in a *Dictyostelium* Model for Juvenile Neuronal Ceroid

Lipofuscinosis. *Cell Adh Migr* 11 (4), 399–418. doi:10.1080/19336918.2016.1236179

Huber, R. J., Myre, M. A., and Cotman, S. L. (2014). Loss of Cln3 Function in the Social Amoeba *Dictyostelium discoideum* Causes Pleiotropic Effects that Are Rescued by Human CLN3. *PLoS ONE* 9 (10), e110544. doi:10.1371/journal.pone.0110544

Jennings, J. J., Jr, Zhu, J. H., Rbaibi, Y., Luo, X., Chu, C. T., and Kiselyov, K. (2006). Mitochondrial Aberrations in Mucolipidosis Type IV. *J. Biol. Chem.* 281 (51), 39041–39050. doi:10.1074/jbc.M607982200

Kilpatrick, B. S., Yates, E., Grimm, C., Schapira, A. H., and Patel, S. (2016). Endo-lysosomal TRP Mucolipin-1 Channels Trigger Global ER Ca^{2+} Release and Ca^{2+} Influx. *J. Cel Sci.* 129 (20), 3859–3867. doi:10.1242/jcs.190322

Kim, H. J., Li, Q., Tjon-Kon-Sang, S., So, I., Kiselyov, K., and Muallem, S. (2007). Gain-of-function Mutation in TRPML3 Causes the Mouse Varitint-Waddler Phenotype. *J. Biol. Chem.* 282, 36138–36142. doi:10.1074/jbc.C700190200

Kiselyov, K., Chen, J., Rbaibi, Y., Oberdick, D., Tjon-Kon-Sang, S., Shcheynikov, N., et al. (2005). TRP-ML1 Is a Lysosomal Monovalent Cation Channel that Undergoes Proteolytic Cleavage. *J. Biol. Chem.* 280, 43218–43223. doi:10.1074/jbc.M508210200

Kotsifas, M., Barth, C., Lay, S. T., Lozanne, A., and Fisher, P. R. (2002). Chaperonin 60 and Mitochondrial Disease in *Dictyostelium*. *J. Muscle Res. Cel Motil* 23, 839–852. doi:10.1023/A:1024444215766

LaPlante, J. M., Falardeau, J., Sun, M., Kanazirska, M., Brown, E. M., Slaugenhaupt, S. A., et al. (2002). Identification and Characterization of the Single Channel Function of Human Mucolipin-1 Implicated in Mucolipidosis Type IV, a Disorder Affecting the Lysosomal Pathway. *FEBS Lett.* 532, 183–187. doi:10.1016/S0014-5793(02)03670-0

LaPlante, J. M., Ye, C. P., Quinn, S. J., Goldin, E., Brown, E. M., Slaugenhaupt, S. A., et al. (2004). Functional Links between Mucolipin-1 and Ca^{2+}-dependent Membrane Trafficking in Mucolipidosis IV. *Biochem. Biophys. Res. Commun.* 322, 1384–1391. doi:10.1016/j.bbrc.2004.08.045

Lawe, D. C., Sitouah, N., Hayes, S., Chawla, A., Virbasius, J. V., Tuft, R., et al. (2003). Essential Role of Ca^{2+}/Calmodulin in Early Endosome Antigen-1 Localization. *Mol. Biol. Cel* 14 (7), 2935–2945. doi:10.1091/mbc.e02-09-0591

Lee, K., Jo, Y. Y., Chung, G., Jung, J. H., Kim, Y. H., and Park, C. K. (2021). Functional Importance of Transient Receptor Potential (TRP) Channels in Neurological Disorders. *Front. Cel. Dev. Biol.* 9, 611773. doi:10.3389/fcell.2021.611773

Lelouvier, B., and Puertollano, R. (2011). Mucolipin-3 Regulates Lumenal Calcium, Acidification, and Membrane Fusion in the Endosomal Pathway. *J. Biol. Chem.* 286, 9826–9832. doi:10.1074/jbc.M110.169185

Lima, W. C., Leuba, F., Soldati, T., and Cosson, P. (2012). Mucolipin Controls Lysosome Exocytosis in *Dictyostelium*. *J. Cel Sci.* 125, 2315–2322. doi:10.1242/jcs.100362

Lima, W. C., Vinet, A., Pieters, J., and Cosson, P. (2014). Role of PKD2 in Rheotaxis in *Dictyostelium*. *PLoS ONE* 9 (2), e88682. doi:10.1371/journal.pone.0088682

Lloyd-Evans, E., Morgan, A., He, X., Smith, D. A., Elliot-Smith, E., Sillence, D. J., et al. (2008). Niemann-Pick Disease Type C1 Is a Sphingosine Storage Disease that Causes Deregulation of Lysosomal Calcium. *Nat. Med.* 14, 1247–1255. doi:10.1038/nm.1876

López-Sanjurjo, C. I., Tovey, S. C., Prole, D. L., and Taylor, C. W. (2013). Lysosomes Shape Ins(1,4,5)P3-Evoked Ca^{2+} Signals by Selectively Sequestering Ca^{2+} Released from the Endoplasmic Reticulum. *J. Cel Sci.* 126 (1), 289–300. doi:10.1242/jcs.116103

López-Sanjurjo, C. I., Tovey, S. C., and Taylor, C. W. (2014). Rapid Recycling of Ca^{2+} between IP3-Sensitive Stores and Lysosomes. *PLoS One* 9 (10), e111275. doi:10.1371/journal.pone.0111275

Lubensky, I. A., Schiffmann, R., Goldin, E., and Tsokos, M. (1999). Lysosomal Inclusions in Gastric Parietal Cells in Mucolipidosis Type IV: a Novel Cause of Achlorhydria and Hypergastrinemia. *Am. J. Surg. Pathol.* 23, 1527–1531.

Lusche, D. F., Wessels, D., Scherer, A., Daniels, K., Kuhl, S., and Sol, I. D. R. (2012). The IplA Ca^{2+} Channel of *Dictyostelium discoideum* Is Necessary for Ca^{2+}, but Not cAMP Chemotaxis, and Plays a Fundamental Role in Natural Aggregation. *J. Cel Sci.* 125 (7), 1770–1783.

Luzio, J. P., Bright, N. A., and Pryor, P. R. (2007). The Role of Calcium and Other Ions in Sorting and Delivery in the Late Endocytic Pathway. *Biochem. Soc. Trans.* 35, 1088–1091. doi:10.1042/BST0351088

Lytton, J., Westlin, M., and Hanley, M. R. (1991). Thapsigargin Inhibits the Sarcoplasmic or Endoplasmic Reticulum Ca^{2+}-ATPase Family of Calcium Pumps. *J. Biol. Chem.* 266, 17067–17071.

Malchow, D., Lusche, D. F., De Lozanne, A., and Schlatterer, C. (2008). A Fast Ca^{2+}-Induced Ca^{2+}-Release Mechanism in *Dictyostelium discoideum*. *Cell Calcium* 43 (6), 521–530. doi:10.1016/j.ceca.2007.08.002

Malchow, D., Lusche, D. F., Schlatterer, C., De Lozanne, A., and Müller-Taubenberger, A. (2006). The Contractile Vacuole in Ca^{2+}-Regulation in *Dictyostelium*: its Essential Function for cAMP-Induced Ca^{2+}-Influx. *BMC Dev. Biol.* 6, 31. doi:10.1186/1471-213X-6-31

Maniak, M. (2011). *Dictyostelium* as a Model for Human Lysosomal and Trafficking Diseases. *Semin. Cel Dev Biol* 22 (1), 114–119. doi:10.1016/j.semcdb.2010.11.001

Manzoni, M., Monti, E., Bresciani, R., Bozzato, A., Barlati, S., Bassi, M. T., et al. (2004). Overexpression of Wild-type and Mutant Mucolipin Proteins in Mammalian Cells: Effects on the Late Endocytic Compartment Organization. *FEBS Lett.* 567, 219–224. doi:10.1016/j.febslet.2004.04.080

Martín-González, J., Montero-Bullón, J. F., and Lacal, J. (2021). *Dictyostelium discoideum* as a Non-mammalian Biomedical Model. *Microb. Biotechnol.* 14 (1), 111–125. doi:10.1111/1751-7915.13692

Martina, J. A., Lelouvier, B., and Puertollano, R. (2009). The Calcium Channel Mucolipin-3 Is a Novel Regulator of Trafficking along the Endosomal Pathway. *Traffic* 10, 1143–1156. doi:10.1111/j.1600-0854.2009.00935.x

Maselli, A., Laevsky, G., and Knecht, D. A. (2002). Kinetics of Binding, Uptake and Degradation of Live Fluorescent (DsRed) Bacteria by *Dictyostelium discoideum*. *Microbiology (Reading)* 148, 413–420. doi:10.1099/00221287-148-2-413

McLaren, M. D., Mathavarajah, S., Kim, W. D., Yap, S. Q., and Huber, R. J. (2021). Aberrant Autophagy Impacts Growth and Multicellular Development in a *Dictyostelium* KO Model of CLN5 Disease. *Front. Cell Dev. Biol.* 9, 657406. doi:10.3389/fcell.2021.657406

Medina, D. L., Di Paola, S., Peluso, I., Armani, A., De Stefani, D., Venditti, R., et al. (2015). Lysosomal Calcium Signalling Regulates Autophagy through Calcineurin and TFEB. *Nat. Cel Biol* 17 (3), 288–299. doi:10.1038/ncb3114

Micsenyi, M. C., Dobrenis, K., Stephney, G., Pickel, J., Vanier, M. T., Slaugenhaupt, S. A., et al. (2009). Neuropathology of the Mcoln1(-/-) KO Mouse Model of mucolipidosis type IV. *J. Neuropathol. Exp. Neurol.* 68, 125–135. doi:10.1097/NEN.0b013e3181942cf0

Miedel, M. T., Rbaibi, Y., Guerriero, C. J., Colletti, G., Weixel, K. M., Weisz, O. A., et al. (2008). Membrane Traffic and Turnover in TRP-ML1-Deficient Cells: a Revised Model for Mucolipidosis Type IV Pathogenesis. *J. Exp. Med.* 205 (6), 1477–1490. doi:10.1084/jem.20072194

Miedel, M. T., Weixel, K. M., Bruns, J. R., Traub, L. M., and Weisz, O. A. (2006). Posttranslational Cleavage and Adaptor Protein Complex-dependent Trafficking of Mucolipin-1. *J. Biol. Chem.* 281 (18), 12751–12759. doi:10.1074/jbc.M511104200

Mills, I. G., Jones, A. T., and Clague, M. J. (1998). Involvement of the Endosomal Autoantigen EEA1 in Homotypic Fusion of Early Endosomes. *Curr. Biol.* 8, 881–884. doi:10.1016/s0960-9822(07)00351-x

Müller, I., Šubert, N., Otto, H., Herbst, R., Rühling, H., Maniak, M., et al. (2005). A *Dictyostelium* Mutant with Reduced Lysozyme Levels Compensates by Increased Phagocytic Activity. *J. Biol. Chem.* 280, 10435–10443. doi:10.1074/jbc.M411445200

Müller-Taubenberger, A., Lupas, A. N., Li, H., Ecke, M., Simmeth, E., and Gerisch, G. (2001). Calreticulin and Calnexin in the Endoplasmic Reticulum Are Important for Phagocytosis. *EMBO J.* 20 (23), 6772–6782. doi:10.1093/emboj/20.23.6772

Morgan, A. J., Platt, F. M., Lloyd-Evans, E., and Galione, A. (2011). Molecular Mechanisms of Endolysosomal Ca^{2+} Signalling in Health and Disease. *Biochem. J.* 439 (3), 349–374.

Nebl, T., and Fisher, P. R. (1997). Intracellular Ca^{2+} Responses by *Dictyostelium* Amoebae to Nanomolar Chemoattractant Stimuli Are Mediated Exclusively by Ca^{2+} Influx. *J. Cel Sci.* 110, 2845–2853.

Nebl, T., Kotsifas, M., Schaap, P., and Fisher, P. R. (2002). Multiple Pathways Connect Chemoattractant Receptors and Ca^{2+} Channels in *Dictyostelium*. *J. Muscle Res. Cel Motil* 23, 853–865. doi: doi:10.1023/a:1024496232604

Nellen, W., Silan, C., and Firtel, R. A. (1984). DNA-mediated Transformation in *Dictyostelium discoideum*: Regulated Expression of an Actin Gene Fusion. *Mol. Cel. Biol.* 4, 2890–2898. doi:10.1128/mcb.4.12.2890-2898.1984

Onyenwoke, R. U., Sexton, J. Z., Yan, F., Díaz, M. C. H., Forsberg, L. J., Major, M. B., et al. (2015). The Mucolipidosis IV Ca^{2+} Channel TRPML1 (MCOLN1) Is Regulated by the TOR Kinase. *Biochem. J.* 470, 331–342. doi:10.1042/BJ20150219

Parikh, A., Miranda, E. R., Katoh-Kurasawa, M., Fuller, D., Rot, G., Zagar, L., et al. (2010). Conserved Developmental Transcriptomes in Evolutionarily Divergent Species. *Genome Biol.* 11 (3), R35. doi:10.1186/gb-2010-11-3-r35

Patel, S., and Cai, X. (2015). Evolution of Acidic Ca^{2+} Stores and Their Resident Ca2+-Permeable Channels. *Cell Calcium* 57 (3), 222–230. doi:10.1016/j.ceca.2014.12.005

Patel, S., and Docampo, R. (2010). Acidic Calcium Stores Open for Business: Expanding the Potential for Intracellular Ca^{2+} Signaling. *Trends Cel Biol* 20 (5), 277–286. doi:10.1016/j.tcb.2010.02.003

Phillips, J. E., and Gomer, R. H. (2015). Partial Genetic Suppression of a Loss-Of-Function Mutant of the Neuronal Ceroid Lipofuscinosis-Associated Protease TPP1 in *Dictyostelium discoideum*. *Dis. Model. Mech.* 8, 147–156. doi:10.1242/dmm.018820

Pikzack, C., Prassler, J., Furukawa, R., Fechheimer, M., and Rivero, F. (2005). Role of Calcium-dependent Actin-Bundling Proteins: Characterization of *Dictyostelium* Mutants Lacking Fimbrin and the 34-kilodalton Protein. *Cell Motil. Cytoskeleton* 62, 210–231. doi:10.1002/cm.20098

Poloz, Y., and O'Day, D. H. (2012). Colchicine Affects Cell Motility, Pattern Formation and Stalk Cell Differentiation in *Dictyostelium* by Altering Calcium Signaling. *Differentiation* 83, 185–199. doi:10.1016/j.diff.2011.12.006

Pryor, P. R., Mullock, B. M., Bright, N. A., Gray, S. R., and Luzio, J. P. (2000). The Role of Intraorganellar Ca^{2+} in Late Endosome-Lysosome Heterotypic Fusion and in the Reformation of Lysosomes from Hybrid Organelles. *J. Cel Biol.* 149 (5), 1053–1062. doi:10.1083/jcb.149.5.1053

Ronco, V., Potenza, D. M., Denti, F., Vullo, S., Gagliano, G., Tognolina, M., et al. (2015). A Novel Ca^{2+}-Mediated Cross-Talk between Endoplasmic Reticulum and Acidic Organelles: Implications for NAADP-dependent Ca^{2+} Signalling. *Cell Calcium* 57 (2), 89–100. doi:10.1016/j.ceca.2015.01.001

Sakamoto, H., Nishio, K., Tomisako, M., Kuwayama, H., Tanaka, Y., et al. (2003). Identification and Characterization of Novel Calcium-Binding Proteins of *Dictyostelium* and Their Spatial Expression Patterns during Development. *Dev. Growth Differ.* 45, 507–514. doi:10.1111/j.1440-169X.2003.00718.x

Santoni, G., Maggi, F., Amantini, C., Marinelli, O., Nabissi, M., and Morelli, M. B. (2020). Pathophysiological Role of Transient Receptor Potential Mucolipin Channel 1 in Calcium-Mediated Stress-Induced Neurodegenerative Diseases. *Front. Physiol.* 11, 251. doi:10.3389/fphys.2020.00251

Schaap, P., Nehl, T., and Fisher, P. R. (1996). A Slow Sustained Increase in Cytosolic Ca^{2+} Levels Mediates Stalk Gene Induction by Differentiation Inducing Factor in *Dictyostelium*. *EMBO J.* 15 (19), 5177–5183. doi:10.1002/j.1460-2075.1996.tb00902.x

Schaloske, H., Lusche, F., Bezares-Roder, K., Happle, K., Malchow, D., and Schlatterer, C. (2005). Ca^{2+} Regulation in the Absence of the ipiA Gene Product in *Dictyostelium discoideum*. *BMC Cel Biol* 6 (1), 13. doi:10.1186/1471-2121-6-13

Scotto-Rosato, A., Montefusco, S., Soldati, C., Di Paola, S., Capuozzo, A., Monfregola, J., et al. (2019). TRPML1 Links Lysosomal Calcium to Autophagosome Biogenesis through the Activation of the CaMKKβ/VPS34 Pathway. *Nat. Commun.* 10 (1), 5630. doi:10.1038/s41467-019-13572-w

Shen, D., Wang, X., Li, X., Zhang, X., Yao, Z., Dibble, S., et al. (2012). Lipid Storage Disorders Block Lysosomal Trafficking by Inhibiting a TRP Channel and Lysosomal Calcium Release. *Nat. Commun.* 3, 731. doi:10.1038/ncomms1735

Smith, D. E., and Fisher, P. A. (1984). Identification, Developmental Regulation, and Response to Heat Shock of Two Antigenically Related Forms of a Major Nuclear Envelope Protein in *Drosophila* Embryos: Application of an Improved Method for Affinity Purification of Antibodies Using Polypeptides Immobilized on Nitrocellulose Blots. *J. Cel. Biol.* 99, 20–28. doi:10.1083/jcb.99.1.20

Smith, P. K., Sen, M. G., Fisher, P. R., and Annesley, S. J. (2019). Modelling of Neuronal Ceroid Lipofuscinosis Type 2 in *Dictyostelium discoideum* Suggests that Cytopathological Outcomes Result from Altered TOR Signalling. *Cells* 8 (5), 469. doi:10.3390/cells8050469

Soyombo, A. A., Tjon-Kon-Sang, S., Rbaibi, Y., Bashllari, E., Bisceglia, J., Muallem, S., et al. (2006). TRP-ML1 Regulates Lysosomal pH and Acidic Lysosomal Lipid Hydrolytic Activity. *J. Biol. Chem.* 281 (11), 7294–7301. doi:10.1074/jbc.M508211200

Stajdohar, M., Rosengarten, R. D., Kokosar, J., Jeran, L., Blenkus, D., Shaulsky, G., et al. (2017). dictyExpress: a Web-Based Platform for Sequence Data Management and Analytics in *Dictyostelium* and beyond. *BMC Bioinformatics* 18 (1), 291. doi:10.1186/s12859-017-1706-9

Sun, M., Goldin, E., Stahl, S., Falardeau, J. L., Kennedy, J. C., Acierno, J. S., Jr., et al. (2000). Mucolipidosis Type IV Is Caused by Mutations in a Gene Encoding a Novel Transient Receptor Potential Channel. *Hum. Mol. Genet.* 9 (17), 2471–2478. doi:10.1093/hmg/9.17.2471

Sun, X., Yang, Y., Zhong, X. Z., Cao, Q., Zhu, X.-H., Zhu, X., et al. (2018). A Negative Feedback Regulation of MTORC1 Activity by the Lysosomal Ca^{2+} Channel MCOLN1 (Mucolipin 1) Using a CALM (Calmodulin)-dependent Mechanism. *Autophagy* 14, 1–15. doi:10.1080/15548627.2017.1389822

Taylor, C. W., Genazzani, A. A., and Morris, S. A. (1999). Expression of Inositol Trisphosphate Receptors. *Cell Calcium* 26, 237–251. doi:10.1054/ceca.1999.0090

Traynor, D., and Kay, R. R. (2017). A Polycystin-type Transient Receptor Potential (Trp) Channel that Is Activated by ATP. *Biol. Open* 6, 200–209. doi:10.1242/bio.020685

Traynor, D., Milne, J. L., Insall, R. H., and Kay, R. R. (2000). Ca^{2+} Signalling Is Not Required for Chemotaxis in *Dictyostelium*. *EMBO J.* 19 (17), 4846–4854. doi:10.1093/emboj/19.17.4846

Treusch, S., Knuth, S., Slaugenhaupt, S. A., Goldin, E., Grant, B. D., and Fares, H. (2004). *Caenorhabditis elegans* Functional Orthologue of Human Protein H-Mucolipin-1 Is Required for Lysosome Biogenesis. *PNAS USA* 101, 4483–4488. doi:10.1073/pnas.0400709101

Venkatachalam, K., Long, A. A., Elsaesser, R., Nikolaeva, D., Broadie, K., and Montell, C. (2008). Motor Decit in a Drosophila Model of Mucolipidosis Type IV Due to Defective Clearance of Apoptotic Cells. *Cell* 135, 838–851. doi:10.1016/j.cell.2008.09.041

Vergarajauregui, S., Connelly, P. S., Daniels, M. P., and Puertollano, R. (2008). Autophagic Dysfunction in Mucolipidosis Type IV Patients. *Hum. Mol. Genet.* 17, 2723–2737. doi:10.1093/hmg/ddn174

Vergarajauregui, S., Martina, J. A., and Puertollano, R. (2009). Identification of the Penta-EF-Hand Protein ALG-2 as a Ca^{2+}-dependent Interactor of Mucolipin-1. *J. Biol. Chem.* 284, 36357–36366. doi:10.1074/jbc.M109.047241

Wilczynska, Z., and Fisher, P. R. (1994). Analysis of a Complex Plasmid Insertion in a Phototaxis-Deficient Transformant of *Dictyostelium discoideum* Selected on a *Micrococcus Luteus* Lawn. *Plasmid* 32, 182–194. doi:10.1006/plas.1994.1054

Wilczynska, Z., Happle, K., Müller-Taubenberger, A., Schlatterer, C., Malchow, D., and Fisher, P. R. (2005). Release of Ca^{2+} from the Endoplasmic Reticulum Contributes to Ca^{2+} Signalling in *Dictyostelium*. *Eukaryot. Cel* 4 (9), 1513–1525. doi:10.1128/EC.4.9.1513-1525.2005

Williams, T. D., and Kay, R. R. (2018). The Physiological Regulation of Macropinocytosis during *Dictyostelium* Growth and Development. *J. Cel Sci.* 131, jcs-213736. doi:10.1242/jcs.213736

Witke, W., Nellen, W., and Noegel, A. (1987). Homologous Recombination in the *Dictyostelium* Alpha-Actinin Gene Leads to an Altered mRNA and Lack of the Protein. *EMBO J.* 6, 4143–4148.

Wong, C. O., Montell, I., R. C., and Venkatachalam, K. (2012). Drosophila TRPML Is Required for TORC1 Activation. *Curr. Biol.* 22, 1616–1621. doi:10.1016/j.cub.2012.06.055

Yap, S. Q., Mathavarajah, S., and Huber, R. J. (2021). The Converging Roles of Batten Disease Proteins in Neurodegeneration and Cancer. *iScience* 24 (4), 102337. doi:10.1016/j.isci.2021.102337

Yuan, A., Siu, C.-H., and Chia, C. P. (2001). Calcium Requirement for Efficient Phagocytosis by *Dictyostelium discoideum*. *Cell Calcium* 29, 229–238. doi:10.1054/ceca.2000.0184

Conflict of Interest: The authors declare that the research was conducted in the absence of any commercial or financial relationships that could be construed as a potential conflict of interest.